Inhibition and Dissociation of Gas Hydrates using Glycols / Alcohols and Biodegradable Kinetic Hydrate Inhibitors

Morteza Aminnaji

Submitted for the degree of Doctor of Philosophy

Petroleum Engineering

Heriot-Watt University

School of Energy, Geoscience, Infrastructure and Society

Institute of Petroleum Engineering

July 2018

ABSTRACT

Gas hydrates are a major flow assurance issue that can cause serious operational and safety problems in the oil and gas industry. In the past decade, low dosage hydrate inhibitors (LDHIs) – including kinetic hydrate inhibitors (KHIs) and anti-agglomerants (AAs), have increasingly been used to prevent hydrate formation/blockage. LDHIs offer significant advantages over thermodynamic hydrate inhibitors (THIs); while LDHIs are used typically dosed at <2.5 wt% in produced water, THIs are used at much higher concentrations, e.g. up to 50 wt%. While KHIs are generally known as hydrate nucleation inhibitors, more recent work (Crystal Growth Inhibition (CGI) method) shows they are powerful crystal growth inhibitors for KHIs which can completely inhibit hydrates indefinitely even in the presence of hydrates. Concerns about their biodegradability have hindered their more widespread usage (in Norwegian waters they cannot be used at all), especially when the produced water containing KHIs is potentially released into the sea, sparking a growing interest in the use of green biodegradable chemicals. While only a limited number of potential green KHI candidates have currently been found, the performance of these KHIs is not well known, and they are not yet used for real applications.

The main objective of this thesis is to investigate Bio KHIs and their potential combination with THIs for prevention and remediation of gas hydrates. Initial findings of experimental studies using CGI method aimed at investigating three green KHIs which have been reported / are produced (Luvicap Bio, ECO-530, and pectin) show Luvicap Bio has better KHIs properties and was selected for further investigation in this thesis.

The performance of Luvicap Bio alone including structure effects and hydrate fraction tolerance was investigated and compared with PVCap. It was concluded that Luvicap Bio is a better inhibitor for s-I methane than for s-II methane, i.e., hydrate growth pattern and structure change studies support the theory of multi-structure hydrate formation in natural gas and s-I and s-II in the methane or ethane system.

In addition, inhibition of hydrates using a combination of Luvicap Bio and THIs (MEG, methanol, and ethanol) was investigated to see whether Luvicap Bio could be used to reduce the required THIs dosage for hydrate inhibition. The results showed that

Luvicap Bio combines well with MEG and it could reduce the methanol requirement, i.e., methanol is toxic, so green KHI replacing is an application with respect to the environment.

Furthermore, work was carried out to investigate hydrate dissociation/remediation using either THIs or KHIs. Hydrate blockage removal in the vertical pipe was investigated using MEG, methanol, and their combination. The results showed that the density of THI mix is a key factor for hydrate plug removal. The initial findings of experimental studies aimed at investigating hydrate dissociation using KHIs demonstrate that, in addition to inhibiting hydrate growth/nucleation, KHI polymers can induce partial or complete hydrate dissociation. It is speculated that it is related to hydrate structure/morphology change. In addition to improving confidence in KHI field use, findings potentially have novel applications with respect to the use of combined THI + KHI (or KHI alone) for hydrate plug remediation and gas production from naturally occurring hydrates in oceanic/permafrost sediments.

DEDICATION

I dedicate my thesis to my beloved wife for her support and patience during my PhD studying. I will always appreciate all she has done for helping me to finish this period of time.

I also dedicate this thesis to my family for their support and encouragement throughout my life.

ACKNOWLEGMENT

This research was undertaken at Institute of Petroleum Engineering, EGIS, Heriot-Watt University, Edinburgh, Scotland, U.K., under the supervision of Professor Bahman Tohidi and Mr. Ross Anderson.

This work is part of the Joint Industry Project (JIP) at the Institute of Petroleum Engineering, Heriot-Watt University. This research programme, JIP, was sponsored by Engie, Nalco-Champion, Statoil, and Total, whose support is gratefully acknowledged.

I would like to thank Professor Bahman Tohidi for offering me the opportunity to work at the well-known centre for gas hydrate, so I had a great opportunity to learn and experience from expertise people in gas hydrate, PVT, and flow assurance.

I would like to thank my second supervisor, Mr. Ross Anderson, for helping me to define, develop, and complete this thesis. In addition, I acknowledge him for experimental assistance and data/results analysis and interpretation. He always teaches me new things and finding a new solution to get the answer.

Moreover, I need to thank Professor Antonin Chapoy, Mr. Rod Burgass, and Dr. Jinhai Yang for their support and valuable discussion about the experimental works during my period of study.

However, I greatly appreciate the comments suggestions from the examiners and reviewers, Professor Jean-Michel Herri from Saint Etienne School of Mines and Dr James M. Somerville from Heriot-Watt University

In Addition, I have to thank my friends in Edinburgh as well as my colleagues in Institute of Petroleum Engineering, Heriot-Watt University. I had a very good time with them. They made my stay in Edinburgh very pleasurable and enjoyable.

Finally, I would like to express my deepest gratitude to my Wife, parents, and brothers for their support, and thanks to my wife's parents and brother.

Morteza Aminnaji

DECLARATION STATEMENT

ACADEMIC REGISTRY
Research Thesis Submission

Name*:*	MORTEZA AMINNAJI		
School:	EGIS/Institute of Petroleum Engineering		
Version: *(i.e. First, Resubmission, Final)*	Final	Degree Sought:	Ph.D. in Petroleum Engineering

Declaration

In accordance with the appropriate regulations I hereby submit my thesis and I declare that:

1) the thesis embodies the results of my own work and has been composed by myself
2) where appropriate, I have made acknowledgement of the work of others and have made reference to work carried out in collaboration with other persons
3) the thesis is the correct version of the thesis for submission and is the same version as any electronic versions submitted*.
4) my thesis for the award referred to, deposited in the Heriot-Watt University Library, should be made available for loan or photocopying and be available via the Institutional Repository, subject to such conditions as the Librarian may require
5) I understand that as a student of the University I am required to abide by the Regulations of the University and to conform to its discipline.
6) I confirm that the thesis has been verified against plagiarism via an approved plagiarism detection application e.g. Turnitin.

* *Please note that it is the responsibility of the candidate to ensure that the correct version of the thesis is submitted.*

Signature of Candidate*:*		Date:	

Submission

Submitted By *(name in capitals):*	MORTEZA AMINNAJI
Signature of Individual Submitting:	
Date Submitted:	

For Completion in the Student Service Centre (SSC)

Received in the SSC by *(name in capitals):*			
Method of Submission *(Handed in to SSC; posted through internal/external mail):*			
E-thesis Submitted ***(mandatory for final theses)***			
Signature:		Date:	

Please note this form should be bound into the submitted thesis.

TABLE OF CONTENTS

LISTS OF TABLES

LIST OF FIGURES

List of Important Symbols and Abbreviations

ΔT_{ex}	Actual cell temperature minus set cell temperature
$\Delta T_{s\text{-}I}$	Subcooling from structure-I hydrate phase boundary
$\Delta T_{s\text{-}II}$	Subcooling from structure-II hydrate phase boundary
A	Motor Current (amps)
AA	Anti-Agglomerant
C_1	Methane
C_2	Ethane
C_3	Propane
iC_4	Iso Butane
nC_4	Normal Butane
CGI	Crystal Growth Inhibition
CIR	Complete Crystal Growth Inhibition Region
CO_2	Carbon dioxide
EtOH	Ethanol
f_w	Water mole fraction
H_n	Hydration Number
hr	Hour
KHI	Kinetic Hydrate Inhibitor
LDHI	Low Dosage Hydrate Inhibitor
M	Medium (Growth Rate)
MEG	Mono Ethylene Glycol
MeOH	Methanol
n	Number of Mole
NG	Natural Gas
P	Pressure

PVCap	Poly-*n*VinylCaprolactam
PVP	Poly-*n*-VinylPyrrolidone
r	% Water Converted to Hydrate per minutes
RGR	Rapid Growth Region
S	Slow (Growth Rate)
s-H	Structure-H hydrate
S-I	Structure-I hydrate
S-II	Structure-II hydrate
t	Time
T	Temperature
T_0	Set Cell Temperature
VS	Very Slow (Growth Rate)
WCH	Water Converted to Hydrate

Chapter 1 – Introduction

1.1 Background on Gas Hydrate

Gas Hydrates are ice-like crystalline compounds which were discovered in 1810 by Sir Humphery Davy [1.1] when he found chlorine hydrate. The composition of chlorine hydrate was characterized by Faraday [1.2]. Nevertheless, it took a century to discover that natural gas hydrates could cause blockage in pipelines. In mid-1930's, Hammerschmidt reported that blockage in the gas pipeline above the ice point was due to natural gas hydrates [1.3]. This discovery of natural gas hydrate was a starting point of research activities on gas hydrates in the oil and gas industries, especially on flow assurance issues.

Gas hydrates or crystalline hydrates are crystalline solids which consist of guest/former molecules (generally gas) and water molecules (host), i.e., the guest molecules are trapped in cages with the different structure formed from hydrogen-bonded water molecules. Gas hydrates are formed as a result of physical combination of gas and water molecules depending on pressure and temperature. Generally, the presence of water/ice, suitable sized gas/liquid molecules, and suitable pressure/temperature condition are the three necessary conditions for gas hydrate formation.

Different hydrate structures can form mainly depending on the hydrate guest size and cage occupancy. However, the stability of cavities and structures can change at high pressure resulting in changing hydrate structure e.g. in methane system [1.4][1.5].

As shown in Figure 1-1, the hydrate cages consists of five polyhedral cavities/cages which are described by general nomenclature ($n_i^{m_i}$) where n_i is the number of edges in face type ''i'' and m_i is the number of faces with n_i edges [1.6]. The description and properties of these cavities are tabulated in Table 1-1.

Most common clathrate hydrate structures are cubic structure I (s-I), cubic structure II (s-II), and hexagonal structure H (s-H). In addition to these structures, some hydrate structures have been discovered which are not common and exist in the natural gas systems e.g. Jeffrey's structures III to VII [1.6].

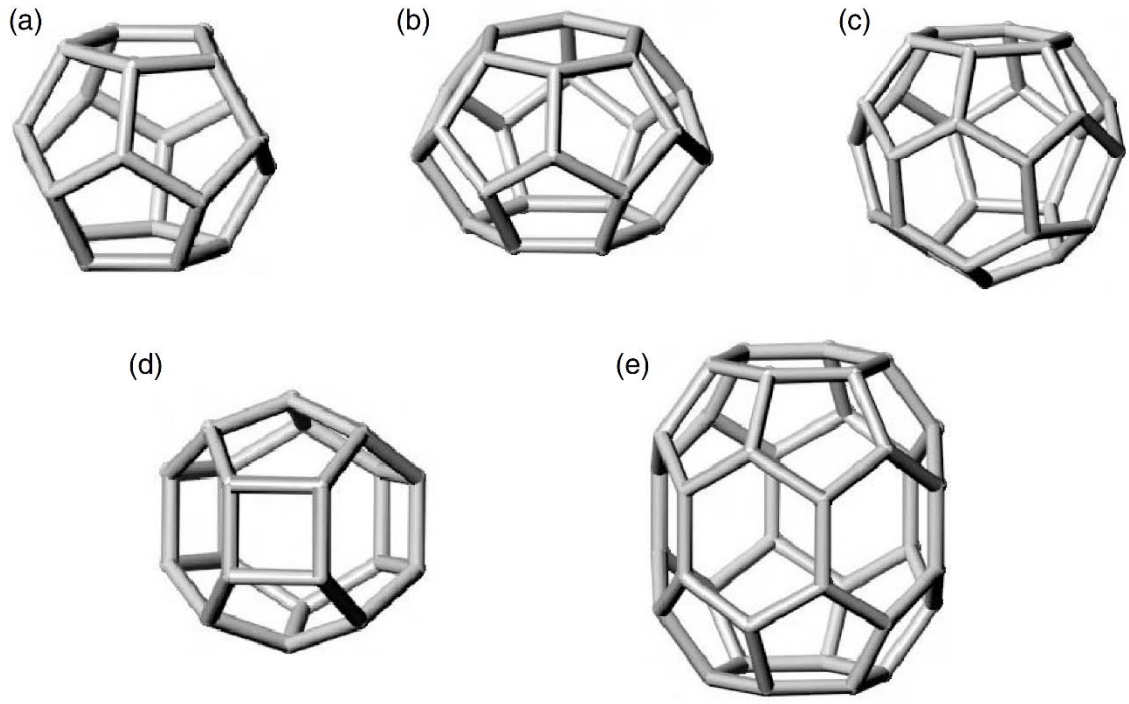

Figure 1-1. (a) pentagonal dodecahedron (5^{12}), (b) tetrakaidecahedron ($5^{12}6^2$), (c) hexakaidecahedron ($5^{12}6^4$), (d) irregular dodecahedron ($4^3 5^6 6^3$), and (e) icosahedron ($5^{12}6^8$) [1.6].

Table 1-1. Geometry of Cages and crystal properties of different hydrate crystal structures [1.6]

Hydrate crystal structure	I		II		H		
Cavity	Small	Large	Small	Large	Small	Medium	Large
Description	5^{12}	$5^{12}6^2$	5^{12}	$5^{12}6^4$	5^{12}	$4^3 5^6 6^3$	$5^{12}6^8$
Number of cavities/unit cell	2	6	16	8	3	2	1
Average cavity radius [a] (Å)	3.95	4.33	3.91	4.73	3.94	4.04	5.79
Variation in Radius [b] (%)	3.4	14.4	5.5	1.73	4.0	8.5	15.1
No. of water molecules/cavity [d]	20	24	20	28	20	20	36

[a] The average cavity radius will vary with temperature, pressure, and guest composition.

[b] Variation in the distance of oxygen atoms from the centre of a cage. A smaller variation in radius reflects a more symmetric cage.

Small molecules/guests (0.4-0.55 nm molecular diameter) e.g. C_1, C_2, and CO_2, form structure I hydrate which is the main structure in natural hydrates in the Earth's natural environment [1.7]. McMullan and Jeffrey (1965) characterised the structure-I using X-ray diffraction method [1.8]. They found that there are 46 water molecules in the cubic unit cell of structure I with a dimension of 12 Å (side) which consists of two type of cages, 2 small cages (5^{12}) and 6 large cages ($5^{12}6^2$). The framework of gas hydrate structure I is illustrated in Figure 1-2.

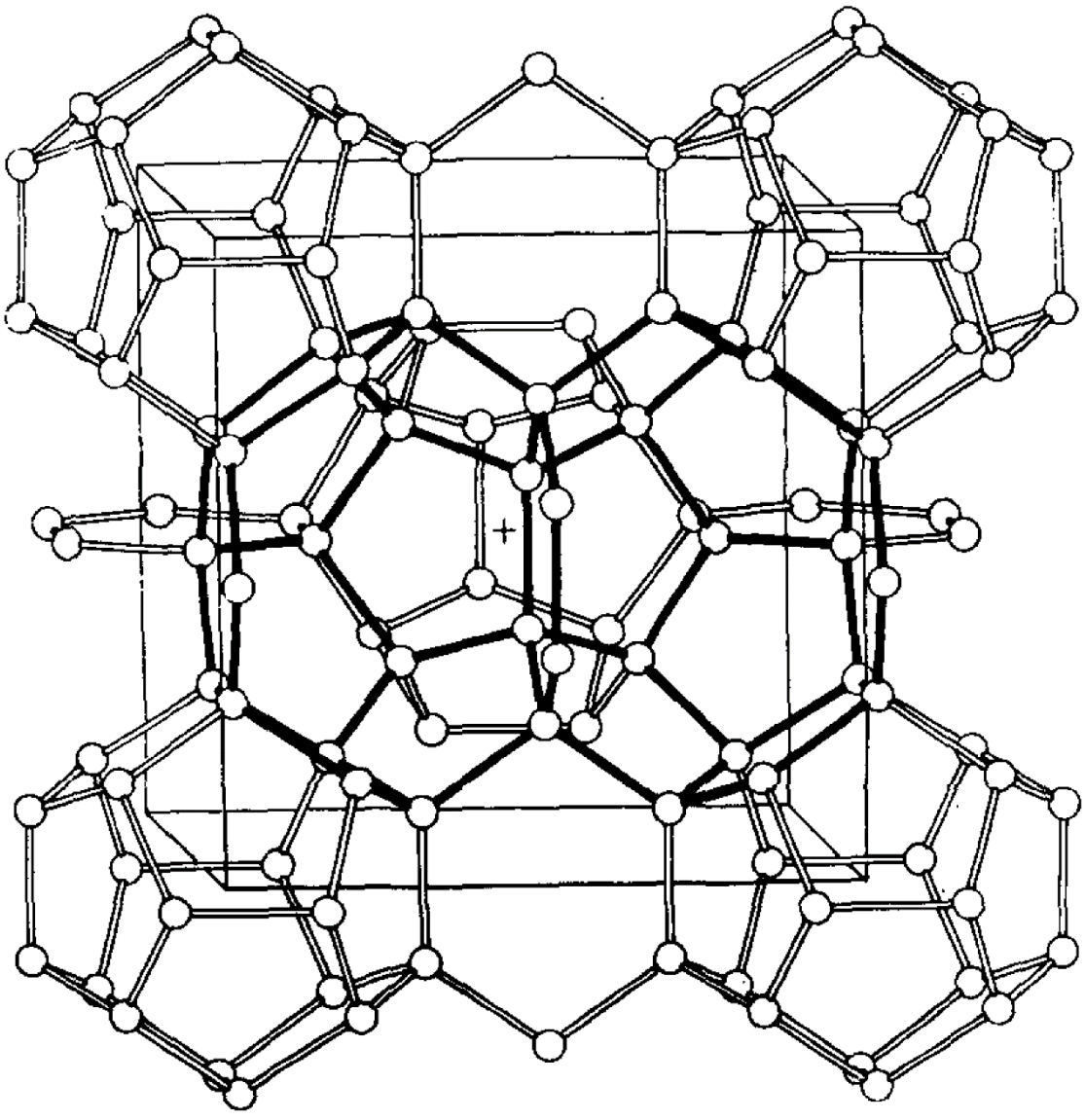

Figure 1-2. The polyhedral oxygen framework of gas hydrate structure I [1.8].

The structure II of gas hydrate was also characterised using the same technique (X-ray diffraction) by Mak and McMullan (1965) [1.9]. They found that cubic structure-II of hydrate with a unit cell dimension of 17.3 Å consists of 136 water molecules. A cubic unit cell of structure-II hydrate consists of 16 small cages (5^{12}) and 8 large cages ($5^{12}6^4$). The framework of gas hydrate structure II is illustrated in Figure 1-3. The cubic structure II generally forms with larger guests (guest diameters: 0.6-07 nm) e.g. propane and iso-butane [1.7]. However, the smallest guest molecules with diameters less than 0.4 nm do form structure II; e.g. Argon, Krypton, Oxygen, and Nitrogen [1.7]. Although some single guest molecules like methane and ethane do form structure-I, they form stable structure II in the binary guest mixture [1.10][1.11][1.12]. However, CO_2 (as an intermediate-sized s-I former) does not form structure II in a system with another s-I former [1.12].

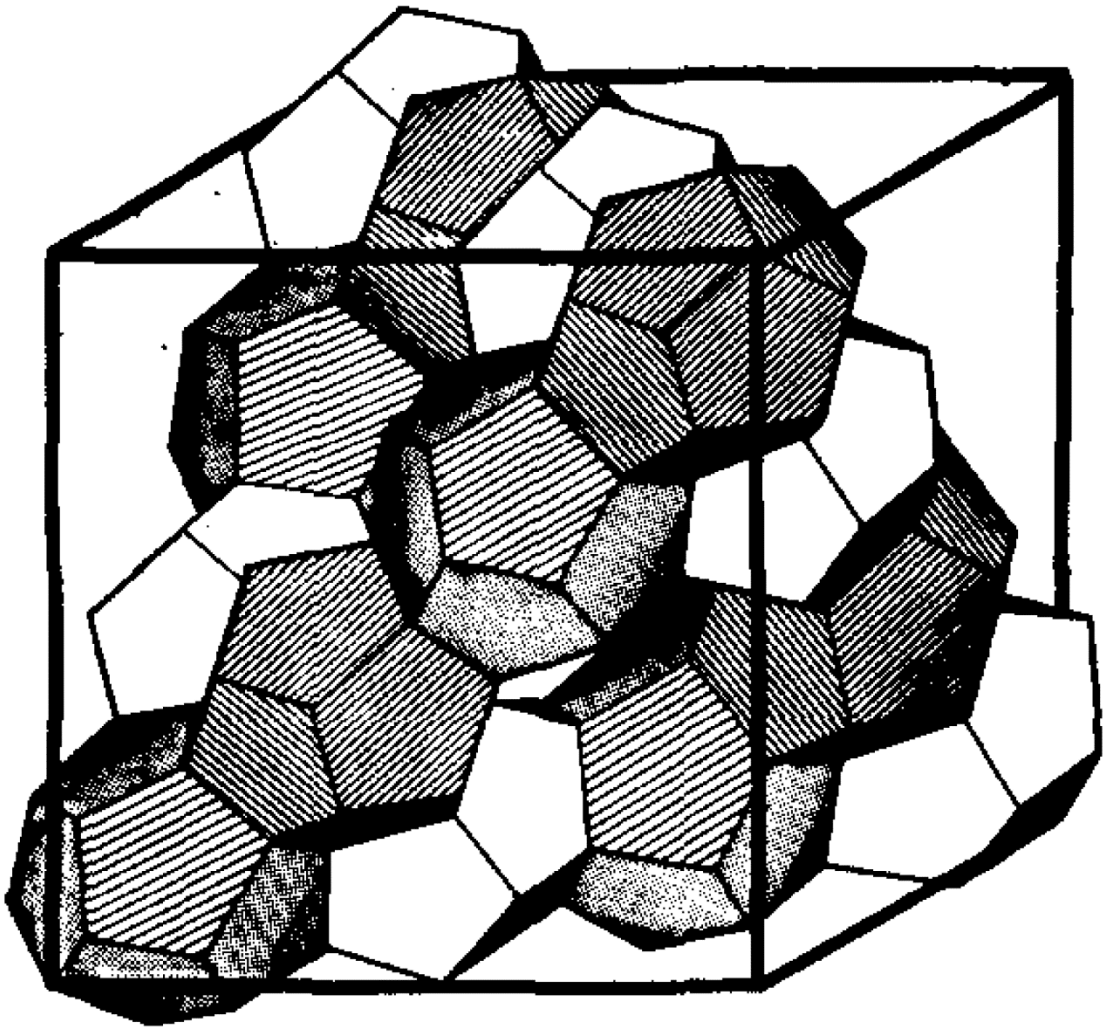

Figure 1-3. The polyhedral oxygen framework of gas hydrate structure II [1.9].

Both structure I and II are the simple hydrates which can be stabilised by a single guest molecule. Unlike structure I and II hydrates, structure-H hydrates, which was discovered using NMR spectroscopy with X-ray and power diffraction in 1987 by Ripmeester et al., require both a small guest molecule and a large guest molecule to form a stable structure H hydrates [1.13]. For example, methane + cycloheptane form structure-H [1.14]. A unit cell structure-H consists of 34 water molecules. Structure-H consists of three small cavities with 12 pentagonal faces (5^{12}), two medium cavities with 3 square faces, 6 pentagonal faces, and 3 hexagonal faces ($4^3 5^6 6^3$), and one large cavity with 12 pentagonal faces and 8 hexagonal faces ($5^{12}6^8$) [1.6]. The framework of gas hydrate structure-H is illustrated in Figure 1-4.

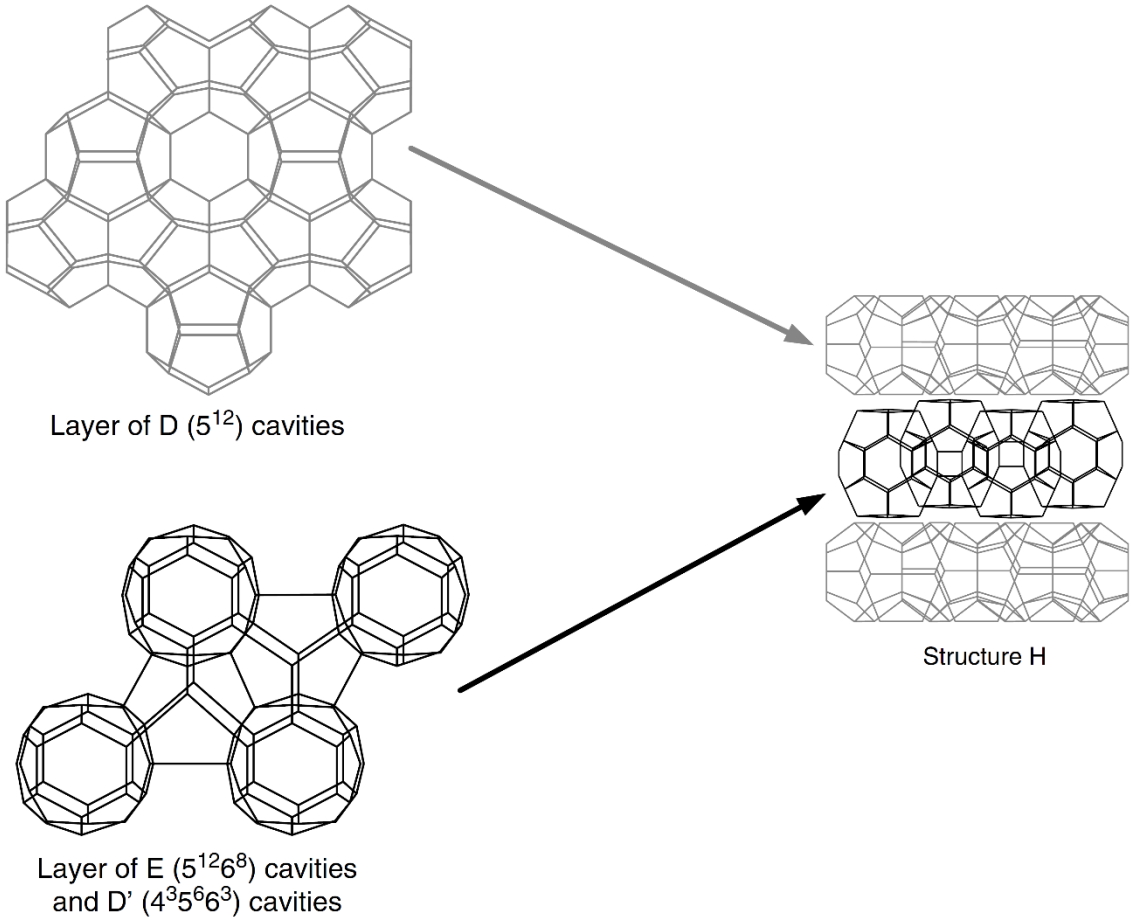

Figure 1-4. Schematic diagram showing structure H is built up of layers of 5^{12} (D) cavities and layers of $5^{12}6^8$ (E) and $4^3 5^6 6^3$ (D') cavities [1.6].

1.2 Hydrate Nucleation and Formation/Growth

Hydrate nucleation is the first step for hydrate formation which is difficult to observe experimentally. The hydrate nucleation is a stochastic phenomenon, so hydrate formation point is not repeatable and depends on many factors including mixing efficiency, cooling rate, the presence of foreign materials, and fluid composition.

There are two types of nucleation theory for crystallization: homogeneous nucleation and heterogeneous nucleation. Homogeneous nucleation would occur in the system without any impurities and foreign materials. According to the theory of nucleation, a critical cluster size/radius is necessary to be reached for nuclei/clusters growth spontaneously [1.6]. In addition, there is a free energy barrier to overcome to form a critical cluster. As subcooling temperature/supersaturation increases, the free energy barrier decreases and then nucleation becomes spontaneous. Practically, homogeneous nucleation does not occur in real systems as they have foreign materials and surface (e.g. fluid interface). Therefore, hydrate nucleation is stochastic and heterogeneous. Nucleation, free energy barrier, and critical cluster radius have been studied by other researchers [1.15][1.16][1.17][1.18].

Hydrate nucleation/initiation usually occurs at the vapour-liquid interface, because not only the Gibbs free energy at the interface is low but also the concentrations of both host and guest molecules are very high at the interface [1.17][1.19]. Generally, there are three postulated mechanisms for hydrate nucleation at the molecular level; labile cluster nucleation hypothesis, nucleation at the interface hypothesis, and local structuring nucleation hypothesis.

In labile cluster nucleation hypothesis, hydrate nucleation occurs inside the aqueous phase. In fact, water molecules spontaneously form labile clusters around the dissolved gas. These labile clusters join together stochastically to create hydrate nucleus and unit cells. The hydrate nucleation does not form until both types of cavities for either s-I or s-II are created (5^{12} and $5^{12}6^2$ for s-I and 5^{12} and $5^{12}6^4$ for s-II). Christiansen and Sloan (1994) developed and hypothesized this model [1.20]. Figure 1-5 and Figure 1-6 show the different steps of hydrate nucleation according to labile cluster nucleation hypothesis.

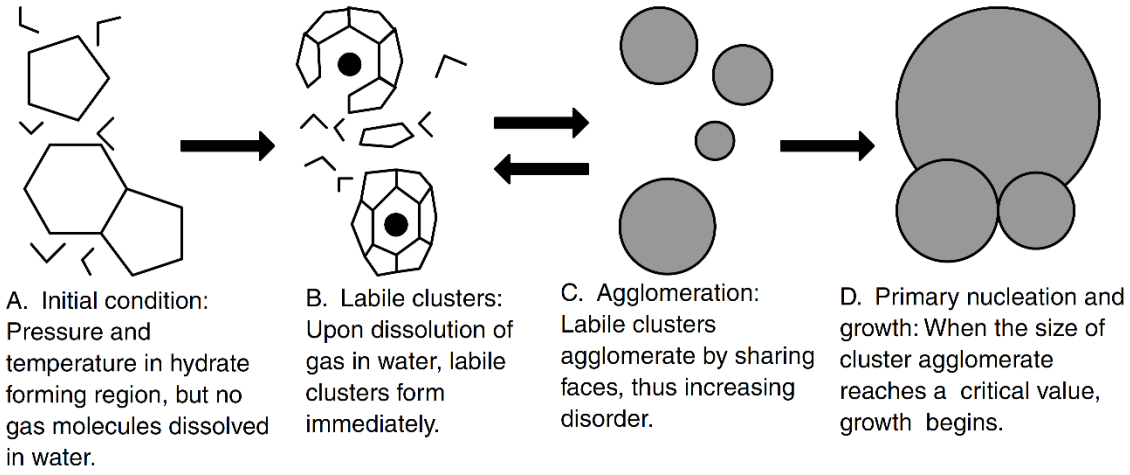

Figure 1-5. Schematic model of labile cluster growth [1.6].

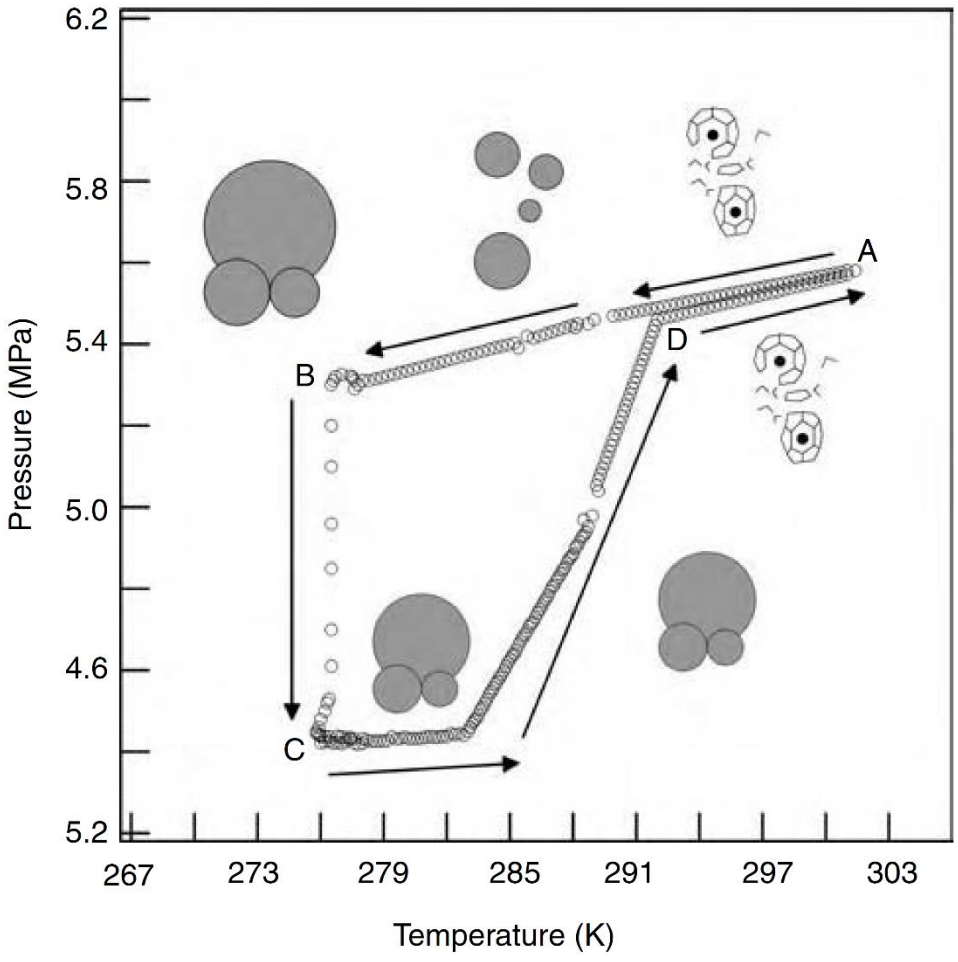

Figure 1-6. Hydrate labile cluster growth mechanism imposed on a pressure–temperature trace [1.6].

Long (1994) and Kvamme (1994) proposed another mechanism for hydrate nucleation. They suggested that labile hydrate cavities occur on the vapour side of interface [1.21][1.22]. Based on this hypothesis, gas molecules are adsorbed and transported to the interface. These gas molecules move to the right position and then adsorb through the surface. At this position, water molecules form some part of cages and then complete these partially open cages. These labile clusters join together and grow on the vapour side to reach the critical size of hydrate nucleus. The schematic of this theory is shown in Figure 1-7.

Molecular dynamic simulation supports the local structuring nucleation hypothesis [1.19][1.23]. The local order model of nucleation proposed that guest molecules are positioned like what it is in clathrate hydrate phase. This arrangement of guest molecules increases to exceed the critical nucleus. Therefore, the increase of guest-guest and host-host cluster order result in critical nucleus formation. Figure 1-8 shows the snapshot of water clathrate ordering at different time using a molecular dynamic simulation by Moon et al. (2003) [1.19].

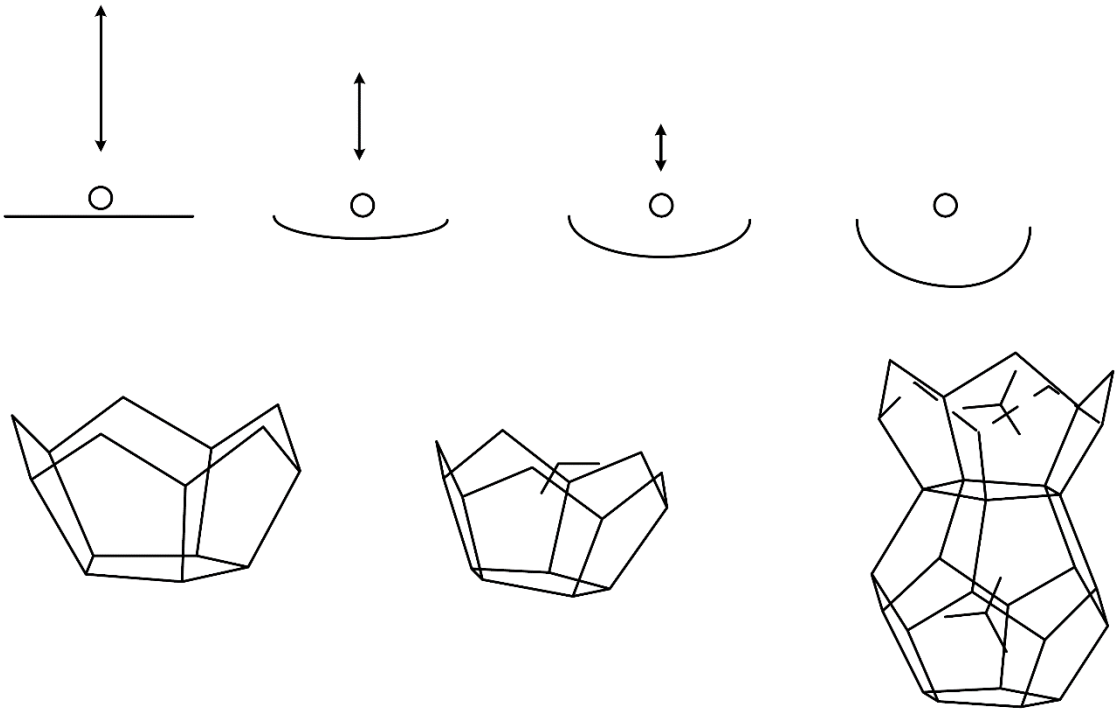

Figure 1-7. Adsorption of gas molecules onto labile hydrate cavities at gas–water interface [1.21].

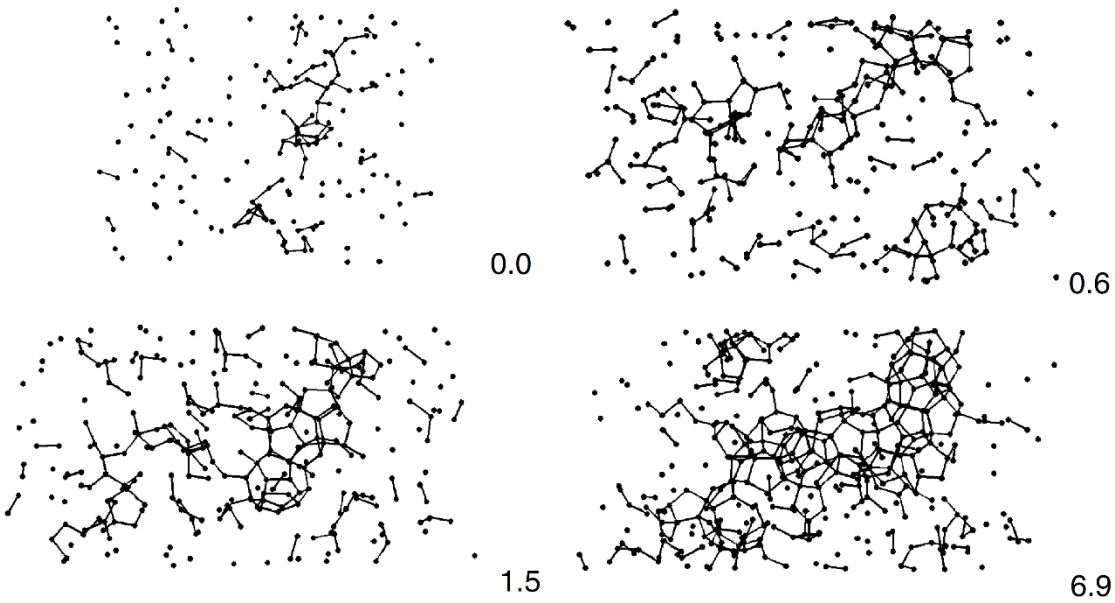

Figure 1-8. Snapshots of clathrate clusters at given times (ns). Only hydrate like waters are shown; lines indicate the hydrogen bond network [1.19].

After hydrate nucleation, hydrate growth would be considered. The hydrate growth rate depends on three factors: (1) the kinetic of crystal growth at the hydrate surface, (2) mass transfer, and (3) heat transfer [1.6]. However, hydrate crystal can grow in different ways including (1) single crystal growth, (2) hydrate film growth at the water-hydrocarbon interface, (3) multiple crystal growths in an agitated system, and (4) growth of metastable hydrate phases [1.6].

Similar to hydrate nucleation, the hydrate crystal growth is stochastic. Although the hydrate growth kinetic is unpredictable [1.6], the pattern of hydrate growth rate can be repeatable at different driving force/subcooling temperatures (see Chapter 3).

Although hydrate formation can cause serious problems and its growth rate and agglomeration tendency need to be considered, increasing of hydrate formation rate is interested in many positive applications of gas hydrates [1.24] including transportation and storage of natural gas [1.25], CO_2 sequestration [1.26], and refrigeration [1.27]. Many techniques have been used to stimulate hydrate formation such as increasing the mass/heat transfer using the higher stirring rate and adding the chemicals e.g. surfactant [1.28] and zeolite [1.29] to the system.

1.3 Gas Hydrates and Flow assurance: Problem

Gas hydrate formation and blockage in the pipelines are still a major flow assurance challenge. There are several options to avoid hydrate formation including: 1. Remove the free water and reduce the water content of the system using different methods such as separator and dehydration using glycol or molecular sieve. 2. Maintain the system at high temperature or low pressure to prevent hydrate formation. 3. Injection of inhibitors such as THIs and LDHIs (See Section 1.4.1 and 1.4.2).

Nevertheless, in some cases, hydrate blockage can form as a result of different scenarios such as restart following an unplanned shut-in, failure of inhibitor delivery pumps, or increased water content. There have been a lot of investigations in association with gas hydrate blockage and different hydrate blockage removal strategies in the literature along with case studies [1.30][1.31].

There are several remediation options for gas hydrate dissociation and hydrate blockage removal such as depressurizing, chemical injection, mechanical methods, and thermal methods. For example, depressurizing method was used to remove hydrate blockage in a >20 miles subsea tieback in the Gulf of Mexico [1.32], gas injector flowline in Gulf of Guinea [1.33], export gas pipeline in the Gulf of Mexico [1.34], and the main gas export pipeline from Pompano platform [1.31]. In addition, BP used a drilling rig for removing fluid from the pipeline and then depressurized it to remove hydrate blockage from a 16 inch jumper connecting the Atlantis gas export line to the Mardi Gras gas transport system in the Gulf of Mexico [1.31]. However, depressurization may result in movement of blockage and its associated consequences. Depressurization may lead to environmental and financial concerns due to gas flaring. In addition, in long vertical lines e.g. riser, depressurization may not be possible due to hydrostatic head associated with the column of liquid, mainly hydrocarbon, on top of the blockage.

In order to dissociate and remove hydrate blockage efficiently, more than one methods is used in many cases. For example, depressurizing and applying electrical heating directly to the pipeline were used by Chevron to remove hydrate blockage [1.35]. In another case, hot glycol circulated using coiled tubing in the gas condensate well in offshore South America was used to remove hydrate blockage [1.36]. In this case, glycol and heated mud and sea water were used first, but these attempts were unsuccessful and did not remove

the blockage. Coiled tubing was deployed to remove hydrate blockage in a Statoil offshore gas field in the Barents Sea as well [1.37].

1.4 Gas Hydrate Inhibtion

One of the most common used methods for hydrate inhibition is the chemical inhibitors which are divided into two main categories, thermodynamic hydrate inhibitors (THIs), and low dosage hydrate inhibitors (LDHIs). In the following, these two main categories of hydrate inhibition are described.

1.4.1 THI Inhibition

THIs, e.g. methanol, ethanol, and mono-ethylene glycol (MEG), shift hydrate phase boundary to the lower temperature at a particular pressure or to the higher pressure at a particular temperature. Basically, the main mechanism of thermodynamic inhibitor is changing intermolecular interaction, i.e., the strong attractive forces between the inhibitor oxygen atoms and water hydrogen atoms which cause hydrogen bond between inhibitor and water molecules [1.6]. One of the problems associated with the use of THIs is that large quantities of inhibitor, e.g. 20-50 mass%, may be required to prevent hydrate formation, which can cause both cost and logistical issues. Figure 1-9 shows the hydrate phase boundary for methane, methane + 20 mass% MEG, and methane + 20 mass% methanol.

1.4.2 KHI Inhibition

In contrast to THIs, LDHIs can inhibit hydrate formation at low dosage e.g. 0.5-2.5 mass%. LDHIs are divided into two groups; anti agglomerants (AAs) and kinetic hydrate inhibitors (KHIs). Both AAs and KHIs were first discovered in the early 1990s [1.38]. While KHIs are known to prevent hydrate nucleation and growth, AAs allow hydrates to form but prevent hydrate agglomeration.

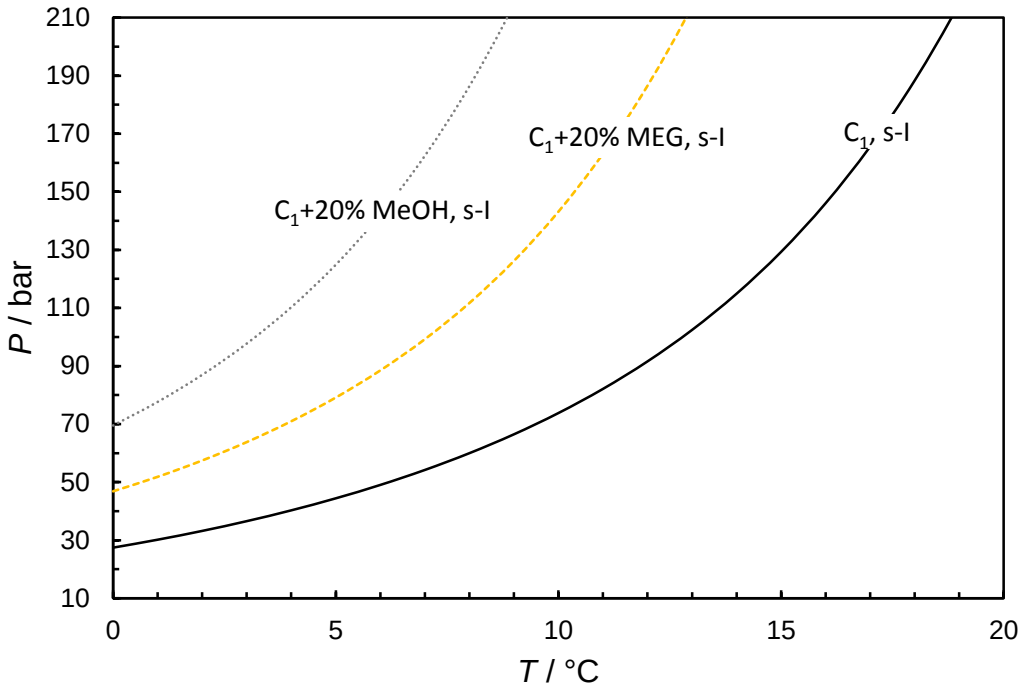

Figure 1-9. Hydrate phase boundary for methane, methane + 20 mass% MEG, and methane + 20 mass% MeOH. The thermodynamic hydrate phase boundaries for these systems were predicted using HydraFLASH®, a thermodynamic model developed by Hydrafact Ltd and Heriot-Watt University.

AAs are surface active agents, usually surfactants, and there are two mechanisms which enable to have AAs effect. One type of AAs produces a water-in-oil emulsion that allows hydrates to form inside the water droplet, enabling slurry of hydrate particles in a hydrocarbon phase [1.38]. Diethanolamides, dioctylsulfosuccinates, sorbitans, ethoxylated polyols, ethoxylated fatty acids, and ethoxylated amines are some examples of this type of AAs [1.38]. The second type of AAs has a hydrate-philic (hydrate seeking) head group and a hydrophobic tail. The hydrate-philic head groups which are quaternary ammonium with n-butyl, n-pentyl, or isopentyl groups (Figure 1-10), adhere to hydrate particles and even can embed in the hydrate surface if hydrates grow around the hydrate-philic head. Meanwhile, hydrophobic tail prevents hydrate formation; making more attractive the hydrate particles to the hydrocarbon phase [1.38].

KHIs are typically low molecular weight polymer or copolymer which were discovered in the 1990s [1.38]. Although KHIs are generally known as anti-nucleators, they can prevent hydrate growth or delay hydrate formation depending on subcooling temperature. poly(vinylpyrrolidone) (PVP) [1.39] and polyvinylcaprolactam (PVCap) [1.40][1.41] are the first groups of polymers known as KHIs. The structure of poly(vinylpyrrolidone) and polyvinylcaprolactam are shown in Figure 1-11 and Figure 1-12 respectively.

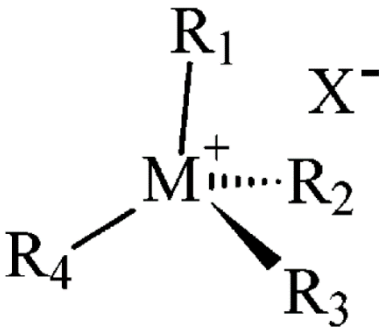

Figure 1-10. Structure of good quaternary ammonium or phosphonium hydrate growth inhibitors, where M=N or P and at least two of the R groups are n-butyl, n-pentyl, or isopentyl [1.38].

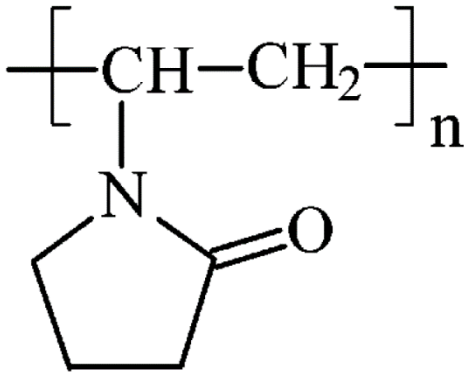

Figure 1-11. Structure of poly(vinylpyrrolidone) [1.38].

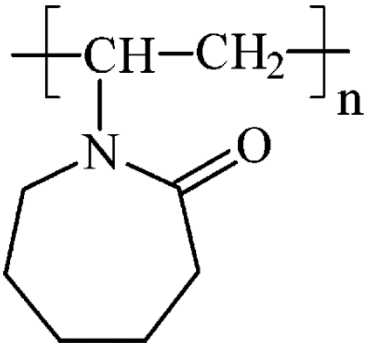

Figure 1-12. Structure of polyvinylcaprolactam [1.38].

1.4.3 Bio KHI

KHIs could offer significant CAPEX and OPEX advantages over other traditional inhibition methods e.g. thermodynamic inhibition using glycols/methanol, insulation, heating, and/or maintaining the system at high temperature or low pressure. Despite this, there are environmental issues in terms of KHIs use and this would be important when the produced water is released to the sea. The common KHIs e.g. PVCap and PVP, are not toxic, but they are poorly biodegradable in terms of structure of active polymer. The large molecule sizes of these KHIs restrict to the breakdown by microorganism and low reactivity of these polymers and therefore result in poor polymer biodegradability of KHIs.

In addition, there has been a trend towards tightening the rules in terms of chemicals use. The chemicals should meet the stringent biodegradability requirement. For example, the KLIF (Norwegian Environmental Agency) puts chemicals with <20% biodegradation and log $P_{ow} \geq 5$ (Log P_{ow}: A product's ability to bioaccumulate) to the black list [1.42]. Therefore, there is a tight restriction towards KHIs, and traditional KHIs cannot be used in the Norwegian water due to its poorly biodegradable.

In the light of above, it raises the potential demand to use green KHIs in the oil and gas industry. However, it is difficult to produce a chemical which has good biodegradability with good KHI properties at the same time. Therefore, there has been effort to balance good biodegradability and good KHI properties. Nevertheless, a new hybrid polymer with good KHI properties together with improved biodegradability has been reported [1.43].

Basically, a common approach to produce green KHIs is bond substitution in backbone chains of conventional KHI polymers e.g. partial substitution of C-C bonds with more reactive/easily broken linkages. Pyroglutamate KHI polymer is an example of green/biodegradable KHI. Figure 1-13 illustrates the structure of one class of pyroglutamate polyester kinetic hydrate inhibitors showing that its pendant groups look like to those found in PVP molecular structure, but the polymer backbone is different [1.42].

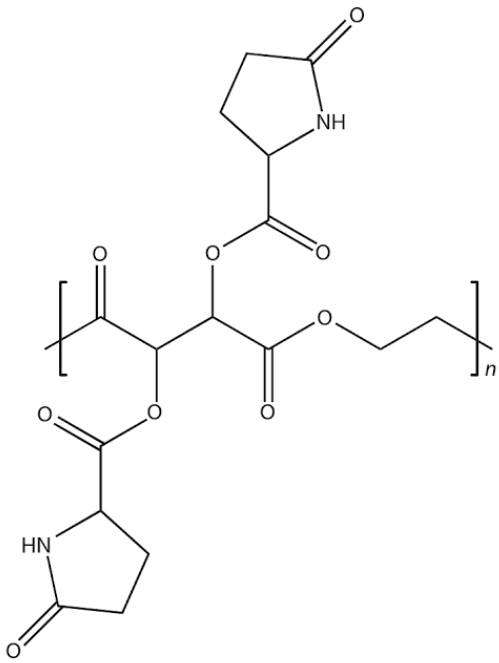

Figure 1-13. One class of pyroglutamate polyester kinetic hydrate inhibitors [1.42].

1.4.4 KHI Evaluation

1.4.4.1 Induction Time

Induction time has been used for a long time to evaluate KHIs, i.e., induction time refers to the period of time between once the system enters the hydrate stability zone and once hydrates are nucleated and formed [1.6][1.38][1.44]. Hydrate crystal nucleation is not detectable with classical macroscopic probe such as pressure transducer. Therefore, induction time refers to time until a detectable volume of hydrates formed. Although induction time is dominated by nucleation period, it consists of the detectable time for hydrate growth. Figure 1-14 shows an example induction time method. As shown in Figure 1-14, although the condition of the system (pressure and temperature) is inside the hydrate stability regions, hydrate nucleation and growth do not occur because of metastability.

As noted, hydrate nucleation is a stochastic phenomenon. Therefore, the results of induction time are not repeatable for evaluation of KHIs, i.e., the induction time is dominated by hydrate nucleation period.

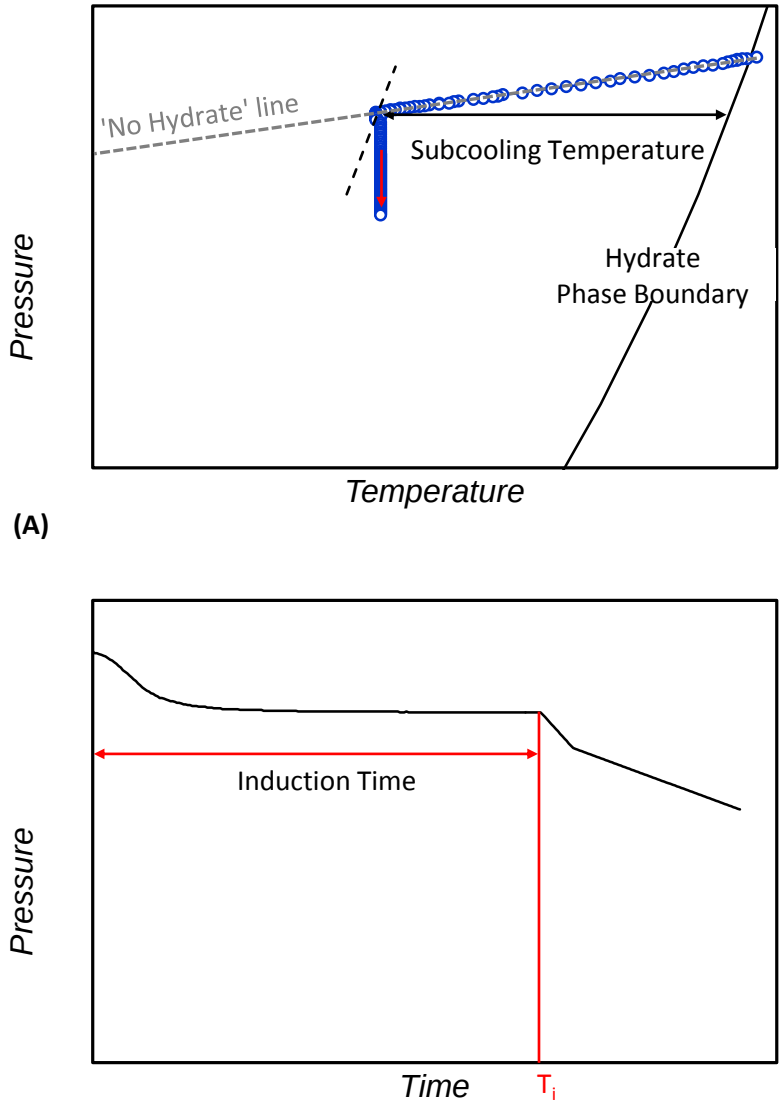

Figure 1-14. An example of induction time method. Part A shows the PT plot for cooling the system to the specific subcooling temperature. Part B shows the same pressure data from part A, but this time as a function of time, showing a clear change in pressure due to hydrate formation at T_i (induction time).

1.4.4.2 Crystal Growth Inhibition (CGI) Method

Recently, the gas hydrate research centre at Heriot-Watt University has developed a method to evaluate KHIs which is highly repeatable [1.45][1.46][1.47][1.48]. In this method which is known as crystal growth inhibition (CGI), the effect of hydrate nucleation is removed from the results. The CGI method determines different regions as a function of subcooling. Complete inhibition region (CIR) (infinite induction time)/green zone, partial inhibition region /amber zone, and rapid failure region/red zone are three main regions which are highly repeatable.

The crystal growth inhibition (CGI) technique was used in this work to evaluate KHI performance. An example CGI method cooling curves for 0.5 mass% PVCap aqueous with decane and natural gas is shown in Figure 1-15 to determine the CGI regions which are described in Table 1-2. The following steps were carried out to determine these regions.

1. After loading the materials, the system was cooled down rapidly to form hydrates.

2. After initial hydrate formation, the system was warmed up to dissociate most of the hydrate crystals. The step heating of the system continued until a few percent of hydrates (roughly 0.5% of water converted to hydrates) remained. As a result, the effect of hydrate nucleation on hydrate formation is removed and the results are repeatable.

3. The system was cooled again with a constant cooling rate, 1 °C/hr. This constant cooling rate allows the system to form hydrates with different growth rate as a function of subcooling temperature and therefore the CGI regions can be defined.

4. Steps 2 and 3 were repeated several times to check repeatability of the results.

5. Finally, the system was step-cooled, 1 °C/24hrs, to determine complete inhibition and very slow growth regions.

Table 1-2. KHI Induced CGI Region Nomenclature and Typical Hydrate Growth Rates [1.45]

Region	Growth rate description	typical growth rates order of magnitude (% water / hr)
CIR	complete inhibition region	0.00
SGR (VS)	slow growth rate (very slow)	0.01 (<0.05%/h)
SGR (S)	slow growth rate (slow)	0.1 (0.05 ≤ growth rate <0.5%/h)
SGR (M)	slow growth rate (medium)	1 (0.5 ≤ growth rate <5%/h)
RGR	rapid growth region	10 (≥5%/h)
SDR	slow dissociation region	dissociation rate 1 order of magnitude less than for no KHI

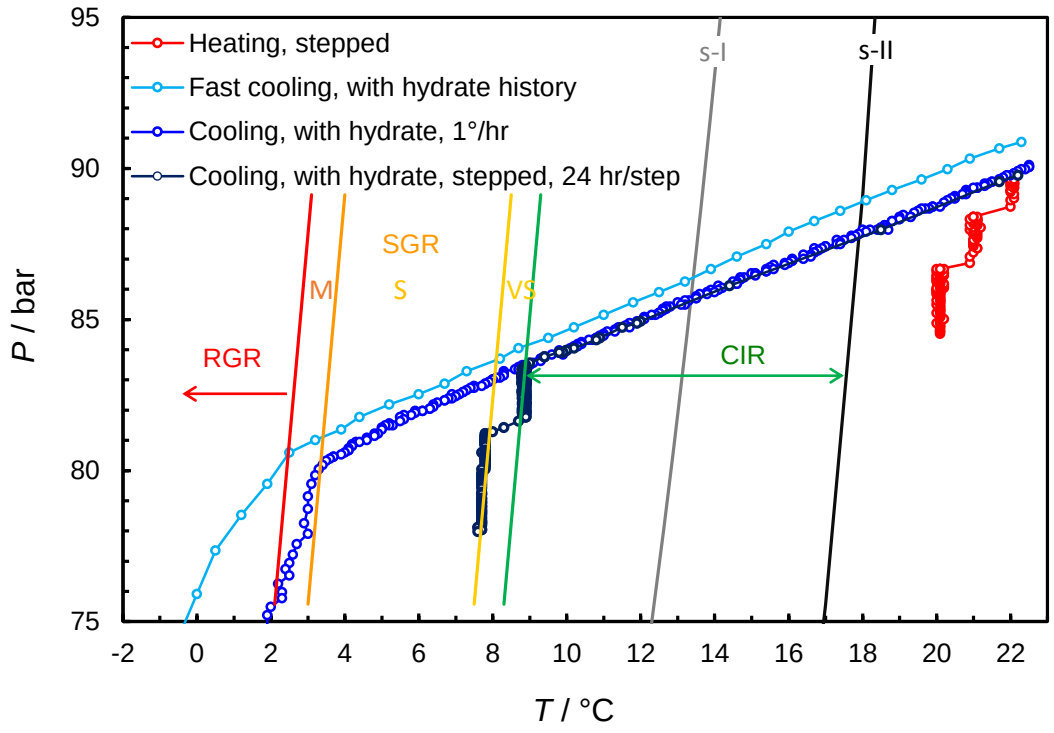

Figure 1-15. Example CGI method cooling curves for 0.5 mass% PVCap aqueous with decane and natural gas (hydrocarbon to water volumetric ration is 1:4) showing CGI regions determined from changes in relative hydrate growth rates. The composition of natural gas is given in Table 2-1.

1.5 Gas Hydrate dissociation

1.5.1 Hydrate Dissociation using THIs

Thermodynamic hydrate inhibitors (THIs) injection as a chemical remediation method is used in some cases to remove hydrate blockage and inhibit further hydrate formation. Methanol (MeOH) and mono-ethylene glycol (MEG) are the two most commonly used THI. Basically, THIs shift the hydrate equilibrium conditions to lower temperature at a particular pressure or higher pressure at a particular temperature [1.31]. Methanol injection in association with pressure reduction is a common method to dissociate hydrate [1.49]. Hydrate properties, inhibitors properties, solid/gel precipitation, and the turbulence of the liquid system affect the hydrate dissociation by THIs [1.50].

The effectiveness of different THIs such as MEG, DEG, TEG, and methanol have been studied [1.50][1.51]. Li et al. (2000) showed experimentally that methanol seems to be the most efficient inhibitor in hydrate plug melting for permeable/porous hydrate plugs. Furthermore, they showed that while MEG can penetrate into a compact plug, it may freeze out, resulting in reduced hydrate melting efficiency [1.50]. They pointed out that TEG is not efficient in hydrate plug removal and should not be used for hydrate plug melting. In addition, Austvik et al. (2000) investigated the efficiency of thermodynamic

hydrate inhibitors in hydrate plug removal [1.51]. They reported that while methanol had no effect in some cases, it could remove the plug in three to four days for several other occasions.

Lysne and Larsen (1995) described the gas hydrate dissociation process using THIs injection [1.49]. Based on this description, hydrate is assumed at thermal equilibrium (no temperature gradients), mechanical equilibrium (no pressure gradients) and thermodynamic equilibrium (no chemical potential gradients) at Point A in Figure 1-16. If the pressure is kept constant, a process A-B will happen. In this process, if THI is injected continuously, the local concentration of THI remains constant, so the temperature at the interface of hydrate and inhibited phase decreases to T_B. At this condition, as the new equilibrium temperature is lower than the ambient temperature, further hydrate dissociation is controlled by heat transfer. In contrast to the continuous THI injection, if a single batch of THI injection is used and pressure is kept constant, the temperature of the hydrate near the interface is initially decreased to T_B. Meanwhile, the fresh water which is produced due to hydrate dissociation, will dilute the THI. Therefore, the effect of THI will diminish gradually and in the case of huge quantities of hydrates, the two curves may merge together into Point A and hydrate dissociation will be stopped (if we ignore the effect of changes in the gas composition).

In contrast to the constant pressure process, the process may follow the A-C path if the system pressure is allowed to increase due to hydrate dissociation. In this process, the temperature at the interface of hydrate and inhibited aqueous phase decreases to TB due to endothermic nature of hydrate dissociation, but can stabilise at T_A. According to the earlier description, if the pressure is kept constant, the inhibited hydrate equilibrium curve may converge to original curve (if the composition changes are ignored) and if the pressure is allowed to increase due to hydrate dissociation, hydrate phase meets the new inhibited curve along curve A-C (at thermodynamic equilibrium). In the latter case, because the temperature is below the ambient temperature, more hydrates should dissociate to reach thermal and thermodynamic equilibrium at Point C.

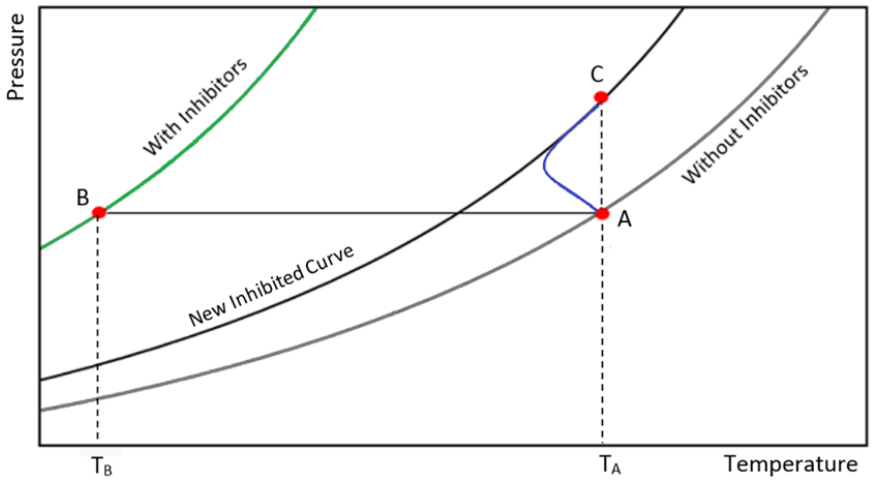

Figure 1-16. Hydrate dissociation process by THIs injection. T_A is ambient temperature.

1.5.2 Hydrate Dissociation using KHIs

While KHI growth inhibition is increasingly well understood, there is much more limited data on the effect of KHIs on gas hydrate dissociation. Recently, it has been reported that PVCap increases the thermodynamic stability of hydrates which causes very slow hydrate dissociation rate outside the hydrate stability zone [1.52]. It is indicated that not only does PVCap increase apparent hydrate dissociation temperatures, but it also caused reduced cage filling typified by a lower large-to-small cage occupancy in hydrates formed from PVCap systems.

In addition, as mentioned in Section 1.4.4.2, during the CGI method development, it was noticed that KHIs reduce the dissociation rate. Therefore, slow dissociation region (SDR) is introduced for the system with KHI. The dissociation rate in this region is one order of magnitude less than for no KHI system[1.45][1.46][1.47][1.48].

Although there are now a number of studies which show that KHIs can affect the hydrate dissociation rate outside the hydrate stability zone, there is very little literature data on the effect of KHIs on hydrate dissociation inside the hydrate region. As discussed, KHIs are known as hydrate nucleation/growth inhibition, so they are not considered as having a thermodynamic THI-type effect. Therefore, dissociation of hydrates using KHIs inside the hydrate stability zone would not be expected. Nevertheless, Anderson et al. reported that PVCap can induce hydrate dissociation inside the thermodynamic hydrate stability region [1.46]. However, the process has mechanisms giving rise to it that have not been investigated in depth (assessing this process and its origins together with the mechanisms have been discussed in Chapter 6).

1.6 Thesis Outline

The main objective of this work is to study Bio KHIs alone and in conjunction with THIs for hydrate prevention / removal (induced dissociation). Furthermore, hydrate fraction tolerance, gas hydrate growth regions, formation of various hydrate structures, and gas hydrate blockage removal are the other topics of this thesis.

In Chapter 2, work has been undertaken to select the Bio KHI for the further studies in this thesis. CGI method was used to evaluate different Bio KHIs, and Luvicap Bio was selected as it has better performance in terms of hydrate inhibition.

Chapter 3 presents results of work undertaken on the topic of KHIs (PVCap and Luvicap Bio), in terms of their general performance and in relation to the issues of structural effects and threshold inhibition. The effect of the fraction of water converted to hydrate on both PVCap and Luvicap Bio performance in the methane system is investigated. Furthermore, studies have focused on Luvicap Bio + PVCap combination with methane and natural gas to see whether better inhibition can be achieved rather than using Luvicap Bio or PVCap alone. In addition, hydrate structure effect on inhibition for Luvicap Bio and PVCap have been studied to support the theory that Luvicap Bio is a better inhibitor for s-I and PVCap is a stronger inhibitor for s-II. The aim is to see whether PVCap and Luvicap Bio show synergism effect, i.e., Luvicap Bio and PVCap are a strong inhibitor for s-I and s-II respectively, so their combination would result in better performance in a multi-structure hydrate system. Moreover, the hydrate growth pattern and hydrate structure change were studied to support the theory of multi-structure hydrate formation in the natural gas system and formation of s-I and s-II in the simple methane or ethane system.

Chapter 4 is focused on the investigation of thermodynamic hydrate inhibitors effect on kinetic hydrate inhibitor. The effectiveness of Luvicap Bio in the presence of MEG, methanol, and ethanol was investigated using the CGI method. The primary aim of this chapter is to assess whether MEG, methanol, or ethanol is a full ‘top-up’ inhibitor or ‘top-up’ inhibitor for Luvicap Bio in the natural gas systems. For example, whether Luvicap Bio can be used to reduce THI requirements in terms of hydrate inhibition. Therefore, the CGI method was carried out to measure CGI regions for 0.5 mass% Luvicap Bio with different THIs concentrations (5, 10, 20, 30, and 50 mass% of MEG,

MeOH, or EtOH). The CGI regions were determined for a range of pressure from 30 bara to 180 bara. Further works in this area to measure the CGI regions with a higher concentration of Luvicap Bio (e.g. 1.0 mass%) with methanol and MEG in the natural gas systems have also been undertaken over the range of pressure from 30 bara to 160 bara. The reason for these measurements is to see if higher methanol/MEG reductions can be achieved by increasing the KHI dosage.

As discussed, one of the aims of this thesis is to investigate the induced hydrate dissociation either using THIs or KHIs especially Luvicap Bio. Therefore, in Chapter 5, the hydrate blockage removal in the vertical pipes using THIs was investigated. One of the problems with natural gas production is gas hydrate formation which can cause blockage. Although there are a number of options to inhibit hydrate formation (e.g. thermodynamic hydrate inhibitors and kinetic hydrates inhibitors), hydrate blockage can occur for some reasons, e.g. underestimation of water cut production, unplanned shut-in, inappropriate inhibitor injection method or failure of inhibitor delivery. There are a number of remediation methods for hydrate blockage removal such as depressurization, chemical injection e.g. methanol and MEG, mechanical, and thermal methods. In the case of chemical usage in vertical pipes, density plays an important role and needs to be considered. Therefore in Chapter 5, the effect of chemical density on removing hydrate blockage in the vertical pipes was assessed using a long window rig. The effectiveness of three chemical mixtures (MEG, MeOH, and MEG/MeOH mixture with a density of 1 g/cc) on hydrate blockage removal in vertical pipes was investigated. The results indicate that a mixture of methanol/MEG with a density of 1 g/cc could remove hydrate blockage more successfully and efficiently than other two mixtures (MEG or MeOH alone). Furthermore, in this chapter, the possibility of ice formation during hydrate dissociation (due to its endothermic nature) and movement of hydrate blockage location during thermodynamic hydrate inhibitor injection were investigated.

In addition, there is a concern about the performance of KHIs in a system with pre-formed hydrates and induced hydrate dissociation using KHIs which are the main objectives of Chapter 6. KHIs are usually used for inhibition of hydrate nucleation and hydrate growth. Therefore, in most of the scenarios, KHI is injected into produced water streams which are hydrates-free. While this is a representative scenario for a perfect situation, there are a number of situations where hydrates could form from produced waters which are KHI-free. The question then may arise as what the influence of KHI is in preformed

hydrates systems. Chapter 6 investigates the performance of Luvicap-EG (PVCap) in the pre-formed hydrate systems (PVCap was used as a well-known reference to compare the performance of Bio KHIs). Furthermore, in Chapter 6, the initial findings of experimental studies aimed at investigating the anomalous hydrate dissociation inside the hydrate stability regions in the presence of Luvicap EG and Luvicap Bio are reported. Results demonstrate that, in addition to inhibiting hydrate growth/nucleation, KHI polymers can induce partial or complete hydrate dissociation inside the hydrate region.

1.7 Reference

[1] H. Davy, "The Bakerian Lecture: On some of the combinations of oxymuriatic gas and oxygene, and on the chemical relations of these principles, to inflammable bodies," *Philos. Trans. R. Soc. London*, vol. 101, pp. 1–35, 1811.

[2] M. Faraday and H. Davy, "On fluid chlorine," *Philos. Trans. R. Soc. London*, vol. 113, pp. 160–165, 1823.

[3] E. G. Hammerschmidt, "Formation of gas hydrates in natural gas transmission lines," *Ind. Eng. Chem.*, vol. 26, no. 8, pp. 851–855, 1934.

[4] H. Hirai, Y. Uchihara, H. Fujihisa, M. Sakashita, E. Katoh, K. Aoki, K. Nagashima, Y. Yamamoto, and T. Yagi, "High-pressure structures of methane hydrate observed up to 8 GPa at room temperature," *J. Chem. Phys.*, vol. 115, no. 15, pp. 7066–7070, 2001.

[5] H. Hirai, T. Kondo, M. Hasegawa, T. Yagi, Y. Yamamoto, T. Komai, K. Nagashima, M. Sakashita, H. Fujihisa, and K. Aoki, "Methane hydrate behavior under high pressure," *J. Phys. Chem. B*, vol. 104, no. 7, pp. 1429–1433, 2000.

[6] E. D. Sloan Jr and C. Koh, *Clathrate hydrates of natural gases*. CRC press, 2007.

[7] E. D. Sloan, "Fundamental principles and applications of natural gas hydrates," *Nature*, vol. 426, no. 6964, pp. 353–363, 2003.

[8] R. K. McMullan and G. A. Jeffrey, "Polyhedral clathrate hydrates. IX. Structure of ethylene oxide hydrate," *J. Chem. Phys.*, vol. 42, no. 8, pp. 2725–2732, 1965.

[9] T. C. W. Mak and R. K. McMullan, "Polyhedral clathrate hydrates. X. Structure of the double hydrate of tetrahydrofuran and hydrogen sulfide," *J. Chem. Phys.*, vol. 42, no. 8, pp. 2732–2737, 1965.

[10] S. Subramanian, R. A. Kini, S. F. Dec, and E. D. Sloan, "Evidence of structure II hydrate formation from methane+ ethane mixtures," *Chem. Eng. Sci.*, vol. 55, no. 11, pp. 1981–1999, 2000.

[11] E. M. Hendriks, B. Edmonds, R. A. S. Moorwood, and R. Szczepanski, "Hydrate structure stability in simple and mixed hydrates," *Fluid Phase Equilib.*, vol. 117, no. 1–2, pp. 193–200, 1996.

[12] K. C. Hester and E. D. Sloan, "sII structural transitions from binary mixtures of simple sI formers," *Int. J. Thermophys.*, vol. 26, no. 1, pp. 95–106, 2005.

[13] J. A. Ripmeester, S. T. John, C. I. Ratcliffe, and B. M. Powell, "A new clathrate hydrate structure," *Nature*, vol. 325, no. 6100, pp. 135–136, 1987.

[14] A. P. Mehta and E. D. Sloan Jr, "Structure H hydrate phase equilibria of paraffins, naphthenes, and olefins with methane," *J. Chem. Eng. Data*, vol. 39, no. 4, pp. 887–890, 1994.

[15] P. Englezos, N. Kalogerakis, P. D. Dholabhai, and P. R. Bishnoi, "Kinetics of gas hydrate formation from mixtures of methane and ethane," *Chem. Eng. Sci.*, vol. 42, no. 11, pp. 2659–2666, 1987.

[16] P. Englezos and P. R. Bishnoi, “Gibbs free energy analysis for the supersaturation limits of methane in liquid water and the hydrate-gas-liquid water phase behavior,” *Fluid Phase Equilib.*, vol. 42, pp. 129–140, 1988.

[17] D. Kashchiev and A. Firoozabadi, “Nucleation of gas hydrates,” *J. Cryst. Growth*, vol. 243, no. 3, pp. 476–489, 2002.

[18] D. Kashchiev and A. Firoozabadi, “Driving force for crystallization of gas hydrates,” *J. Cryst. Growth*, vol. 241, no. 1, pp. 220–230, 2002.

[19] C. Moon, P. C. Taylor, and P. M. Rodger, “Molecular dynamics study of gas hydrate formation,” *J. Am. Chem. Soc.*, vol. 125, no. 16, pp. 4706–4707, 2003.

[20] R. L. Christiansen and E. D. Sloan, “Mechanisms and kinetics of hydrate formation,” *Ann. N. Y. Acad. Sci.*, vol. 715, no. 1, pp. 283–305, 1994.

[21] J. Long, “Gas Hydrate Formation Mechanism and Its Kinetic Inhibition,” Ph.D. Thesis, Colorado School of Mines, Golden, CO, 1994.

[22] B. Kvamme, “A new theory for the kinetics of hydrate formation,” in *Proceedings of the Second International Conference on Natural Gas Hydrates, Toulouse, France*, 1996, pp. 131–146.

[23] R. Radhakrishnan and B. L. Trout, “A new approach for studying nucleation phenomena using molecular simulations: Application to CO2 hydrate clathrates,” *J. Chem. Phys.*, vol. 117, no. 4, pp. 1786–1796, 2002.

[24] I. Chatti, A. Delahaye, L. Fournaison, and J.-P. Petitet, “Benefits and drawbacks of clathrate hydrates: a review of their areas of interest,” *Energy Convers. Manag.*, vol. 46, no. 9, pp. 1333–1343, 2005.

[25] S. Thomas and R. A. Dawe, “Review of ways to transport natural gas energy from countries which do not need the gas for domestic use,” *Energy*, vol. 28, no. 14, pp. 1461–1477, 2003.

[26] J. C. Stevens, J. J. Howard, B. A. Baldwin, G. Ersland, J. Husebø, and A. Graue, “Experimental hydrate formation and gas production scenarios based on CO2 sequestration,” in *Proceedings of the 6th International Conference on Gas Hydrates*, 2008, pp. 6–10.

[27] L. Fournaison, A. Delahaye, I. Chatti, and J.-P. Petitet, “CO2 hydrates in refrigeration processes,” *Ind. Eng. Chem. Res.*, vol. 43, no. 20, pp. 6521–6526, 2004.

[28] S. Fan, L. Yang, Y. Wang, X. Lang, Y. Wen, and X. Lou, “Rapid and high capacity methane storage in clathrate hydrates using surfactant dry solution,” *Chem. Eng. Sci.*, vol. 106, pp. 53–59, 2014.

[29] N.-J. Kim, S.-S. Park, S.-W. Shin, J.-H. Hyun, and W. Chun, “An experimental investigation into the effects of zeolites on the formation of methane hydrates,” *Int. J. Energy Res.*, vol. 39, no. 1, pp. 26–32, 2015.

[30] S. Cochran, “Hydrate control and remediation best practices in deepwater oil developments,” in *Offshore Technology Conference, OTC 15255. Houston, TX*, 2003.

[31] Sloan, E. D.; Koh, C. A.; Sum, A.; Ballard, A. L.; Creek, J. L.; Eaton, M.; Lachance, J.; McMullen, N.; Palermo, T.; Shoup, G.; Talley, L., 2010. Natural Gas Hydrates in Flow Assurance; Gulf Professional Publishing (Elsevier): Oxford, U.K., ISBN: 978-1-85617-945-4

[32] J. Lee, B. Hampton, R. R. Alapati, E. a Sanford, and S. O'Brien, "OTC 20171 Innovative Technique for Flowline Plug Remediation," *Otc*, no. May, pp. 4–7, 2009.

[33] M. Piemontese, M. Rotondi, A. Genesio, A. Perciante, and F. Iolli, "Successful experience of hydrate plug removal from deepwater gas injection flowline" 12th Offshore Mediterr. Conf., pp. 1–9, 2015.

[34] S. Kashou, S. Subramanian, P. Matthews, and L. Thummel, "OTC 16691 GOM Export Gas Pipeline, Hydrate Plug Detection and Removal," *Otc*, 2004.

[35] J. Davalath, "Methods to Clear Blocked Flowlines," *Mentor Subsea, Deep. IIA CTR A208-1*, vol. 157, 1997.

[36] J. Davalath and J. W. Barker, "Hydrate Inhibition Design for Deepwater Completions," *SPE Drill. Complet.*, vol. 10, no. June, pp. 115–121, 1995.

[37] M. Nepomiluev and V. Streletskaya, "Subsea Gas Pipeline Coiled Tubing Intervention for Hydrate Plug Removal," *SPE Russ. Oil Gas Explor. Prod. Tech. Conf.*, 2014.

[38] M. A. Kelland, "History of the development of low dosage hydrate inhibitors," *Energy & Fuels*, vol. 20, no. 3, pp. 825–847, 2006.

[39] E. D. Sloan Jr, "Method for controlling clathrate hydrates in fluid systems, U.S. Patent 5,420,370, issued May 30." Google Patents, 1995.

[40] E. D. Sloan Jr, "Method for controlling clathrate hydrates in fluid systems, U.S. Patent 5,432,292, issued July 11." Google Patents, 1995.

[41] E. D. Sloan Jr, "Method for controlling clathrate hydrates in fluid systems, U.S. Patent 5,880,319, issued March 9." Google Patents, 1999.

[42] M. A. Kelland, Production chemicals for the oil and gas industry. CRC press, 2014.

[43] O. M. Musa, C. Lei, J. Zheng, and M. M. Alexandre, "Advances in Kinetic Gas Hydrate Inhibitors," in *RSC Manchester*, 2009.

[44] U. Klomp, "The world of LDHI: From conception to development to implementation," in *Proceedings of the 6th International Conference on Gas hydrates, Vancouver, Canada*, 2008, vol. 5409.

[45] E. Luna-Ortiz, M. Healey, R. Anderson, and E. Sørhaug, "Crystal Growth Inhibition Studies for the Qualification of a Kinetic Hydrate Inhibitor under Flowing and Shut-In Conditions," *Energy & Fuels*, vol. 28, no. 5, pp. 2902–2913, 2014.

[46] R. Anderson, H. Mozaffar, and B. Tohidi, "Development of a crystal growth inhibition based method for the evaluation of kinetic hydrate inhibitors," in *Proceedings of the 7th International Conference on Gas Hydrates*, 2011, pp. 17–21.

[47] P. Glénat, R. Anderson, H. Mozaffar, and B. Tohidi, “Application of a new crystal growth inhibition based KHI evaluation method to commercial formulation assessment,” in *Proceedings of the 7th International Conference on Gas Hydrates*, 2011, pp. 17–21.

[48] H. Mozaffar, R. Anderson, and B. Tohidi, “Reliable and Repeatable Evaluation of Kinetic Hydrate Inhibitors Using a Method Based on Crystal Growth Inhibition,” *Energy & Fuels*, vol. 30, no. 12, pp. 10055–10063, 2016.

[49] D. Lysne and R. Larsen, “Hydrate Problems in Pipelines : A Study from Norwegian Continental Waters,” *Int. Offshore Polar Eng. Conf.*, vol. I, pp. 257–262, 1995.

[50] X. Li, L. H. Gjertsen, and T. Austvik, “Thermodynamic inhibitors for hydrate plug melting,” *Ann. N. Y. Acad. Sci.*, vol. 912, no. 1, pp. 822–831, 2000.

[51] Austvik, T., Li, X. and Gjertsen, L.H., 2000. Hydrate plug properties: Formation and removal of plugs. Annals of the New York Academy of Sciences, 912(1), pp.294-303.

[52] A. C. Gulbrandsen and T. M. Svartås, “Effects of PVCap on gas hydrate dissociation kinetics and the thermodynamic stability of the hydrates,” Energy & Fuels, vol. 31, no. 9, pp. 9863–9873, 2017.

Chapter 2 – Bio KHI Selection

2.1 Introduction

This chapter presents the results of work undertaken on the topic of Bio KHIs selection. The CGI method (see Section 1.4.4.2) has been undertaken to assess different Bio KHIs.

Luvicap Bio from BASF and ECO-530 as a Bio KHI from ECO Inhibitors (CGI regions for ECO-530 is taken from 6th report of 2012-2015 JIP phase project [2.1]) were selected to assess which one has a better performance in terms of hydrate inhibition both in simple gas or natural gas systems.

In addition, it is reported that pectin could inhibit the hydrate formation as a KHI [2.2]. Xu et al. (2016) reported that both CGI-type method and induction time method strongly suggest that biodegradable fruit pectin has powerful KHI properties [2.2]. They claimed that pectin could inhibit methane hydrate formation at subcoolings up to 12.5 °C, at doses of 0.25 to 0.50 mass% aqueous phase. If it is true, pectin can be used as an excellent Bio KHI, i.e., having excellent biodegradation properties together with powerful KHI properties. Therefore, it was decided to quickly assess pectin's potential in methane and natural gas systems.

The chemical structure of pectin is illustrated in Figure 2-1 [2.3]. Pectin is a mixture of polysaccharides which found in cell wall dry substance of higher plants. The repeating sections of pectin molecule consist of carboxyl, ester, and amide; the strong polarity of carboxyl and hydroxyl groups contributing to its affinity for water and gelling properties at modest aqueous concentrations.

Initial findings of experimental studies using CGI method aimed at investigating three potential green KHIs which have been reported / are produced (Luvicap Bio, ECO-530, and pectin) are reported in this chapter. The results of this chapter were used to select the best biochemical in terms of hydrate inhibition in both single gas and multicomponent natural gas for further investigation in the rest of this thesis.

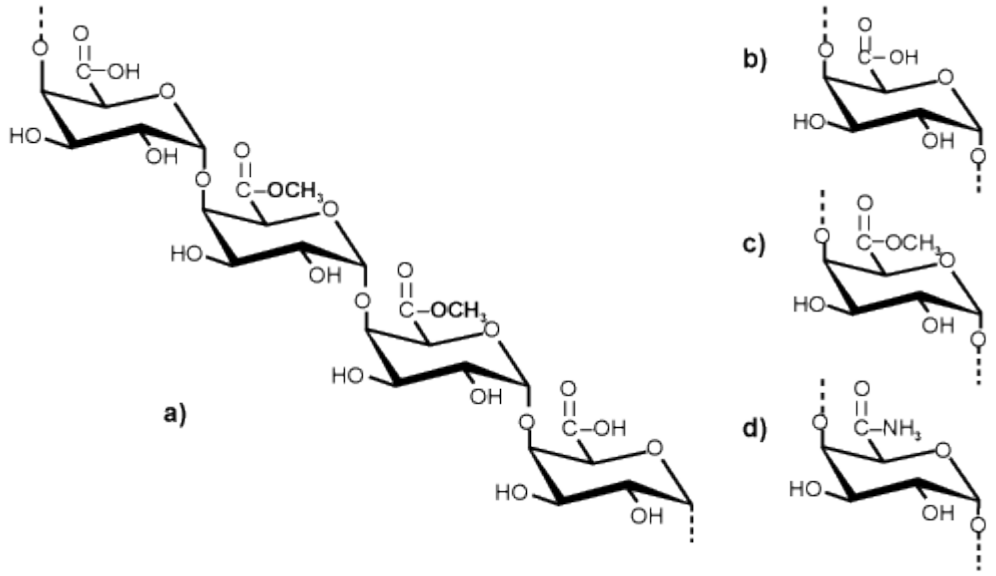

Figure 2-1. (a) A repeating segment of pectin molecule and functional groups: (b) carboxyl; (c) ester; (d) amide in pectin chain [2.3].

2.2 Experimental Equipment & Materials

Studies were carried out using in-house standard high-pressure, ~300 ml volume, stirred autoclaves (Figure 2-2). Autoclave mixing rates were typically ~500 rpm (as normally used for KHI evaluation studies). Some autoclaves were equipped with motor power (amps), voltage and rpm recording, possibly allowing assessment of transportability of fluids (e.g. from power required in an attempt to maintain rpm) and onset of blockage (rpm reduced to zero).

The temperature probe was calibrated with a measurement accuracy of 0.1 °C. Cell pressure was measured by a Druck strain gauge (±0.07 bar), calibrated using a Budenberg dead weight tester. Both thermometer and pressure transducer are connected to a data acquisition unit and a computer with the ability to continuously record the temperature and the cell pressure.

Methane was 99.99% pure. The multi-component natural gas was supplied by BOC, the composition is given in Table 2-1. Deionised water was used in all tests.

The Luvicap Bio base polymer used was supplied by BASF in a water + MEG solvent mix at ~30 mass% active polymer. However, Bio KHI from Eco Inhibitors (ECO-530) was supplied at a concentration of 40 mass% active polymer in ethylene glycol. The

Bio KHI concentrations in the aqueous phase in all tests are based on the dose of active polymer, i.e., to have 0.5 mass% dose of active polymer of Luvicap Bio in the aqueous phase. Pectin was standard food grade fruit extract apple pectin.

2.3 Predicting Hydrate Phase Boundary and Hydrate Calculation

In this thesis, the thermodynamic hydrate phase boundary was predicted using HydraFLASH®, a thermodynamic model by Hydrafact Ltd and Heriot-Watt University. The sCPA (Simplified Cubic Plus Association) was used as the equation of state to predict phase equilibria and hydrate phase boundary. The estimated percentage of water converted to hydrate (WCH %) was calculated based on the calculation presented in Appendix B.

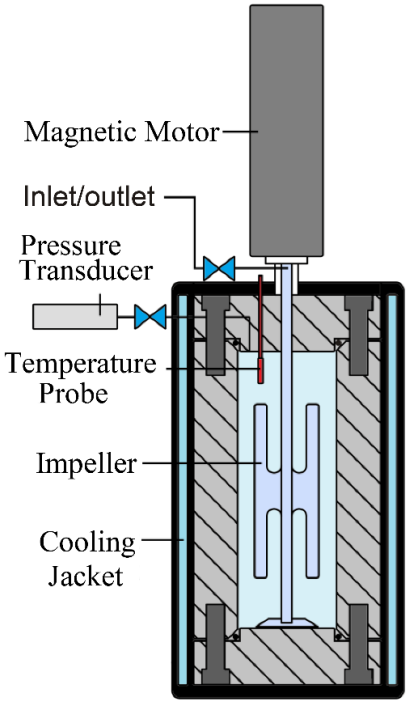

Figure 2-2. Schematic illustration of standard autoclaves used in experimental studies.

Table 2-1. Composition of the natural gases used in experiments.

Component	Mole%
Methane	87.9
Ethane	6.0
Propane	2.0
i-Butane	0.2
n-Butane	0.3
CO2	2.0
Nitrogen	1.5

2.4 Results and Discussion

As discussed, the main objective of this chapter was to choose the best Bio KHI in terms of hydrate inhibition among main available Bio KHIs. Based on this, two main sets of experiments using standard CGI method were carried out in methane and natural gas systems and their measured subcooling extents of CGI regions were compared at ~70 bar. In the methane system, CGI cooling/heating were carried out in 0.5% Luvicap Bio, 0.5% pectin, 0.25% Luvicap Bio, and 0.25% Luvicap Bio + 0.25% pectin (a mixture of polymers was used to see if the best option was a mixture rather than a single polymer). In the natural gas system, CGI cooling/heating runs were carried out in 0.5% Luvicap Bio, 0.5% Pectin, and 0.25% Luvicap Bio + 0.25% pectin. In addition, the subcooling extents of CGI regions for ECO-530 is taken from 6th report of 2012-2015 JIP phase project [2.1].

Figure 2-3 and Figure 2-4 are examples of heating/cooling curves (CGI method) for 0.5 mass% aqueous Luvicap Bio and pectin with natural gas respectively. Points are every five minutes. Figure 2-5 and Figure 2-6 show a comparison of subcooling extents of measured CGI regions for Luvicap Bio, pectin, Luvicap Bio-pectin, and ECO-530 combinations for various aqueous polymer concentrations at ~70 bar pressure with methane and natural gas respectively.

As can be seen, Luvicap Bio has more powerful KHI properties compared to pectin and ECO-530, i.e., the largest CIR region (green zone: complete hydrate inhibition) is achieved by Luvicap Bio both in methane and natural gas system. The CIR extents for 0.5 mass% Luvicap Bio for methane from s-I phase boundary and natural gas from s-II phase boundary are 3 °C and 10.5 °C respectively.

The subcooling extents of CGI regions for ECO-530 in methane and natural gas suggest that ECO-530 does not have KHI properties like Luvicap Bio. As can be seen in Figure 2-6, no obvious CIR extent is seen for 0.5 mass% ECO-530 in the natural gas system, with only limited SGR(S) largely observed.

In addition, as can be seen, results strongly suggest that pectin does not have notable KHI properties, at least in the case of the sample tested in methane and natural gas. As shown in Figure 2-4, no obvious CIR extent is seen for pectin alone in the natural gas system, with only limited SGR(S) largely observed for both methane and natural gas.

However, studies in this area have focussed on 0.25% Luvicap Bio + 0.25% pectin mixtures with methane and natural gas to see if pectin might still offer useful KHI properties (to assess potential synergism) if used in combination with another, effective Bio KHI. As shown in Figure 2-5 and Figure 2-6, in combination with Luvicap Bio, pectin likewise shows no measurable inhibition effect; CGI behavior appears essentially identical to pectin-free cases / Luvicap Bio alone.

Therefore, it is concluded that the findings of Xu et al. (2016) are in error, and pectin does not have significant potential as a bio KHI, at least in terms of crystal growth inhibition. The probable explanation for reported literature findings is that pectin does seem to have some history elimination effects. This probably suggests that in those systems where pectin was the only polymer, the hydrate history could be disappeared during heating cycle even if the temperature was kept close to the phase boundary. Consequently, on the next cooling, it appeared some inhibition region due to lack of hydrate nucleation/history in the system, so Xu et al. (2016) suggest the pectin as a Bio KHI which is wrong.

However, as shown in Figure 2-4, in the 0.5% pectin + NG system with hydrates (where a clear ΔP was evident), slow to medium growth rate patterns were observed at low subcoolings in re-cooling immediately after heating. As a result, the long induction time due to pectin which was observed by Xu et al. (2016) could be explained by the role of hydrate history in KHI evaluation. Therefore, it is crucially important that the CGI studies always should run with hydrate / hydrate history (obvious ΔP due to hydrate during re-cooling)

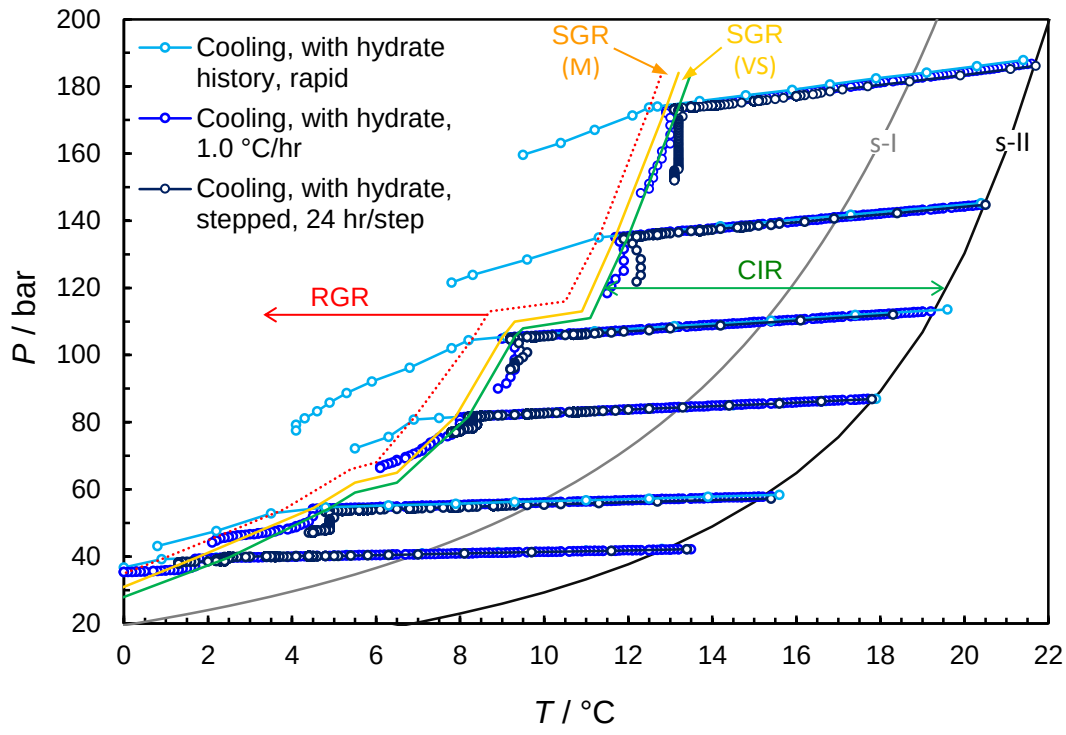

Figure 2-3. Example cooling curves (CGI method) for 0.5 mass% Luvicap Bio with natural gas. Points are every five minutes.

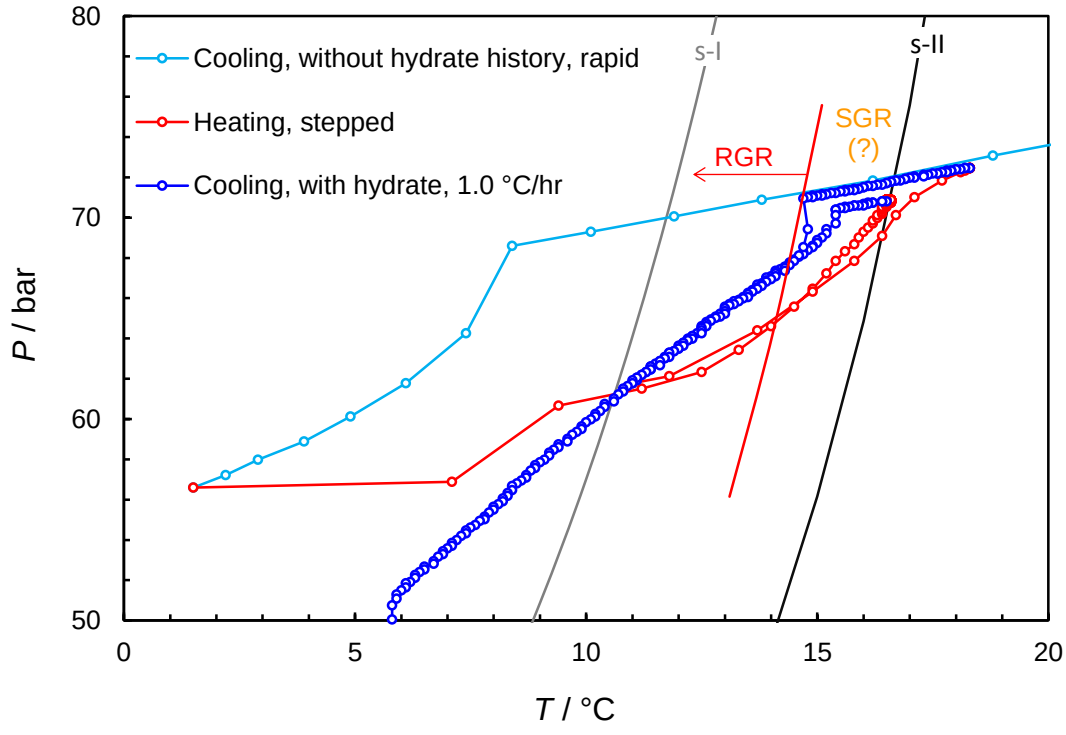

Figure 2-4. Example cooling/Heating curves (CGI method) for 0.5 mass% pectin with natural gas. Points are every five minutes.

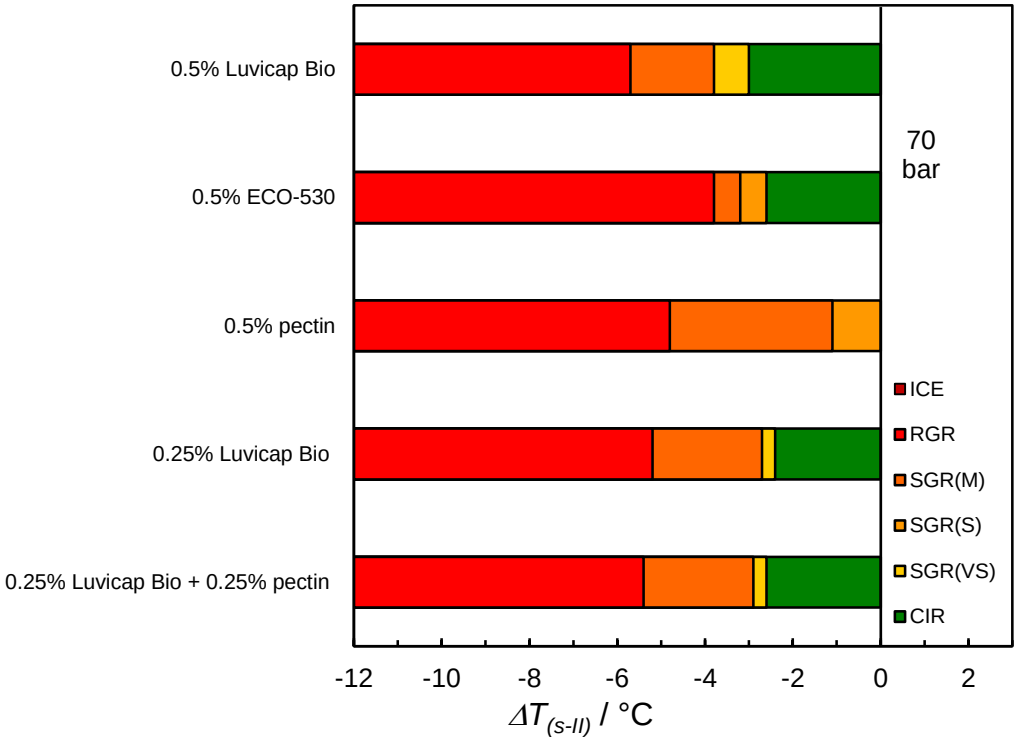

Figure 2-5. Comparison of subcooling extents of CGI regions from the s-I phase boundary for 0.5 mass% Luvicap Bio, 0.5 mass% ECO-530, 0.5 mass% pectin, 0.25 mass% Luvicap Bio, and 0.25 mass% Luvicap Bio + 0.25 mass% pectin, all in methane system. The subcooling extents of CGI regions for ECO-530 is taken from 6th report of 2012-2015 JIP phase project [2.1].

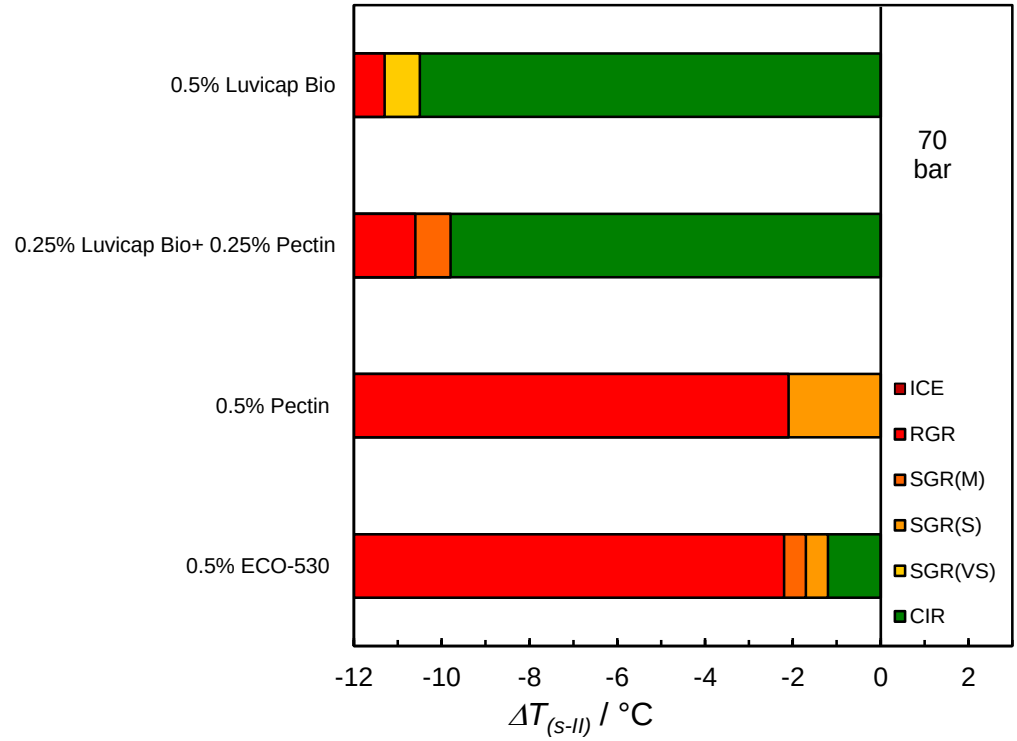

Figure 2-6. Comparison of subcooling extents of CGI regions from the s-II phase boundary for 0.5 mass% Luvicap Bio, 0.5 mass% ECO-530, 0.5 mass% pectin, and 0.25 mass% Luvicap Bio + 0.25 mass% pectin, all in the natural gas system. The subcooling extents of CGI regions for ECO-530 is taken from 6th report of 2012-2015 JIP phase project [2.1].

2.5 Summary

From preliminary CGI studies of Luvicap Bio, ECO-530, and pectin in methane and natural gas system, it is concluded that:

- Luvicap Bio could be used as a strong Bio KHI, i.e., the large CIR extent was observed in the system with Luvicap Bio, e.g. the CIR extents for 0.5 mass% Luvicap Bio for methane from s-I phase boundary and natural gas from s-II phase boundary are 3 °C and 10.5 °C respectively

- Pectin does not seem to be a strong KHI, at least in the case of the sample tested here (apple pectin), i.e. no obvious CIR extent was observed, with only limited SGR(S) largely observed in both methane and natural gas system

- Pectin does not seem to be behaving like synergise materials, at least in the case of 0.25 mass% Luvicap Bio + 0.25 mass% Pectin with methane

- It seems that pectin removes the hydrate history from the system and which could result in observing some CGI behavior

- This finding from pectin strongly suggests that it is crucial to have hydrate memory or clear presence of hydrate (clear pressure drop ΔP) in the system for cooling runs in CGI method

Therefore, Luvicap Bio was selected for further investigation in this thesis to study of hydrate inhibition using a combination of THIs and Luvicap Bio, hydrate fraction tolerance, and induced hydrate dissociation using Luvicap Bio.

2.6 Reference

[1] R. Anderson, B. Tohidi, and F. Tohidi, "evaluation of low dosage hydrate inhibitors" Edinburgh:Heriot-Watt University, Institute of Petroleum Engineering-Joint Industry Project Report-2012-2015, Report 6.

[2] S. Xu, S. Fan, S. Fang, X. Lang, Y. Wang, and J. Chen, "Pectin as an extraordinary natural kinetic hydrate inhibitor," Sci. Rep., vol. 6, p. 23220, 2016.

[3] P. Sriamornsak, "Chemistry of pectin and its pharmaceutical uses: A review," Silpakorn Univ. Int. J., vol. 3, no. 1–2, pp. 206–228, 2003.

Chapter 3– Luvicap Bio: Structure Effects Inhibition, Hydrate Fraction Tolerance

3.1 Introduction

This chapter reports the results of KHI hydrate fraction tolerance and structure effect inhibition studies. As discussed in Section 1.4.2, KHIs polymers are known as nucleation inhibitors and most of the KHIs are designed for nucleation inhibition. Although most of the KHIs are successful in induction time test in terms of hydrate inhibition, some of them fail at high hydrate fraction or even at low aqueous fractions of hydrate (only a few % of water converted to hydrate). Generally, a KHI that can inhibit per unit dosage at a higher fraction of hydrate is better in terms of hydrate blockage prevention.

In this chapter, the CGI method (see Section 1.4.4.2) was carried out to evaluate the performance of Luvicap Bio and PVCap polymers in terms of hydrate inhibition at various hydrate fractions in the methane system, i.e., PVCap which is well studied / known was used through the thesis as a comparison with Luvicap Bio, so makes a good reference. The results potentially suggest that Luvicap Bio is a better inhibitor for s-I methane than for s-II methane hydrates and PVCap is better for s-II hydrates; the formation of both s-I and s-II methane hydrate is speculated. In addition, as Luvicap Bio is better for s-I and PVCap is better for s-II, it was speculated that the combination of Luvicap Bio and PVCap can inhibit further in terms of subcooling temperature, i.e., one inhibits s-II and the other inhibits s-I, resulting in improved CGI regions. Therefore, the CGI method was carried out to evaluate the performance of Luvicap Bio/PVCap combination in terms of hydrate inhibition in both methane and natural gas systems.

As discussed later in this chapter, the initial findings of experimental studies of hydrate fraction tolerance suggest potentially formation of s-I and s-II methane and multi-structure formation in the natural gas system. In addition, it is speculated that the common CGI regions observed for the KHI system are not as a result of KHI polymers directly and there is an interaction between KHIs and hydrate structures and morphology. In other words, 3 °C subcooling temperature observed as a CIR for Luvicap Bio in the methane (see Section 2.4) could be as a result of a change in hydrate growth rate or hydrate structures, not as a direct result of KHI polymers. Accordingly, it was speculated that there are different hydrate growth/structure regions in those systems that can potentially form more than one structures. Therefore, these different hydrate growth/structure regions can induce the behaviour seen for Luvicap Bio/PVCap and also the common CGI regions. Therefore, the hydrate growth rates and various potential hydrate structure formation were studied in methane, ethane, propane, $C_1 + C_3$, and $C_1 + C_2 + C_3$ systems.

3.2 Experimental Equipment, and materials

All experiments were carried out using high pressure stirred autoclaves (see Section 2.2 for a more detailed description of equipment). Distilled water was used in all tests. Luvicap Bio base polymer was supplied in water by BASF. The PVCap used was standard Luvicap-EG base polymer (average MW = ~7000) supplied by BASF, with an ethylene glycol solvent removed by vacuum oven drying. Methane, propane, and ethane were 99.99% pure. The multi-component natural gas was supplied by BOC, the composition is given in Table 3-1.

3.3 Experimental Principles and Methodologies

The CGI method (see Section 1.4.4.2) was carried out to study the structure effects inhibition and hydrate fraction tolerance for Luvicap Bio / PVCap and the performance of Luvicap Bio/PVCap combination in terms of hydrate inhibition.

In addition, a number of experimental methods have been applied in high pressure stirred autoclaves to study and investigate the hydrate growth rate/patterns and formation of various hydrate structures in different gas systems including methane, ethane, propane, C_1+C_3, and C_1+C_2+C_3. These methods including equilibrium step heating/cooling measurements and shut-in restart (SIR) runs are described in the Sections 3.3.1 and 3.3.2. Furthermore, the method for predicting hydrate stability regions for different gas hydrate structures and their phase boundaries is described in Section 3.3.3.

Table 3-1. Composition of natural gas used

Component	Mole%
Methane	87.93
Ethane	6.00
Propane	2.04
i-Butane	0.20
n-Butane	0.30
CO_2	2.03
Nitrogen	1.50

3.3.1 Equilibrium Step-Heating & Cooling Measurements

For step-heating measurements, the system was cooled down into the hydrate phase region and allowed to form hydrate as much as possible. Following hydrate growth, the system was heated up in steps; the system temperature was raised ~1 °C/step. A long time was given to the system to achieve the equilibrium point for each step; the time required to achieve the equilibrium point may be weeks or months. This step heating was continued until all hydrate dissociated; the system pressure moves back to the initial system pressure without hydrates.

Almost the same procedure was applied for equilibrium step-cooling measurement. The system was cooled immediately into the hydrate region to form hydrates and heated up close to phase boundary to dissociate most of the hydrate crystals (with hydrates or history/nuclei), allowing to have a 'seeded' system. Following this, the seeded system was cooled down in steps (~1 °C/step) and the sufficient time was given to each step to achieve the equilibrium points.

In the equilibrium step heating/cooling measurements, the equilibrium points were confirmed when a stabilised pressure at constant temperature was recorded for a long time. Although the system was mixed during measurements to achieve the equilibrium, more time (weeks or months) was given to the system in the case of blockages where mass transfer is limited.

3.3.2 Shut-in Restart (SIR)

The shut-in restart run is similar to the step-cooling measurements, but the system initiated to form hydrates at a set subcooling temperature. The seeded system was cooled down to a set subcooling temperature while the stirrer was shut off; the lack of mixing in the system prevents any measurable hydrate formation in the system. Following this, mixing was restarted allowing the system to form hydrates. The purpose of this type test is to study hydrate growth rate patterns and structure effects on growth rate during the SIR runs at various subcooling temperatures. However, the system temperature may increase and deviate from the set subcooling temperature due to the exothermic nature of hydrate formation. As discussed later in this chapter, this thermal aspect of detection could be also used to study for various hydrate structures formation. This method was developed through the JIP project (2015-2018) at Heriot-Watt University [3.3].

3.3.3 Predicting Hydrate Stability Regions for Different Structures

The thermodynamic hydrate phase boundary for gas was predicted using HydraFLASH®; a thermodynamic model developed by Hydrafact Ltd and Heriot-Watt University. The sCPA (Simplified Cubic Plus Association) was used as the equation of state to predict phase equilibria and hydrate phase boundary.

As discussed later in this chapter (see section 3.4.5), more than one hydrate structure can be formed in the natural gas system or even in a simple methane/ethane system, i.e., instead of forming single s-II natural gas hydrate, various hydrate structures e.g. C_3/C_4 s-II, C_2 s-II, C_2 s-I, C_1 s-I, and C_1 s-II are formed in order.

Propane and butane (particularly iso-butane) can only enter and stabilise the large cavity of s-II ($5^{12}6^4$) and they are the most stable hydrates in natural gas system [3.1]. Therefore, in step cooling measurements, the first hydrate structures formed in the natural gas systems are C_3/C_4 s-II hydrates. As subcooling temperature increases, the less stable hydrate structure s-II/s-I ethane hydrate can be formed. Ethane can enter the large cavity of s-I ($5^{12}6^2$) and the large cavity of s-II ($5^{12}6^4$) to form both stable s-I and s-II hydrates respectively. Finally, methane dominates both small and large cavities of s-I. However, as discussed in Section 3.4.5.3, s-II methane may be formed in a simple methane system even it might be metastable. Therefore, the most thermodynamically stable hydrate formers are C_3/C_4, C_2, C_1, CO_2, and N_2 in order (decreasing in stability) [3.2].

Based on the above, for step cooling measurement, various hydrate structures would be expected to form and become thermodynamically stable in order as subcooling temperature increases. This is the same for step heating measurements; various hydrate structures would be expected to disappear/dissociate in order as system temperature rises.

As can be seen in Figure 3-1, step-heating equilibrium run for 85% C_1 + 12% C_2 + 3% C_3 shows a clear change pattern/transition, indicating dissociation of different hydrate structures formed in the systems (see Section 3.4.5.5). To predict the phase boundary for this transition, simple removal component method was used; each phase boundary is related to formation or dissociation of different hydrate structures. This method was developed through the JIP project (2015-2018) at Heriot-Watt University [3.3].

Based on this method, to predict the phase boundary of ethane hydrates for $C_1 + C_2 + C_3$ system shown in Figure 3-1, the fraction of those components which are more stable than ethane (e.g. C_3 and C_4 fraction) should be removed. Therefore, propane fraction is removed from the composition and the model is run for a new normalised composition to predict both s-I and s-II ethane phase boundary.

A similar procedure is used to predict the phase boundary of methane, so the fraction of those components which are more stable than methane is removed from the composition (e.g. C_2, C_3, and C_4 fraction). For the system used in Figure 3-1, only methane remained, so the methane phase boundary for this system is as same as for simple methane system.

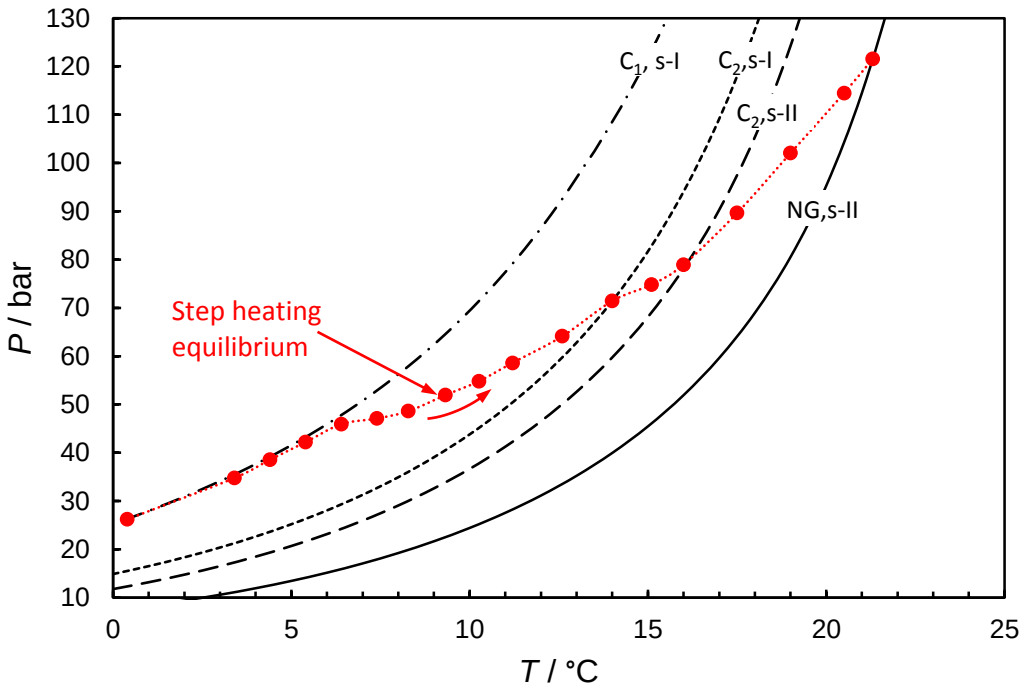

Figure 3-1. Plot of measured equilibrium (step-heating) dissociation behaviour for 85% C_1 + 12% C_2 + 3% C_3 (80% cell volume as aqueous phase) compared to model predictions for the NG (s-II), ethane (large cage) dominated s-II then s-I, then finally methane (large cage) dominated s-I. As can be seen, predictions commonly are a reasonable match for observed structural transitions.

3.4 Results and Discussion

3.4.1 Luvicap Bio Hydrate Fraction Tolerance in Methane System

To study the hydrate fraction tolerance, work on the Luvicap Bio has been done. The main objectives of this test were to assess the performance of Luvicap Bio as a function of increasing hydrate fraction and to assess any potential polymer-hydrate stoichiometry. A specific hydrate fraction will use a specific fraction of KHIs polymer which depends on whether these polymer-hydrate complexes have any polymer-water stoichiometry.

Figure 3-2 shows a plot of CGI method heating and cooling curves for 0.5% Luvicap Bio with methane for increasing fractions of water converted to hydrate with interpretation for the CIR region. The method for calculation of fractions of water converted to hydrate is described in Appendix B. The initial pressure of this experiment was 150 bar at 20 °C with 70:30 water/gas volume ratio. Figure 3-3 shows calculated %water converted to hydrate as a function of subcooling temperature for the same data plotted in Figure 3-2. As can be seen, as a fraction of water converted to hydrate increases, the performance of Luvicap Bio reduces in terms of inhibition. For example, the CIR is ~3.8 °C subcooling at a low fraction hydrate, and it reduced to 1 °C subcooling as the hydrate fraction approaches 30%. As shown in Figure 3-3, the SGR (S-M) type conditions have been seen beyond this CIR condition at higher subcooling temperature up to ~5.2 °C subcooling.

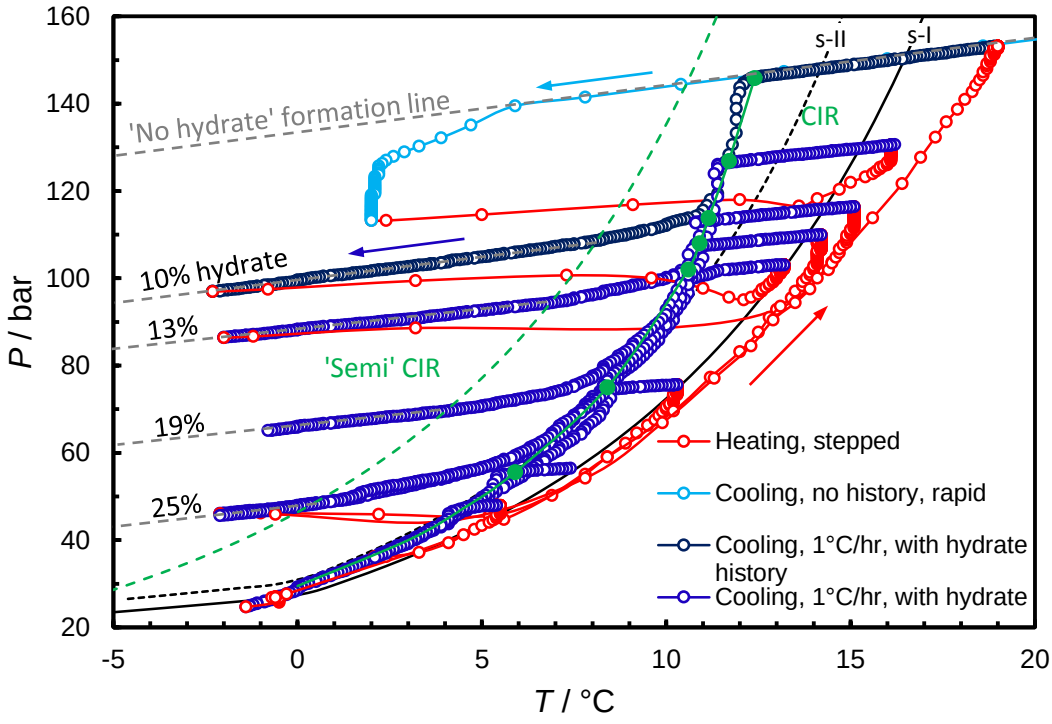

Figure 3-2. Plot of CGI method heating and cooling curves for 0.5% Luvicap Bio with methane for increasing fractions of water converted to hydrate with interpretation for the CIR region. Initial pressure of ~150 bar, with water 70% of cell volume.

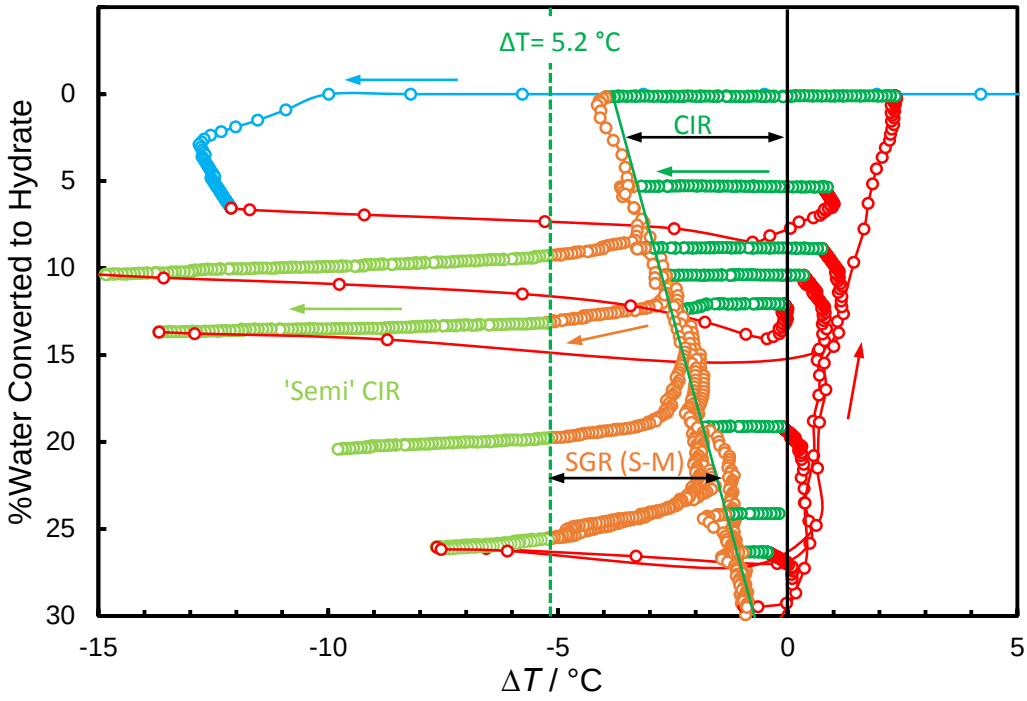

Figure 3-3. Plot of CGI method heating and cooling curves for 0.5% Luvicap Bio with methane hydrate threshold test plotted as %water converted to hydrate versus subcooling. After growth commences within the SGR(S-M), results then show it largely halts ~ 5.2 °C subcooling, at least up to ~25% water converted to hydrate.

As would be expected, the hydrate growth rate and the fraction of water converted to hydrate increases with increasing subcooling temperature beyond the CIR. In contrast to what would be expected, in this case with Luvicap Bio in methane system, beyond the narrow region of SGR (S-M) conditions, the hydrate growth rate decreased significantly. As shown in Figure 3-2 and Figure 3-3, the fraction of water converted to hydrate remains constant (hydrate growth was observed to apparently stop) at higher subcooling temperature beyond the 5.2 °C subcooling.

Several cooling runs with a different fraction of water converted to hydrate were carried out to assess the repeatability of this patterns. As shown in Figure 3-3, this pattern was observed up to the 25% water converted to hydrate. Furthermore, in all cases, this pattern was observed consistently beyond the ~5.2 °C subcooling temperature. This subcooling temperature (5.2 °C) is associated with CGI boundaries, i.e., for example, the CIR for 0.5 mass% PVCap in methane system is 5.2 °C where hydrates start to grow, as reported in the Section 3.4.2.

As shown in Figure 3-3, Luvicap Bio in the methane system shows an initial strong inhibition region (CIR region), following by weak inhibition region (SGR), then strong inhibition region (Semi CIR). Figure 3-4 shows CGI regions for Luvicap Bio in the methane system with different hydrate fraction showing CIR, SGR (S-M), and 'Semi' CIR (beyond the 5.2 °C subcooling temperature) up to 25% water converted to hydrates.

This growth pattern, inhibition of hydrate growth ('Semi' CIR) following by weak inhibition region (SGR), is unusual if one type of hydrate structure formed in the system e.g. s-I methane hydrate. As discussed in Section 3.4.5.3, the evidence and results for methane system strongly suggest and support the formation of both s-I and s-II hydrates in the methane system at different conditions. Therefore, if it is true, Luvicap Bio is a strong inhibitor for s-I methane and poor inhibitor for s-II methane, i.e., as shown in Figure 3-4, Luvicap Bio could inhibit the hydrate growth in CIR region (s-I methane hydrate formed), then allowed hydrate growth in SGR (s-II methane hydrate formed), then prevented again hydrate growth in 'Semi' CIR beyond the 5.2 °C subcooling temperature (s-I methane hydrate formed again). In addition, as shown in Figure 3-4, the start of SGR (S-M) for the higher hydrate fraction coincides with the s-II methane phase boundary predicted by the model, i.e., at higher hydrate fraction, the free active polymer of Luvicap Bio for hydrate inhibition is lower. This interpretation for the 'Semi' CIR is a joint work product of M. Aminnaji and R. Anderson which is taken from JIP Project at Heriot-Watt University [3.3]).

However, as evidence presented in Section 3.4.5.3, the 5.2 °C subcooling temperature phase boundary is believed a limit for formation of s-II methane beyond this phase boundary. As a result, s-I methane hydrate becomes more stable than s-II methane in 'Semi' CIR region, so Luvicap Bio could inhibit hydrate formation again beyond 5.2 °C subcooling temperature.

These results probably suggest the formation of both s-I and s-II methane hydrate at different conditions. However, it is proposed the formation of s-I methane hydrate in CIR and 'Semi' CIR regions which could be inhibited by Luvicap Bio, and formation of s-II methane hydrate in SGR (S-M) which could not be inhibited by Luvicap Bio. Consequently, it is proposed that Luvicap Bio is a strong inhibitor for s-I methane hydrate, but a poor inhibitor for s-II methane hydrate.

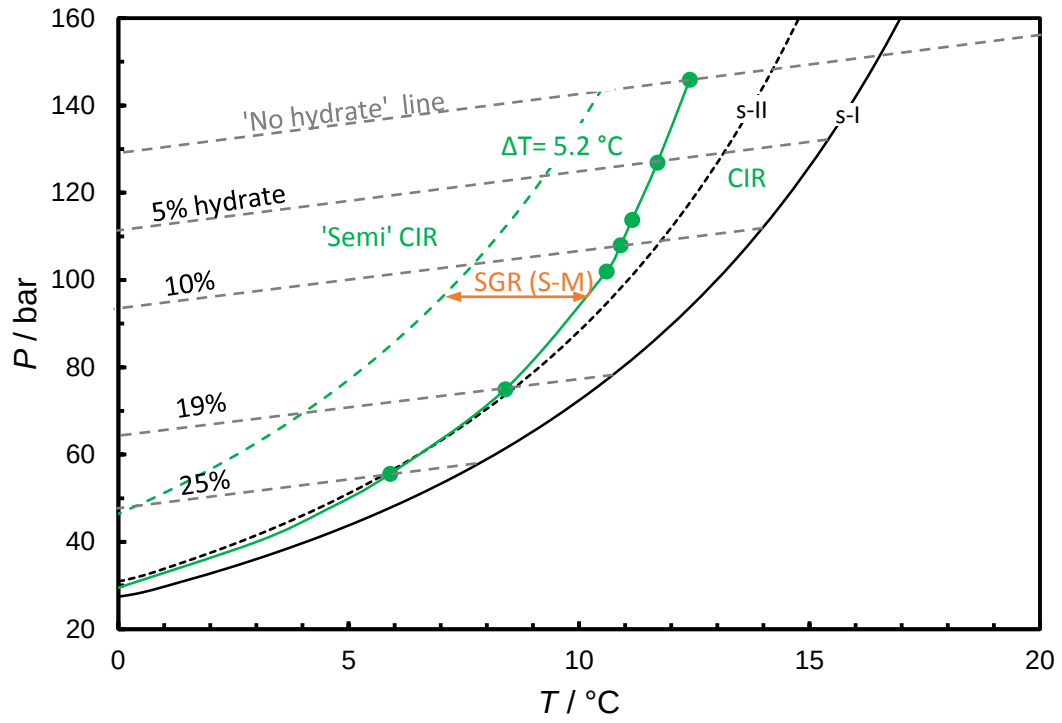

Figure 3-4. Plot of determined Luvicap Bio test CGI regions (from Figure 3-2) showing the apparent band of SGR(S-M) conditions between the CIR and the 'semi CIR' beyond 5.2 °C subcooling, where growth halted again for cooling runs with up to 25% water as hydrate. The position of the currently predicted s-II phase boundary is also shown for reference.

3.4.2 PVCap Hydrate Fraction Tolerance in Methane System

Following work on hydrate fraction tolerance tests on Luvicap Bio, tests were repeated with PVCap. PVCap which is well known was used as a comparison with Luvicap Bio, so makes a good reference. It is speculated that whether CGI regions can remain constant at higher PVCap concentration regardless of water fraction converted to hydrate, i.e., hydrate growth in the system with PVCap (with concentration more than stoichiometric composition) should not change the aqueous PVCap level. As discussed in previous section, Luvicap Bio was found to be a better inhibitor for s-I than s-II methane hydrate, so another aim of this section was to assess the PVCap in terms of structural effect on CGI regions.

Figure 3-5 shows a plot of CGI heating and cooling curves for 1.4% PVCap aqueous with methane for increasing fractions of water converted to hydrate with interpretation for the CIR region. The initial pressure of this system was 150 bar at 20 °C with 70:30 water/gas volume ratio in the cell. In addition, Figure 3-6 shows calculated %water converted to hydrate as a function of subcooling temperature for the same data plotted in Figure 3-5. As can be seen, the CIR (5.2 °C) is preserved at increasing fraction of water converted to hydrate up to ~29%. In addition, the heating stepped curves even at higher hydrate

fraction in Figure 3-5 (red points at contestant temperature) confirms the induced gas hydrate dissociation inside the CIR region. In theory, this suggests that the PVCap concentration in the aqueous phase did not drop below the stoichiometric composition up to 29% water converted to hydrate.

As shown in Figure 3-5, assessing PVCap at higher hydrate fraction (>29%) may result in ice formation, i.e., it reaches below zero temperature. Therefore, to prevent ice formation in the system, more methane was added to the system (new initial pressure of ~310 bar at 20 °C) and the same procedure was carried out to study hydrate fraction tolerance on PVCap. Figure 3-7 shows a plot of CGI heating and cooling curves for 1.4% PVCap aqueous with methane with a new initial pressure of ~310 bar for increasing fractions of water converted to hydrate with interpretation for the CIR region. In addition, Figure 3-8 shows calculated %water converted to hydrate as a function of subcooling temperature for the same data plotted in Figure 3-7.

Figure 3-7 shows that the CIR of ~5.2 °C subcooling temperature is preserved up to ~30% water converted to hydrate. As can be seen, beyond this hydrate fraction, the CIR extend starts to reduce. For example, the CIR extend is only ~1 °C, at ~60% water converted to hydrate. Therefore, this reduction of CIR region may suggest that 1.4 mass% of PVCap is lower than the stoichiometric composition for the system with more than 30% hydrates.

In contrast to the data for Luvicap Bio, the results for PVCap does not show any 'Semi' CIR region, suggesting PVCap is not a good inhibitor for s-I methane hydrate at least at higher subcooling temperature. In addition, the results suggest that PVCap is better inhibitor for s-II methane hydrate, because CIR extent (5.2 °C) was preserved over the range of hydrate fraction up to 30% hydrate for PVCap, but was not for Luvicap Bio. Formation of s-II methane hydrate in the region with a subcooling temperature between s-II phase boundary predicted by the model and 5.2 °C subcooling from s-I methane was investigated in JIP project at Heriot-Watt University [3.3]. To put this in perspective, as PVCap is a strong inhibitor for s-II methane, PVCap could inhibit the s-II methane hydrate formation in the region with a subcooling temperature between s-II phase boundary predicted by the model and 5.2 °C subcooling from s-I methane.

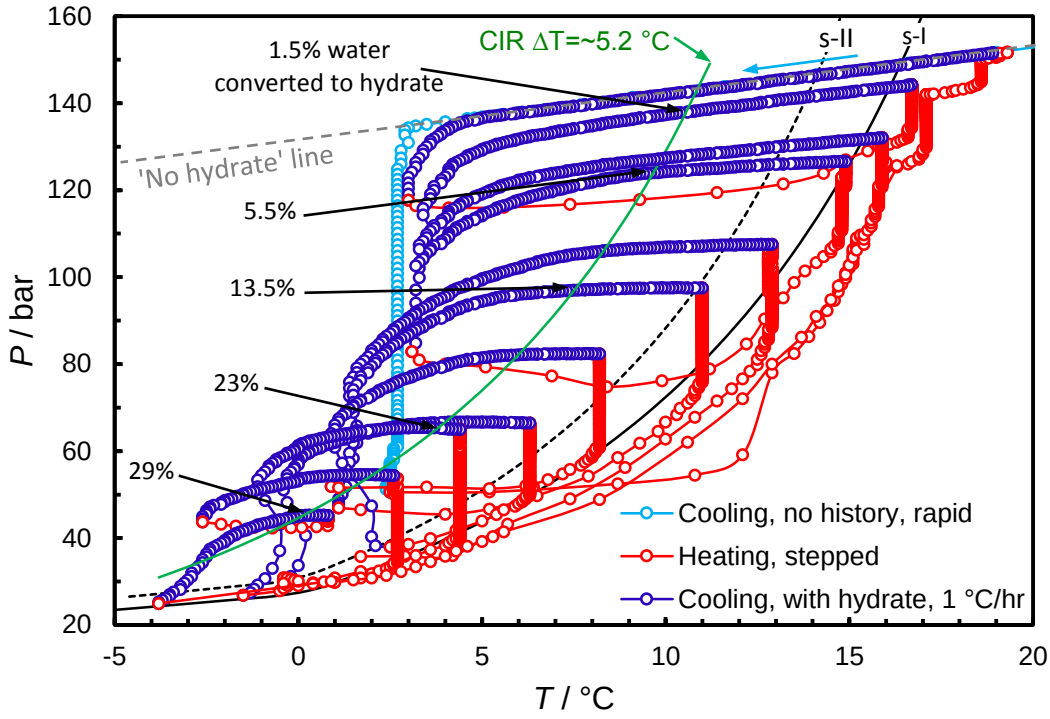

Figure 3-5. Plot of CGI heating and cooling curves for 1.4% PVCap aqueous with methane for increasing fractions of water converted to hydrate (calculated from pressure drop due to gas consumption) with interpretation for the extent of the CIR. Initial pressure was ~150 bar at 20 °C, with water 70% of cell volume.

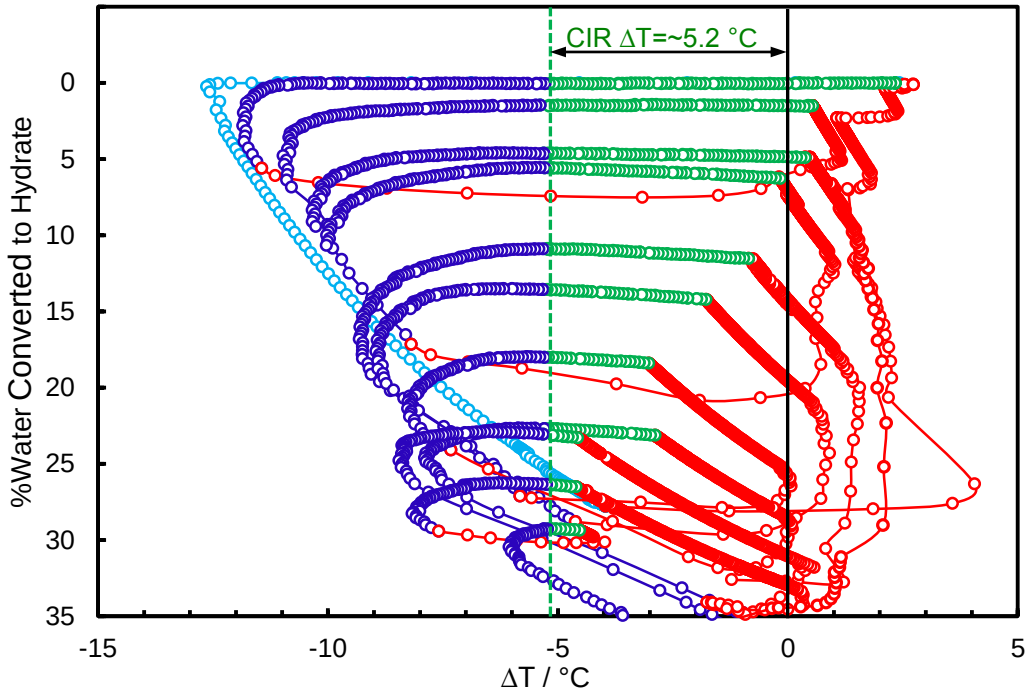

Figure 3-6. Plot of CGI method heating and cooling curves for 1.4% PVCap with methane hydrate threshold test (from Figure 3-5) plotted as %water converted to hydrate versus subcooling.

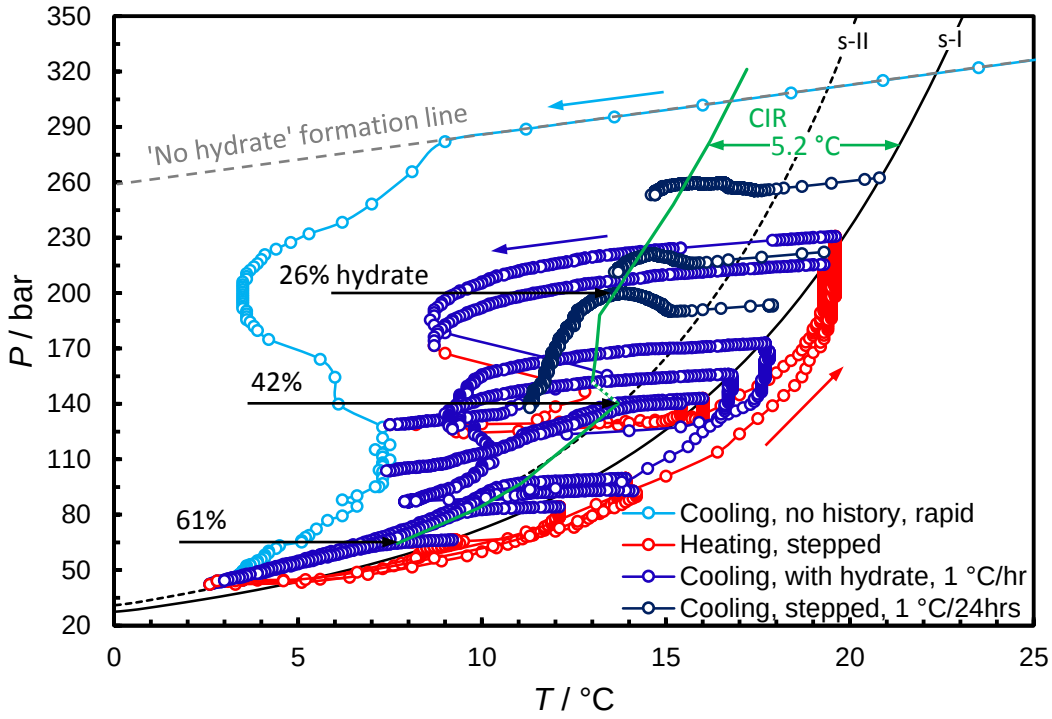

Figure 3-7. Plot of CGI method cooling curves for 1.4% PVCap aqueous with methane for increasing fractions of water converted to hydrate (calculated from pressure drop due to gas consumption) with interpretation for the extent of the CIR. Initial pressure was ~310 bar at 20 °C, with water 70% of cell volume.

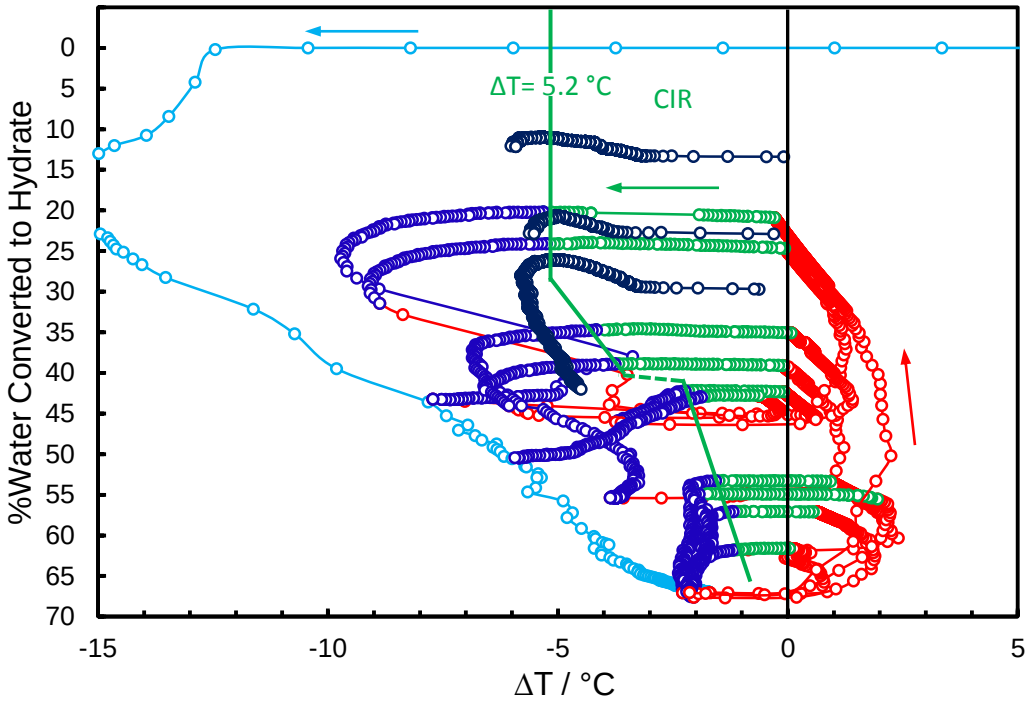

Figure 3-8. Plot of CGI method heating and cooling curves for 1.4% PVCap with methane hydrate threshold test (from Figure 3-7) plotted as %water converted to hydrate versus subcooling.

3.4.3 Combination of Luvicap Bio + PVCap in Methane System

As noted, results strongly support the theory that Luvicap Bio is a better inhibitor for s-I methane than it is for s-II. In contrast to Luvicap Bio, PVCap is a better inhibitor for s-II methane than it is for s-I. Therefore, it is speculated that if these polymers target different hydrate structures in terms of growth inhibition, the combination of these polymers should perform better, i.e., evidence show formation of both s-I and s-II methane, so Luvicap Bio and PVCap can prevent the formation of s-I and s-II methane respectively. Therefore, work progressed onto the CGI regions measurement for 0.25% Luvicap Bio + 0.25% PVCap in the methane system.

Figure 3-9 shows example CGI method cooling curves with measured points on CGI region boundaries with interpolations for 0.25 mass% PVCap + 0.25 mass% Luvicap Bio with methane. Data are reported in Table 3-2. Figure 3-10 shows a comparison of subcooling extents of measured CGI regions for 0.25 mass% PVCap + 0.25 mass% Luvicap Bio, 0.5 mass% Luvicap Bio, and 0.5 mass% PVCap, all with methane at ~70 bar pressure.

As can be seen, the combination of Luvicap Bio and PVCap improves the CGI regions in terms of hydrate inhibition performance compared to these polymers alone. For example, while the CIR extend for combination of Luvicap Bio and PVCap is ~5.8 °C at ~70 bar, the CIR extent for Luvicap Bio and PVCap alone are ~2.9 °C and ~5.2 °C subcoolings respectively. In addition, the results show an additional SGR (VS) region to ~7.2 °C subcooling temperature for the combination of these polymers compared to the PVCap alone. Moreover, as shown in Figure 3-10, the combination of these polymers is far superior and much better compared to Luvicap Bio alone in terms of hydrate inhibition. Therefore, these results do more additional support the formation of both s-I and s-II methane hydrates and to this theory that LuviCap Bio is better for s-I and PVCap is better for s-II.

Finally, as shown in Figure 3-9, the inhibition of hydrate growth beyond ~7.2 °C subcooling from s-I phase boundary is very difficult, i.e., evidence shows the formation of s-I methane in this region. It may suggest that the lean s-I gases are the most difficult system for KHIs in terms of inhibition.

Table 3-2. Measured points on CGI region boundaries with interpolations for 0.25 mass% PVCap / 0.25 mass% Luvicap Bio with methane.

CGR boundary	Growth rate	T / °C (±0.5)	P / bar (±0.2)	ΔT_{s-I} / °C (±0.5)
CIR-SGR(VS)	No growth	2.5	60.1	-5.9
		7.0	95.6	-5.8
		10.4	138.5	-5.6
SGR(VS-S)	Very slow to Slow	1.0	59.2	-7.3
		5.5	94.1	-7.1
		9.1	138	-6.8
SGR(S-M)	Slow to Medium	0.3	59.5	-8.0
		4.5	93.4	-8.1
		8.1	136	-7.8
SGR(M-R)	Medium to Rapid	2.8	92	-9.6
		6.1	134.5	-9.6

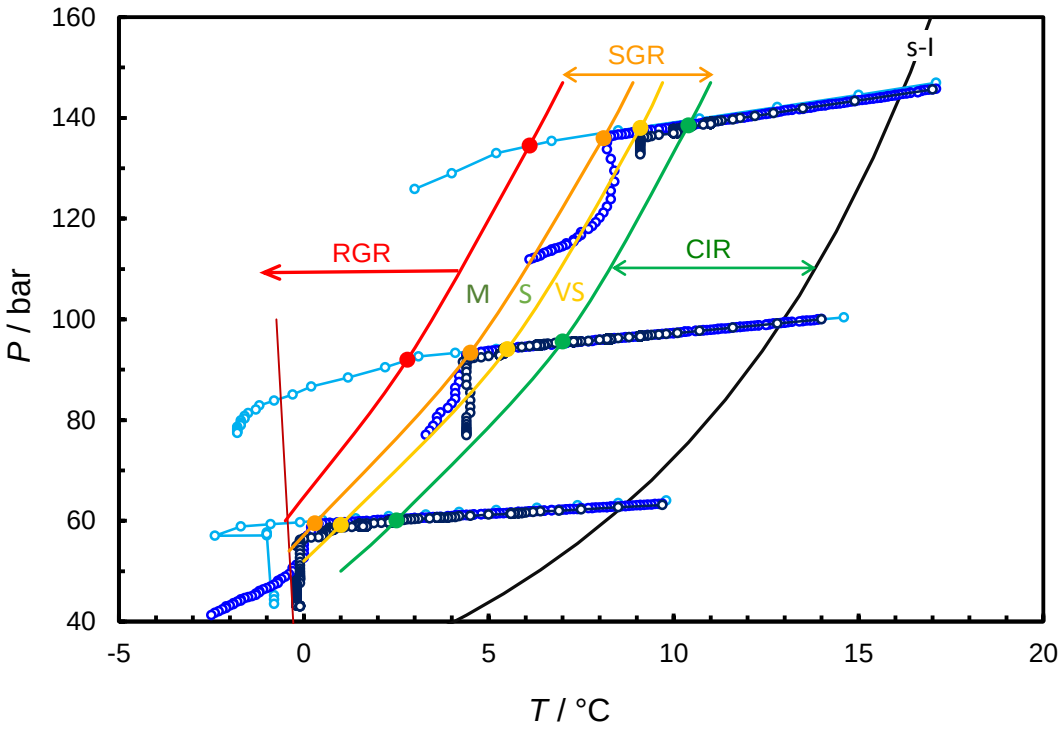

Figure 3-9. Plot of CGI method cooling curves and measured points on CGI region boundaries with interpolations for 0.25 mass% PVCap / 0.25 mass% Luvicap Bio with methane.

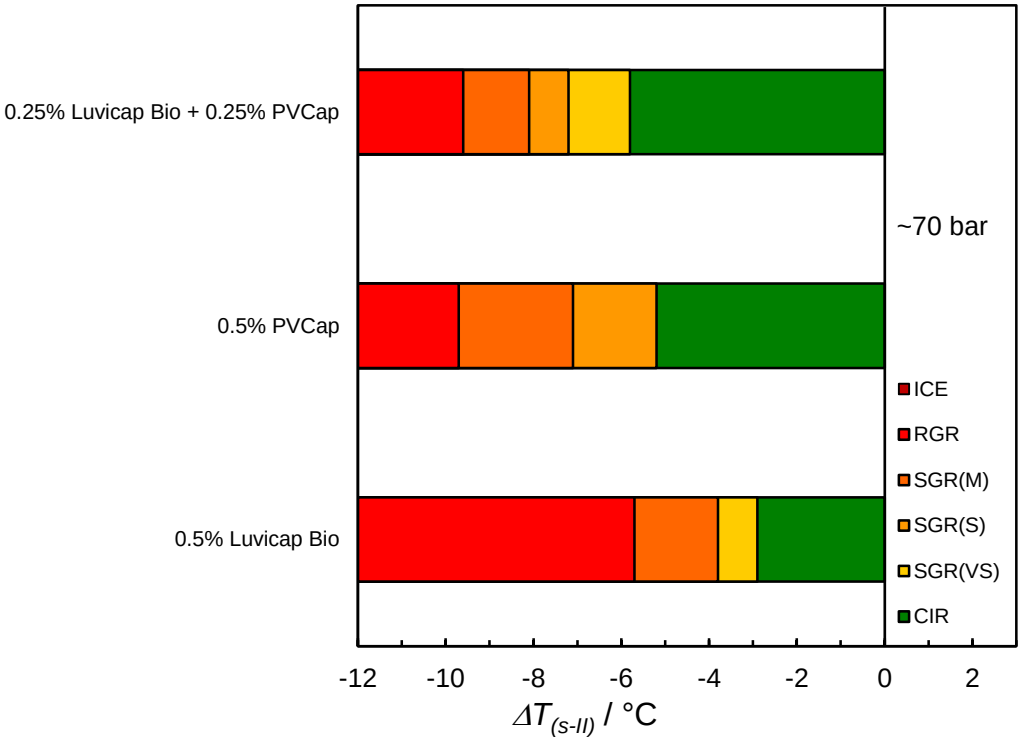

Figure 3-10. Comparison of subcooling extents of measured CGI regions at low hydrate fraction for 0.25 mass% PVCap / 0.25 mass% Luvicap Bio, 0.5% Luvicap Bio, and 0.5% PVCap, all with methane at ~70 bar pressure.

3.4.4 Combination of Luvicap Bio + PVCap in Natural Gas System

In light of the above results to find more evidence and support the theory that Luvicap Bio is a better inhibitor for s-I than it is for s-II and the opposite for PVCap (it is a better inhibitor for s-II), work progressed onto the CGI regions measurement for the combination of Luvicap Bio and PVCap in the natural gas system (composition given in Table 3-1). The reason for this is that it is speculated a better performance of combination of these polymers compared to these polymers alone (at the same aqueous concentration); one inhibiting s-II, the other s-I.

Figure 3-11 shows example CGI method cooling curves with measured points on CGI region boundaries with interpolations for 0.25 mass% PVCap + 0.25 mass% Luvicap Bio with natural gas. Data are reported in Table 3-3. Figure 3-12 and Figure 3-13 show a comparison of subcooling extents of measured CGI regions for 0.25 mass% PVCap + 0.25 mass% Luvicap Bio, 0.5 mass% Luvicap Bio, and 0.5 mass% PVCap, all with natural gas.

As shown in Figure 3-12 and Figure 3-13, the combination of Luvicap Bio and PVCap shows a better performance compared to these polymers alone in terms of improving hydrate inhibition performance. For example, while the CIR extend for the combination of these polymers is 12.9 °C subcooling temperature at 70 bar, the CIR for Luvicap Bio and PVCap alone are 9.4 °C and 9.8 °C respectively. In addition, the results show an additional SGR (VS) region for the combination of these polymers compared to the PVCap or Luvicap Bio alone. Therefore, the results indicate the strong synergism in combination of these polymers in natural gas.

Figure 3-12 and Figure 3-13 show that the synergism effect of PVCap/Luvicap Bio is most evident at lower pressure. Although this is not clear, this might be due to the changes in hydrate structures. If s-II methane hydrates form at lower presser where they are stable, the synergism effect of PVCap /Luvicap Bio would be more expected. In contrast, if one type of structure forms at higher pressure e.g. s-I, the combination of these polymers does not improve hydrate inhibition performance. Meanwhile, the evidence shows that different hydrate structures (C_3/C_4 s-II, C_2 s-II, C_2 s-I, C_1 s-I, C_1 s-II) could be formed in the natural gas system (see Section 3.4.5).

Table 3-3. Measured points on CGI region boundaries with interpolations for 0.25 mass% PVCap / 0.25 mass% Luvicap Bio with natural gas (composition given in Table 3-1).

CGR boundary	Growth rate	T / °C (±0.5)	P / bar (±0.2)	ΔT_{s-I} / °C (±0.5)	ΔT_{s-II} / °C (±0.5)
CIR-SGR(VS)	No growth	1.5	53.5	-8	-13.2
		3.8	72.2	-8.2	-12.9
		6	95.6	-8.2	-12.4
		9	138.4	-7.9	-11.3
		13.5	227	-6.7	-9.1
SGR(S-M)-RGR	Very slow	0.3	53.5	-9.2	-14.4
		2.7	72.2	-9.3	-14
		4.8	94.7	-9.3	-13.5
		8	138.1	-8.9	-12.3
		11.6	223.3	-8.5	-11

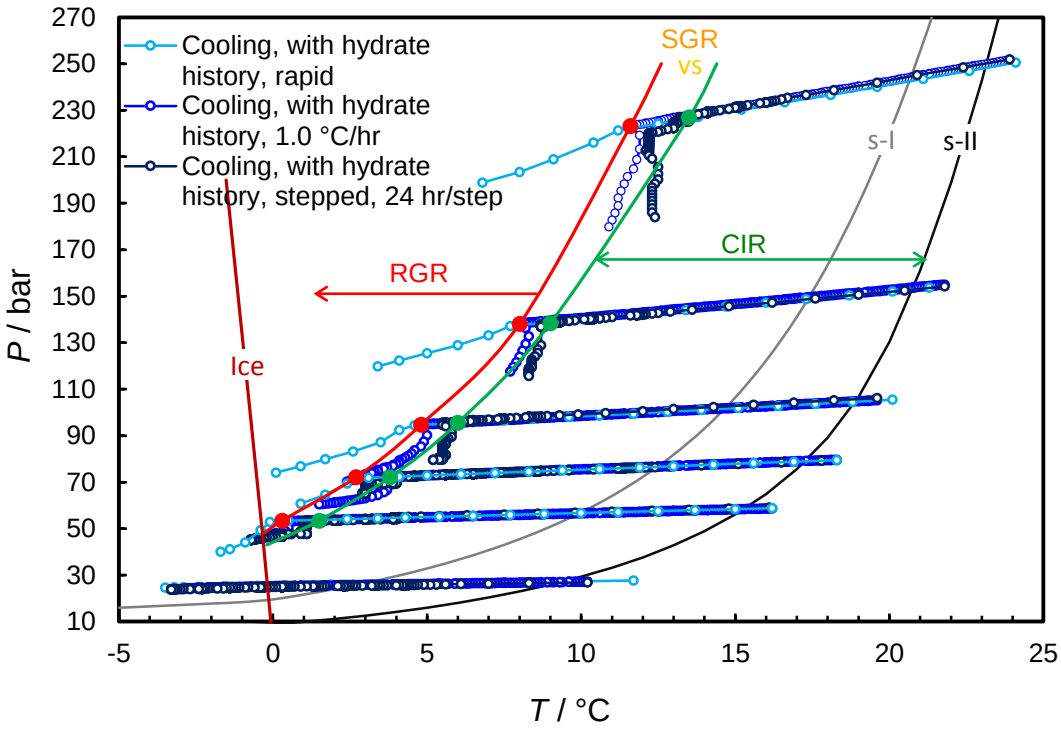

Figure 3-11. Plot of CGI method cooling curves and measured points on CGI region boundaries with interpolations for 0.25 mass% PVCap / 0.25 mass% Luvicap Bio with natural gas (composition given in Table 3-1).

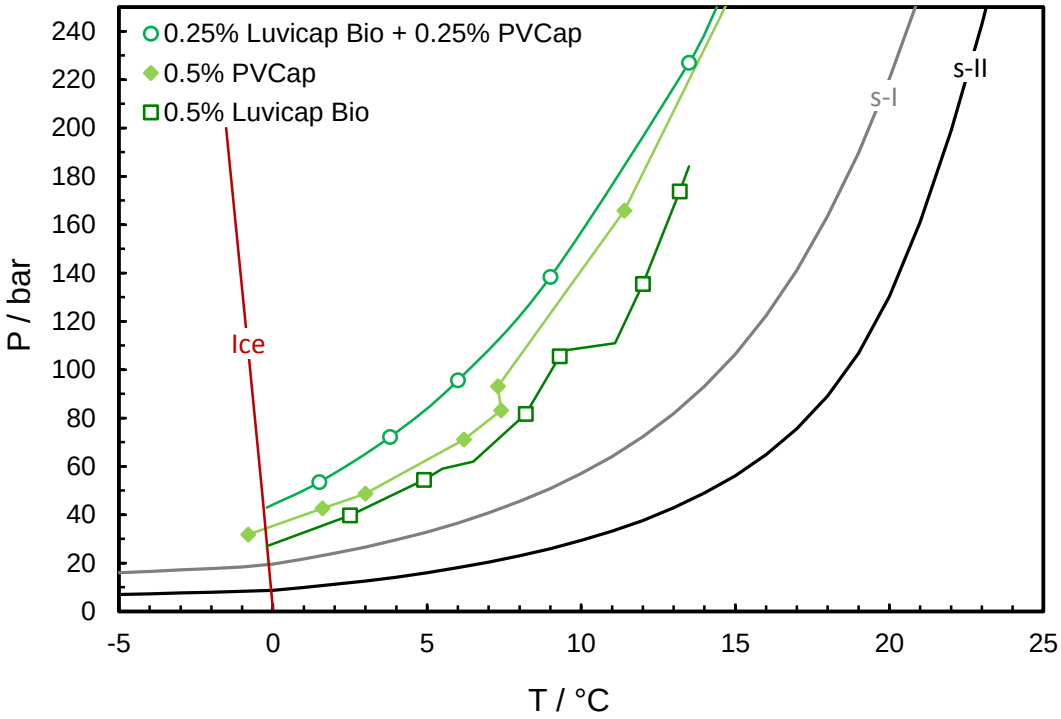

Figure 3-12. Comparison of measured CIR boundaries for 0.25 mass% PVCap / 0.25 mass% Luvicap Bio, 0.5 mass% Luvicap Bio (PT plot showing measured experimental points is reported in A.6), and 0.5 mass% PVCap, all with natural gas. (CGI regions for 0.5 mass% PVCap with natural gas are taken from [3.4])

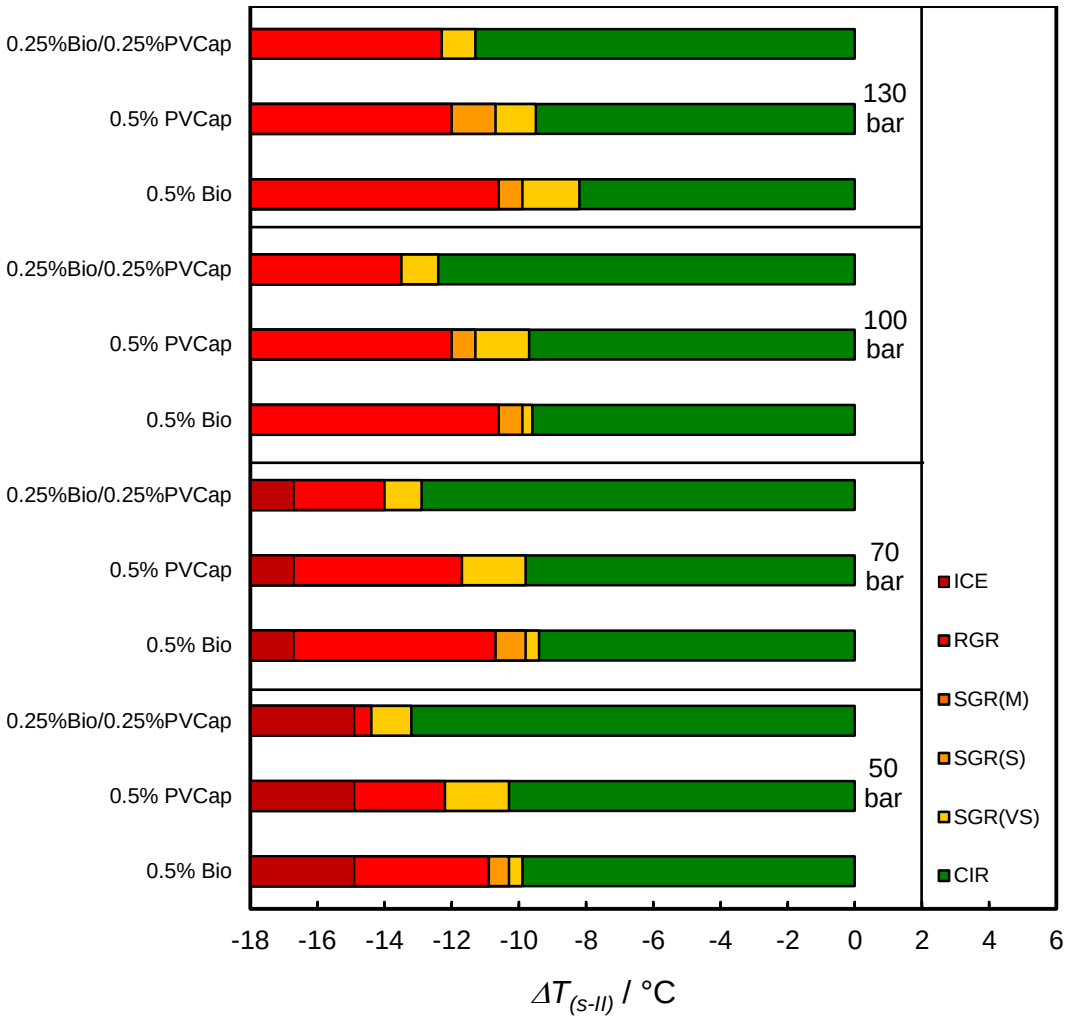

Figure 3-13. Comparison of subcooling extents of measured CGI regions for 0.25 mass% PVCap / 0.25 mass% Luvicap Bio, 0.5% Luvicap Bio, and 0.5% PVCap, all with JIP standard natural gas, for various pressure conditions. (CGI regions for 0.5% PVCap with natural gas are taken from [3.4]).

3.4.5 Gas Hydrate Structure Study in different systems

As discussed, it is speculated that there is formation of s-I and s-II methane hydrate. In addition, it is speculated that there is formation of different hydrate structures (C_3/C_4 s-II, C_2 s-II, C_2 s-I, C_1 s-I, and C1 s-II) in the natural gas system. To study the formation of different hydrate structures, equilibrium step heating/cooling measurement and shut-in-restart run were used. Therefore, works progressed onto the gas hydrate structure study in different systems including propane, ethane, methane, 98 mole% C_1 + 2 mole% C_3, and 85 mole% C_1 + 12 mole% C_2 + 3 mole% C_3. The main purpose of this section is to study the change in hydrate structure, morphology, or growth rate, because it is speculated that the common CGI regions observed for the Luvicap Bio or PVCap system are not as a result of KHI polymers directly and there is an interaction between KHIs and hydrate structures and morphology. So, it is important to find out whether various hydrate structures could be formed in the natural gas system (or even in the simple methane or ethane system) rather than the simple formation of s-II hydrate in the natural gas system.

3.4.5.1 Crystal Growth regions in Propane Systems

To study the crystal growth region in propane system, shut-in-restart run (SIR, see Section 3.3.2) has been carried out for the seeded (hydrate history present) propane-water system (water 70% of cell volume). Figure 3-14 shows PT data for multiple growth rate measurement runs (SIR runs) at different subcoolings for the simple propane-water system. Figure 3-15 shows the pressure drop as a function of time for four different subcoolings with the calculated hydrate growth rate (%hydrate/min) versus time data in Figure 3-16. In addition, hydrate growth rate following restart versus subcooling data at various initial subcoolings is shown in Figure 3-17. As shown in Figure 3-17, subcooling temperature of each SIR run reduced with hydrate formation, i.e., at 0 °C subcooling temperature, conditions have reached equilibrium on the propane hydrate phase boundary, so hydrate growth rate should be zero.

As shown in Figure 3-14, hydrate growth rates are very slow at low subcoolings, points are every minute. Results show that, as would be expected, initial hydrate growth rate increases with increasing of subcooling temperature (driving force). In addition, as shown in Figure 3-14, hydrate growth rates were highest at the beginning of all SIR runs, and the growth rates reduced as the condition reached equilibrium (driving force / subcooling temperature decreased). Figure 3-16 shows the reduction exponential pattern of the reaction process in the formation of propane hydrate at different initial subcoolings. Furthermore, Figure 3-17 clearly indicates the continuous reduction of growth rate as subcooling decreases. Therefore, this pattern of growth rate indicates the formation of a single phase, i.e., a typical exponential type decay is observed as conditions approach equilibrium which is quite similar to the single phase growth reaction pattern. In this system, this single phase should be structure-II propane hydrates, i.e., propane is too large to enter and stabilise the large cavity of s-I ($5^{12}6^2$), it can only enter the largest structure-II hydrate cavity ($5^{12}6^4$) [3.1].

Another point from these results is the possible formation of metastable propane hydrate (green points) below the ice point of water. As shown in Figure 3-15, those SIR runs which initiated at the subcooling below the ice line (red points) reached to the Hydrate + Liquid + Gas (H_m + L + G) line which is metastable. The reason for this is that ice did not nucleate at those SIR runs.

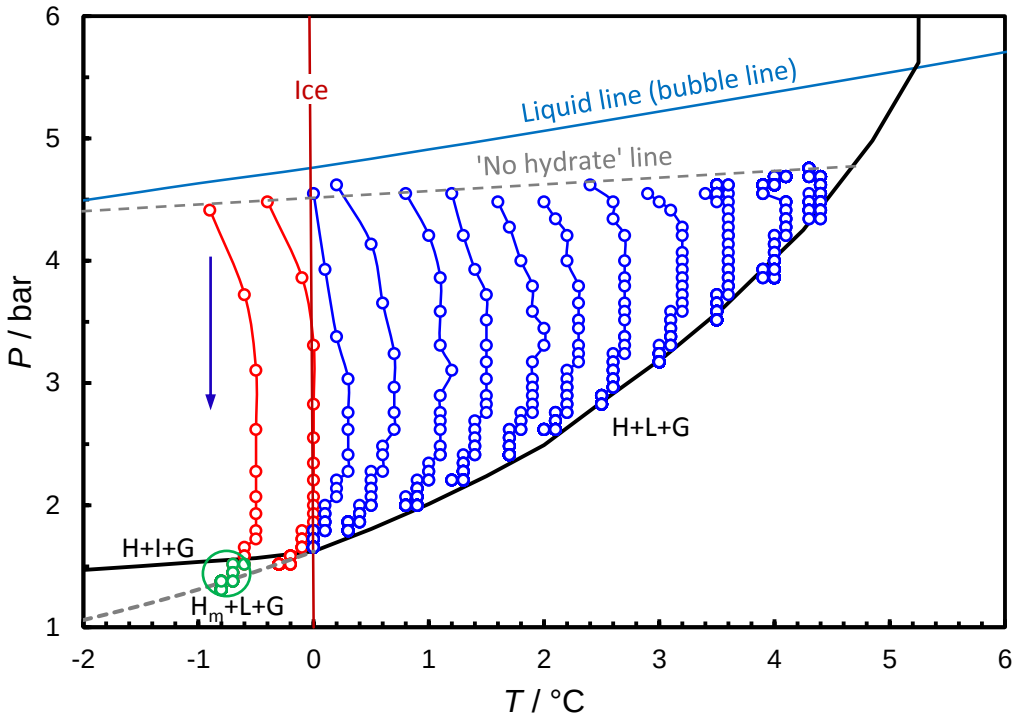

Figure 3-14. Example PT data for multiple growth rate measurement runs at different subcoolings for the simple propane-water system. Points are every minute.

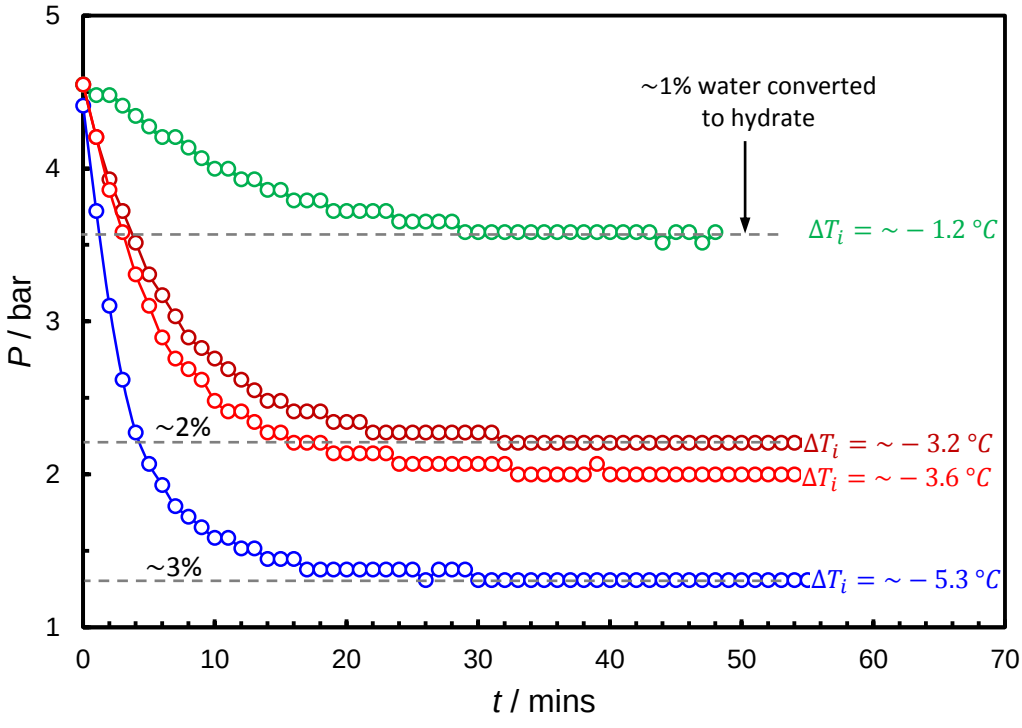

Figure 3-15. Plot of example pressure versus time following restart data for seeded propane-water systems at various initial subcoolings.

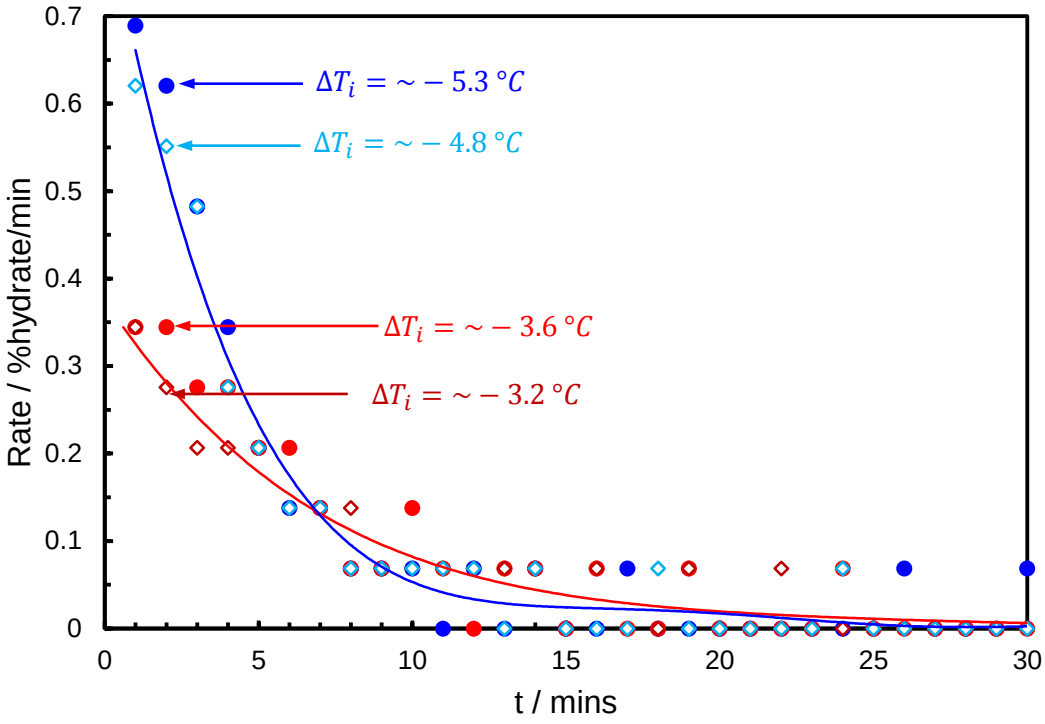

Figure 3-16. Plot of example hydrate growth rate (pressure drop rate) versus time following restart for seeded propane-water systems at various initial subcoolings. Lines are polynomial fits. A typical exponential type decay is observed as conditions approach equilibrium.

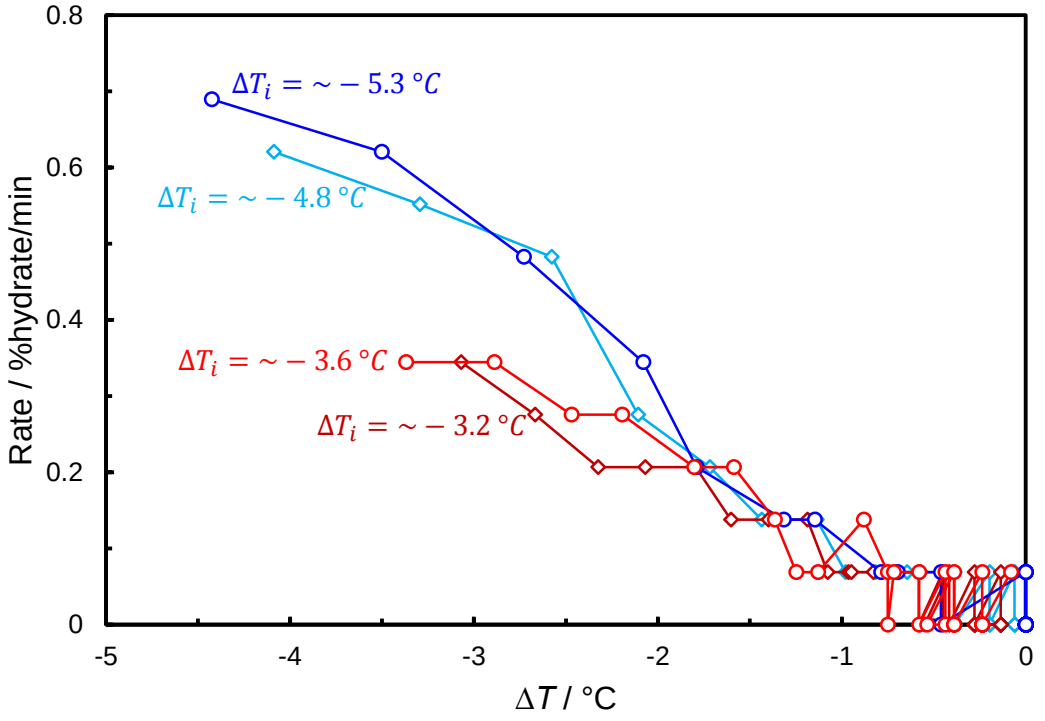

Figure 3-17. Plot of example hydrate growth rate (pressure drop rate) following restart versus subcooling data for seeded propane-water systems at various initial subcoolings. At 0 °C subcooling, conditions have reached equilibrium on the propane hydrate phase boundary.

3.4.5.2 Crystal Growth regions in Ethane Systems

Further investigation on crystal growth regions studies progressed to the ethane system. In theory, ethane can enter the large cavity of s-I ($5^{12}6^2$) and the large cavity of s-II ($5^{12}6^4$) to form both stable s-I and s-II hydrates respectively. Furthermore, it is reported the formation of both stable s-II and s-I of ethane in the presence of methane depending on the pressure/temperature conditions and ethane fraction [3.5][3.6]. Based on this, formation of metastable s-II (or even stable) in the ethane systems is speculated. Therefore, shut-in-restart run (SIR, see Section 3.3.2) has been carried out for the seeded (hydrate history present) ethane-water system (water 70% of cell volume).

Figure 3-18 shows PT data for multiple growth rate measurement runs (SIR runs) at different subcoolings for the simple ethane-water system. Figure 3-19 and Figure 3-20 show example pressure drop and normalised pressure drop ($^{\Delta P}/_{\Delta P_f}$) versus time following restart data for runs initiated at various initial subcoolings respectively. In addition, Figure 3-21 and Figure 3-22 show example hydrate growth rate versus time and subcooling temperature respectively for seeded ethane-water systems at various initial subcoolings.

As shown in Figure 3-18, the pattern for ethane growth rate is different from the data for propane system (Figure 3-14), i.e., while growth rates increase with subcooling temperature in propane system, the growth rates are generally slower at higher subcoolings in the ethane system. As can be seen in Figure 3-18, for the data coloured blue, the same pattern for growth rates similar to propane system has been seen for ethane system. For example, as shown in Figure 3-19, for those SIR initiated at lower subcoolings e.g. -2.6 °C subcooling temperature, rates reduce in an exponential decay-type manner as equilibrium is approached. This indicates a growth of single new hydrate phase, i.e., a typical exponential type decay is observed as conditions approach equilibrium. In addition, in this region (blue data in Figure 3-18), the growth rate increases with increasing subcooling temperature (point are every minute).

As can be seen in Figure 3-18, at higher subcooling temperature (beyond the ~6 °C subcooling temperature), the pattern of growth rate (for the data coloured grey) starts to change. As can be seen, the hydrate growth rate starts to decrease at higher subcoolings after an initial high growth rate. As shown in Figure 3-19 and Figure 3-20, this hydrate

growth rate is almost constant up to ~2 °C subcooling temperature and then the hydrate growth rates increase at subcooling temperature between ~2 °C and ~1 °C before final equilibrium is achieved. This peak growth rate is clearly shown in Figure 3-21 and Figure 3-22. Therefore, two peaks for hydrate growth rate in the ethane system at higher subcooling temperature have been seen; the first one is at initial growth and the second is at subcoolings lower than ~2 °C before final equilibrium is achieved. This result suggests the formation of more than one hydrate phase, i.e., it is not like a typical exponential type decay which is seen in a single phase growth reaction pattern.

As discussed, in theory, ethane can enter both cavity of s-I ($5^{12}6^2$) and the large cavity of s-II ($5^{12}6^4$), i.e., ethane can form stable s-II in the presence of methane as a help gas in the smaller cavities. Furthermore, the results of ethane suggest the formation of more than one hydrate phase in the simple ethane system, and these phases can be s-I and s-II ethane. However, this s-II ethane hydrate is probably a metastable phase and should change to s-I ethane hydrate at equilibrium, though this is speculative still.

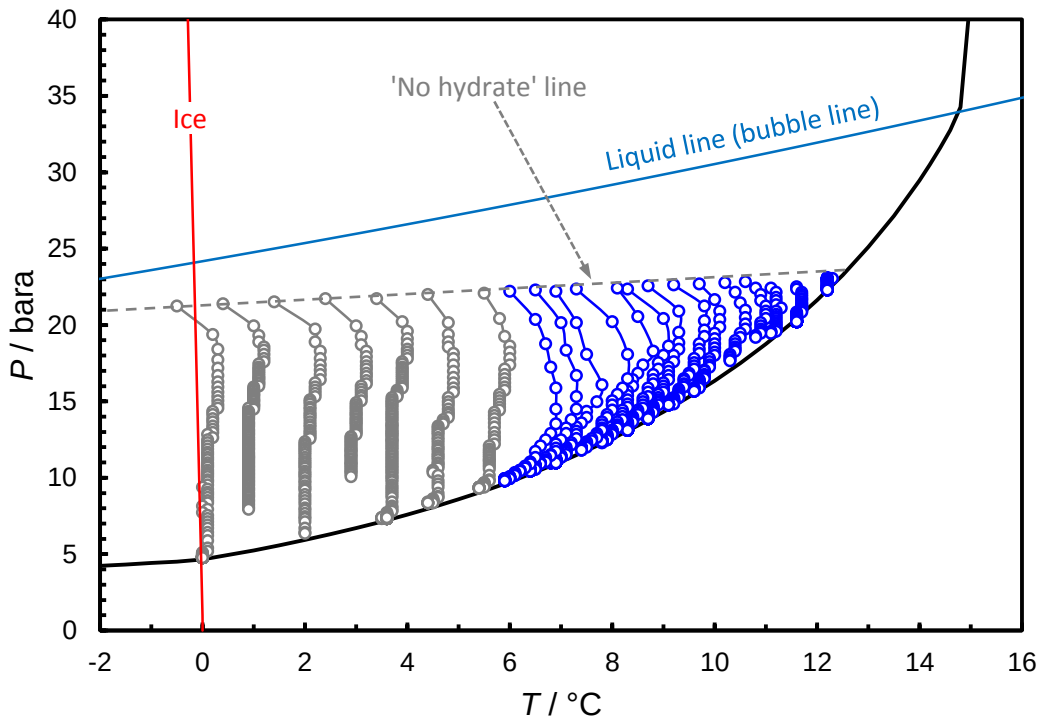

Figure 3-18. Example PT data for multiple growth rate measurement runs at different subcoolings for a simple ethane-water system. Points are every minute. Colours are based on different growth rate pattern.

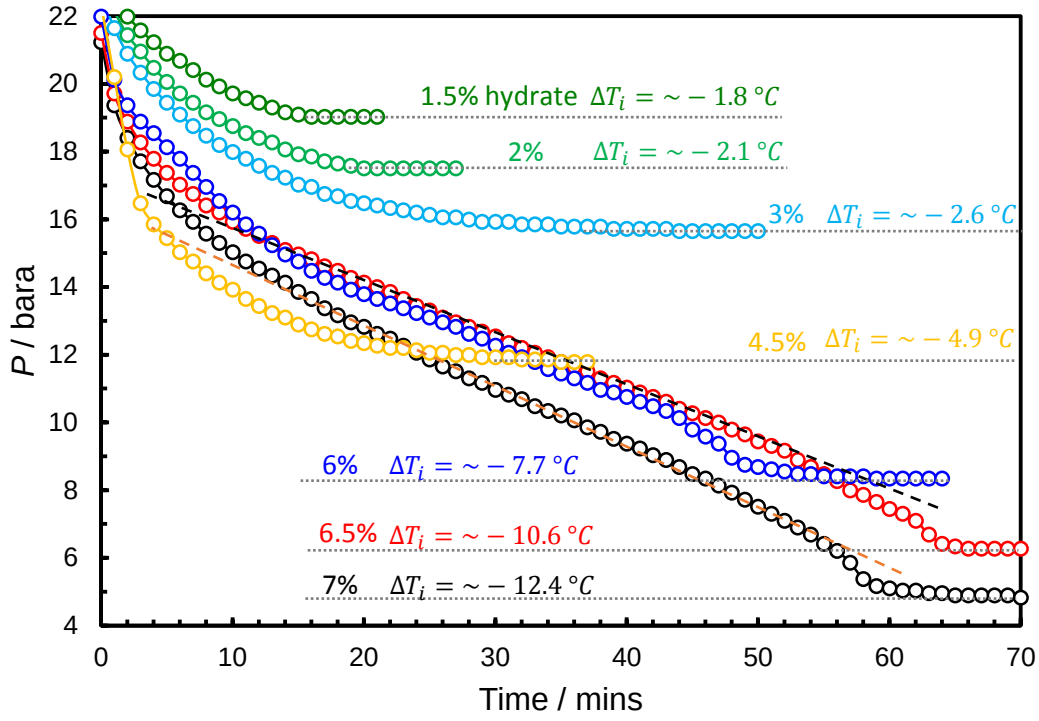

Figure 3-19. Plot of example pressure versus time following restart data for seeded ethane-water systems at various initial subcoolings.

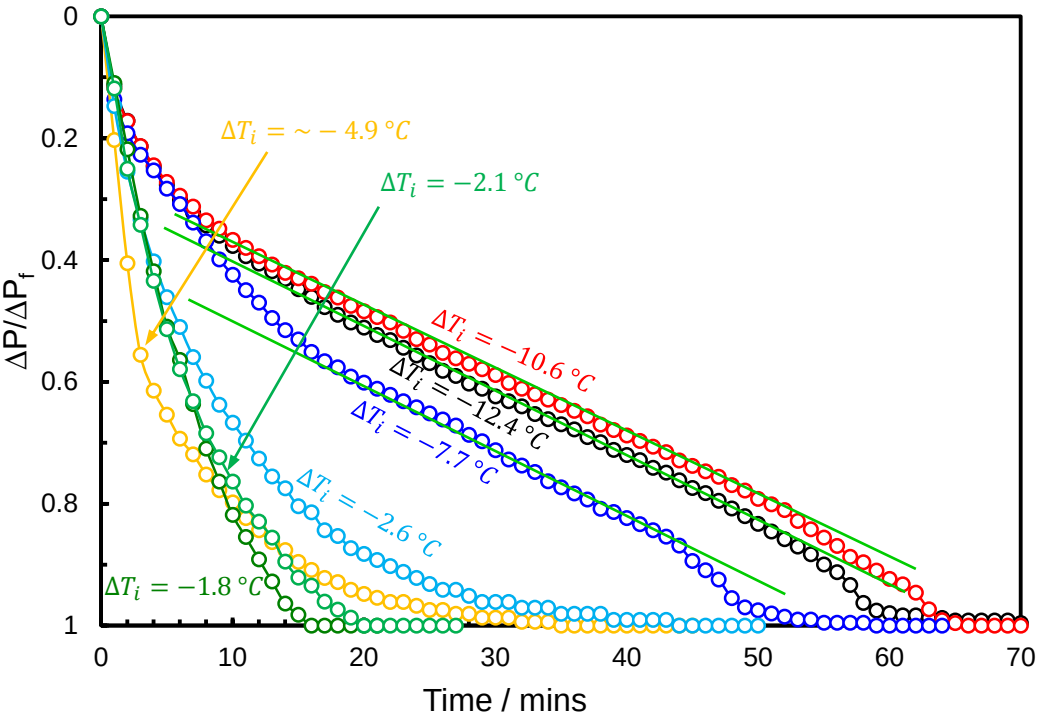

Figure 3-20. Plot of example normalised pressure drop versus time following restart data for seeded ethane-water systems at various initial subcoolings.

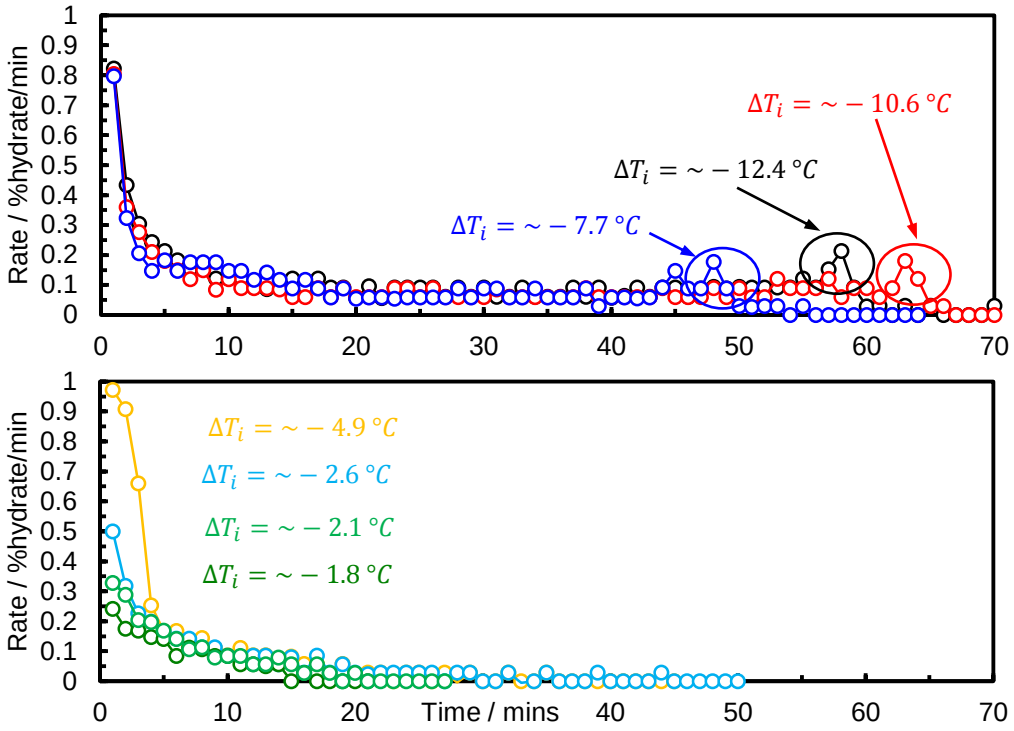

Figure 3-21. Plot of example hydrate growth rate versus time following restart data for seeded ethane-water systems at various initial subcoolings.

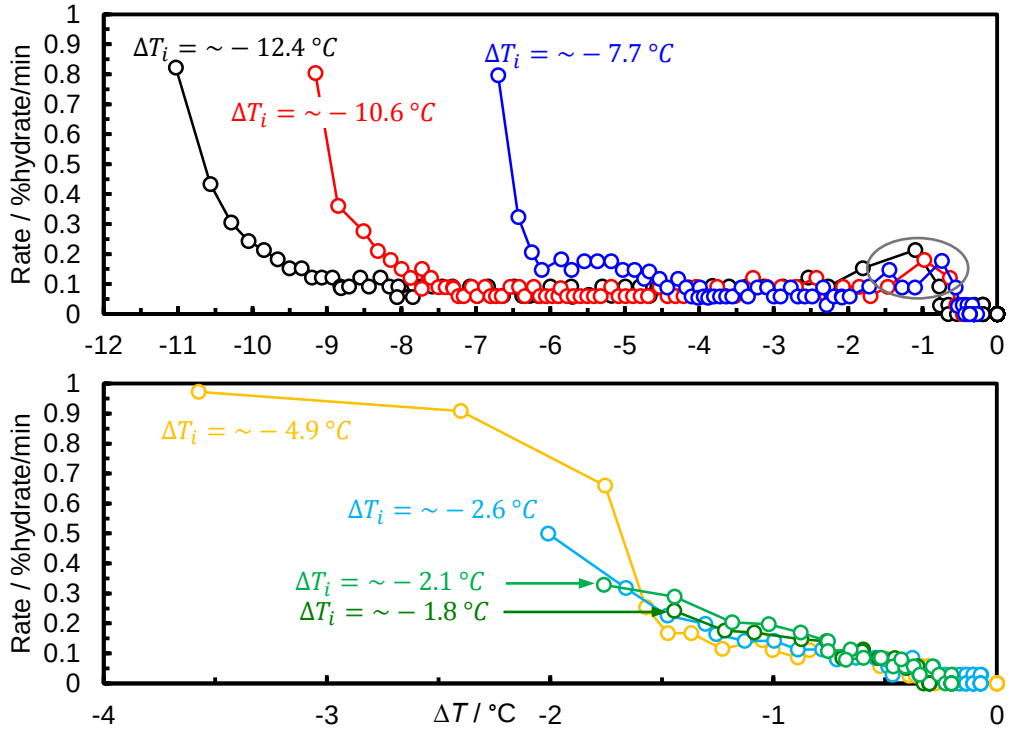

Figure 3-22. Plot of example hydrate growth rate following restart versus subcooling data for seeded ethane-water systems at various initial subcoolings. At 0 °C subcooling, conditions have reached equilibrium on the ethane hydrate phase boundary.

3.4.5.3 Crystal Growth regions in Methane Systems

The shut-in-restart (SIR) tests were undertaken for a simple methane-water system to evaluate the hydrate growth rates/regions as a function of subcooling. To confirm the repeatability of the results, SIR runs were undertaken for three different methane systems; Test-A: methane-water system at ~100 bar with 80:20 water to gas volume ratio, cell position was horizontal; Test-B: methane-water system at ~100 bar with 80:20 water to gas volume ratio, cell position was vertical; Test-C: methane-water system at ~100 bar with 50:50 water to gas volume ratio, cell position was vertical.

Figure 3-23 shows pressure/temperature data for multiple growth rate measurement runs (SIR runs) at different subcoolings for a simple methane-water system at 100 bar (Test- A). As can be seen, a clear change in hydrate growth rate as a function of subcooling temperature could be observed in Test-A. As it is expected, the hydrate growth rates are very slow at low subcoolings and the growth rates were observed to increase progressively as subcooling increases up to 3.8 °C (CIR for the 0.5% Luvicap Bio in the methane system). Beyond this subcooling temperature, the hydrate growth rates start to decrease; the region between 3.8 °C and 7.2 °C subcooling temperature as shown in Figure 3-23. As subcooling temperature increases, clear jumps in hydrate growth rates were observed beyond 7.2 °C; the hydrate growth rates start to increase suddenly beyond this subcooling temperature, then remain constant after it. This 7.2 °C subcooling temperature from s-I methane is a common CGI boundary seen for KHIs.

In addition, SIR runs were carried out for another water-methane system (Test-B) at ~100 bar with 80:20 water to gas volume ratio in an autoclave, but the experimental setup was positioned in vertical orientation. Figure 3-24 shows pressure/temperature data for multiple growth rate measurement runs (SIR runs) at different subcoolings for a simple methane-water system at 100 bar (Test-B). In contrast to Test-A, this system (Test-B) was allowed to form hydrates to reach the equilibrium, s-I methane hydrate phase boundary. As Test-A, a clear change in hydrate growth rate as a function of subcooling temperature could be observed in Test-B.

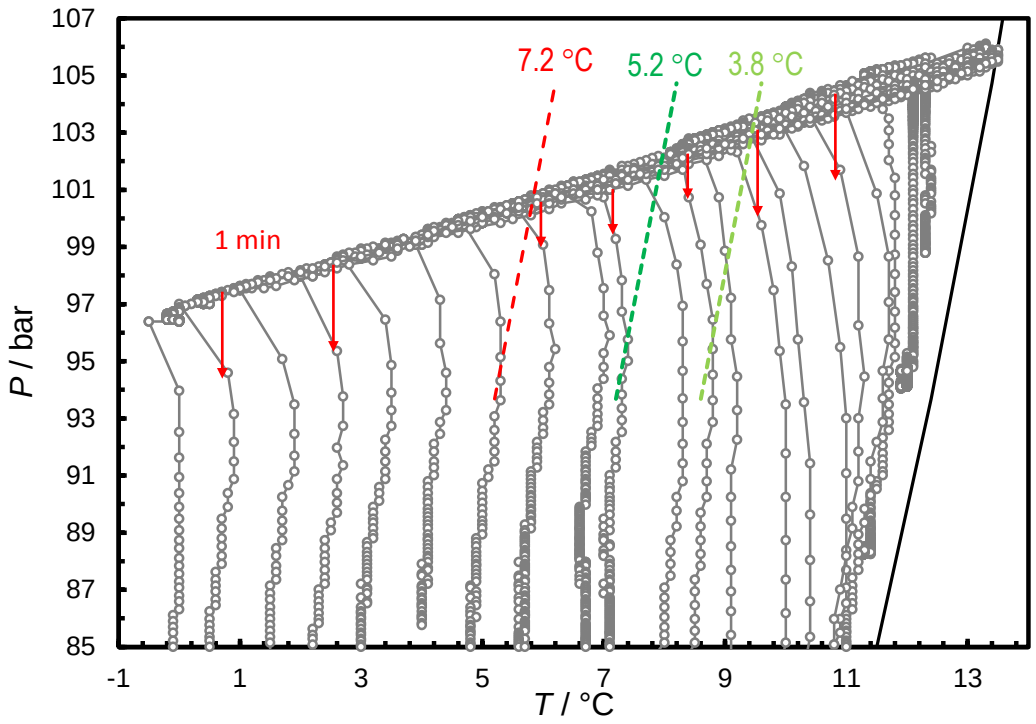

Figure 3-23. Example PT data for multiple growth rate measurement runs at different subcoolings for a simple methane-water system at ~100 bar (Test-A). Points are every minute. Test with 80% water cut was carried out in autoclave. Cell position was horizontal. 3.8 °C and 5.2 °C subcooling temperature are the CIR for 0.5% Luvicap Bio and 0.5% PVCap in the methane system respectively.

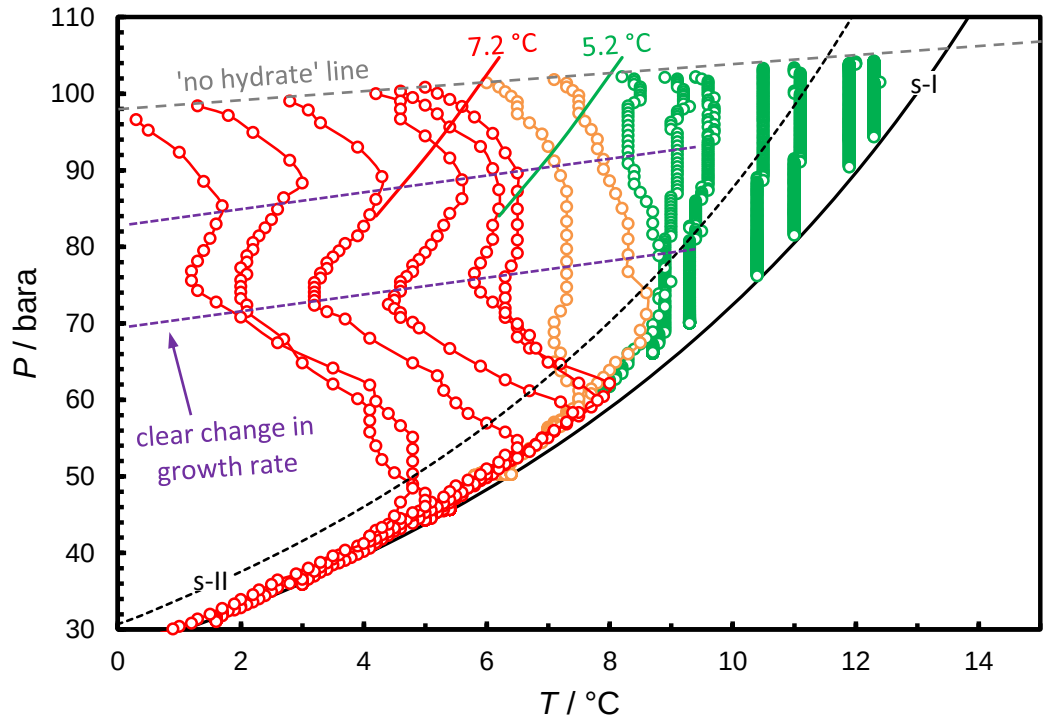

Figure 3-24. PT data for multiple growth rate measurement runs at different subcoolings for the 80:20 water to gas volume ratio, methane-water system (Test-B). Points are every minute. Colours are based on CGI region extents for 0.5% PVCap with methane. Cell position was vertical.

Figure 3-25 shows the time in minutes taken for 1% water conversion to hydrate upon restart as a function of subcooling for autoclave methane experiments with an initial starting pressure of ~100 bar (Test-B). As would be expected, the growth rate for the initial small fraction of hydrate (e.g. 1% water converted to hydrates) increases with subcooling temperature. As shown in Figure 3-24, if a larger pressure drop (higher hydrate fraction) is considered for initial growth rate, reduction of hydrate growth rate at higher subcooling temperature could be observed. As can be seen in red points in Figure 3-24, the growth rates were initially very high, then reduced significantly as hydrate fraction increased, and finally increased as the system reached to the s-I methane hydrate phase boundary. This behaviour was also observed in the simple ethane system, as shown in Figure 3-18.

The question may then arise as whether this reduction of hydrate growth rate was because of the mixing problem or whether increasing of hydrate growth rate after the initial reduction in growth rate was due to mixing; as results show the hydrate growth rate was highest as the system moved back to the equilibrium which is not expected for a normal progress of chemical reaction (a typical exponential type decay is expected as conditions approach equilibrium). Therefore, to assess whether the mixing problem was the case, different parameters were checked. As discussed, the SIR runs were done for the methane-water system in two different cell positions; horizontal (Test-A) and vertical (Test-B). Results for both cell positions showed a general same pattern for hydrate growth rate. In addition, it was not observed any blockage of stirrers during hydrate formation; the rpm remained constant through each SIR run. Furthermore, it was checked that if the impellers could shear the water/gas interface in both horizontal and vertical positions (this was the case for all systems); if impellers cannot shear the water/gas interface, there is a possibility of a layer of hydrate forming between gas and water, resulting in hydrate growth rate reduction. However, the maximum calculated water converted to hydrates at highest subcooling test (for Test-A, 80% water cut) is around 6% conversion which is relatively very low to reduce heat/mass transfer requirement. Nevertheless, the repeatability of the results in all systems, no blockage of stirrers (constant rpm) during hydrate formation, and ensuring the shearing of water/gas interface by impellers indicate that reduction of hydrate growth rate after initial high growth rate was not due to mixing problem. Therefore, the clear changes in hydrate growth rate should be possible due to phase changes, as was the case for ethane.

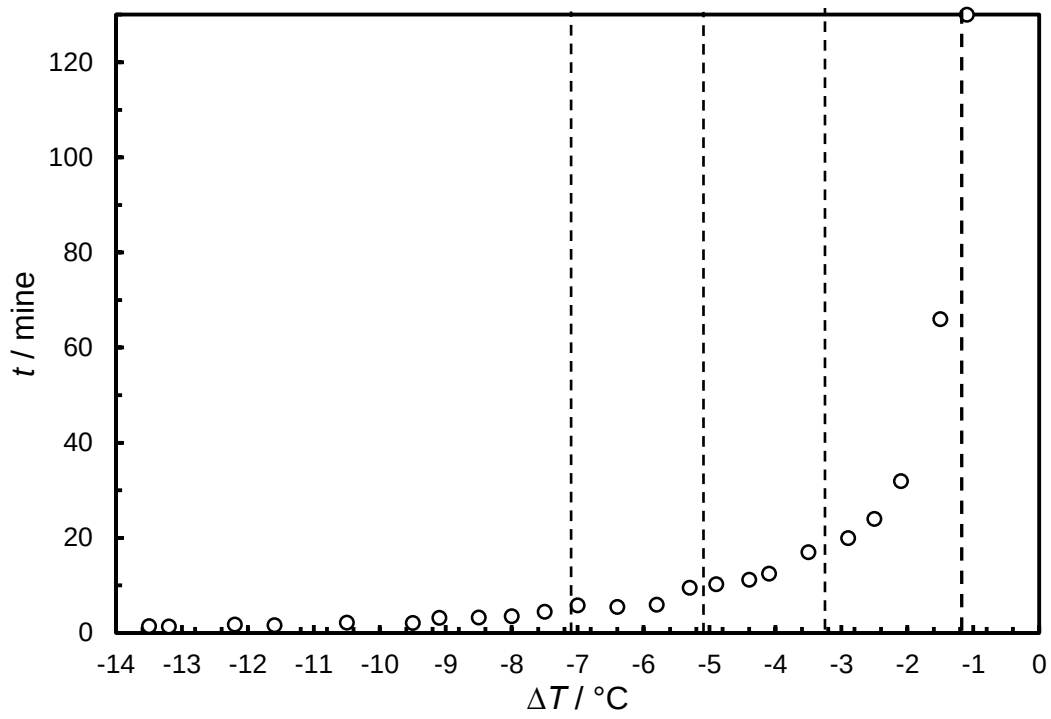

Figure 3-25. Time in minutes taken for 1% water conversion to hydrate upon restart as a function of subcooling for autoclave methane experiments with an initial starting pressure of ~100 bar (Test-B). Dashed lines are the subcoolings where KHI CGI region boundaries are commonly observed. Water cut was 80%. The cell position was vertical.

Figure 3-26 and Figure 3-27 show example normalised pressure drop ($^{\Delta P}/_{\Delta P_f}$) versus time and subcooling temperature respectively, following restart data for runs initiated at various initial subcoolings for seeded methane-water system (Test-B). In addition, Figure 3-28 and Figure 3-29 show example hydrate growth rate versus time and subcooling temperature respectively for seeded methane-water system (Test-B) at various initial subcoolings.

As shown in Figure 3-27, clear changes in hydrate growth rates are obvious at high subcooling temperatures. As can be seen in Figure 3-28, the hydrate growth rate pattern was not a typical exponential decline type reaction, and various peaks were observed. For example, for the SIR run initiated at 5.5 °C subcooling temperature, the highest growth rate was observed at the end of SIR run, before going back to the equilibrium (1.1 °C subcooling). For those SIR run initiated at higher subcoolings (>~5 °C initial subcooling), more than one peak was observed. These peaks probably suggest the formation of new hydrate phase.

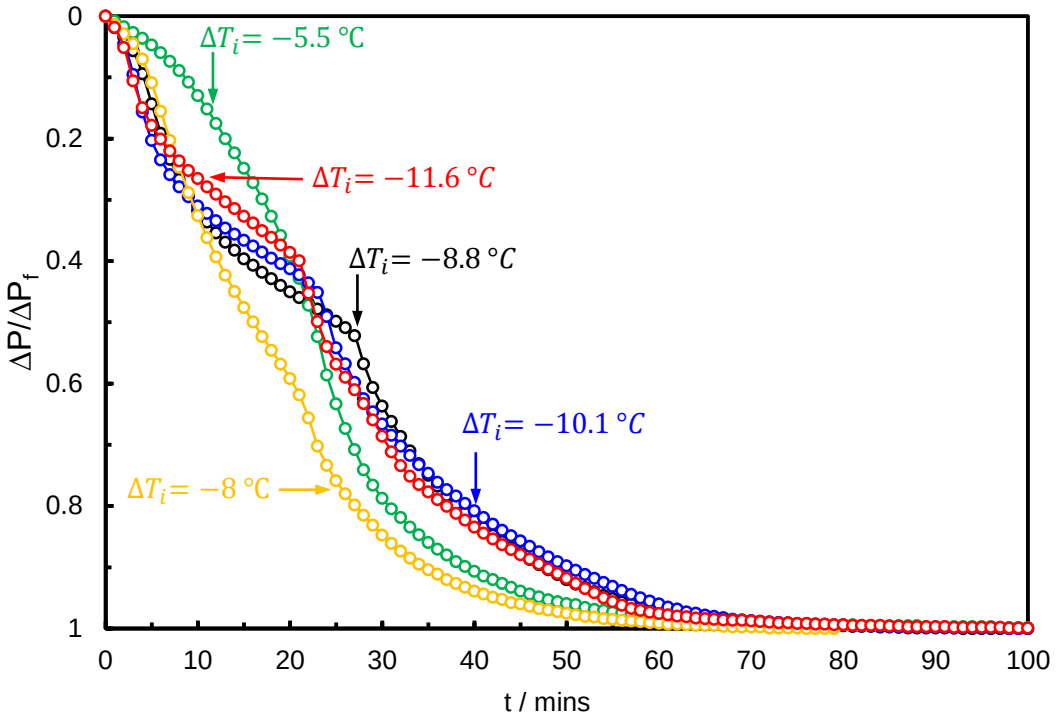

Figure 3-26. Plot of example normalised pressure drop versus time following restart data for seeded methane-water system with an initial starting pressure of ~100 bar (Test-B) at various initial subcoolings. Water cut was 80%. The cell position was vertical.

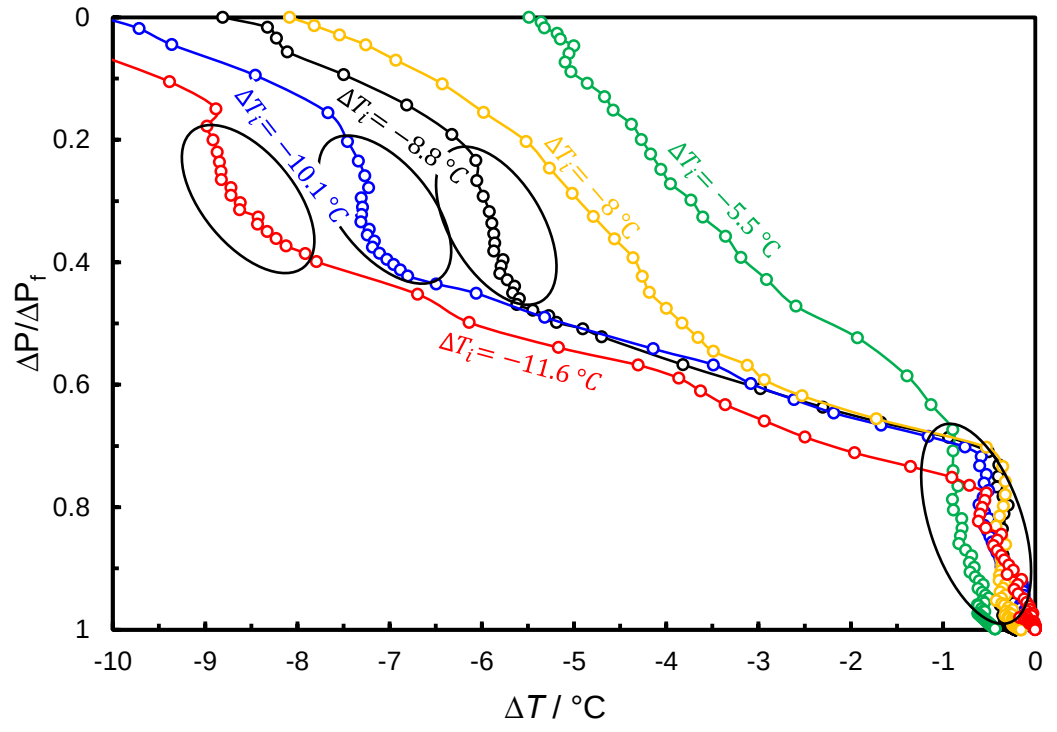

Figure 3-27. Plot of example normalised pressure drop versus subcooling temperature following restart data for seeded methane-water system with an initial starting pressure of ~100 bar (Test-B) at various initial subcoolings. Water cut was 80%. The cell position was vertical.

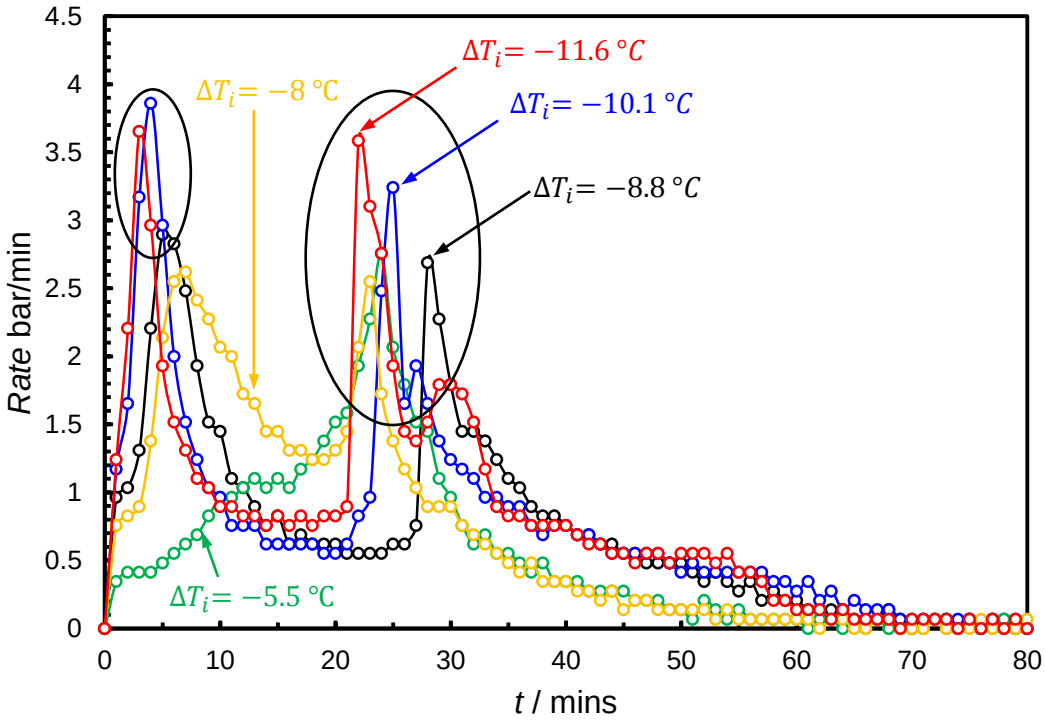

Figure 3-28. Plot of pressure drop rate (approximately corresponds to hydrate growth rate) versus time for example seeded methane-water system with an initial starting pressure of ~100 bar (Test-B) at various initial starting subcoolings (indicated). Water cut was 80%. The cell position was vertical.

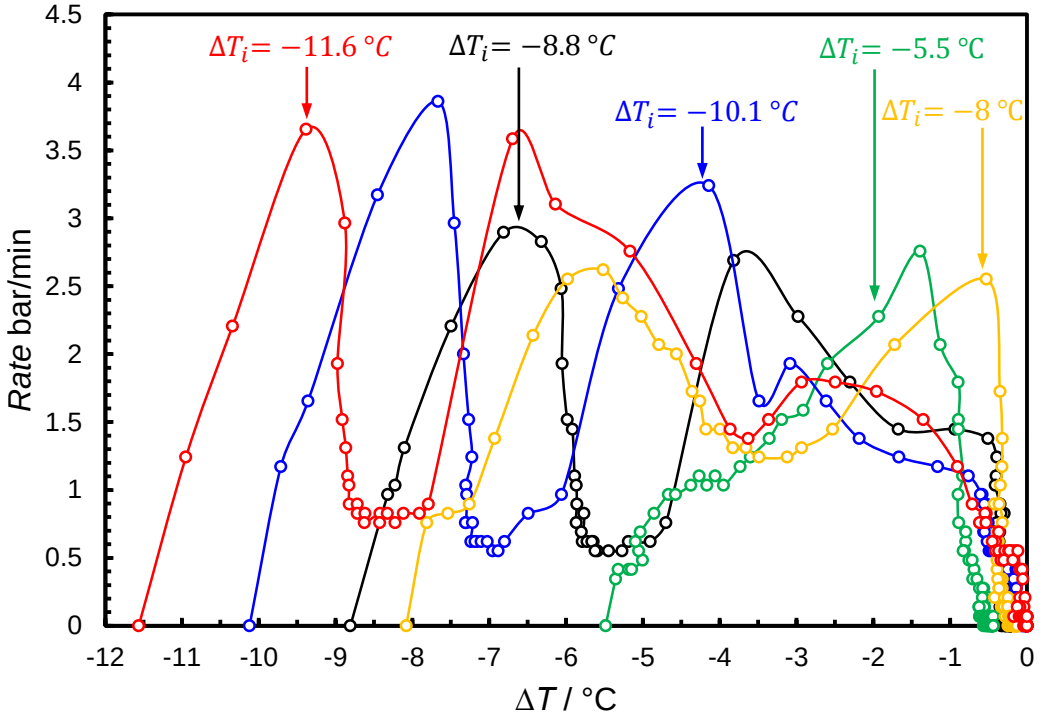

Figure 3-29. Plot of pressure drop rate (approximately corresponds to hydrate growth rate) versus subcooling temperature for example seeded methane-water system with an initial starting pressure of ~100 bar (Test-B) at various initial starting subcoolings (indicated). Water cut was 80%. The cell position was vertical.

Figure 3-30 shows the size of the measured exotherm (cell T minus set temperature T_0) as a function of subcooling for various hydrate growth runs on the methane-water system (Test-B). As can be seen, two peaks for the measured exotherm were observed and the biggest peak occurred towards the end of the hydrate formation process (~1.8 °C subcooling temperature which is predicted by HydraFLASH as a phase boundary for s-II methane hydrate). Therefore, the thermal aspect of detection studies, as another evidence, support the potential formation of more than one hydrate phase e.g. two methane structures, i.e., once a new hydrate phase starts to grow, hydrate growth rate and heat released due to exothermic nature of hydrate formation start to change.

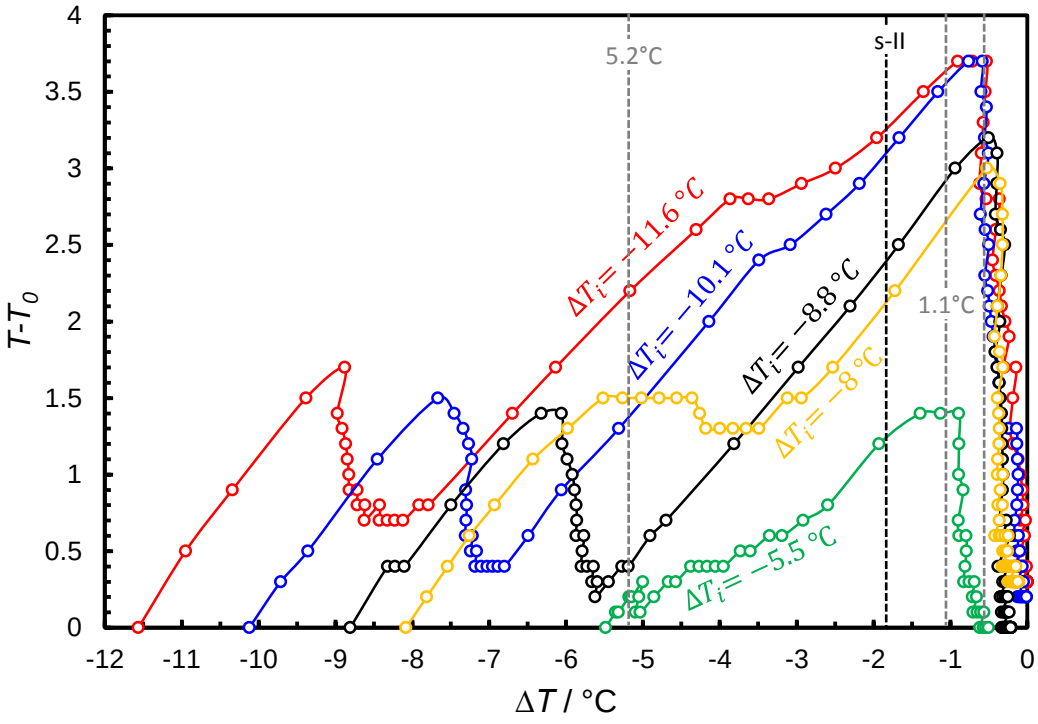

Figure 3-30. Size of the measured exotherm (cell T minus set Temperature T_0) as a function of subcooling for various hydrate growth runs on the methane-water system with an initial starting pressure of ~100 bar (Test-B). Dashed lines are for where changes in growth patterns are seen in this test and also historically in the presence of KHI polymers. Water cut was 80%. The cell position was vertical.

As discussed, the thermal aspect of detection in methane hydrate growth rate support the potential theory of formation of more than one hydrate phase in the methane systems, i.e., formation of two structures or solid-solid transition from one structure to another could be observed thermally. The water to gas volume ratio for the Test-A and Test-B was 80%; this high water to gas ratio reduces the potential thermal detection. Therefore, another test (Test-C) was carried out for a methane-water system at ~100 bar with 50:50 water to gas volume ratio, cell position was vertical. The aim was to allow the system to have higher hydrate fraction during SIR runs; the heat released during hydrate formation could affect the system temperature which is more quantifiable. In addition, the cell was equipped with motor current recording (amps to maintain set rpm) which could support more for formation of two phases/structures in the methane system, as discussed later.

Figure 3-31 shows pressure/temperature data for multiple growth rate measurement runs (SIR runs) at different subcoolings for the simple methane-water system (Test-C). Figure 3-32 shows the size of the measured exotherm (cell T minus set temperature T_0) as a function of subcooling for various hydrate growth runs on the methane-water system (Test-C).

Similar to the previous results for methane hydrate growth rate experiments (Test-A and Test-B), Figure 3-31 shows that the initial hydrate growth rates (initial pressure drop) increased with subcooling for Test-C. In addition, for those subcoolings higher than 5.2 °C, hydrate growth rate increased after an initial slower rate which is in contrast to exponential type decay rate. Furthermore, after this rate acceleration, hydrate growth rate decreased, then accelerated again close to around 1.8 °C subcooling temperature. These results are pretty similar to the results for Test-A and Test-B.

Furthermore, exploring the exothermic behaviour of this experiment reveals more evidence of formation of more than one structure in the methane systems. As shown in Figure 3-32, for those SIR runs initiated at low subcoolings (green points), the system temperature did not change; hydrate growth rates were very slow and heat released was insufficient to increase the cell temperature. In contrast, while temperature increased for those SIR runs initiated at higher subcoolings (amber and red points), some peaks of exotherm were observed. Similar to Test-B, the peaks of all exotherms were observed at the end of hydrate formation, around 1.8 °C subcooling temperature which is the theoretical stability limit for s-II methane predicted by HydraFLASH.

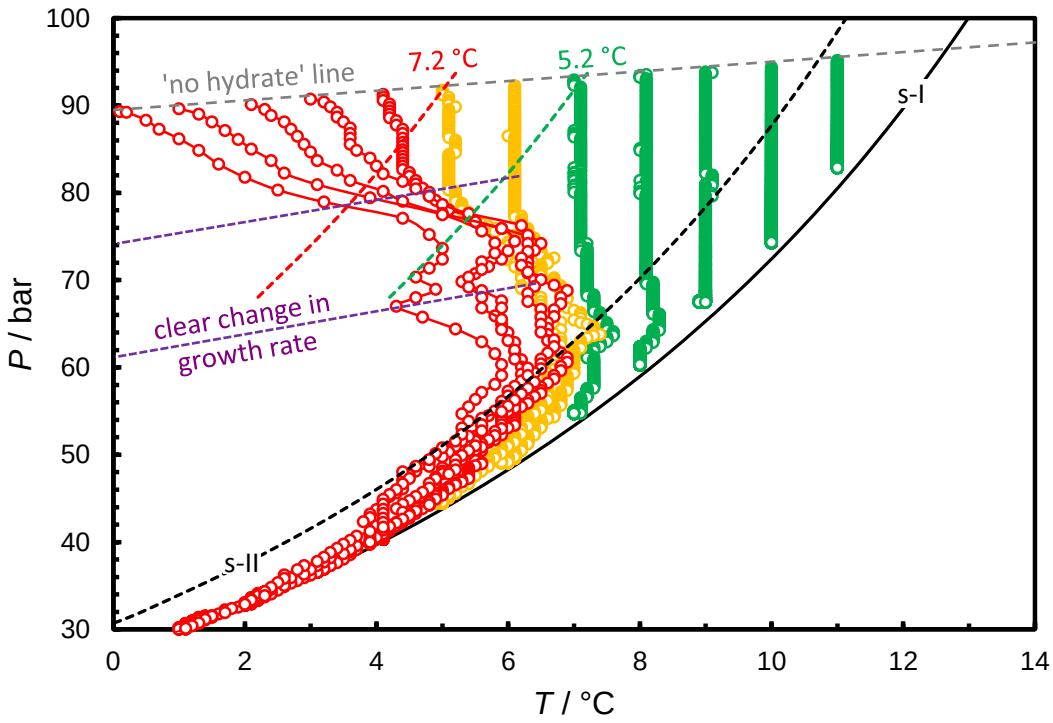

Figure 3-31. PT data for multiple growth rate measurement runs at different subcoolings for the 50:50 water to gas volume ratio, methane-water system (Test-C). Points are every minute. Colours are based on CGI region extents for 0.5% PVCap with methane. Cell position was vertical.

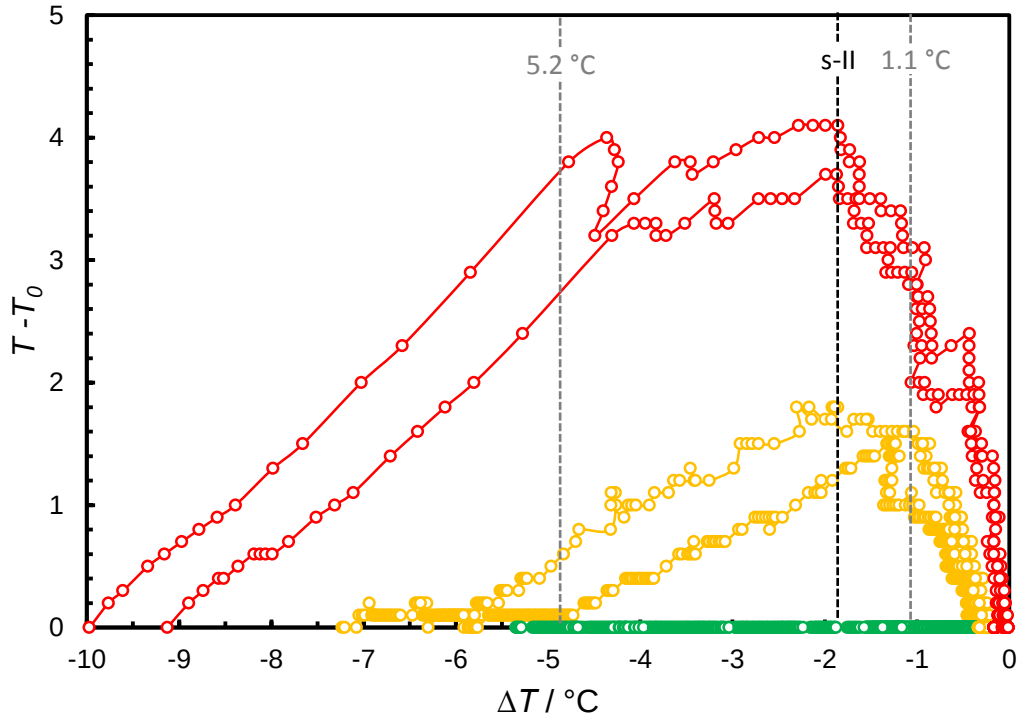

Figure 3-32. Size of the measured exotherm (cell T minus set Temperature T0) as a function of subcooling for various hydrate growth runs on the methane-water system (Test-C). Dashed lines are for where changes in growth patterns are seen in this test and also historically in the presence of KHI polymers. Water cut was 50%. The cell position was vertical.

As shown in Figure 3-32, the measured exotherm at the subcooling temperature around 2 °C is strongly sustained; suggesting although very little hydrates formed, some reaction occurred which could release too much heat and sustain the system temperature. This might be due to solid-solid transition (s-II to s-I transition). Further support from solid-solid transition could be observed from the motor current data during SIR runs (This interpretation is a joint work product of R. Anderson and M. Aminnaji which is taken from JIP Project at Heriot-Watt University [3.3]). Figure 3-33 and Figure 3-34 show a plot of change in stirrer motor current as a function of subcooling temperature and time respectively for the methane hydrate growth rate tests (Test-C) for various initial subcoolings.

As can be seen, for those SIR runs initiated at high subcooling temperature (red and amber points), the motor current starts to increase after the 5.2 to 4.0 °C subcooling range. From the previous results, it was suggested that a new phase of hydrates (it might be s-II methane) formed in the 5.2 to 4.0 °C subcooling range. The motor current continued to rise up to 1.8 to 1.1 °C subcooling range, then reduced as the system moved back to equilibrium. The motor current at the equilibrium conditions was as same as the system with a subcooling temperature beyond the 5.2 °C. While the fraction of hydrate increased, these peaks at the lowest subcooling around 1.8 °C (predicted as the limit of s-II methane hydrate stability) suggesting solid-solid transition which coincides with the other results e.g. the peaks for growth rate and exothermic s-II to s-I transition. However, this solid-solid transition needs dissociation and regrowth of hydrate phase which could be exothermic.

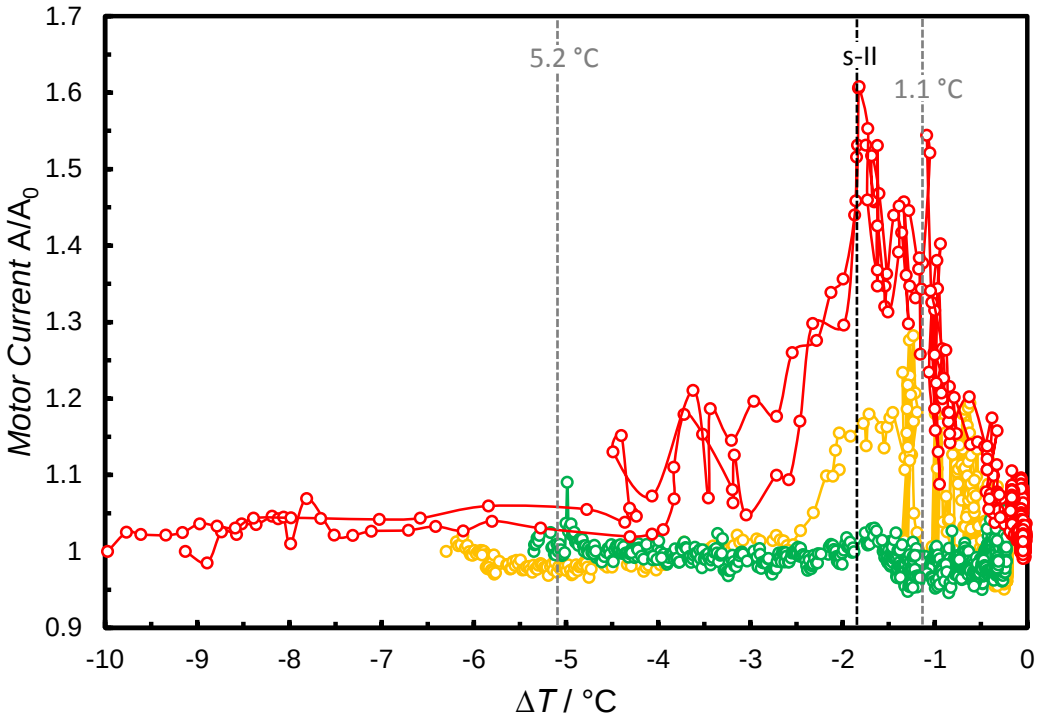

Figure 3-33. Plot of change in stirrer motor current (amps divided by initial amps, A/A0) as a function of subcooling for various hydrate growth runs on the methane-water system (Test-C). Water cut was 50%. The cell position was vertical.

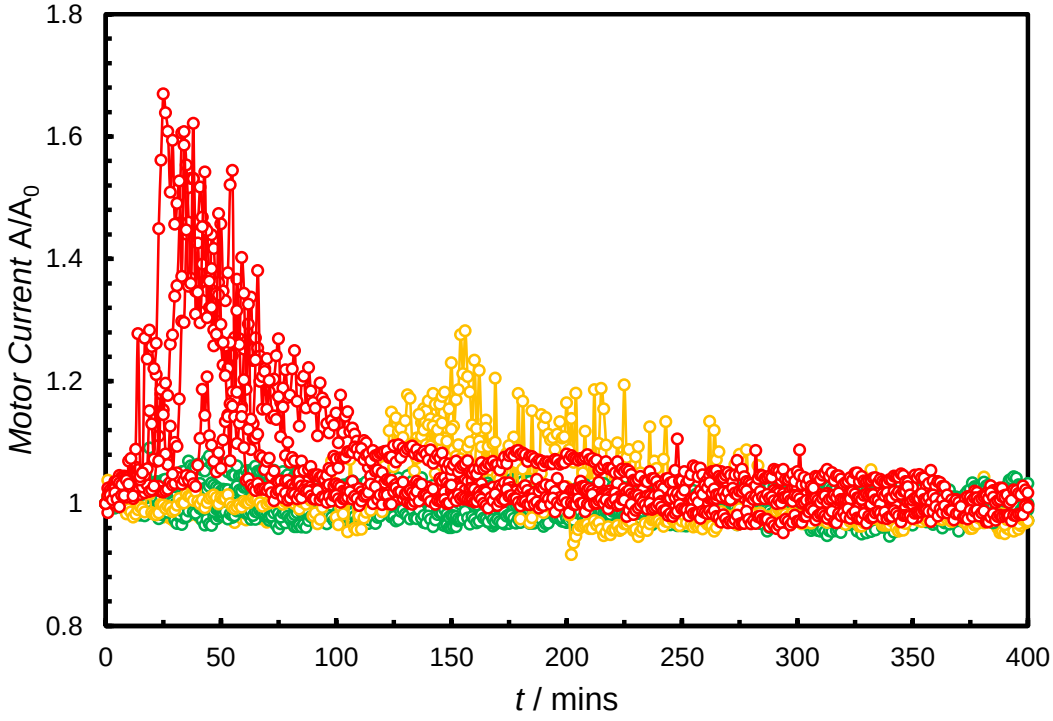

Figure 3-34. Plot of change in stirrer motor current (amps divided by initial amps, A/A0) as a function of time for various hydrate growth runs on the methane-water system (Test-C). Water cut was 50%. The cell position was vertical.

As methane hydrate is generally known to form s-I hydrates, these results are not as would be expected. As discussed, while a typical growth rate for reaction process is the exponential type decay, more than one reaction rate peaks were observed in the simple methane hydrate formation systems. These peaks strongly suggest the formation of more than one phase in the system; as discussed, mixing problem and mass/heat transfer limitation were not the case for the methane systems tested. Therefore, it is speculated that the second phase could be s-II methane hydrate, although it might be metastable.

Although in theory, methane can enter the 5^{12} and $5^{12}6^4$ cavities for s-II, it is too small to stabilise the large cavity of structure-II. Therefore, methane can better stabilise the large cavity of s-I than s-II. However, this is not meaning that s-II methane hydrate cannot form; it means that s-I methane is more stable than s-II methane, depending on PT conditions. Some limited studies confirm the formation of s-II methane as a stable phase at lower temperatures / higher pressures [3.7][3.8][3.9][3.10].

Schicks and Ripmeester (2004) reported the formation of both s-I and s-II methane hydrate at the conditions of 30 to 90 bar and 1.5 to 12 °C which are similar to the experiments studied here [3.11]. Although the authors showed the co-existence of the two structures of methane, they indicated that the s-II methane was a metastable phase and finally converted to s-I methane. Nevertheless, the formation of the two structures of methane at the conditions of the experiments studied here are possible and can describe the behaviour of methane growth rates seen here.

Furthermore, as discussed, the pattern of simple propane hydrate growth rate which can form only s-II (exponential type decay as exactly would be expected for the growth of a single new phase) is another evidence to support the theory of formation of more than one structure in the methane systems, i.e., different growth rate changes and various growth rate peaks were observed in the methane systems.

In addition, s-II methane hydrate phase boundary predicted by HydraFLASH® (which is at around 2 °C subcooling temperature from s-I) is another evidence to support the theory of formation of s-II methane hydrates and its potential transient to s-I methane hydrates. As results show, a clear change/peak in hydrate growth rate was observed around 1.8 °C subcooling temperature for all SIR runs.

3.4.5.4 Crystal Growth regions in $C_1 + C_3$

As discussed, the results indicate the formation of s-I and s-II in both simple methane and ethane. Further investigation on the formation of various hydrate structures progressed on the system with 98 mole% C_1 + 2 mole% C_3. In contrast to the previous procedure (SIR runs) for hydrate growth rate studies, step heating and step cooling measurements (see Section 3.3.1) were carried out in this experiment, to investigate multiple hydrate structures in the natural gas system and possible hydrate equilibrium phase boundary associated with different hydrate structures. This is because that it is speculated the common CGI regions observed for the KHI system are not as a result of KHI polymers directly and there is an interaction between KHIs and hydrate structures.

Figure 3-35 shows a plot of pressure / temperature data for constant cooling (1 °C / hour) then equilibrium step heating and step cooling measurements in the two components natural gas system (98 mole% C_1 + 2 mole% C_3). As can be seen, a clear change in the slope of the measured equilibrium step heating/cooling curve was observed. As shown in Figure 3-35, data points for both equilibrium step cooling and step heating runs indicate the sequential formation of multiple hydrate phases of different composition and structures during hydrate growth, as evidenced by changes the slope of the measured equilibrium step heating and step cooling curve. Moreover, constant cooling confirms this sequential formation of multiple hydrate phases of different compositions and structures.

Propane can only enter and stabilise the large cavities of structure-II ($5^{12}6^4$) and methane can form both s-I and s-II. Based on model predictions and established thermodynamic stability, these hydrates formed in this system are understood to be C_3 (in the large cage) dominated s-II and methane dominated s-I, as subcooling increases. At lower subcooling temperature (< 4 °C), the region between the black line and black dashed line predicted by HydraFLASH®, propane can only form as a stable phase. As subcooling increases, step cooling/heating curves followed the methane phase boundary (structure-I). Therefore, as shown in Figure 3-35, the results strongly suggest the order of hydrate formation. This order of hydrate formation is based on the order of stability, i.e., the most thermodynamically stable hydrate formers. This might suggest that the simple formation of s-II hydrate in the natural gas system is not true and various hydrate structures with a sequential formation can be formed in order of decreasing stability ($C_3/C_4 \rightarrow C_2 \rightarrow C_1$ / $CO_2 \rightarrow N_2$). (This interpretation is a joint work product of R. Anderson and M. Aminnaji which is taken from JJI Project at Heriot-Watt University [3.1]).

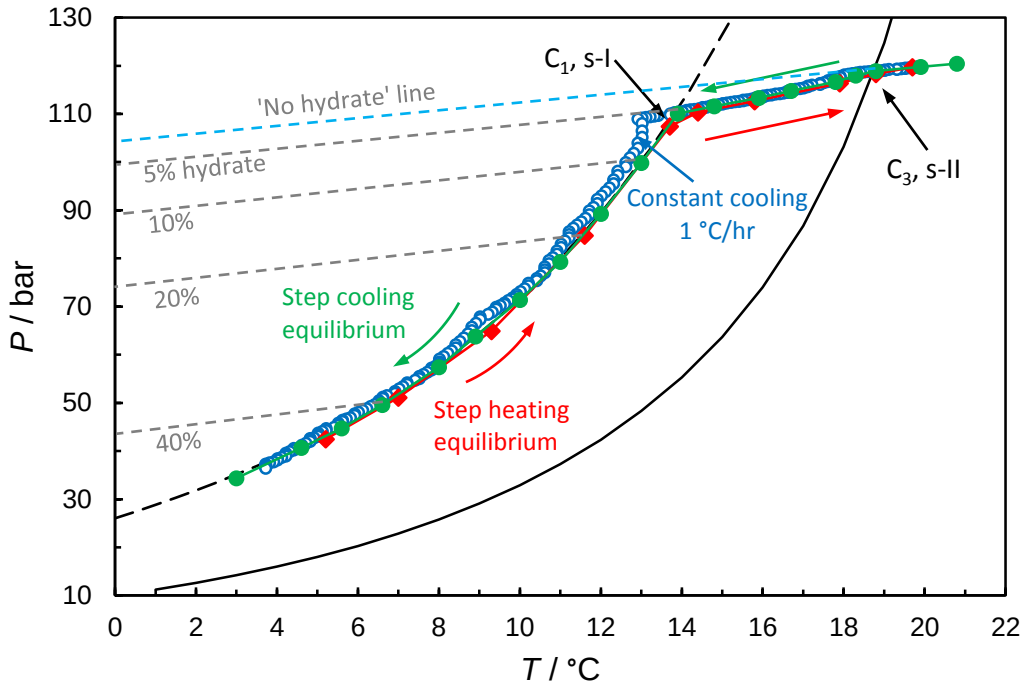

Figure 3-35. Plot of PT data for constant cooling (1.0 °C / hour) then equilibrium step heating and step cooling measurements on the 98 mole% C1 + 2 mole% C3 system. Black line and dashed line are model predictions (adjusted slightly as required to match measurements) for the stability of different potential structures which can form.

3.4.5.5 Crystal Growth regions C_1 + C_2 + C_3

Work progressed onto the more complex natural gas with three components to investigate the multiple hydrate structures formation in the natural gas systems. Therefore, step heating equilibrium measurement was carried out for the system with 85 mole% C_1 + 12 mole% C_2 + 3 mole% C_3. This is crucial to find out whether various hydrate structures could be formed in the natural gas system rather than the simple formation of s-II hydrate; because it is speculated that there is an interaction between KHIs and hydrate structures which may result in the common CGI regions observed for the KHI system.

Figure 3-36 shows a plot of pressure / temperature data for seeded constant cooling (1 °C / hour) then equilibrium step heating measurements in the three components natural gas system (85% C_1 + 12% C_2 + 3% C_3). As can be seen, clear transitions and changes in the slope of the measured equilibrium step heating curve were observed. As shown in Figure 3-36, these clear changes/transitions coincide with the model predictions for the stability of different structures which can be formed e.g. C_3 s-II, C_2 s-II, C_2 s-I, and C_1 s-I (Section 3.3.3).

As would be expected, the results of this experiment indicate the sequential dissociation of different hydrate phases with different compositions and structures. As shown in Figure 3-36, the first few step heating equilibrium points coincide with C_1 s-I phase boundary predicted by the model, indicating the dissociation of s-I methane hydrates. As temperature raised, the slope of measured equilibrium step heating curve was changed in the region between C_1 s-I and C_2 s-I phase boundary, specifying dissociation of C_2 s-I hydrates. In addition, measured equilibrium step heating curve for those points in the region between C_2 s-I and C_2 s-II phase boundary followed by different slope, indicating dissociation of C_2 s-II hydrates. Finally, as would be expected, C_3 s-II hydrate dissociated which is the most thermodynamically stable hydrate former in this system. A straight line was observed for the measured equilibrium step heating points in the region between C_2 s-II and NG s-II phase boundary, i.e., NG s-II phase boundary refers to the hydrate phase boundary of the system with full composition (85% C_1 + 12% C_2 + 3% C_3). Therefore, similar to the results for C_1 + C_3 mixture, the results of step heating equilibrium measurements for this system strongly suggest the order of hydrate formation/dissociation which is based on the order of stability.

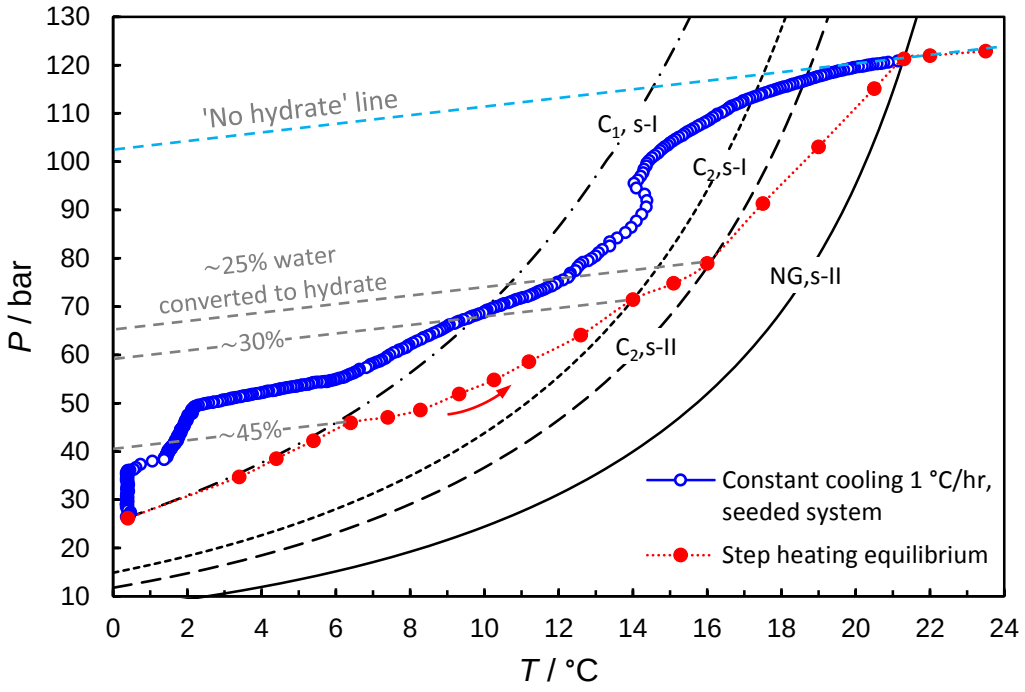

Figure 3-36. Plot of measured equilibrium (step-heating) dissociation behaviour for 85% C_1 + 12% C_2 + 3% C_3 (80% cell volume as aqueous phase). Black dashed lines are model predictions (adjusted slightly as required to match measurements) for the stability of different potential structures which can form.

3.5 Summary

From hydrate fraction tolerance on Luvicap Bio and PVCap in the methane system and performance of combined Luvicap Bio + PVCap in both methane and natural gas system in terms of hydrate inhibition, the following conclusions could be drawn:

- As the hydrate fraction increases, the CIR subcooling extent decreases for both Luvicap Bio and PVCap.

- Results suggest that Luvicap Bio is a better inhibitor for s-I methane than for s-II methane hydrate. Luvicap Bio prevents successfully s-I hydrate formation at low subcooling temperature up to ~3 °C subcooling temperature, then struggles to inhibit the s-II methane hydrates up to 5.2 °C subcooling temperature; but shows a good inhibition for s-I hydrates beyond the 5.2 °C subcooling temperature.

- In contrast to Luvicap Bio, PVCap is probably a better s-II hydrate inhibitor. PVCap prevents successfully s-I hydrate formation at low subcooling temperature, then inhibits the s-II methane hydrates up to 5.2 °C subcooling temperature; but struggles to inhibit s-I hydrates beyond the 5.2 °C subcooling temperature.

- Furthermore, the CGI test on combined 0.25% Luvicap Bio + 0.25% PVCap with both methane and natural gas shows significantly improved hydrate inhibition region compared to these polymers alone.

- The results for the combined Luvicap Bio + PVCap support the theory that Luvicap Bio is better for s-I and PVCap is better for s-II, i.e., the synergism effect could be achieved when these polymers combined; one inhibits s-II and the other inhibits s-I, resulting in improved CGI regions.

Furthermore, from the results for hydrate growth rate regions/patterns and the hydrate structure studies in methane, ethane, propane, $C_1 + C_3$, and $C_1 + C_2 + C_3$, it is concluded that:

- The SIR runs for simple methane and ethane systems reveal the clear and distinct changes in hydrate growth rates and exothermic heat release rates which correspond to the CGI-type regions observed in Luvicap Bio and PVCap systems (1.1-2, 5.2, 7.2 °C subcooling temperature)

- The hydrate growth rate patterns and exothermic heat release rates in both simple ethane and methane systems support the possible theory of formation both s-I and s-II methane and ethane; but not propane which could form only s-II due to its large molecular diameter (a typical exponential type decay was observed for growth rate in simple propane system)

- In addition, equilibrium step heating/cooling measurements in the multicomponent gas systems suggest the multiple hydrate structures formation.

3.6 Reference

[1] E. D. Sloan, “Fundamental principles and applications of natural gas hydrates,” Nature, vol. 426, no. 6964, pp. 353–363, 2003.

[2] E. D. Sloan Jr and C. Koh, *Clathrate hydrates of natural gases*. CRC press, 2007.

[3] R. Anderson, M. Aminnaji, B. Tohidi. “Evaluation of low dosage hydrate inhibitors: Pushing the Boundaries of Low Dosage Hydrate Inhibition: Challenging Conditions & Novel Solutions” Edinburgh: Heriot-Watt University, Institute of Petroleum Engineering- Joint Industry Project Report, 2015-2018.

[4] Mozaffar, Houra. "Development and application of a novel crystal growth inhibition (CGI) method for evaluation of kinetic hydrate inhibitors." PhD thesis, Heriot-Watt University, 2013.

[5] S. Takeya, Y. Kamata, T. Uchida, J. Nagao, T. Ebinuma, H. Narita, A. Hori, and T. Hondoh, “Coexistence of structure I and II hydrates formed from a mixture of methane and ethane gases,” *Can. J. Phys.*, vol. 81, no. 1–2, pp. 479–484, 2003.

[6] S. Subramanian, R. A. Kini, S. F. Dec, and E. D. Sloan, “Evidence of structure II hydrate formation from methane+ ethane mixtures,” *Chem. Eng. Sci.*, vol. 55, no. 11, pp. 1981–1999, 2000.

[7] I.-M. Chou, A. Sharma, R. C. Burruss, J. Shu, H. Mao, R. J. Hemley, A. F. Goncharov, L. A. Stern, and S. H. Kirby, “Transformations in methane hydrates,” *Proc. Natl. Acad. Sci.*, vol. 97, no. 25, pp. 13484–13487, 2000.

[8] H. Shimizu, T. Kumazaki, T. Kume, and S. Sasaki, “In situ observations of high-pressure phase transformations in a synthetic methane hydrate,” *J. Phys. Chem. B*, vol. 106, no. 1, pp. 30–33, 2002.

[9] H. Hirai, T. Kondo, M. Hasegawa, T. Yagi, Y. Yamamoto, T. Komai, K. Nagashima, M. Sakashita, H. Fujihisa, and K. Aoki, “Methane hydrate behavior under high pressure,” *J. Phys. Chem. B*, vol. 104, no. 7, pp. 1429–1433, 2000.

[10] J. S. Loveday, R. J. Nelmes, M. Guthrie, S. A. Belmonte, D. R. Allan, D. D. Klug, J. S. Tse, and Y. P. Handa, “Stable methane hydrate above 2 GPa and the source of Titan’s atmospheric methane,” *Nature*, vol. 410, no. 6829, pp. 661–663, 2001.

[11] J. M. Schicks and J. A. Ripmeester, “The coexistence of two different methane hydrate phases under moderate pressure and temperature conditions: kinetic versus thermodynamic products,” *Angew. Chemie Int. Ed.*, vol. 43, no. 25, pp. 3310–3313, 2004.

Chapter 4 – Inhibition of Hydrates Using Combination of MeOH / MEG / EtOH and Luvicap Bio for Natural Gas Systems

4.1 Introduction

The main objective of this chapter was to investigate whether Bio KHIs could be used to reduce or eliminate THIs, particularly more toxic MeOH. This chapter presents the results of application of the crystal growth inhibition (CGI) method to investigate the effect of MeOH, EtOH, and MEG on biodegradable polymers of KHIs like Luvicap Bio. Methanol (MeOH) and ethylene glycol (MEG) are the two most common thermodynamic hydrate inhibitors, and they are also being used either as solvents in LDHI formulations or as a 'top-up' inhibitor to increase the subcooling temperature to which KHIs can be used. The term of 'full top-up' inhibitor refers to those THIs inhibitors that do not have negative effect on KHI performance, i.e., the CIR extent (complete inhibition region, green zone) is fully preserved when THIs is combined with KHIs. Similarly, KHIs can be used to reduce the amount of thermodynamic inhibitor required in terms of hydrate inhibition at high subcooling temperatures.

There is limited data showing the effect of alcohols on KHIs. There are two conflicting studies about the effect of MeOH in mixtures with KHIs. Sloan et al. (1998) showed the negative effect of MeOH on PVCap [4.1] while there is one study showing the synergy effect of MeOH [4.2]. In addition to this, there are two theoretical and experimental studies concerning the effect of alcohol on anti-agglomeration [4.3][4.4]. In the theoretical study, very little effect of MeOH as a co-solvent on anti-agglomeration was proposed, yet in the experimental studies, a significant effect of small amounts of alcohol co-surfactant (MeOH) on hydrate anti-agglomeration was one of the main conclusions, and authors have shown that alcohol co-surfactants could be effective at low concentrations.

In addition to the published data, a lot of researches have been done to evaluate the effect of alcohol on the KHIs within the various phases of Joint Industrial Project (JIP) at Heriot Watt University. The following paragraphs summarize the research on the effect of THIs on KHIs using CGI methods.

Previous studies (induction time measurements carried out during the 2006-2009 project phase) have shown that methanol (MeOH) has a generally negative effect on PVCap performance [4.5]. Furthermore, CGI experiments on methanol-PVCap systems with methane carried out in another project phase (2009-2012) support these findings [4.6];

methanol consistently reducing the extent of PVCap-induced CGI regions as the aqueous concentration is increased.

To better understand the impact of alcohols on KHI performance, experiments on the effect of ethanol (EtOH), n-propanol (n-POH), i-propanol (i-POH) and n-butanol (n-BOH) on PVCap performance in methane systems were undertaken within another phase of the project [4.6]. Results showed that the above alcohols do not act as full top-up thermodynamic inhibitors and all have negative effect on the PVCap-induced complete inhibition region (CIR) with the exception of n-butanol. In addition, the results indicate that the molecular weight is not the only factor which controls this kind of negative behaviour effect, i.e., results showed that n-propanol is less negative than i-propanol. Moreover, results show that the higher subcooling temperature of CGI region extents (more preservation of the CIR) are achieved for those ones that have longer alkyl tail. Nevertheless, it was concluded that the combination of alcohol + PVCap does still offer better inhibition by mass of inhibitor than any of the alcohols alone even though they have some negative effect on PVCap performance.

In contrast to data for PVCap + methanol + methane system which strongly suggests the negative effect of MeOH on PVCap performance, results for the natural gas systems showed the modestly positive effect of methanol (at 2.5 and 5.0 mass% concentrations) on PVCap performance, indicating a full ‘top-up’ thermodynamic inhibitor [4.7]. Conversely, at a higher concentration of methanol (25 mass%), crystal growth regions reduced compared to PVCap alone showing negative effect of MeOH on PVCap performance at higher concentration of methanol.

The different effect of methanol on PVCap performance in s-I forming methane systems and s-II/s-I forming multicomponent gases probably suggests the methanol involvement in hydrate growth/nucleation, e.g. potentially though temporary cage occupation [4.7]. Certainly, methanol has a molecular diameter sufficiently small to enter hydrate cavities and is known to form hydrates at low temperatures [4.8][4.9].

However, the CGI studies on MEG + PVCap in the natural gas systems showed that MEG has positive effect on PVCap, i.e., evidenced by the increase in CGI region subcoolings [4.7]. The reason for this could be increase in the strength of polymer adsorption on hydrate crystal surfaces due to presence of MEG in the system.

In addition to work on methanol and MEG, studies were undertaken on the systems with 5.0 and 25.0 mass % ethanol, PVCap, and natural gas to investigate the effect of ethanol on PVCap in natural gas systems in terms of hydrate inhibition [4.7]. The results for both concentration of ethanol support the generally negative effect of ethanol on PVCap performance indicating ethanol does not act as a full top-up thermodynamic inhibitor for PVCap.

In addition to the PVCap, some work has been undertaken on one commercial polymer (Nalco-Champion T1441), i.e., the effect of alcohols on Nalco-Champion T1441 in the natural gas systems has been studied [4.7]. The results showed that methanol has general negative effect on performance of Nalco-Champion T1441 in terms of hydrate inhibition, reducing the CGI extents regions [4.7].

However, there is a question in terms of if the negative effect of ethanol on PVCap performance is due to ethanol enclathration, i.e., ethanol is known to form binary hydrates in both methane and ethane systems [4.10]. Therefore, the effect of ethanol on PVCap performance in methane and ethane systems was investigated and the results showed that although both systems are known as s-I hydrates formation, CGI inhibition being considerably greater in ethane than methane systems [4.7]. In addition, the CGI method was carried out for the 5.56 mole% ethanol + PVCap in an ethane system. The 5.56 mole% ethanol is the stoichiometric ratio for ethanol entry into the hydrate lattice. The results also showed the strongly negative effect of ethanol on PVCap performance in terms of hydrate growth in ethane-ethanol systems. Therefore, it is concluded that the negative effect of ethanol is considerably less for ethane than it is for methane. Consequently, these findings strongly suggest the molecules occupancy of cages is the important/single biggest factor in KHIs performance in terms of the ability of KHIs polymers to inhibit crystal growth as a function of pressure and composition.

As discussed in Section 1.4.3, there is growing interest in 'green' KHIs and as noted in Chapter 2, results showed that Luvicap Bio has better performance in terms of hydrates inhibition and powerful KHIs properties. Therefore, following work on PVCap, the effect of methanol on Bio-KHI (Luvicap Bio Polymer) performance in a natural gas system was examined to assess whether the negative effect seen in PVCap systems also applies to Luvicap Bio polymer systems. In addition, the effect of ethanol and MEG on Luvicap Bio were examined.

4.2 Experimental Methods and Materials

The purity of the methanol, ethanol, and MEG used were 99.9%. Distilled water was used in all tests. Luvicap Bio base polymer was supplied in water by BASF. The composition of natural gas used in tests (including that used in previous tests for PVCap in JIP) is given in Table 4-1. The volume ratio of liquid/gas in the cell was 70/30.

All experiments were carried out using high pressure stirred autoclaves (see Section 2.2 for a more detailed description of equipment), using the new CGI method (see Section 1.4.4.2).

The thermodynamic hydrate phase boundaries for systems were predicted using HydraFLASH®, a thermodynamic model developed by Hydrafact Ltd and Heriot-Watt University.

Table 4-1. Composition of the standard North Sea natural gas used in CGI experiments

Component	Mole%
Methane	87.93
Ethane	6.00
Propane	2.04
i-Butane	0.20
n-Butane	0.30
CO2	2.03
Nitrogen	1.50

4.3 Results and Discussion

4.3.1 0.5 Mass% Luvicap Bio with Methanol in a Natural Gas System

Figure 4-1 and Figure 4-2 show example CGI method cooling/heating curves for Luvicap Bio + natural gas systems with 5 and 50 mass% aqueous methanol (relative to water + Luvicap Bio) respectively. Complete measured CGI boundary data points with interpolations for all systems studied (5, 10, 20, 30 and 50 mass% MeOH) are reported in Table 4-2 to Table 4-6, and presented in Figure 4-3 to Figure 4-7. Pressure / temperature plots showing measured experimental points delineating the various crystal growth inhibition regions for these systems are reported in Appendix A.1. Figure 4-8 shows average induced CGI regions for 0.5 mass% Luvicap Bio aqueous as a function of methanol mass% relative to the MeOH-inhibited s-II boundary for the natural gas + methanol + water system. Figure 4-9 shows a comparison of subcooling extents of CGI regions from the s-II phase boundary for 0.5 mass% Luvicap Bio aqueous with natural gas and different methanol mass% over the range of pressures studied. Figure 4-10 shows average Luvicap Bio induced CIR region for 0.5 mass% Luvicap Bio aqueous as a function of methanol mass% + MeOH thermodynamic inhibition for the natural gas-water system, while Figure 4-11 shows calculated mass% methanol inhibition equivalent to methanol + 0.5 mass% Luvicap Bio as a function of methanol mass% + 0.5 mass% Luvicap Bio.

As discussed, it was concluded from past studies that methanol has an overall negative effect on PVCap (and another non-bio polymer) performance in s-I forming methane hydrate systems. Likewise, while methanol had a moderate positive effect on PVCap performance in s-II forming natural gas at lower concentrations (2.5 and 5 mass% methanol), it had an increasingly negative effect at higher concentrations. However, the combination of methanol and PVCap still offered a greater degree of inhibition by mass of inhibitor than methanol alone, even though it was not a full ‘top-up’ inhibitor.

In contrast to PVCap, results of tests on 0.5 mass% Luvicap Bio with methanol at concentrations up to 30% with natural gas show that while it has a moderately negative effect on the SGR region, the important complete inhibition region / CIR (considered safe for operating) remains largely preserved, making it generally a consistent top up inhibitor for Luvicap Bio for the conditions / concentrations tested. Only at the higher methanol concentration of 50 mass% does the methanol start to have a significant detrimental effect

on the KHI performance, reducing the CIR, although even then this is primarily confined to pressures below ~100 bar. Another significant point is that slow dissociation region decreases as methanol concentration increases. Results show that there is no significant SDR in those systems with methanol concentration higher than 30 mass%.

Results do therefore suggest much greater potential for Luvicap Bio + methanol combinations for reducing methanol requirements than is the case for other polymers such as PVCap. For example, as shown in Figure 4-11, 0.5 mass% Luvicap Bio + 26 mass% MeOH offers the complete inhibition (MeOH + Bio CIR) equivalent of 40 mass% Methanol, which would constitute a 35% methanol reduction. At lower subcooling / methanol dose requirements, the percent reductions are even greater; 0.5 mass% Luvicap Bio could replace all methanol where it was currently being dosed at ~23 mass%. Certainly data suggest large cost savings could be made, with additional environmental benefits by replacing methanol with Luvicap Bio based KHIs.

Finally, while this has not been examined in detail, it is notable that, in contrast to data for PVCap [4.7], CGI boundaries in Luvicap Bio + MeOH + natural gas systems seem primarily related to s-II (in terms of subcooling extents) instead of s-I. This potentially relates to the different abilities of these two polymers to inhibit different hydrate structures that can form in natural gas systems, as discussed in Chapter 3. It may also give clues to the role of methanol (and ethanol) in hydrate nucleation and growth. Methanol is known to enter hydrate cavities under certain conditions [4.11] (with ethanol a known s-II type hydrate former), and this may be a factor in the different behaviours seen for PVCap and Luvicap Bio with methanol if it is considered these polymers have different abilities to inhibit different types of structure. For example, if methanol encouraged the formation of e.g. s-I, then a KHI with less ability to inhibit s-I would be expected to be poorer in the presence of methanol, and vice versa for a KHI poor with s-II if MeOH encouraged that structure. Certainly, methanol (and ethanol) partial enclathration looks increasingly likely as the factor behind the contrasting top-up effects observed for different KHI polymers.

Table 4-2. Experimental natural gas hydrate CGI region data for 0.5 mass% Luvicap Bio aqueous (relative to water) with 5 mass% MeOH (relative to water + Luvicap Bio).

CGR boundary	Growth rate	T / °C (±0.5)	P / bar (±0.2)	ΔT_{s-I} / °C (±0.5)	ΔT_{s-II} / °C (±0.5)
CIR-SGR(VS)	No growth	-2.7	24.6	-2.9	-9.3
		3.5	53.1	-3.8	-9.1
		5.5	71.3	-4.3	-9.1
		7.5	99.8	-4.9	-9.1
		9.7	132.2	-4.6	-8.3
SGR(VS)-RGR	Very slow	2.2	53.1	-5.1	-10.4
		4.7	71.3	-5.1	-9.9
		6.7	99.7	-5.7	-9.9
		9.3	132.4	-5.0	-8.7
SDR	Slow dissociation	10.8	27.0	-	3.5
		16.6	57.2	-	3.5
		18.6	77.5	-	3.5
		20.5	108.5	-	3.5
		22.1	146.4	-	3.5

Table 4-3. Experimental natural gas hydrate CGI region data for 0.5 mass% Luvicap Bio aqueous (relative to water) with 10 mass % methanol (relative to water + Luvicap Bio).

CGR boundary	Growth rate	T / °C (±0.5)	P / bar (±0.2)	ΔT_{s-I} / °C (±0.5)	ΔT_{s-II} / °C (±0.5)
CIR-SGR(VS)	No growth	-6.0	23.0	-3.4	-9.9
		0.4	53.1	-4.7	-10.0
		2.7	75.8	-5.3	-10.1
		4.2	95.2	-5.5	-9.9
		7.0	134.5	-5.1	-8.8
SGR(VS)-RGR	Very slow	0.0	52.8	-5.0	-10.4
		2.3	78.5	-5.7	-10.7
		3.8	96.6	-6.0	-10.4
		6.2	133.4	-5.8	-9.5
SDR	Slow dissociation	7.0	25.0	-	2.3
		13.3	57.7	-	2.3
		15.6	82.9	-	2.3
		16.9	106.2	-	2.3
		18.5	148.4	-	2.3

Table 4-4. Experimental natural gas hydrate CGI region data for 0.5 mass% Luvicap Bio aqueous (relative to water) with 20 mass % methanol (relative to water + Luvicap Bio).

CGR boundary	Growth rate	T / °C (±0.5)	P / bar (±0.2)	ΔT_{s-I} / °C (±0.5)	ΔT_{s-II} / °C (±0.5)
CIR-SGR(VS)	No growth	-9.3	23.6	-2.3	-8.7
		-3.2	52.7	-3.4	-8.8
		-1.1	72.8	-3.9	-8.8
		0.5	95.1	-4.2	-8.7
		3.3	125.5	-3.2	-7.2
SGR(VS)-RGR	Very slow	-10.2	23.6	-3.2	-9.6
		-4.1	52.3	-4.2	-9.6
		-2.0	72.5	-4.7	-9.7
		-0.7	94.4	-5.4	-9.8
		1.7	123.3	-4.7	-8.7
SDR	Slow dissociation	1.6	25.6	-	1.5
		7.6	57.2	-	1.5
		9.6	78.2	-	1.5
		11.1	102.9	-	1.5
		12.3	134.9	-	1.5

Table 4-5. Experimental natural gas hydrate CGI region data for 0.5 mass% Luvicap Bio aqueous (relative to water) with 30 mass % methanol (relative to water + Luvicap Bio).

CGR boundary	Growth rate	T / °C (±0.5)	P / bar (±0.2)	ΔT_{s-I} / °C (±0.5)	ΔT_{s-II} / °C (±0.5)
CIR-SGR(VS)	No growth	-13.5	24.3	-1.6	-8.0
		-7.9	51.6	-2.5	-8.1
		-6.0	68.8	-2.8	-8.0
		-4.6	87.9	-3.2	-8.0
		-3.1	126.0	-3.9	-8.0
		-2.4	148.0	-4.1	-8.0
		0.0	209.3	-3.8	-7.0
		1.6	282.2	-4.0	-6.8
SGR(VS)-RGR	Very slow	-15.8	24.5	-3.9	-10.3
		-8.6	51.8	-3.1	-8.7
		-6.7	68.5	-3.5	-8.7
		-5.5	86.9	-4.0	-8.8
		-3.8	125.8	-4.6	-8.7
		-3	146.6	-4.7	-8.5
		-0.7	205.3	-4.4	-7.6
		1.0	279.2	-4.5	-7.4
SDR	Slow dissociation	-4.7	26.0	-	0.3
		1.3	58.5	-	0.3
		2.7	73.4	-	0.3
		4.0	94.7	-	0.3
		5.6	138.3	-	0.3
		6.2	162.7	-	0.3
		7.7	229.4	-	0.3
		9.2	307.9	-	0.3

Table 4-6. Experimental natural gas hydrate CGI region data for 0.5 mass% Luvicap Bio aqueous (relative to water) with 50 mass % methanol (relative to water + Luvicap Bio).

CGR boundary	Growth rate	T / °C (±0.5)	P / bar (±0.2)	ΔT_{s-I} / °C (±0.5)	ΔT_{s-II} / °C (±0.5)
CIR-SGR(VS)	No growth	-21.9	34.4	0.2	-5.7
		-18.8	61.2	-1.2	-6.6
		-16.8	76.9	-0.7	-5.9
		-16.5	93.4	-1.5	-6.5
		-16.3	122.6	-2.7	-7.3
		-13.5	194.5	-2.3	-6.2
		-10.4	317.6	-2.0	-5.5
SGR(VS)-RGR	Very slow	-22.2	34.9	-0.2	-6.1
		-19.0	61.2	-1.4	-6.8
		-17.1	76.8	-1.0	-6.2
		-16.8	93.4	-1.8	-6.8
		-16.7	122.0	-3.1	-7.7
		-14.3	191.8	-3.0	-6.9
		-10.9	317.2	-2.5	-6.0
SDR	Slow dissociation	No SDR			

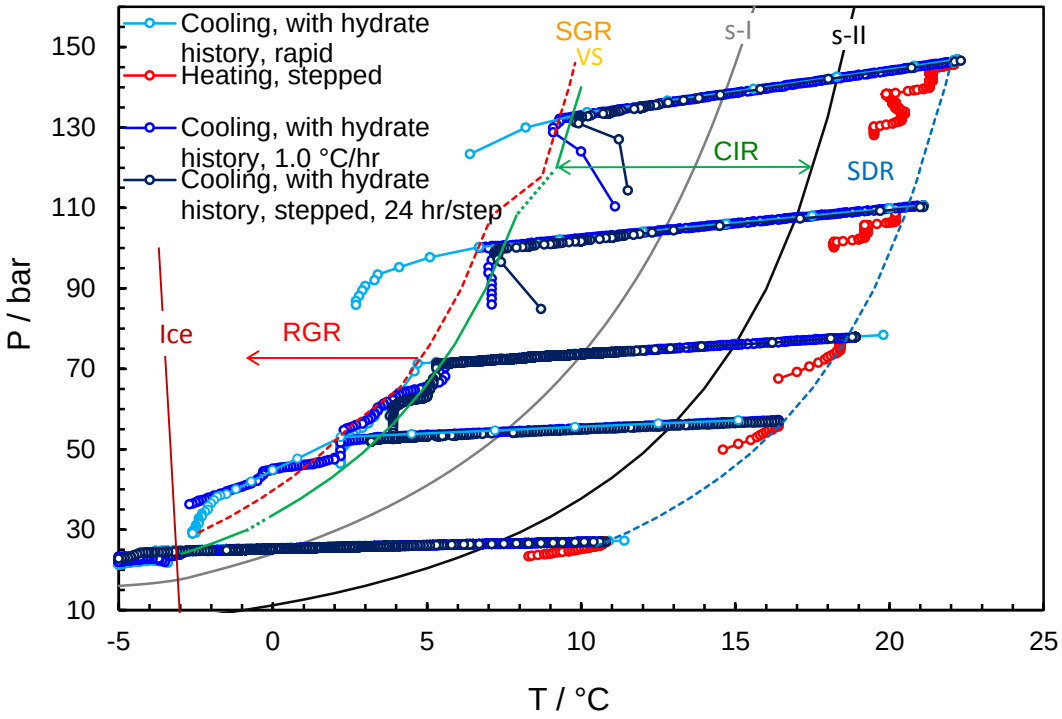

Figure 4-1. Example CGI method cooling curves for 0.5 mass% Luvicap Bio / 5 mass % methanol aqueous with natural gas.

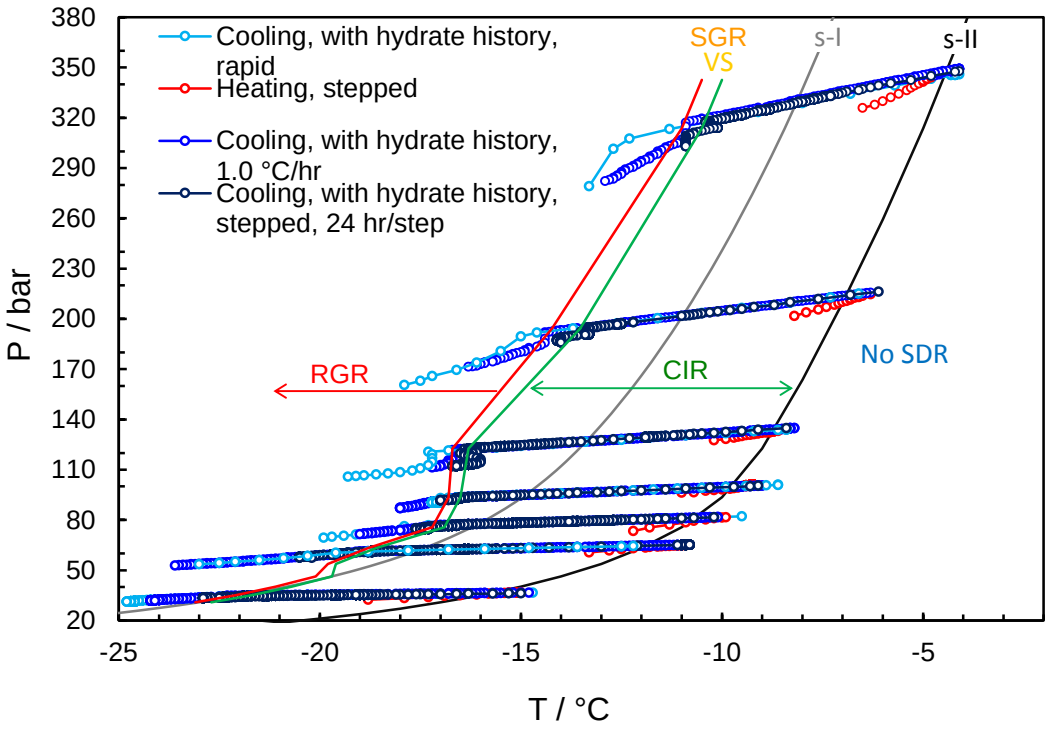

Figure 4-2. Example CGI method cooling curves for 0.5 mass% Luvicap Bio / 50 mass % methanol aqueous with natural gas.

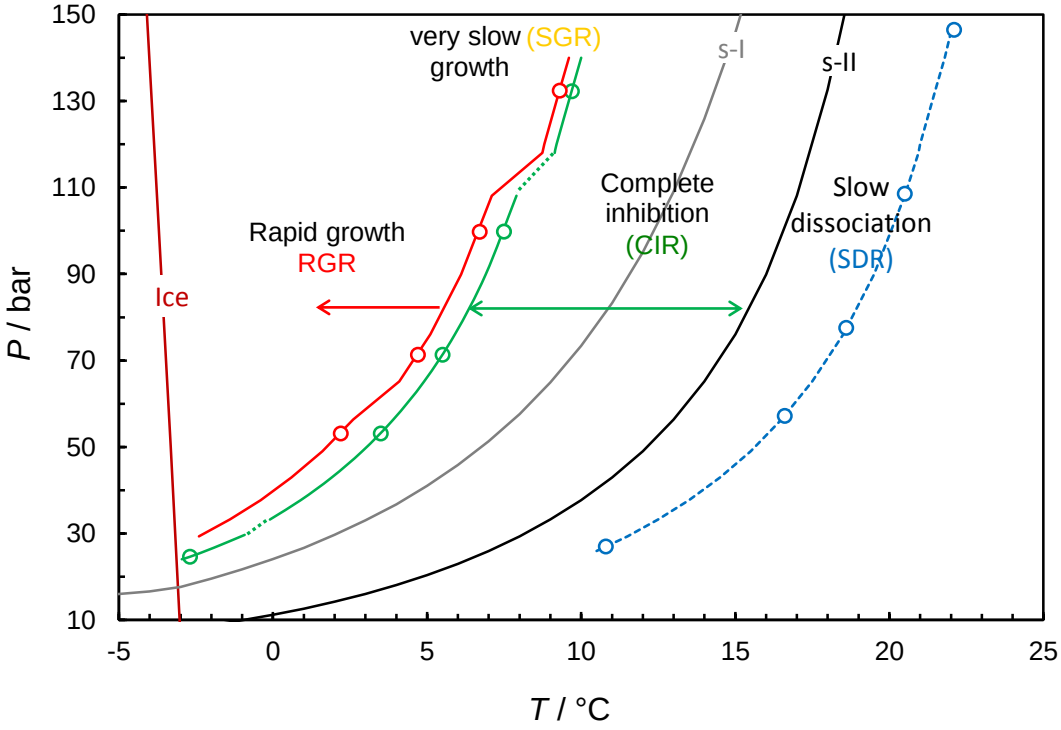

Figure 4-3. Experimental natural gas hydrate CGI region data for 0.5 mass% Luvicap Bio aqueous with 5.0 mass % methanol (relative to water + Luvicap) showing CGI regions determined from changes in relative hydrate growth rates.

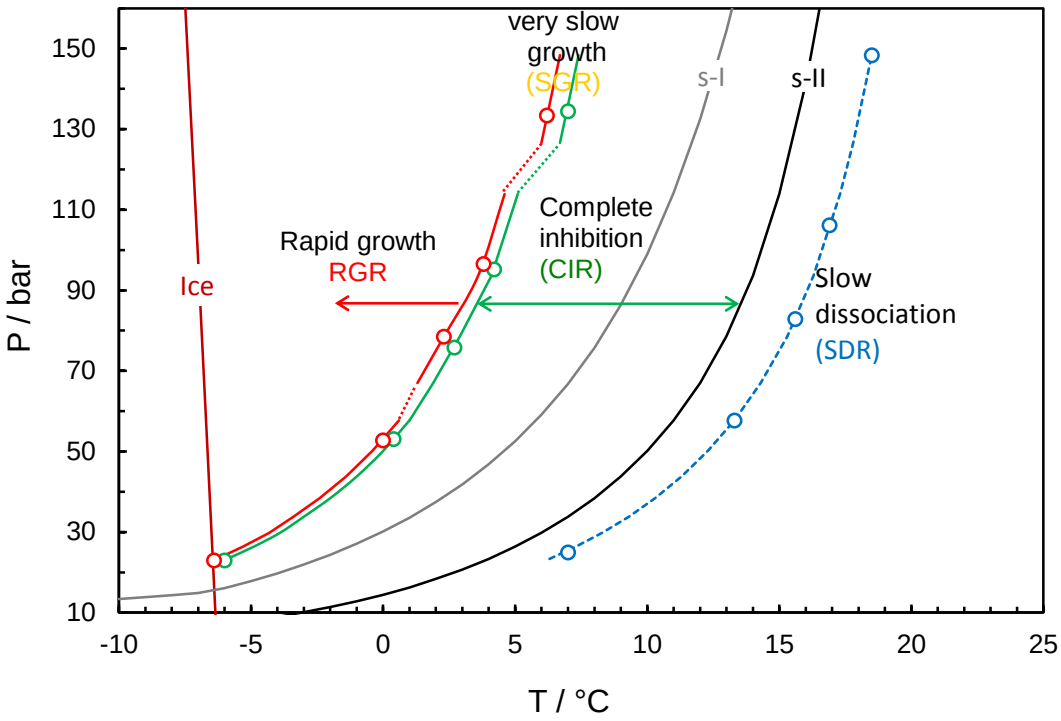

Figure 4-4. Experimental natural gas hydrate CGI region data for 0.5 mass% Luvicap Bio aqueous with 10 mass % methanol (relative to water + Luvicap) showing CGI regions determined from changes in relative hydrate growth rates.

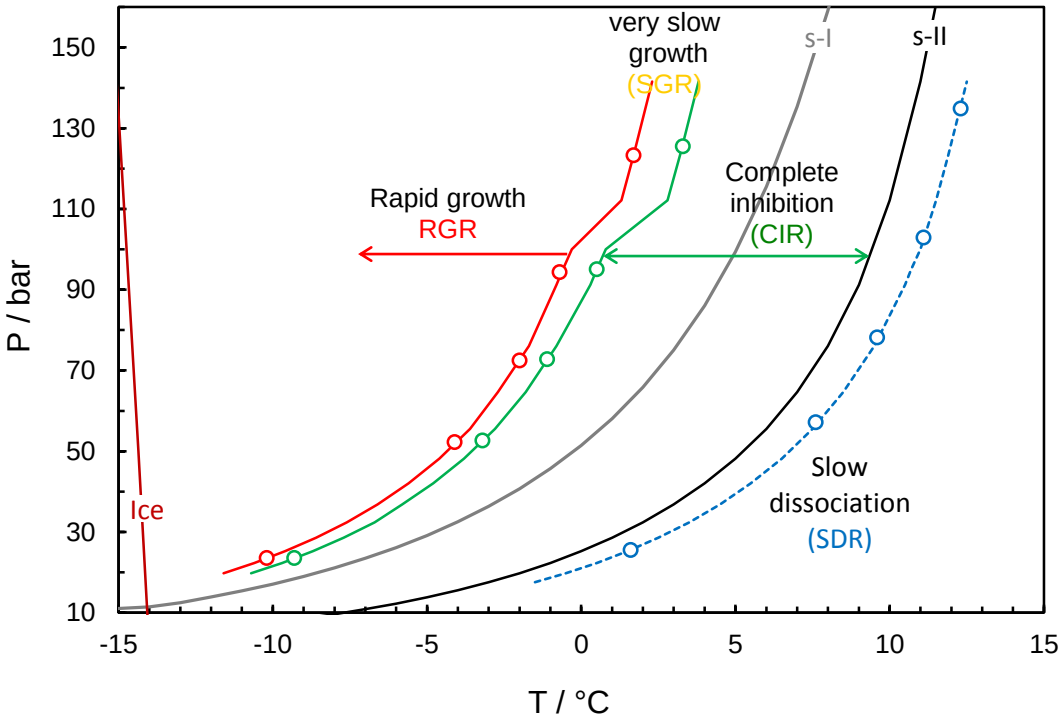

Figure 4-5. Experimental natural gas hydrate CGI region data for 0.5 mass% Luvicap Bio aqueous with 20 mass % methanol (relative to water + Luvicap) showing CGI regions determined from changes in relative hydrate growth rates.

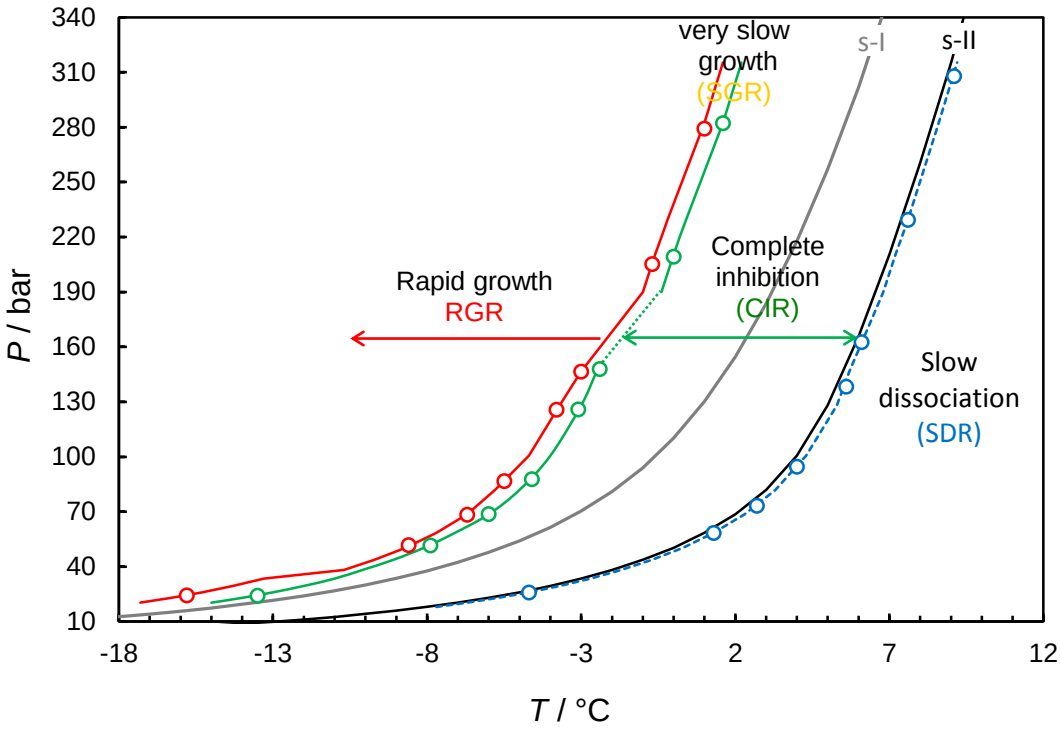

Figure 4-6. Experimental natural gas hydrate CGI region data for 0.5 mass% Luvicap Bio aqueous with 30 mass % methanol (relative to water + Luvicap) showing CGI regions determined from changes in relative hydrate growth rates.

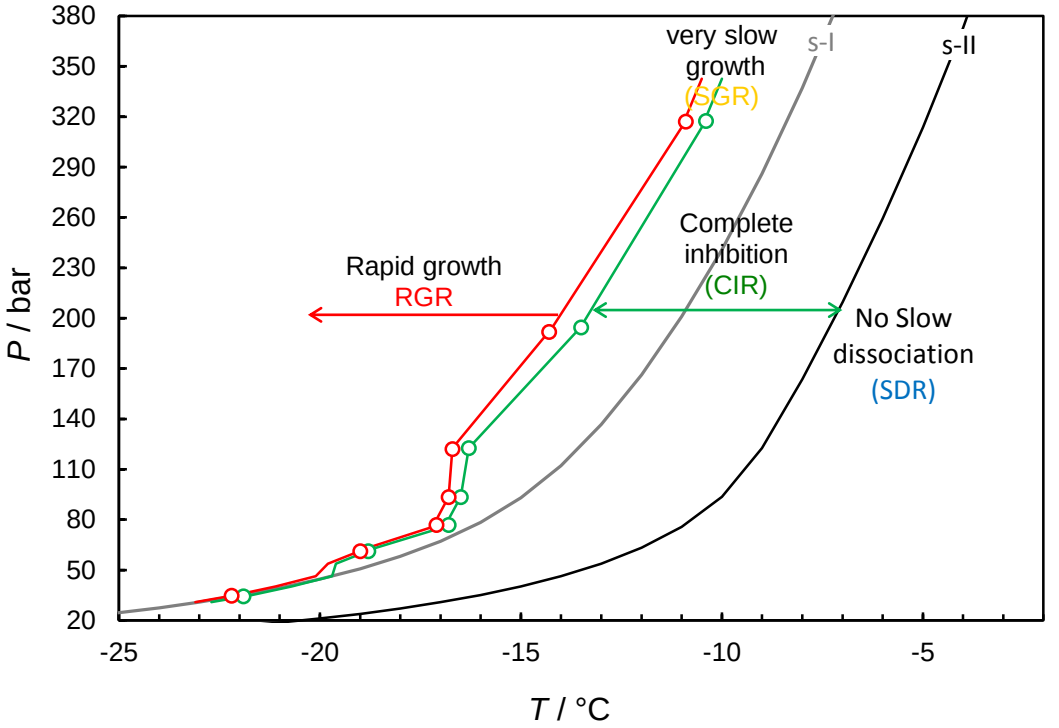

Figure 4-7. Experimental natural gas hydrate CGI region data for 0.5 mass% Luvicap Bio aqueous with 50 mass % methanol (relative to water + Luvicap) showing CGI regions determined from changes in relative hydrate growth rates.

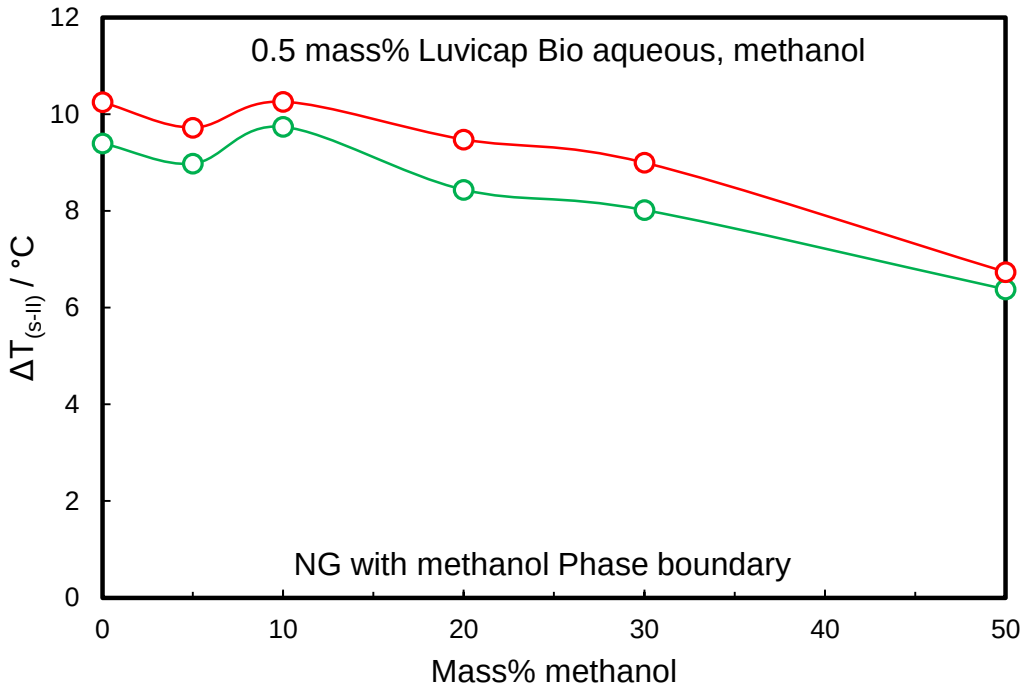

Figure 4-8. Average (25 to 130 bar) Luvicap Bio induced CGI regions for 0.5 mass% Luvicap Bio aqueous as a function of methanol mass% (relative to water + Luvicap Bio) relative to the MeOH-inhibited s-II boundary for the natural gas-methanol-water system.

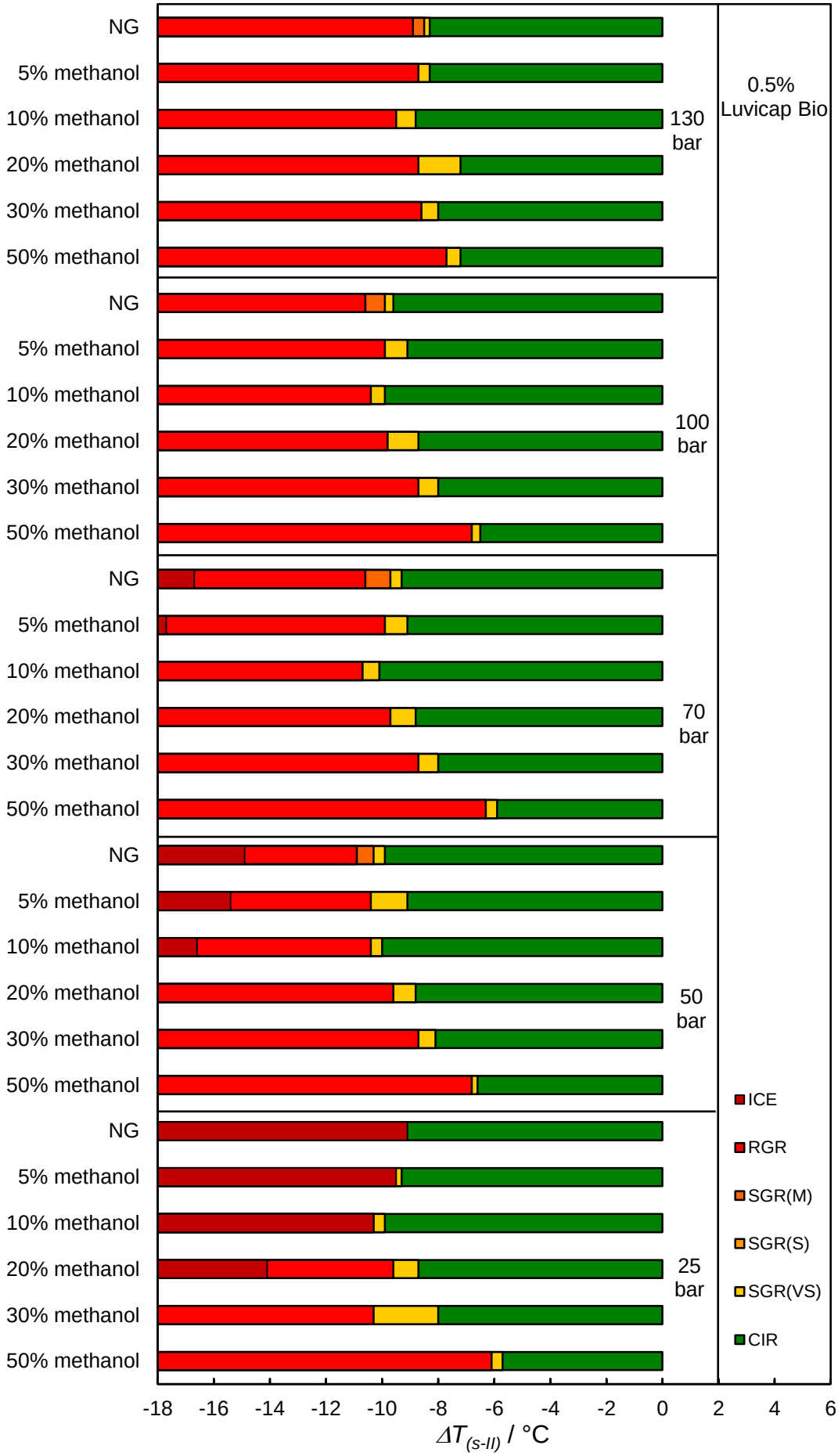

Figure 4-9. Comparison of subcooling extents of CGI regions from the s-II phase boundary for 0.5 mass% Luvicap Bio aqueous with natural gas and different methanol mass%.

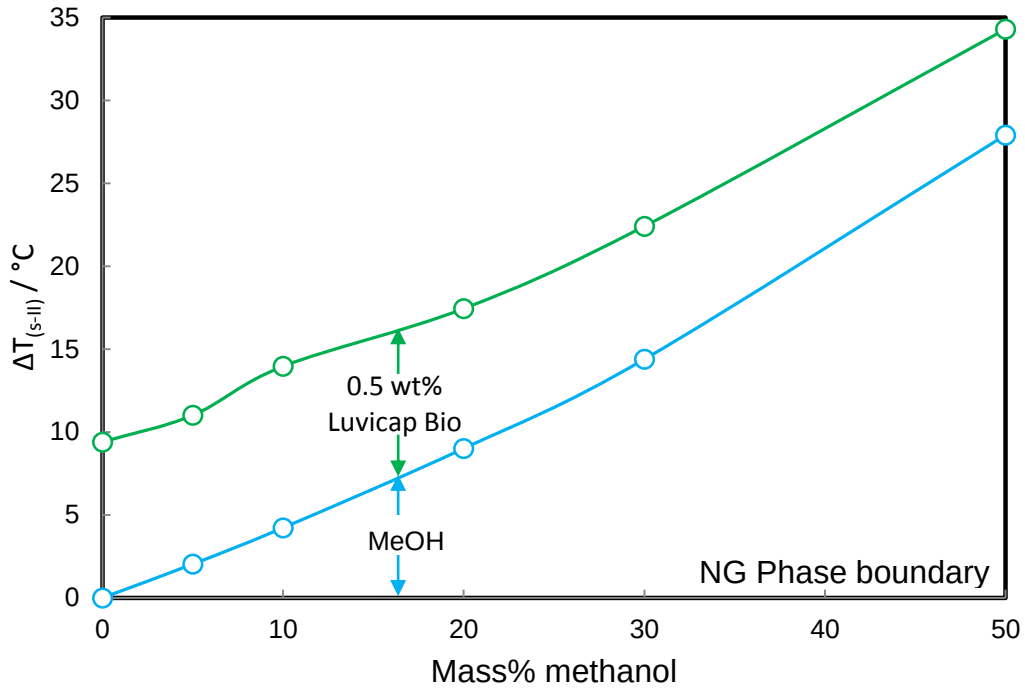

Figure 4-10. Average (25 to 130 bar) Luvicap Bio induced CIR region for 0.5 mass% Luvicap Bio aqueous as a function of methanol mass% (relative to water + Luvicap Bio) + MeOH thermodynamic inhibition for the natural gas-water system.

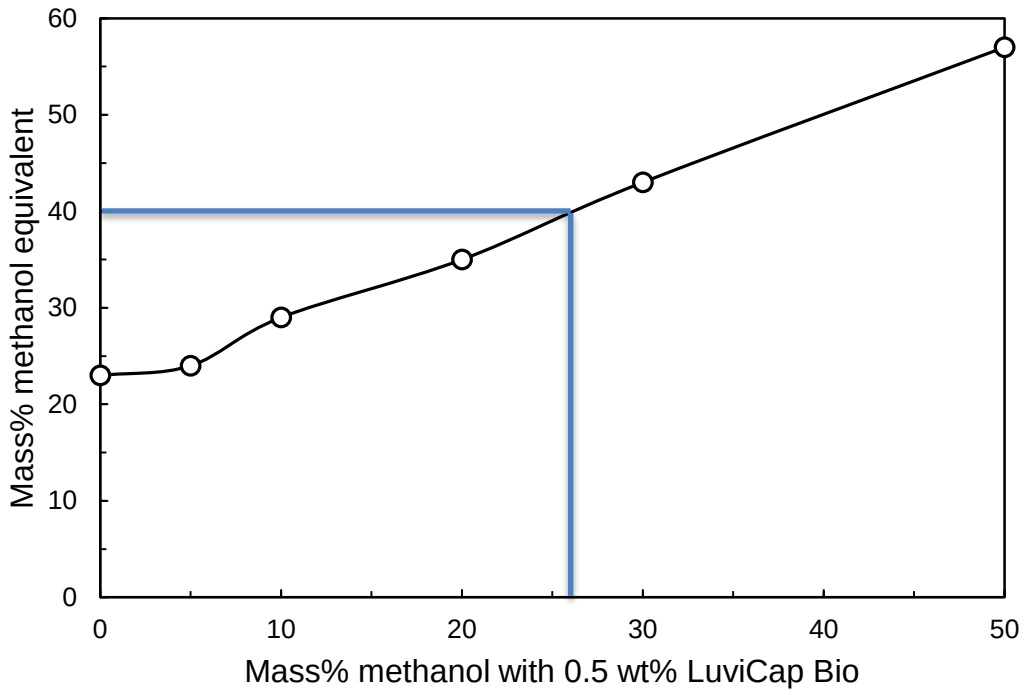

Figure 4-11. Calculated mass% methanol inhibition equivalent to methanol + 0.5 mass% Luvicap Bio (thermodynamic methanol inhibition + CIR) as a function of methanol mass% (+0.5 mass% Luvicap Bio). 40 mass% methanol can be replaced by 26 mass% MeOH + 0.5 mass% Luvicap Bio.

4.3.2 1.0 Mass% Luvicap Bio with Methanol in a Natural Gas System

As discussed, methanol was found to generally act as a top-up inhibitor for 0.5 mass% Luvicap Bio with natural gas. It was decided to investigate the effect of a higher concentration of Luvicap Bio in natural gas systems with methanol. CGI studies have been carried out on 1.0 mass% Luvicap Bio aqueous (relative to water) with 5, 10, 20, and 30 mass% methanol (relative to water + Luvicap Bio) and natural gas. Measured CGI region boundary data for these systems are presented in Figure 4-12 to Figure 4-15 and reported in Table 4-7 to Table 4-10. Pressure / temperature plots showing measured experimental points delineating the various crystal growth inhibition regions for these systems are reported in Appendix A.2.

Figure 4-16 shows average induced CGI regions for 1.0 mass% Luvicap Bio aqueous as a function of methanol mass% relative to the MeOH-inhibited s-II boundary for the natural gas-methanol-water system. In addition, Figure 4-17 shows the average (25 to 150 bar) Luvicap Bio induced CIR region for 1.0 mass% (and 0.5 mass%) Luvicap Bio aqueous as a function of methanol mass% (relative to water + Luvicap Bio) + MeOH thermodynamic inhibition for the natural gas-water system. Figure 4-18 shows a comparison of subcooling extents of CGI regions from the s-II phase boundary for 1.0 mass% Luvicap Bio aqueous with natural gas and different methanol mass% over the range of pressures studied.

As can be seen, results suggest methanol generally acts as good top-up inhibitor for 1.0 mass% Luvicap Bio, although a complete top-up additive effect is restricted to 5 mass% methanol; at higher concentrations, there is a modest negative effect of methanol on Luvicap Bio performance which increases with methanol concentration and pressure, as shown in Figure 4-18.

Figure 4-19 to Figure 4-22 show the comparison of measured CIR boundaries for 0.5 and 1.0 mass% Luvicap Bio, both with 5, 10, 20, and 30 mass% MeOH in the natural gas system respectively. As can be seen, the CIR relative to s-II phase boundary at 30 bar for 1.0 mass% Luvicap Bio + 5 mass% methanol is ~10.8 °C. This is larger than the ~9.3 °C found for 0.5 mass% Luvicap Bio, indicating an apparent increase in Luvicap Bio CGI performance at this higher polymer concentration, with top-up effects retained. It clearly shows that Luvicap Bio performance is generally improved at the higher polymer concentration, i.e. as shown in Figure 4-19, the CIR increases ~1.7 °C for 1 mass%

Luvicap Bio compared to 0.5 mass%, both with 5.0 mass% methanol over the range of pressure tested. This increase in CIR is more obvious at higher pressure, e.g. ~2 °C at 120 bar.

In contrast to data for 5 mass% methanol, the CIR boundaries for 1.0 and 0.5 mass% Luvicap Bio, both with 10% MeOH, are very similar, as shown in Figure 4-20. In addition, as can be seen in Figure 4-21, for 20 mass% MeOH, the CIR increases ~1.0 °C at the higher polymer dose (1.0% compared to 0.5% in this case). However, as shown in Figure 4-22, the result for 30 mass% methanol shows that while CIR increases ~1.5 °C for 1 mass% Luvicap Bio compared to 0.5 mass% for low pressure, the CIR boundaries for these two systems are similar at high pressure.

Figure 4-23 shows the CGI boundaries for 1.0 and 0.5 mass% Luvicap Bio alone in the natural gas system, indicating the CIR increases modestly at higher polymer dose, i.e. ~1.0 °C for 1 mass% Luvicap Bio compared to 0.5 mass%. This, and data for 5 mass% methanol (Figure 4-19) suggests that the benefits of using a higher polymer dose is most evident at the lowest methanol concentrations (~2 °C for 1.0% Bio + 5% MeOH compared to 0.5% Bio + 5 % MeOH), although this is overall fairly marginal, and the net CGI gains of using 1.0% Bio compared to 0.5% are quite limited per unit dose, as can be seen in averaged data in Figure 4-17. Nevertheless, methanol does still act more as a full top-up inhibitor for 1.0 mass% Luvicap Bio compared to 0.5 mass%, and the negative effect of methanol on Luvicap Bio performance decreases at higher Luvicap Bio concentrations.

Table 4-7. Experimental natural gas hydrate CGI region data for 1.0 mass% Luvicap Bio aqueous (relative to water) with 5 mass% methanol (relative to water + Luvicap Bio).

CGR boundary	Growth rate	T / °C (±0.5)	P / bar (±0.2)	ΔTs-I / °C (±0.5)	ΔTs-II / °C (±0.5)
CIR-SGR(VS)	No growth	-2.8	29.4	-4.7	-10.8
		1.8	53.3	-5.5	-10.8
		4.3	74.4	-5.8	-10.6
		6.0	100.5	-6.4	-10.6
		7.4	126.6	-6.6	-10.4
		9.0	148.7	-6.1	-9.5
SGR(VS)-RGR	Very Slow	1.2	53.0	-6.1	-11.4
		3.4	73.8	-6.7	-11.4
		5.2	99.7	-7.2	-11.4
		6.8	125.6	-7.2	-10.9
		7.8	147.7	-7.4	-10.7
SDR	Slow dissociation	11.3	32.0	-	2.6
		15.8	58.1	-	2.6
		18.0	81.3	-	2.6
		19.8	111.5	-	2.6
		20.9	141.1	-	2.6
		21.7	166.9	-	2.6

Table 4-8. Experimental natural gas hydrate CGI region data for 1.0 mass% Luvicap Bio aqueous (relative to water) with 10 mass% methanol (relative to water + Luvicap Bio).

CGR boundary	Growth rate	T / °C (±0.5)	P / bar (±0.2)	ΔTs-I / °C (±0.5)	ΔTs-II / °C (±0.5)
CIR-SGR(VS)	No growth	-4.5	29.1	-4.2	-10.3
		-0.1	51.2	-4.9	-10.3
		2.5	75.4	-5.5	-10.2
		3.9	93.8	-5.7	-10.1
		6.0	120.6	-5.4	-9.3
		7.9	153.3	-5.1	-8.5
SGR(VS)-RGR	Very Slow	-5.0	29.1	-4.7	-10.8
		-0.6	51.2	-5.4	-10.8
		2.0	75.4	-6.0	-10.7
		3.4	93.8	-6.2	-10.6
		5.5	120.6	-5.9	-9.8
		7.4	153.3	-5.6	-9.0
SDR	Slow dissociation	8.4	31.4	-	2.0
		12.8	55.8	-	2.0
		15.3	82.5	-	2.0
		17.8	134.0	-	2.0
		18.8	170.4	-	2.0

Table 4-9. Experimental natural gas hydrate CGI region data for 1.0 mass% Luvicap Bio aqueous (relative to water) with 20 mass% methanol (relative to water + Luvicap Bio).

CGR boundary	Growth rate	T / °C (±0.5)	P / bar (±0.2)	ΔTs-I / °C (±0.5)	ΔTs-II / °C (±0.5)
CIR-SGR(VS)	No growth	-9.9	25.6	-3.7	-10.0
		-3.5	58.3	-4.5	-9.8
		-2.0	74.0	-4.9	-9.8
		-0.1	96.1	-4.9	-9.4
		1.3	118.5	-4.9	-8.9
		3.5	161.5	-4.6	-8.0
SGR(VS)-RGR	Very Slow	-11.0	25.4	-4.7	-11.0
		-3.9	58.2	-4.9	-10.2
		-2.4	73.8	-5.3	-10.2
		-0.9	95.4	-5.6	-10.1
		0.3	116.9	-5.8	-9.9
		2.5	160.1	-5.5	-9.0
SDR	Slow dissociation	1.8	27.8		1.0
		7.8	63.1	-	1.0
		9.2	79.4	-	1.0
		10.6	103.9	-	1.0
		11.6	128.8	-	1.0
		12.9	176.6	-	1.0

Table 4-10. Experimental natural gas hydrate CGI region data for 1.0 mass% Luvicap Bio aqueous (relative to water) with 30 mass% methanol (relative to water + Luvicap Bio).

CGR boundary	Growth rate	T / °C (±0.5)	P / bar (±0.2)	ΔTs-I / °C (±0.5)	ΔTs-II / °C (±0.5)
CIR-SGR(VS)	No growth	-12.7	33.6	-3.7	-9.7
		-8.7	58.7	-4.3	-9.7
		-6.9	78.9	-4.7	-9.7
		-5.6	100.9	-5.0	-9.6
		-3.9	136.0	-5.2	-9.1
		-1.5	173.4	-4.2	-7.7
		0.2	229.2	-4.1	-7.2
		1.5	290.0	-4.3	-7.1
SGR(VS)-RGR	Very Slow	-13.9	33.4	-4.8	-10.9
		-9.3	58.3	-4.9	-10.3
		-7.5	78.5	-5.3	-10.3
		-6.3	100.4	-5.7	-10.3
		-4.6	135.4	-5.8	-9.8
		-3.0	172	-5.6	-9.1
		-1.1	225.1	-5.3	-8.4
		0.3	285.8	-5.4	-8.2
SDR	Slow dissociation	No SDR			

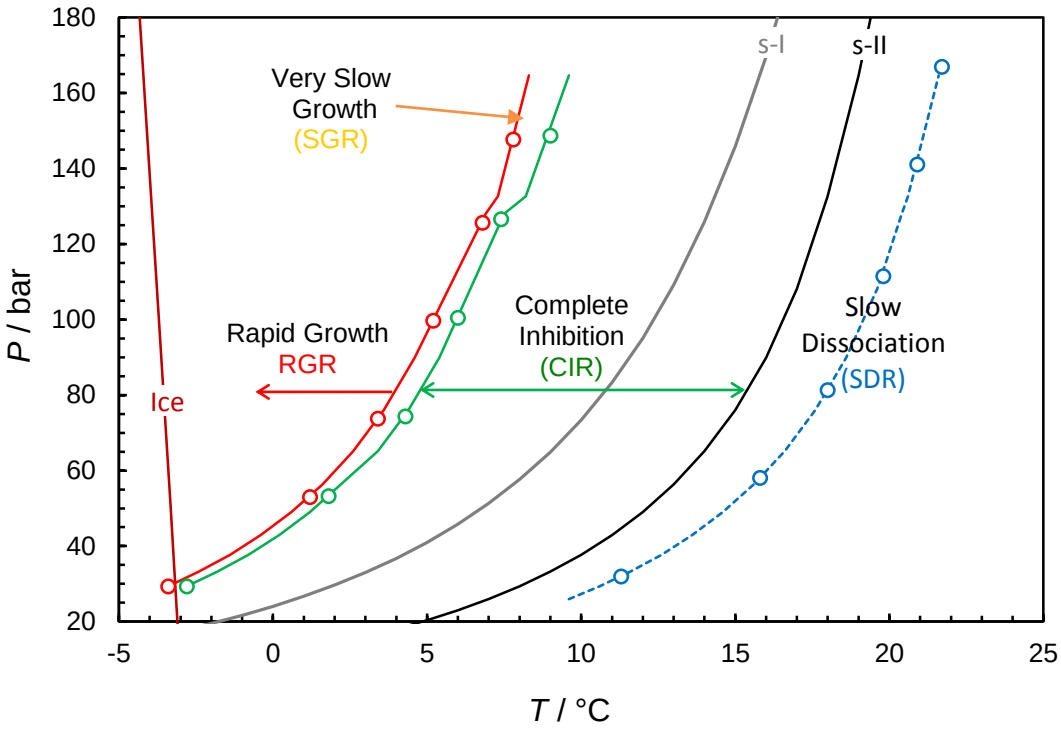

Figure 4-12. Experimental natural gas hydrate CGI region data for 1.0 mass% Luvicap Bio aqueous with 5.0 mass% methanol (relative to water + Luvicap) showing CGI regions determined from changes in relative hydrate growth rates.

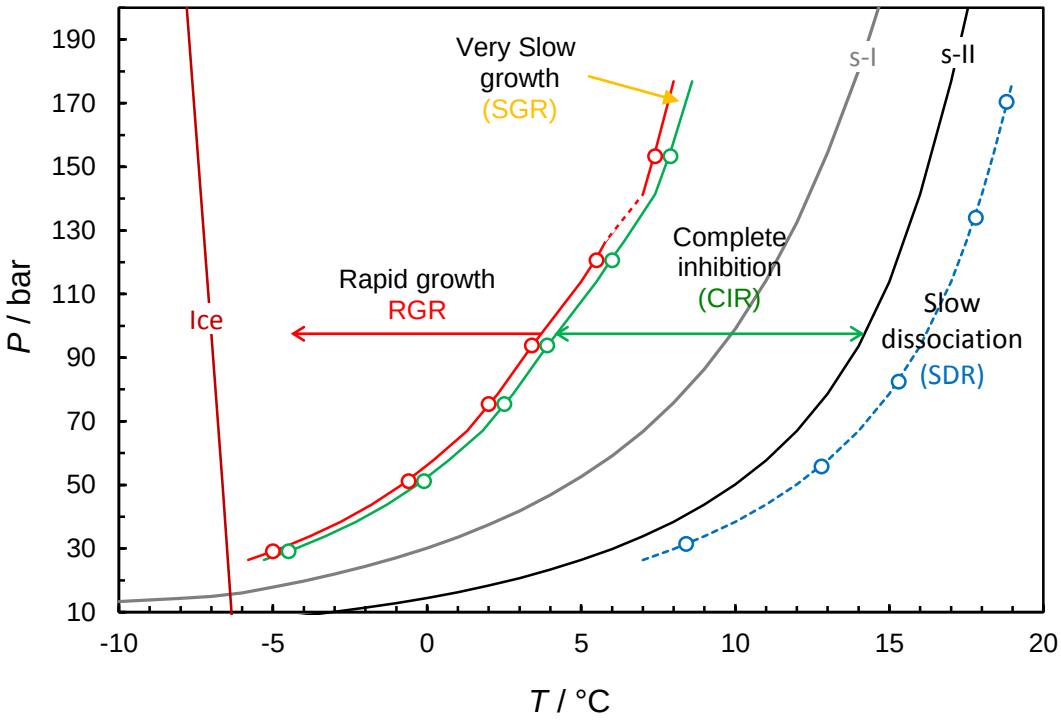

Figure 4-13. Experimental natural gas hydrate CGI region data for 1.0 mass% Luvicap Bio aqueous with 10 mass% methanol (relative to water + Luvicap) showing CGI regions determined from changes in relative hydrate growth rates.

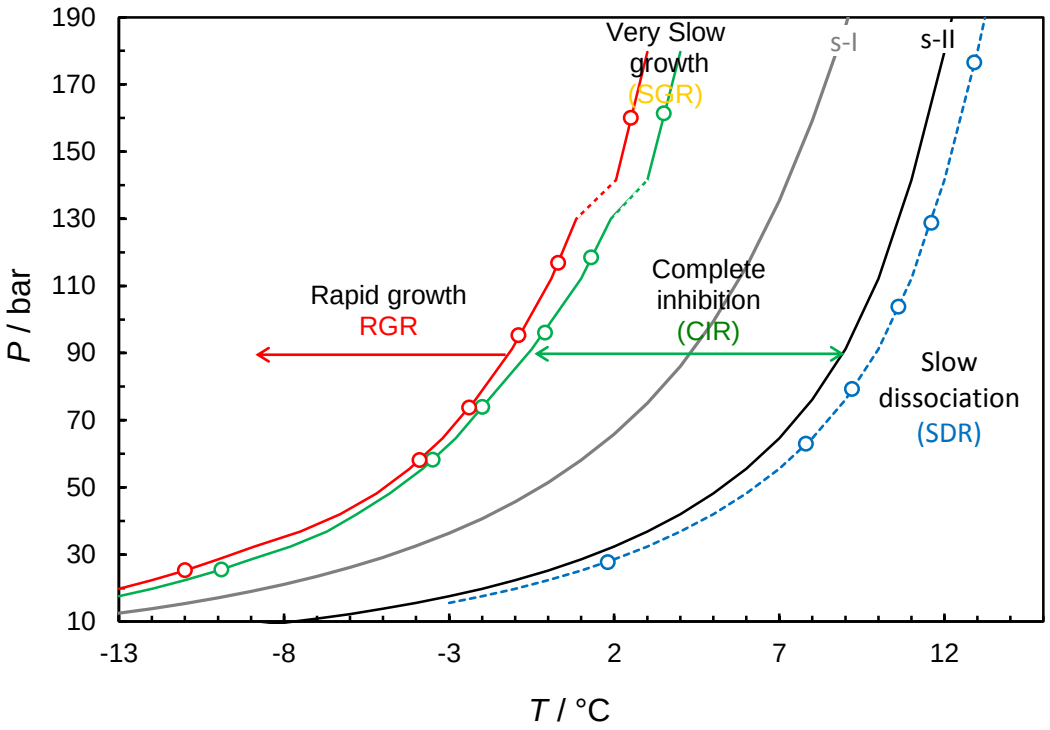

Figure 4-14. Experimental natural gas hydrate CGI region data for 1.0 mass% Luvicap Bio aqueous with 20 mass% methanol (relative to water + Luvicap) showing CGI regions determined from changes in relative hydrate growth rates.

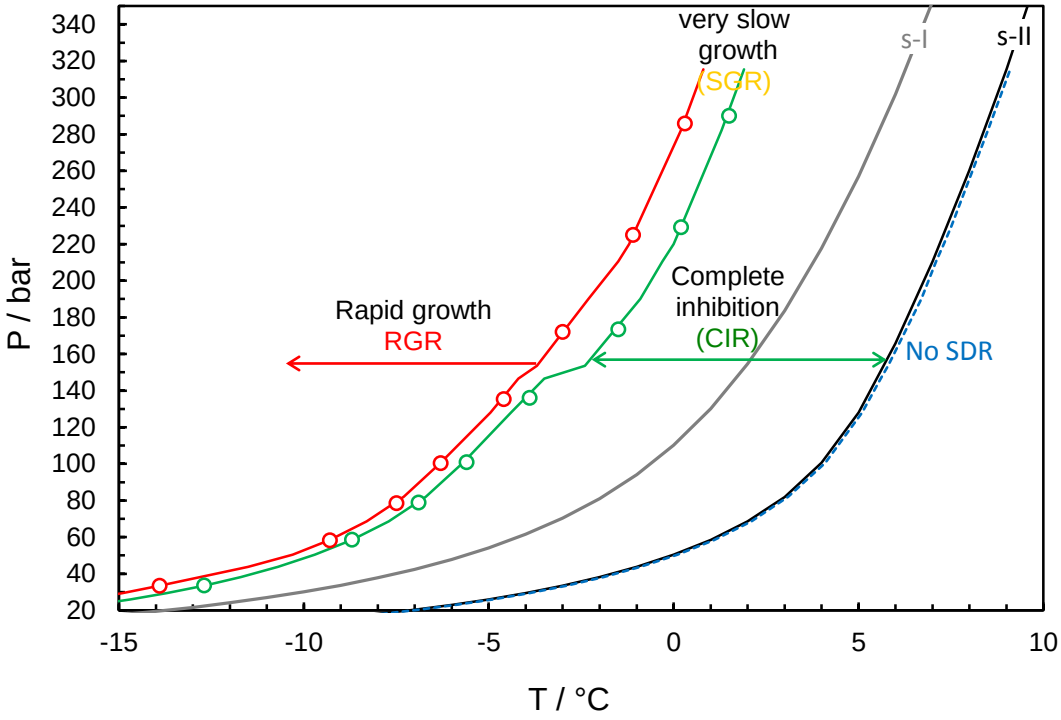

Figure 4-15. Experimental natural gas hydrate CGI region data for 1.0 mass% Luvicap Bio aqueous with 30 mass% methanol (relative to water + Luvicap) showing CGI regions determined from changes in relative hydrate growth rates.

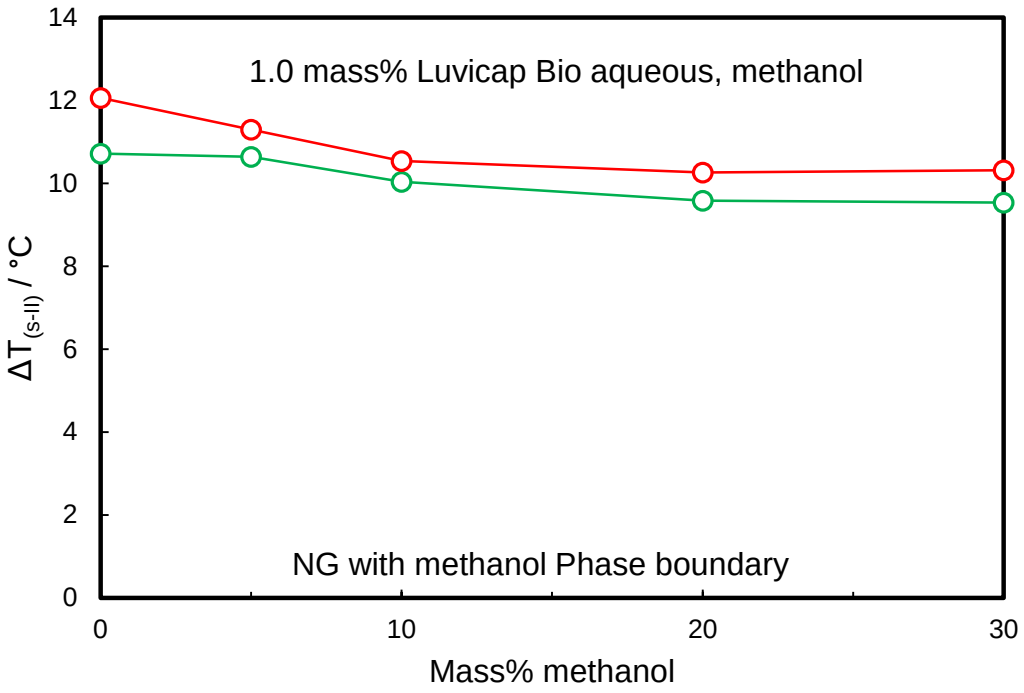

Figure 4-16. Average (25 to 150 bar) Luvicap Bio induced CGI regions for 1.0 mass% Luvicap Bio aqueous as a function of methanol mass% (relative to water + Luvicap Bio) relative to the MeOH-inhibited s-II boundary for the natural gas-methanol-water system.

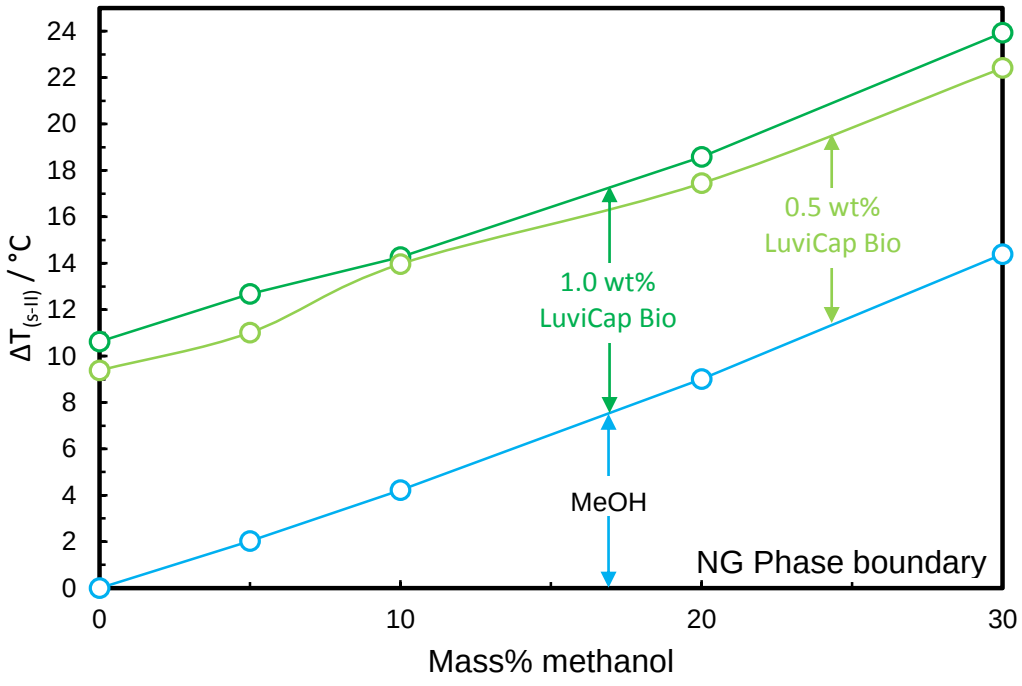

Figure 4-17. Average (25 to 150 bar) Luvicap Bio induced CIR region for 1.0 and 0.5 mass% Luvicap Bio aqueous as a function of methanol mass% (relative to water + Luvicap Bio) + MeOH thermodynamic inhibition for the natural gas-water system.

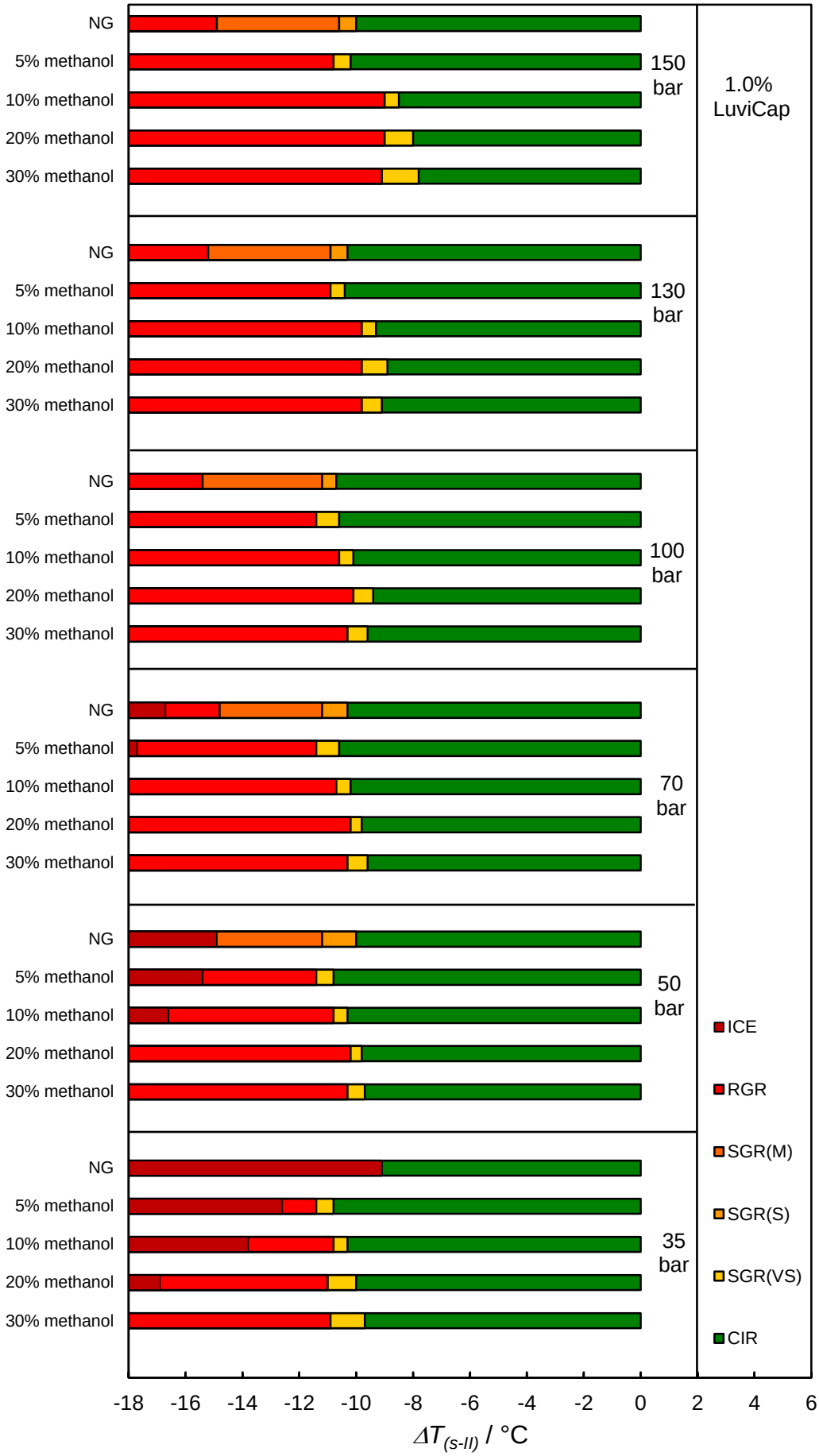

Figure 4-18. Comparison of subcooling extents of CGI regions from the s-II phase boundary for 1.0 mass% Luvicap Bio aqueous with natural gas and different methanol mass%.

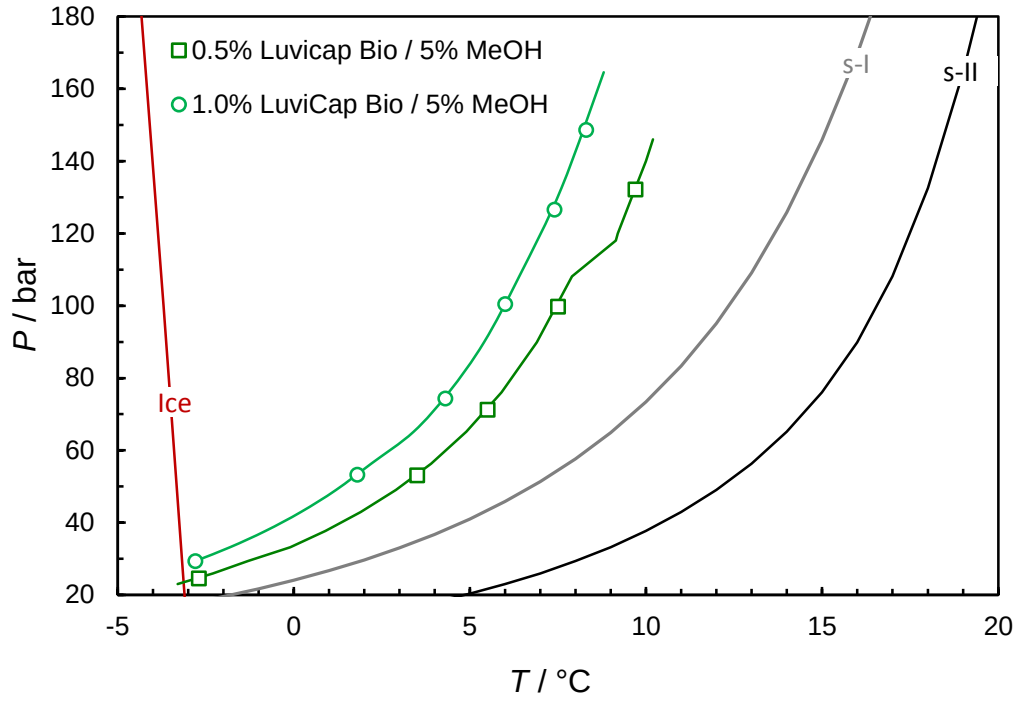

Figure 4-19. Comparison of measured CIR boundaries for 0.5 and 1.0 mass% Luvicap Bio, both with 5 mass% MeOH and natural gas.

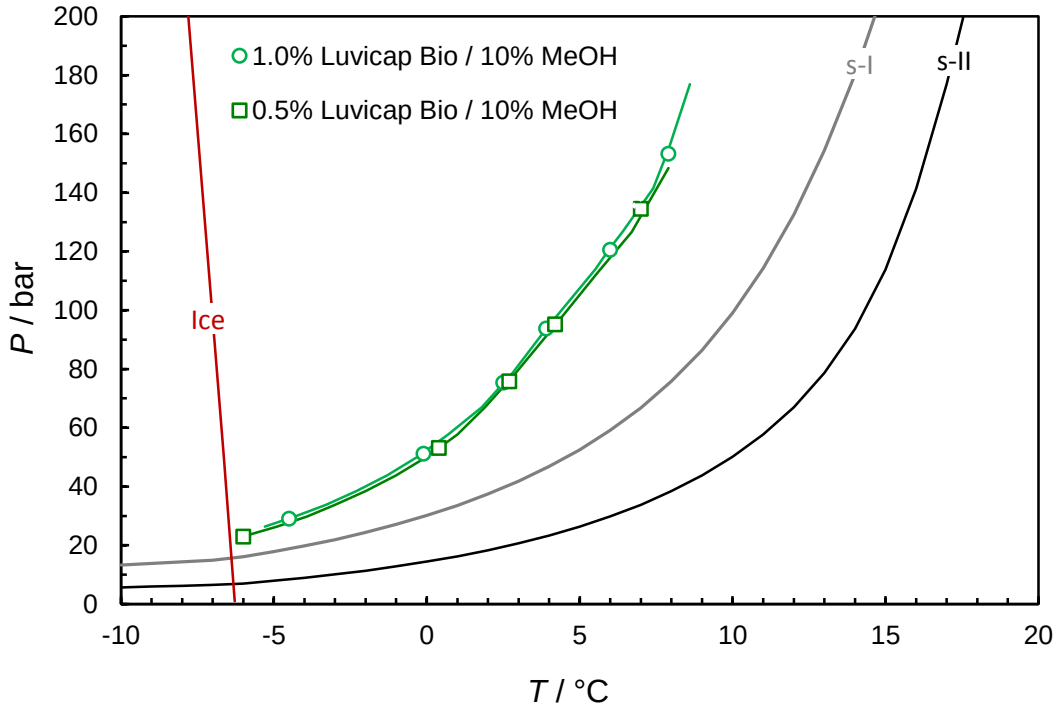

Figure 4-20. Comparison of measured CIR boundaries for 0.5 mass% Luvicap Bio and 1.0 mass% Luvicap Bio with 10 mass% MeOH and natural gas.

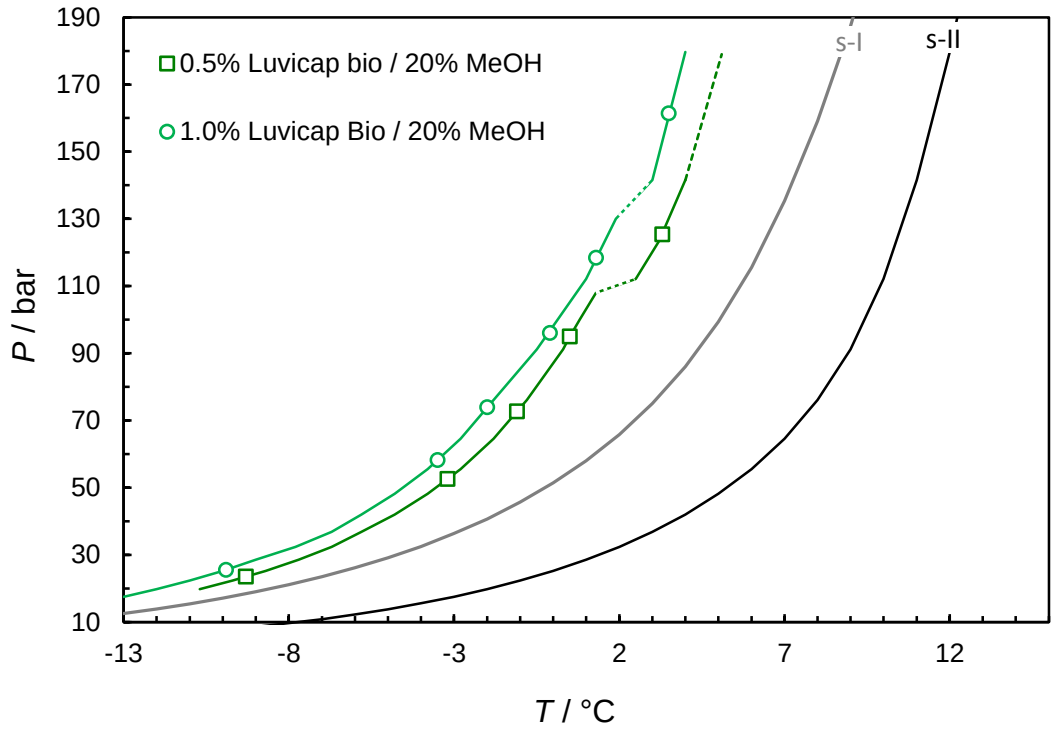

Figure 4-21. Comparison of measured CIR boundaries for 0.5 mass% Luvicap Bio and 1.0 mass% Luvicap Bio with 20 mass% MeOH and natural gas.

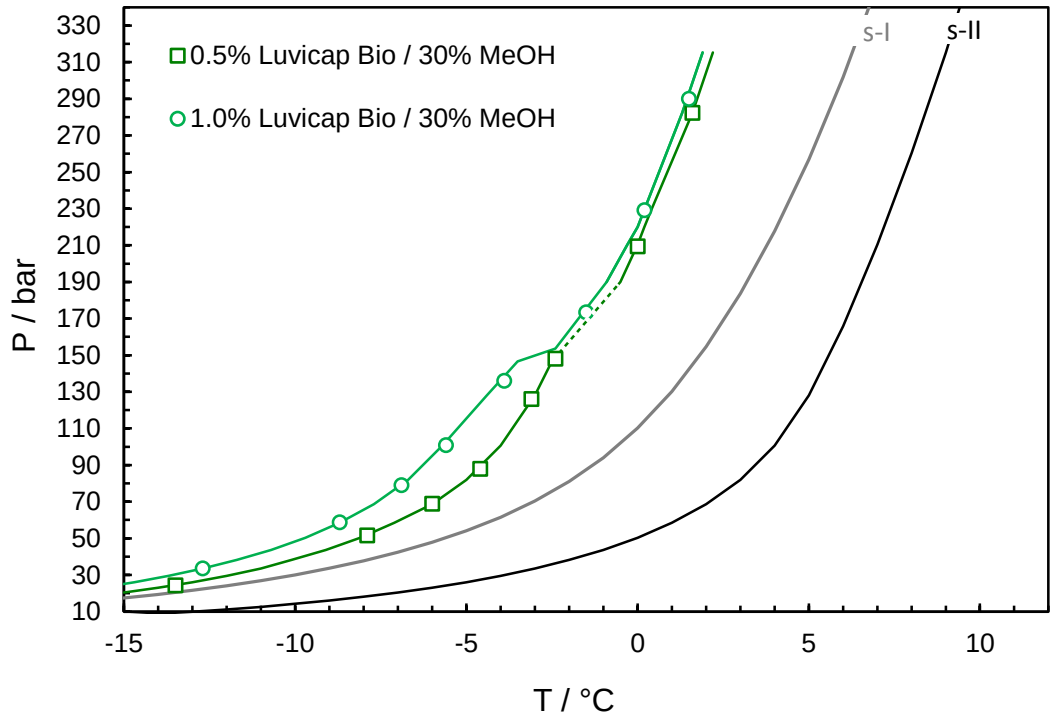

Figure 4-22. Comparison of measured CIR boundaries for 0.5 mass% Luvicap Bio and 1.0 mass% Luvicap Bio with 30 mass% MeOH and natural gas.

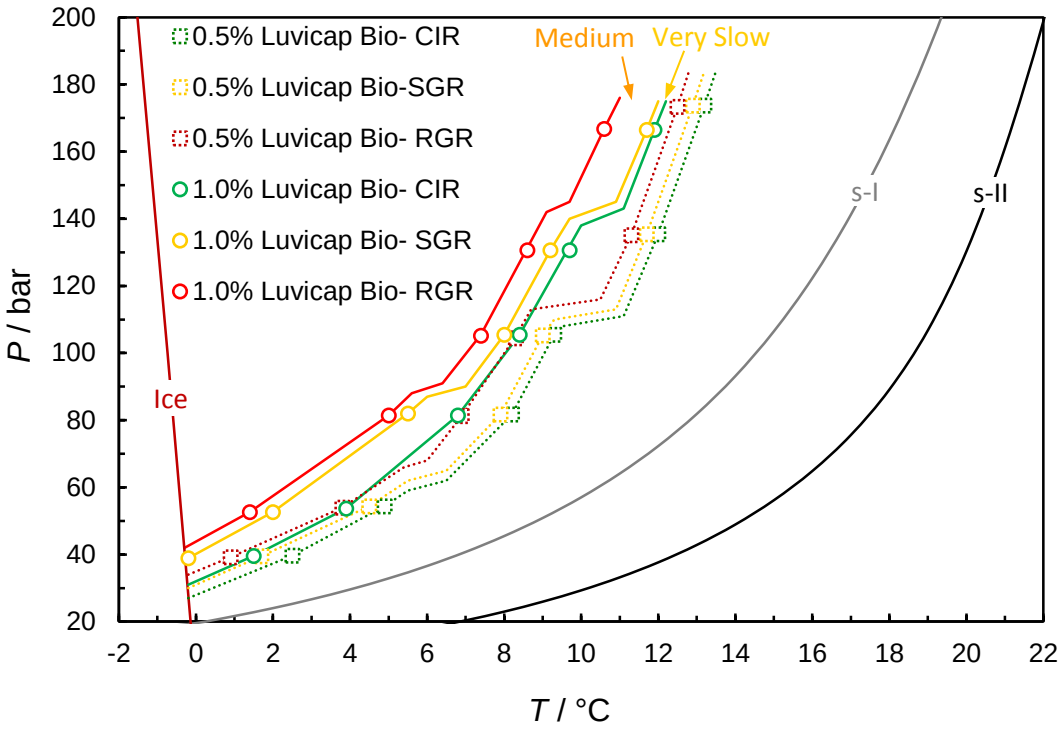

Figure 4-23. Comparison of measured CGI boundaries for 0.5 and 1.0 mass% Luvicap Bio (no methanol), both with natural gas. PT plot showing measured experimental points delineating the various crystal growth inhibition regions for these two system (0.5 and 1.0 mass% Luvicap) with natural gas are reported in Appendix A.6.

4.3.3 0.5 Mass% Luvicap Bio with Ethanol in a Natural Gas system

As noted, given that methanol seems to act as a top-up inhibitor for Luvicap Bio in contrast to behaviour for other polymers (e.g. PVCap), it was decided to see whether this was the case also for ethanol; a more environmentally friendly alternative which also shows poor top-up effects typically for KHIs [4.7]. Therefore, CGI tests were carried out for 5, 10, 20, and 30 mass% ethanol with 0.5 mass% Luvicap Bio in a natural gas system.

Figure 4-24 shows example CGI method cooling/heating curves for 0.5 mass% Luvicap Bio with 5 mass% aqueous ethanol (relative to water + Luvicap Bio) in the natural gas system. CGI boundary data points for these systems tested so far are reported in Table 4-11 to Table 4-14, and presented in Figure 4-25 to Figure 4-28. Pressure / temperature plots showing measured experimental points delineating the various crystal growth inhibition regions for these systems are reported in Appendix A.3. As can be seen, for example, the CIR at 20 mass% ethanol ranges from ~9.1 °C at low pressures (25 bar) to ~4.9 °C at high pressures (300 bar), so could offer top-up potential.

Figure 4-29 shows the average (25 to 150 bar) Luvicap Bio induced CGI regions for 0.5 mass% Luvicap Bio aqueous as a function of EtOH mass% (relative to water + Luvicap Bio) relative to the EtOH-inhibited s-II boundary for the natural gas-EtOH-water

system. As can be seen, while EtOH has an increasingly negative effect on Bio performance with increasing concentration, there is still a reasonable top-up effect, with a CIR of ~7 °C at 30 mass% EtOH.

Figure 4-30 shows a comparison of the subcooling extents of CGI regions from the s-II phase boundary measured for 0.5 mass% Luvicap Bio aqueous with natural gas and different EtOH concentrations over the range of pressures studied. As can be seen, the CIR extent is completely preserved for 5 mass% ethanol up to 70 bar. Therefore, ethanol could act as a full-top up inhibitor for combination with Luvicap Bio at low pressure and low ethanol concentration. Figure 4-30 shows the CIR and RGR extent reduces with pressure measurably, indicating the negative effect of ethanol on Luvicap Bio at higher pressure. While the CIR extent reduces with pressure measurably, it is quite comparable to the same mass% methanol aqueous to around 70 bar, meaning ethanol could offer a more environmentally friendly top-up inhibitor for combination with Luvicap Bio, at least at low pressure and lower ethanol concentration, depending on operating conditions. But, generally, the CIR extent, in a natural gas system with 0.5 mass% Luvicap Bio, is more preserved in the presence of methanol rather than ethanol.

Figure 4-31 shows the average (25 to 150 bar) Luvicap Bio induced CIR region for 0.5 mass% Luvicap Bio aqueous as a function of EtOH mass% (relative to water + Luvicap Bio) + EtOH thermodynamic inhibition for the natural gas-water system. Figure 4-32 shows calculated mass% EtOH inhibition equivalent to EtOH + 0.5 mass% Luvicap Bio (thermodynamic ethanol inhibition + CIR) as a function of EtOH mass% (+0.5 mass% Luvicap Bio). For example, as shown in Figure 4-32, 16 mass% EtOH + 0.5 mass% Luvicap Bio offers the complete inhibition equivalent of 40 mass% ethanol. This would constitute a 60% ethanol reduction. The same value for 0.5 mass% Luvicap Bio + methanol + natural gas, as reported before, is a 35% methanol reduction. It suggests that Luvicap Bio could reduce ethanol more than methanol, although methanol acts as a more top-up inhibitor than ethanol in 0.5 mass% Luvicap Bio, i.e., the CIR extent is more preserved in methanol + Luvicap Bio rather than ethanol + Luvicap Bio in the natural gas system. This could be due to the fact that, in terms of mole%, methanol is stronger than ethanol in shifting hydrate phase boundary to lower temperature and higher pressure, i.e., methanol is more polar than ethanol. However, if mass% is used, methanol is much stronger than ethanol, because methanol has lower molecular weight, so more moles in the same mass%.

Table 4-11. Experimental natural gas hydrate CGI region data for 0.5 mass% Luvicap Bio aqueous (relative to water) with 5 mass% EtOH (relative to water + Luvicap Bio).

CGR boundary	Growth rate	T / °C (±0.5)	P / bar (±0.2)	ΔTs-I / °C (±0.5)	ΔTs-II / °C (±0.5)
CIR-SGR(S)	No growth	-1.7	28.9	-4.1	-10.2
		3.0	52.5	-4.8	-10.2
		5.7	77.4	-5.4	-10.2
		8.3	101.8	-4.9	-9.2
		10.8	137.7	-4.5	-8.2
		12.1	160.9	-4.3	-7.5
SGR(S)-RGR	Slow	2.0	52.2	-5.8	-11.2
		4.9	76.7	-6.1	-10.9
		7.4	101.4	-5.8	-10.0
		9.7	135.6	-5.5	-9.2
		11.1	160.4	-5.2	-8.5
SDR	Slow dissociation	11.0	31.5	-	1.7
		15.5	56.8	-	1.7
		18.1	83.9	-	1.7
		19.6	111.1	-	1.7
		21.1	149.5	-	1.7
		21.7	176.2	-	1.7

Table 4-12. Experimental natural gas hydrate CGI region data for 0.5 mass% Luvicap Bio aqueous (relative to water) with 10 mass% EtOH (relative to water + Luvicap Bio).

CGR boundary	Growth rate	T / °C (±0.5)	P / bar (±0.2)	ΔTs-I / °C (±0.5)	ΔTs-II / °C (±0.5)
CIR-SGR(S)	No growth	-2.0	29.6	-3.2	-9.4
		2.6	52.7	-3.8	-9.3
		5.3	77.2	-4.3	-9.2
		7.1	98.3	-4.3	-8.8
		9.2	127.9	-4.1	-8.0
		11.5	168.6	-3.6	-7.0
SGR(S)-RGR	Slow	-3.0	29.6	-4.2	-10.4
		1.5	52.6	-4.9	-10.4
		4.3	77.0	-5.2	-10.2
		6.0	97.2	-5.3	-9.8
		7.9	126	-5.2	-9.2
		10.1	166.7	-4.9	-8.4
SDR	Slow dissociation	9.3	32.0	-	1.2
		13.5	56.0	-	1.2
		16.1	83.2	-	1.2
		17.4	105.4	-	1.2
		18.8	138.7	-	1.2
		20.1	181.9	-	1.2

Table 4-13. Experimental natural gas hydrate CGI region data for 0.5 mass% Luvicap Bio aqueous (relative to water) with 20 mass% EtOH (relative to water + Luvicap Bio).

CGR boundary	Growth rate	T / °C (±0.5)	P / bar (±0.2)	ΔTs-I / °C (±0.5)	ΔTs-II / °C (±0.5)
CIR-SGR(S)	No growth	-6.5	24.3	-2.5	-9.1
		-0.4	49.7	-2.9	-8.7
		3.4	75.6	-2.6	-7.7
		5.2	97.0	-2.6	-7.3
		7.9	138	-2.4	-6.3
		11.0	220.8	-2.4	-5.4
		13.3	307.1	-2.3	-4.9
SGR(S)-RGR	Slow	-7.5	24.5	-3.6	-10.2
		-2.1	48.5	-4.4	-10.2
		1.1	74.0	-4.7	-9.9
		3.8	97.0	-4.1	-8.7
		6.2	136.4	-4.0	-7.9
		10.4	220.8	-3.0	-6.0
		12.6	306.4	-3.0	-5.6
SDR	Slow dissociation	No SDR			

Table 4-14. Experimental natural gas hydrate CGI region data for 0.5 mass% Luvicap Bio aqueous (relative to water) with 30 mass% EtOH (relative to water + Luvicap Bio).

CGR boundary	Growth rate	T / °C (±0.5)	P / bar (±0.2)	ΔTs-I / °C (±0.5)	ΔTs-II / °C (±0.5)
CIR-SGR(S)	No growth	-7.2	28.7	-1.4	-7.9
		-2.2	50.7	-1.5	-7.3
		0.0	71.8	-2.1	-7.2
		2.0	96.0	-2.3	-7.0
		4.0	126.3	-2.1	-6.2
		5.3	160.0	-2.3	-5.9
SGR(S)-RGR	Slow	-9.5	28.2	-3.6	-10.1
		-4.1	50.3	-3.3	-9.1
		-1.5	71.1	-3.5	-8.7
		0.5	95.0	-3.7	-8.4
		2.5	125.0	-3.5	-7.7
		4.2	158.0	-3.3	-6.9
SDR	Slow dissociation	No SDR			

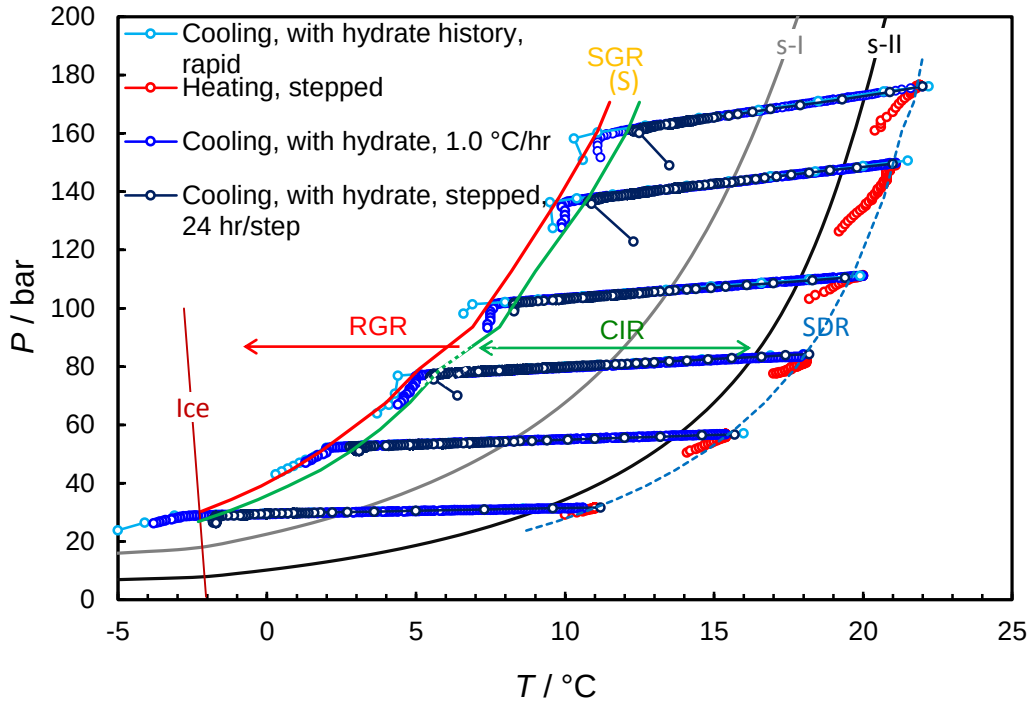

Figure 4-24. Example CGI method cooling curves for 0.5 mass% Luvicap Bio / 5 mass % EtOH aqueous with natural gas.

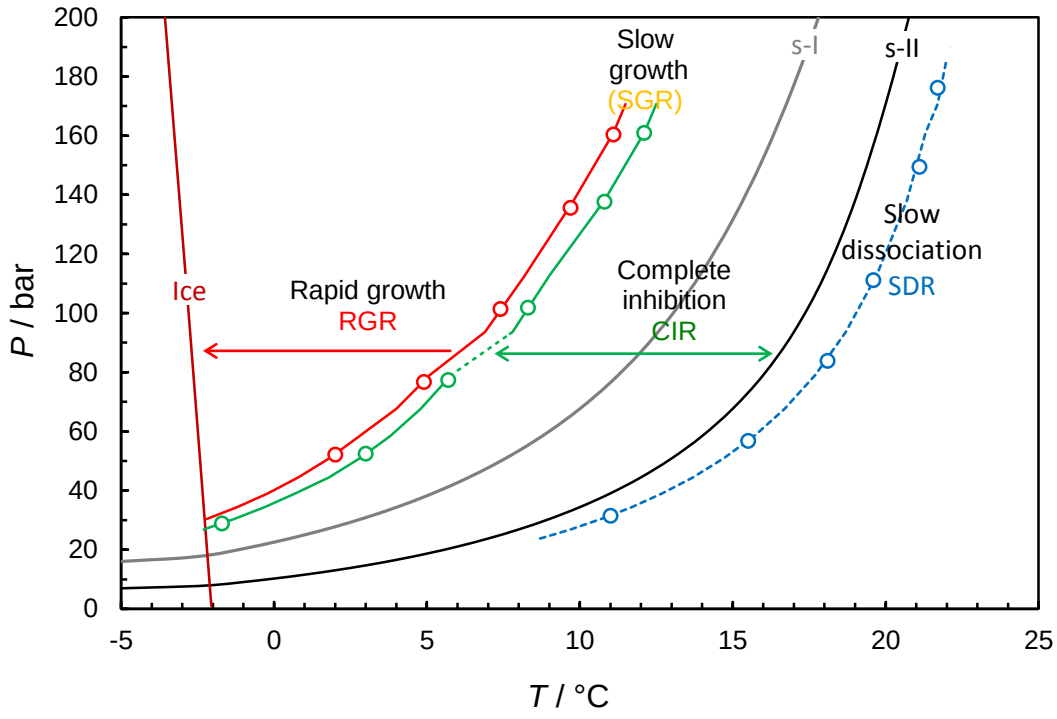

Figure 4-25. Experimental natural gas hydrate CGI region data for 0.5 mass% Luvicap Bio aqueous with 5.0 mass % EtOH (relative to water + Luvicap) showing CGI regions determined from changes in relative hydrate growth rates.

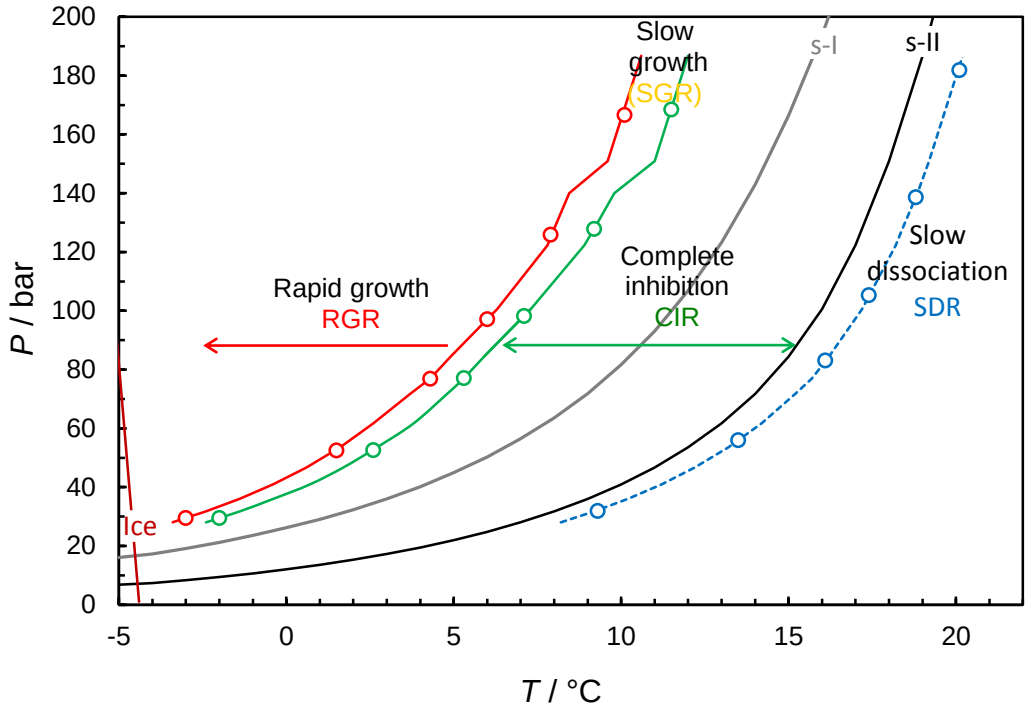

Figure 4-26. Experimental natural gas hydrate CGI region data for 0.5 mass% Luvicap Bio aqueous with 10 mass % EtOH (relative to water + Luvicap) showing CGI regions determined from changes in relative hydrate growth rates.

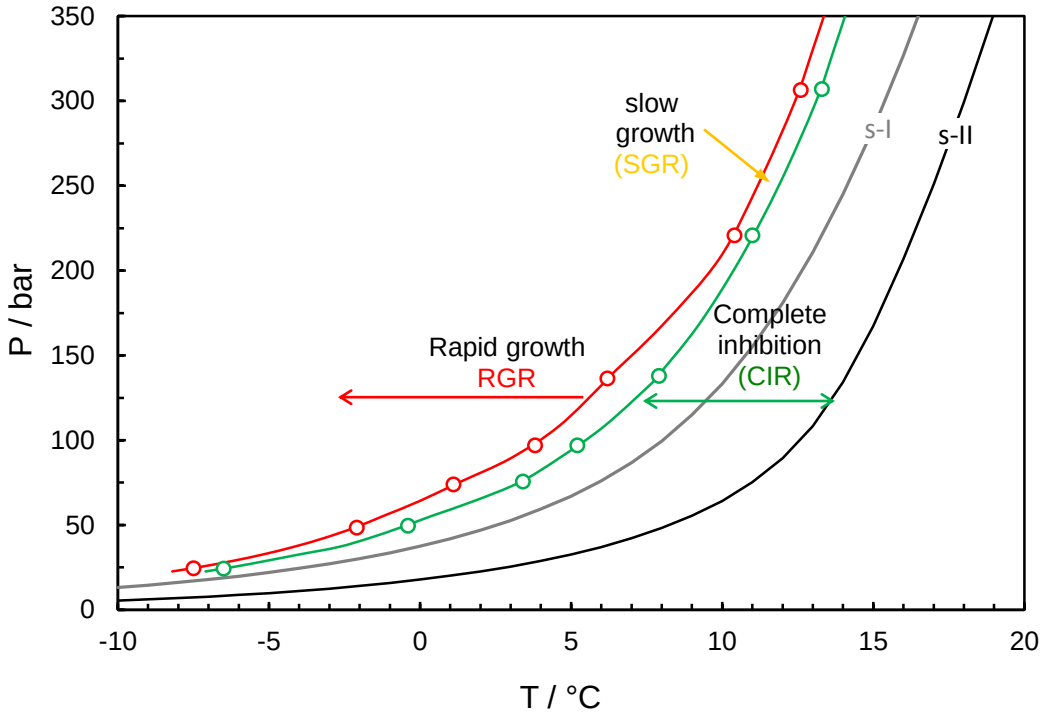

Figure 4-27. Experimental natural gas hydrate CGI region data for 0.5 mass% Luvicap Bio aqueous with 20 mass % EtOH (relative to water + Luvicap) showing CGI regions determined from changes in relative hydrate growth rates.

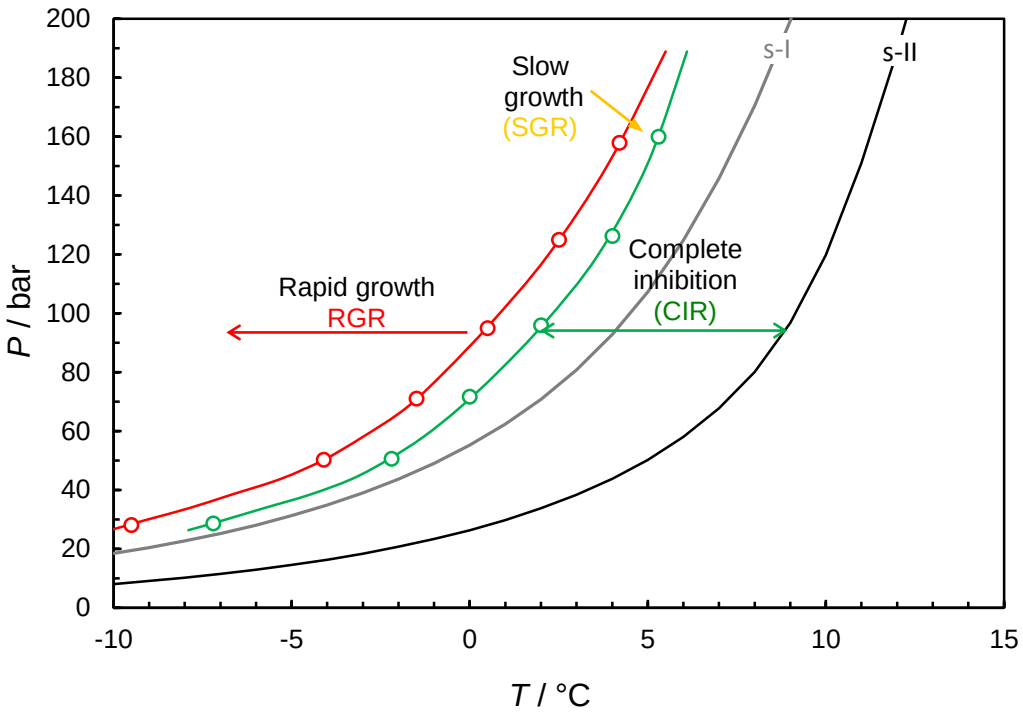

Figure 4-28. Experimental natural gas hydrate CGI region data for 0.5 mass% Luvicap Bio aqueous with 30 mass % EtOH (relative to water + Luvicap) showing CGI regions determined from changes in relative hydrate growth rates.

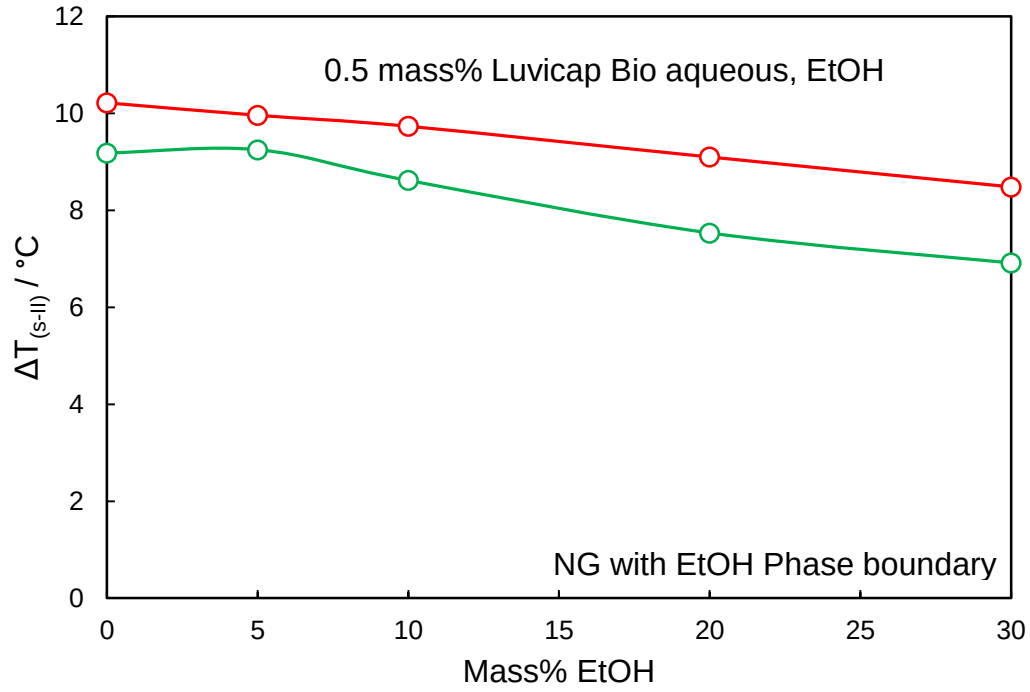

Figure 4-29. Average (25 to 150 bar) Luvicap Bio induced CGI regions for 0.5 mass% Luvicap Bio aqueous as a function of EtOH mass% (relative to water + Luvicap Bio) relative to the EtOH-inhibited s-II boundary for the natural gas-EtOH-water system.

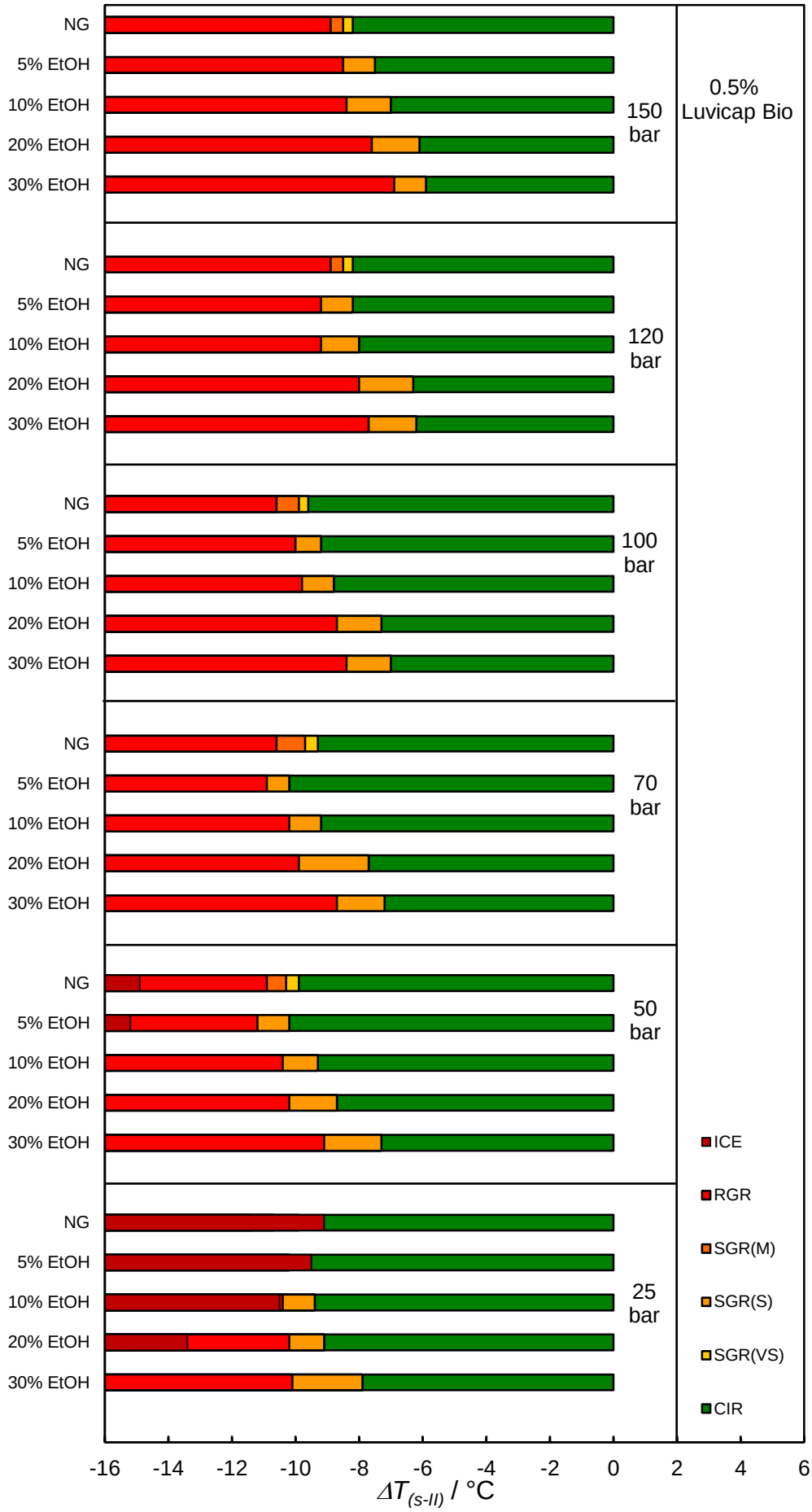

Figure 4-30. Comparison of subcooling extents of CGI regions from the s-II phase boundary for 0.5 mass% Luvicap Bio aqueous with natural gas and different EtOH mass%.

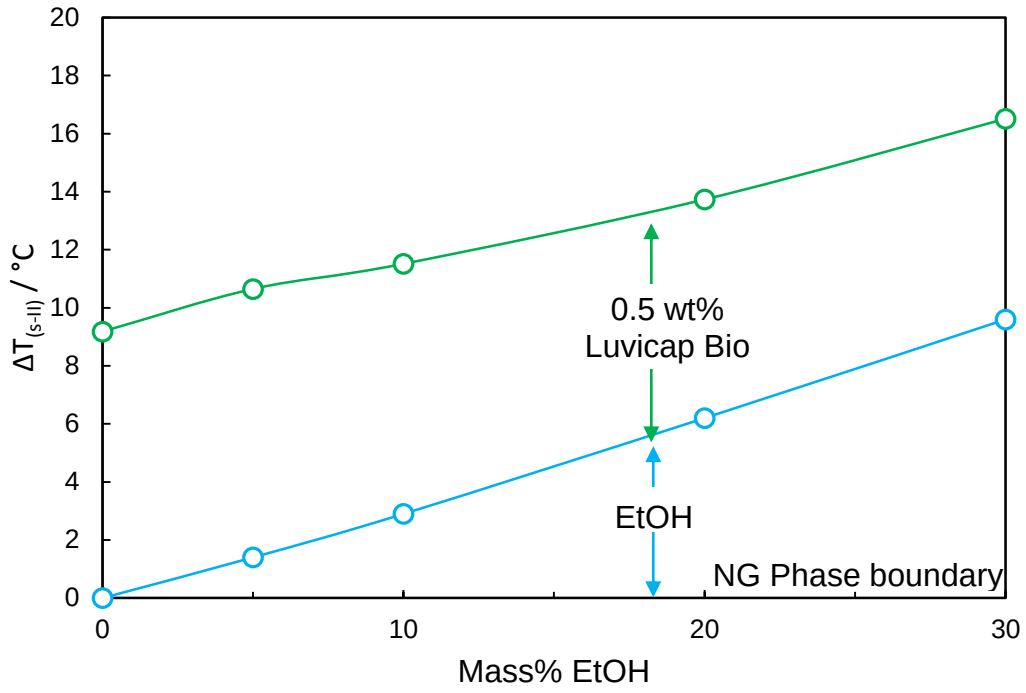

Figure 4-31. Average (25 to 150 bar) Luvicap Bio induced CIR region for 0.5 mass% Luvicap Bio aqueous as a function of EtOH mass% (relative to water + Luvicap Bio) + EtOH thermodynamic inhibition for the natural gas-water system.

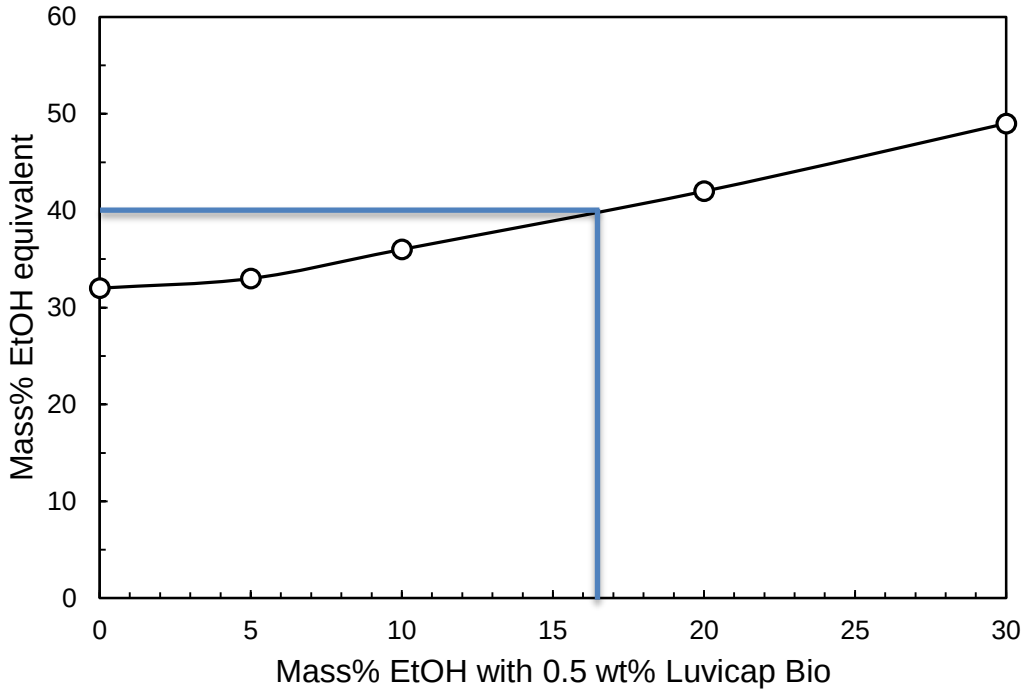

Figure 4-32. Calculated mass% EtOH inhibition equivalent to EtOH + 0.5 mass% Luvicap Bio (thermodynamic ethanol inhibition + CIR) as a function of EtOH mass% (+0.5 mass% Luvicap Bio). 40 mass% EtOH can be replaced by 16 mass% EtOH + 0.5 mass% Luvicap Bio.

4.3.4 0.5 Mass% Luvicap Bio with MEG in a Natural Gas system

As noted, measurements on combined MEG-PVCap inhibition showed that MEG has a generally positive effect, and is normally a full top-up inhibitor for PVCap in both methane and natural gas systems, at least up to the concentration of 50 mass% tested [4-7]. In contrast, while methanol has a negative effect on PVCap, CGI measurements showed that methanol is normally a full top-up inhibitor for Luvicap Bio in a natural gas system, at least up to 20 mass% methanol. Therefore, to complete the performance evaluation of Luvicap Bio for different thermodynamic inhibitors, CGI measurements were carried out on combined MEG-Luvicap Bio systems.

Figure 4-33 shows example CGI method cooling/heating curves for Luvicap Bio + natural gas system with 5 mass% MEG aqueous. Measured CGI boundary data points with interpolations for 0.5 mass% Luvicap Bio with 5, 10, 20 and 30 mass% MEG and natural gas are plotted in Figure 4-34 to Figure 4-37, with completed data sets reported in Table 4-15 to Table 4-18. Pressure / temperature plots showing measured experimental points delineating the various crystal growth inhibition regions for these systems are reported in Appendix A.4. The average Luvicap Bio induced CGI regions for 0.5 mass% Luvicap Bio as a function of MEG mass% relative to the MEG-inhibited s-II boundary for the natural gas-MEG-water system is plotted in Figure 4-38. Figure 4-39 shows a comparison of the subcooling extents of CGI regions from the s-II phase boundary measured for 0.5 mass% Luvicap Bio aqueous with natural gas and different MEG concentrations over the range of pressures studied.

As can be seen, results suggest that MEG generally acts as a top-up inhibitor in terms of the most important CIR is preserved. Figure 4-39 indicates that MEG could act as a full top-up inhibitor for the range of MEG concentration tested (except for 5 mass% MEG), up to 150 bar.

While the top-up effect is fairly consistent with pressure in the case of >10 mass% MEG, at 5 mass% MEG, there is a more marked reduction in the extent of the CIR at higher pressure conditions. Therefore, except at 5 mass% MEG and higher pressure, MEG is normally a full top-up inhibitor for 0.5 mass% Luvicap Bio in natural gas systems.

As is the case for methanol with Luvicap Bio, CGI extents with MEG also seem to be related primarily to the s-II phase boundary, supporting the theory that Luvicap Bio is a stronger inhibitor for s-I, with s-II formation leading to 'failure'.

Figure 4-40 shows the average (25 to 150 bar) Luvicap Bio induced CIR region for 0.5 mass% Luvicap Bio aqueous as a function of MEG mass% (relative to water + Luvicap Bio) + MEG thermodynamic inhibition for the natural gas-water system. It clearly shows that the CIR extent is preserved for the MEG concentration up to 30 mass%, except with the exception of 5 mass%, indicating the full top-up inhibitor effect of MEG. The general top-up effect means that MEG could be used to extend the subcooling range of Luvicap Bio, or Luvicap Bio be used to reduce MEG dosage requirements. Figure 4-41 shows calculated mass% MEG inhibition equivalent to MEG + 0.5 mass% Luvicap Bio (thermodynamic MEG inhibition + CIR) as a function of MEG mass% (+ 0.5 mass% Luvicap Bio). For example, as shown in Figure 4-41, 14 mass% MEG with 0.5 mass% Luvicap Bio could offer a full inhibition equivalent to 40 mass% MEG in the natural gas systems. This could reduce MEG consumption by 65%.

In contrast to methanol, the CGI results for PVCap + MEG (JIP report, [4-7]) and Luvicap Bio + MEG (this work) show that MEG is generally a full top-up inhibitor for both PVCap and Luvicap Bio inhibitors, suggesting this positive top-up effect is largely generic.

Table 4-15. Experimental natural gas hydrate CGI region data for 0.5 mass% Luvicap Bio aqueous (relative to water) with 5 mass% MEG (relative to water + Luvicap Bio).

CGR boundary	Growth rate	T / °C (±0.5)	P / bar (±0.2)	ΔT_{s-I} / °C (±0.5)	ΔT_{s-II} / °C (±0.5)
CIR-SGR(VS)	No growth	3.1	54.8	-5.4	-10.7
		6.3	78.1	-5.2	-9.8
		9.4	100.9	-4	-8.2
		11.1	124.7	-3.9	-7.6
		12.7	156.4	-3.8	-7.1
SGR(S)-RGR	Slow	1.9	53.8	-6.5	-11.7
		4.9	76.7	-6.4	-11.1
		7.0	98.2	-6.2	-10.5
		8.7	120.5	-6.0	-9.8
		10.4	149.7	-5.8	-9.2
SDR	Slow dissociation	12.0	27.3	-	3.7
		18.0	59.2	-	3.7
		20.4	85.6	-	3.7
		21.8	110.1	-	3.7
		22.9	136.7	-	3.7
		23.9	170.9	-	3.7

Table 4-16. Experimental natural gas hydrate CGI region data for 0.5 mass% Luvicap Bio aqueous (relative to water) with 10 mass% MEG (relative to water + Luvicap Bio).

CGR boundary	Growth rate	T / °C (±0.5)	P / bar (±0.2)	ΔT_{s-I} / °C (±0.5)	ΔT_{s-II} / °C (±0.5)
CIR-SGR(VS)	No growth	-2.6	27.8	-3.7	-9.9
		2.2	52.9	-4.8	-10.1
		4.7	75.5	-5.2	-10.0
		6.7	109.4	-6.0	-10.1
		7.4	124	-6.2	-10.0
		8.8	150.7	-6.1	-9.5
SGR(VS)-RGR	Very Slow	-3.5	27.5	-4.5	-10.7
		1.5	52.6	-5.4	-10.7
		4.1	75.2	-5.8	-10.5
		6.2	109	-6.5	-10.5
		7.3	124	-6.3	-10.1
		8.7	150.7	-6.2	-9.6
SDR	Slow dissociation	11.6	30.2	-	3.6
		16.4	57.2	-	3.6
		18.8	82.4	-	3.6
		20.9	121.9	-	3.6
		21.5	139.2	-	3.6
		22.4	168.4	-	3.6

Table 4-17. Experimental natural gas hydrate CGI region data for 0.5 mass% Luvicap Bio aqueous (relative to water) with 20 mass% MEG (relative to water + Luvicap Bio).

CGR boundary	Growth rate	T / °C (±0.5)	P / bar (±0.2)	ΔT_{s-I} / °C (±0.5)	ΔT_{s-II} / °C (±0.5)
CIR-SGR(VS)	No growth	-7.3	24.5	-4.3	-10.6
		-1.1	53.9	-5.2	-10.5
		1.4	79.2	-5.8	-10.5
		2.5	95.4	-6.1	-10.5
		3.5	117.4	-6.5	-10.5
		5.0	147.1	-6.5	-10.0
SGR(VS)-RGR	Very Slow	-7.9	24.2	-4.7	-11.1
		-1.6	54.3	-5.8	-11.1
		0.8	78.8	-6.4	-11.1
		1.9	95.0	-6.6	-11.1
		2.9	117.4	-7.1	-11.1
		4.5	146.5	-7.0	-10.5
SDR	Slow dissociation	7.7	26.8	-	3.6
		13.7	59.7	-	3.6
		16.0	87.0	-	3.6
		17.1	106.5	-	3.6
		18.2	132.7	-	3.6
		19.2	167.2	-	3.6

Table 4-18. Experimental natural gas hydrate CGI region data for 0.5 mass% Luvicap Bio aqueous (relative to water) with 30 mass% MEG (relative to water + Luvicap Bio).

CGR boundary	Growth rate	T / °C (±0.5)	P / bar (±0.2)	ΔT_{s-I} / °C (±0.5)	ΔT_{s-II} / °C (±0.5)
CIR-SGR(VS)	No growth	-10	26.9	-4.1	-10.4
		-5.0	51.4	-4.8	-10.3
		-2.3	75.3	-5.2	-10.1
		-0.4	100.9	-5.3	-9.8
		0.4	117.4	-5.5	-9.7
		2.3	146.7	-5.0	-8.7
SGR(VS)-RGR	Very Slow	-10.8	26.7	-4.8	-11.1
		-5.8	50.7	-5.5	-11.1
		-2.8	74.5	-5.7	-10.6
		-0.9	100.8	-5.8	-10.2
		0.1	117.4	-5.8	-10.0
		1.7	144.9	-5.6	-9.2
SDR	Slow dissociation	4.7	29.3	-	3.6
		9.5	55.8	-	3.6
		12	83.2	-	3.6
		13.5	112.6	-	3.6
		14.1	131.6	-	3.6
		15.1	165.3	-	3.6

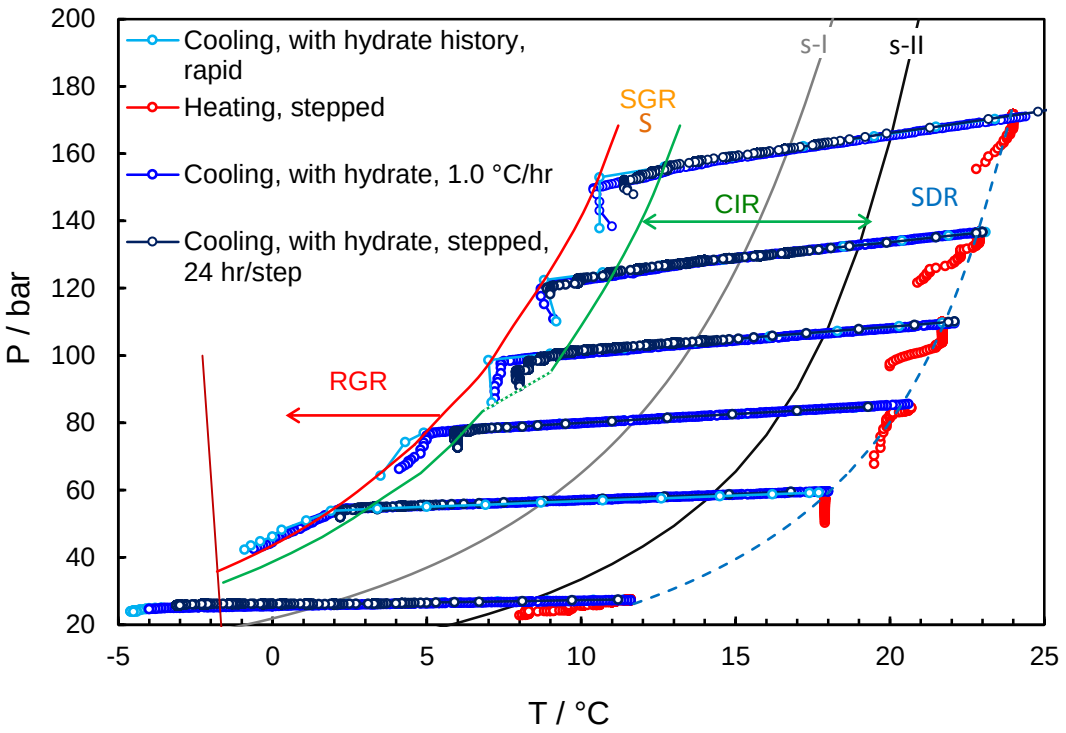

Figure 4-33. Example CGI method cooling curves for 0.5 mass% Luvicap Bio / 5 mass % MEG aqueous with natural gas.

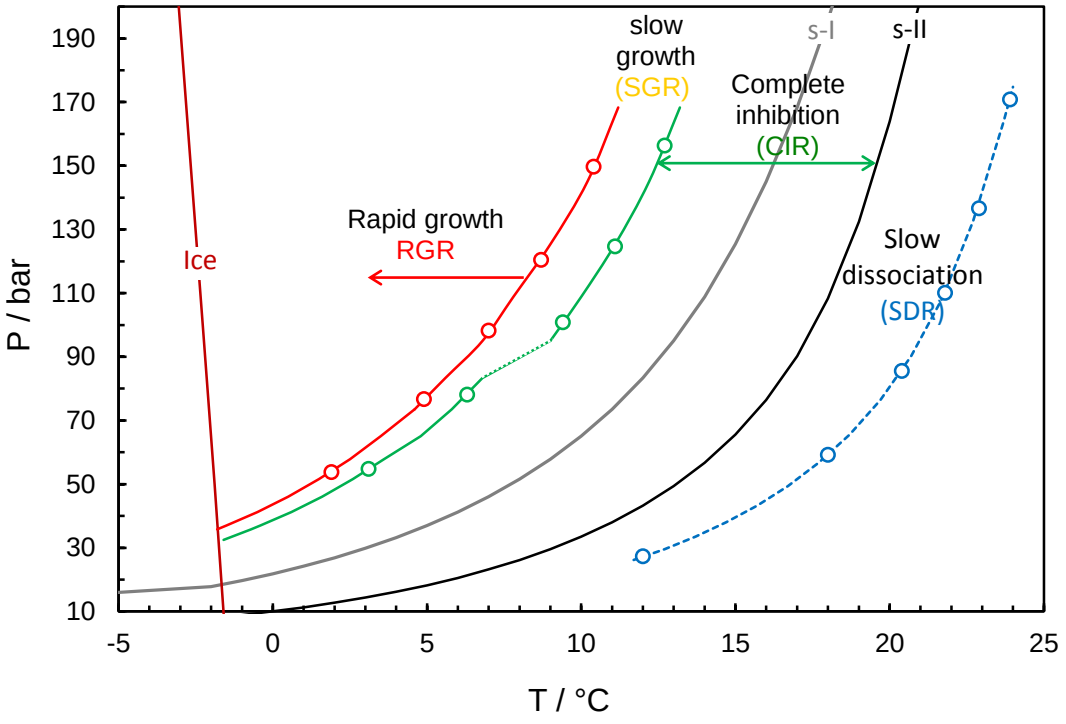

Figure 4-34. Experimental natural gas hydrate CGI region data for 0.5 mass% Luvicap Bio aqueous with 5.0 mass % MEG (relative to water + Luvicap) showing CGI regions determined from changes in relative hydrate growth rates.

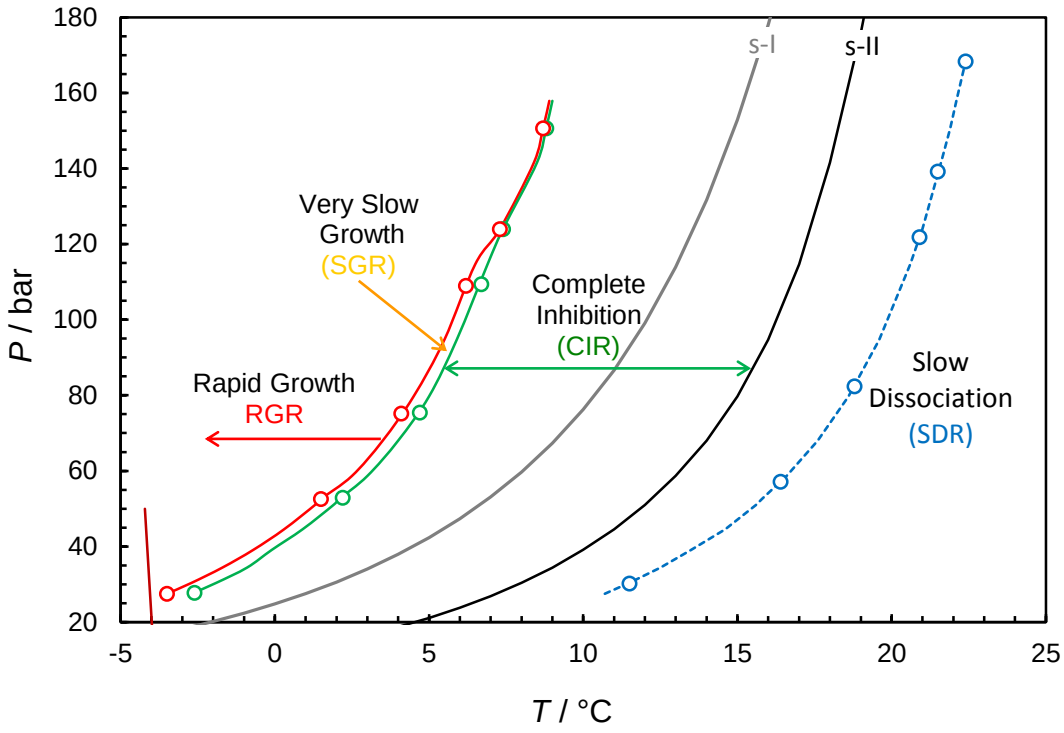

Figure 4-35. Experimental natural gas hydrate CGI region data for 0.5 mass% Luvicap Bio aqueous with 10 mass % MEG (relative to water + Luvicap) showing CGI regions determined from changes in relative hydrate growth rates.

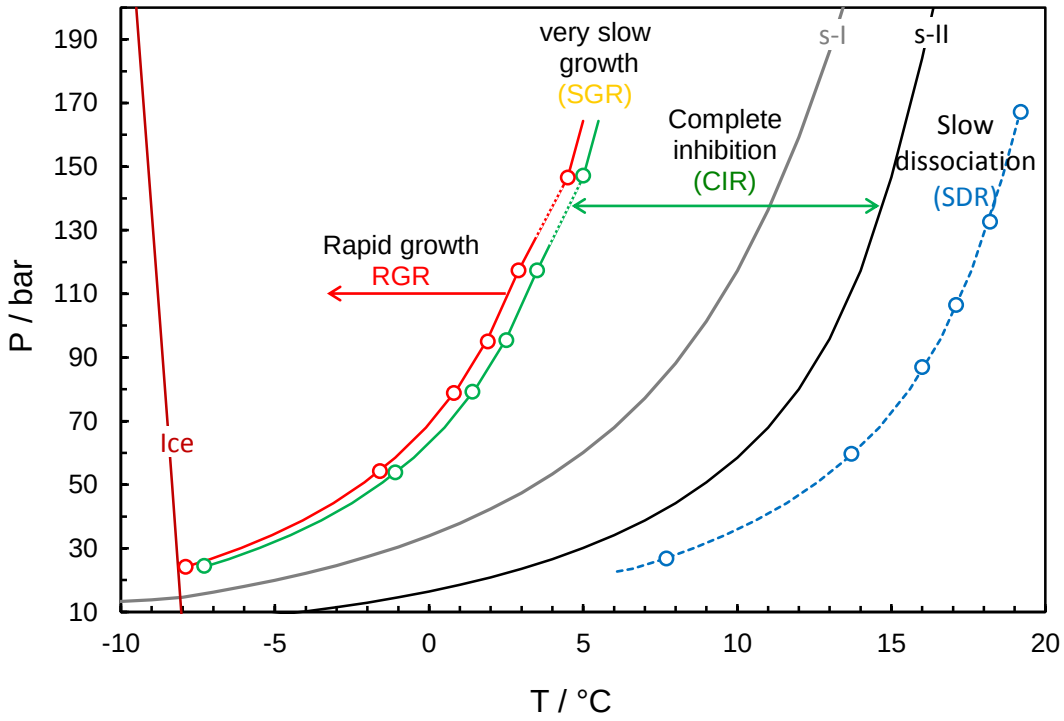

Figure 4-36. Experimental natural gas hydrate CGI region data for 0.5 mass% Luvicap Bio aqueous with 20 mass % MEG (relative to water + Luvicap) showing CGI regions determined from changes in relative hydrate growth rates.

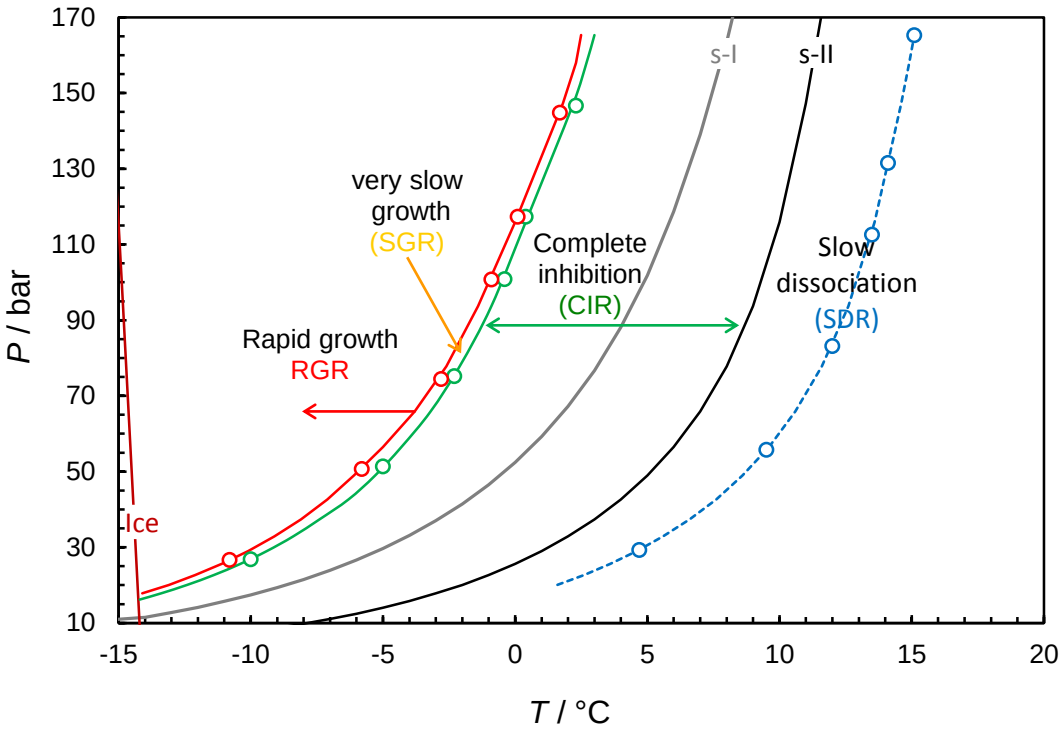

Figure 4-37. Experimental natural gas hydrate CGI region data for 0.5 mass% Luvicap Bio aqueous with 30 mass % MEG (relative to water + Luvicap) showing CGI regions determined from changes in relative hydrate growth rates.

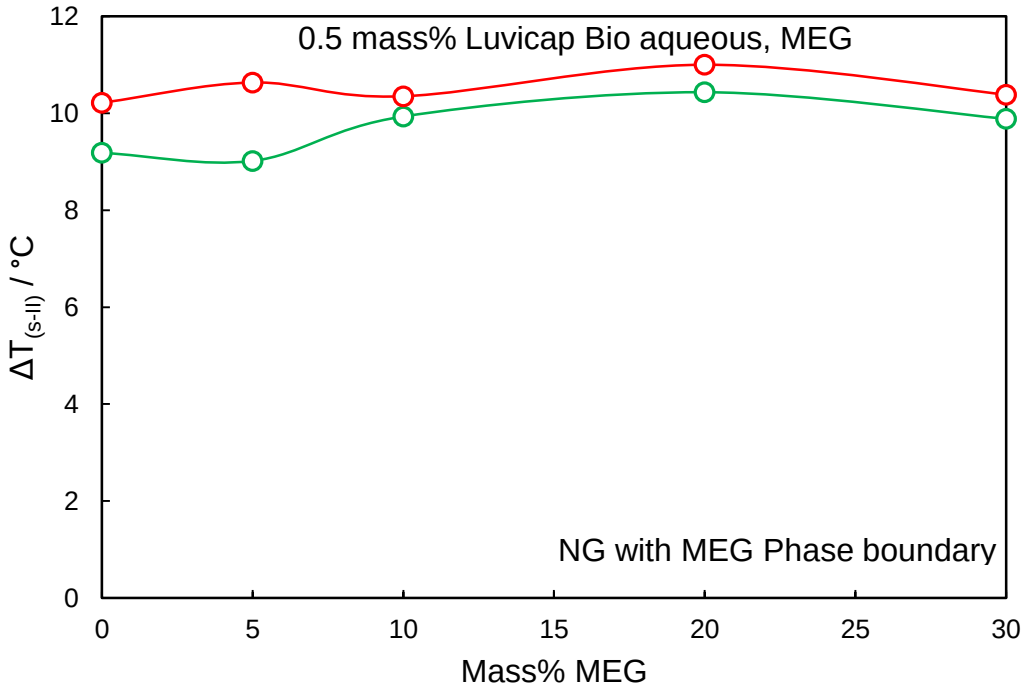

Figure 4-38. Average (25 to 150 bar) Luvicap Bio induced CGI regions for 0.5 mass% Luvicap Bio aqueous as a function of MEG mass% (relative to water + Luvicap Bio) relative to the MEG-inhibited s-II boundary for the natural gas-MEG-water system.

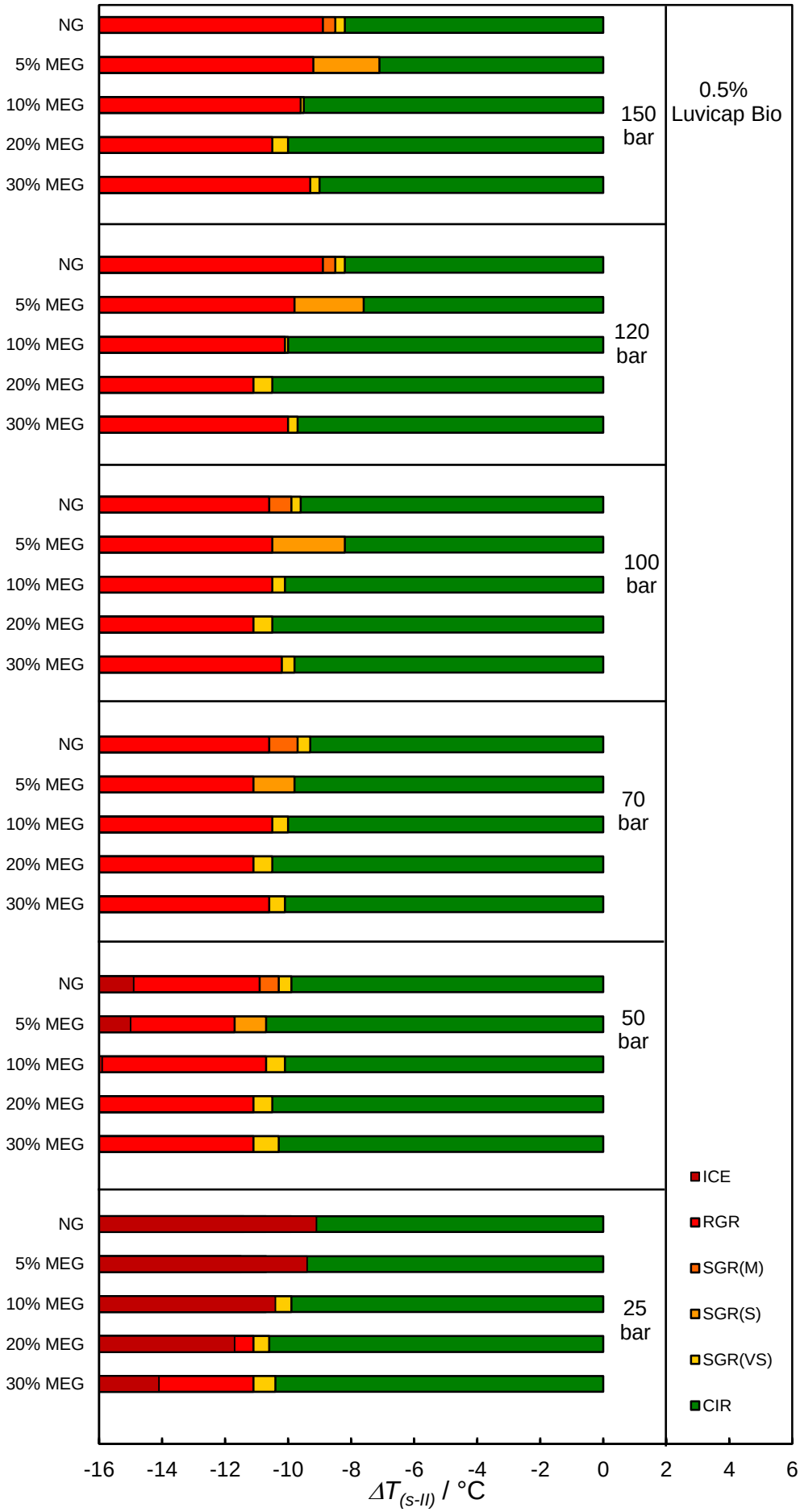

Figure 4-39. Comparison of subcooling extents of CGI regions from the s-II phase boundary for 0.5 mass% Luvicap Bio aqueous with natural gas and different MEG mass%.

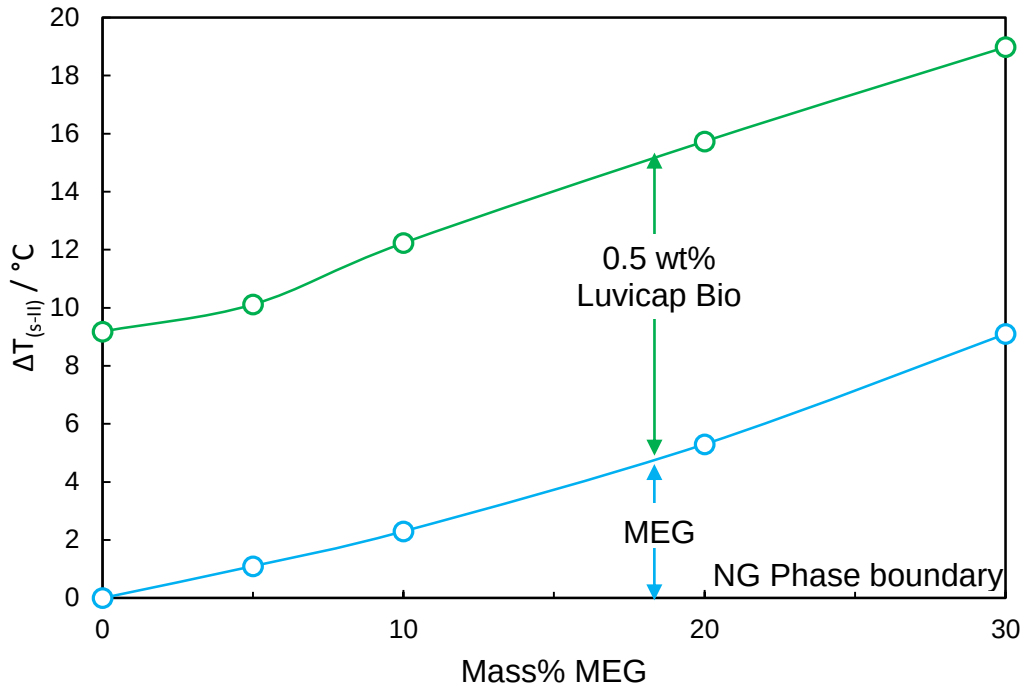

Figure 4-40. Average (25 to 150 bar) Luvicap Bio induced CIR region for 0.5 mass% Luvicap Bio aqueous as a function of MEG mass% (relative to water + Luvicap Bio) + MEG thermodynamic inhibition for the natural gas-water system.

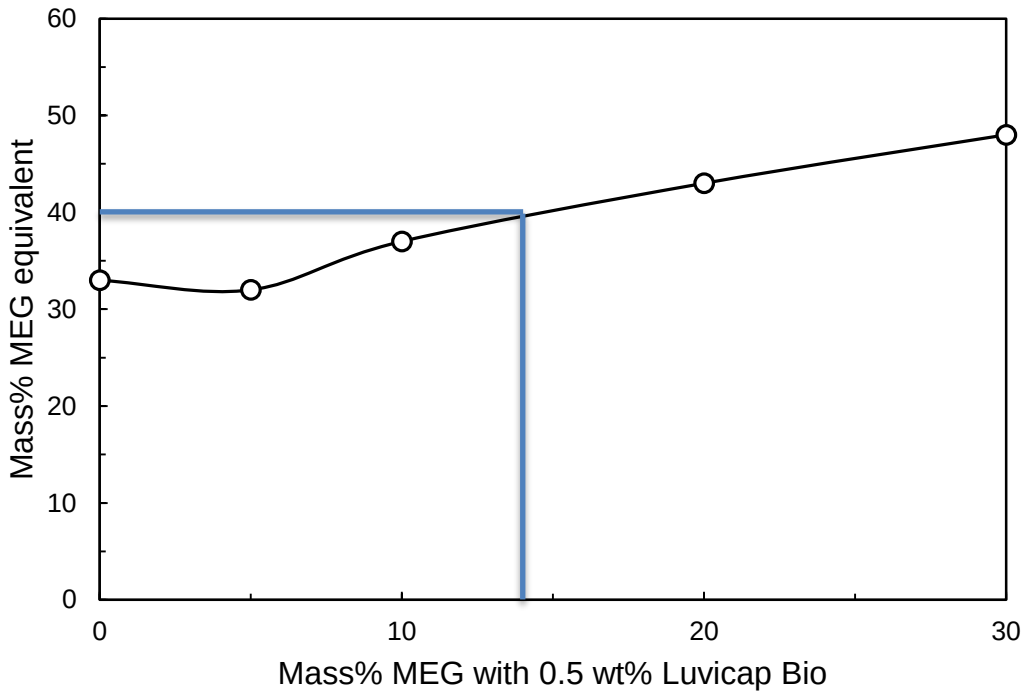

Figure 4-41. Calculated mass% MEG inhibition equivalent to MEG + 0.5% Luvicap Bio (thermodynamic MEG inhibition + CIR) as a function of MEG mass% (+ 0.5 mass% Luvicap Bio). 40 mass% MEG can be replaced by 14 mass% MEG + 0.5 mass% Luvicap Bio.

4.3.5 1.0 Mass% Luvicap Bio with MEG in a Natural Gas system

As discussed, MEG was found to act as a top-up inhibitor for 0.5 mass% Luvicap Bio with natural gas. CGI tests were carried out on a higher concentration of Luvicap Bio (1.0 mass%) with 5, 10, 20 and 30 mass% MEG (relative to water + Luvicap Bio) and natural gas to see whether there is a benefit to using a higher polymer dose. Figure 4-42 to Figure 4-45 show measured CGI boundaries for 1.0 mass% Luvicap Bio with 5, 10, 20 and 30 mass% MEG with natural gas, with tabulated data for each system in Table 4-19 to Table 4-22. Pressure / temperature plots showing measured experimental points delineating the various crystal growth inhibition regions for these systems are reported in Appendix A.5.

Figure 4-46 shows average induced CGI regions for 1.0 mass% Luvicap Bio aqueous as a function of MEG mass% relative to the MEG-inhibited s-II boundary for the natural gas-MEG-water system. Figure 4-47 shows average (25 to 150 bar) Luvicap Bio induced CIR region for 1.0 mass% (and 0.5 mass%) Luvicap Bio aqueous as a function of MEG mass% (relative to water + Luvicap Bio) + MEG thermodynamic inhibition for the natural gas-water system. Figure 4-48 shows a comparison of subcooling extents of CGI regions from the s-II phase boundary for 1.0 mass% Luvicap Bio aqueous with natural gas and different MEG mass% over the range of pressures studied.

As can be seen, results show that not only is MEG is a full top-up inhibitor for Luvicap Bio, but it also has a positive, synergistic effect on the CGI boundaries of Luvicap Bio over the range of pressure and MEG concentrations tested so far. For example, there is a clear ~1.9 °C increase in the CIR at 20 mass% MEG compared to 1 mass% Luvicap Bio alone. Such synergism is common to MEG and KHIs.

Figure 4-49 to Figure 4-52 show a comparison of measured CIR boundaries for 0.5 and 1.0 mass% Luvicap Bio, both with 5, 10, 20, and 30 mass% MEG in the natural gas system respectively. As can be seen, the CIR boundary generally increases at the higher 1.0% polymer dose. For example, the CIR boundary is ~2.3 °C higher at higher pressure for the 1.0% Bio + 5% MEG system compared to the 0.5% Bio + 5% MEG system. Results therefore show MEG to be a full top-up inhibitor for Luvicap Bio with a clear synergistic effect on it, particularly at 1.0 mass% polymer.

Table 4-19. Experimental natural gas hydrate CGI region data for 1.0 mass% Luvicap Bio aqueous (relative to water) with 5 mass% MEG (relative to water + Luvicap Bio).

CGR boundary	Growth rate	T / °C (±0.5)	P / bar (±0.2)	ΔTs-I / °C (±0.5)	ΔTs-II / °C (±0.5)
CIR-SGR(VS)	No growth	3.2	58.7	-6.0	-11.1
		5.2	75.7	-6.0	-10.7
		7.1	99.2	-6.2	-10.4
		8.8	126.1	-6.2	-10.0
		10.5	158.7	-6.1	-9.3
SGR(VS)-RGR	Very Slow	1.8	58.3	-7.3	-12.4
		3.9	75.3	-7.3	-12.0
		5.8	98.1	-7.4	-11.7
		7.8	126.2	-7.3	-11
		9.4	157.8	-7.2	-10.4
SDR	Slow dissociation	13.1	30.1	-	4.0
		18.9	64.7	-	4.0
		20.6	83.6	-	4.0
		22.1	110.5	-	4.0
		23.3	142.4	-	4.0
		24.4	180.4	-	4.0

Table 4-20. Experimental natural gas hydrate CGI region data for 1.0 mass% Luvicap Bio aqueous (relative to water) with 10 mass% MEG (relative to water + Luvicap Bio).

CGR boundary	Growth rate	T / °C (±0.5)	P / bar (±0.2)	ΔTs-I / °C (±0.5)	ΔTs-II / °C (±0.5)
CIR-SGR(VS)	No growth	-2.8	36.3	-6.4	-12.2
		1.0	60.4	-7.1	-12.2
		3.3	79.8	-7.1	-11.7
		4.9	98.3	-7.0	-11.3
		7.7	132.9	-6.4	-10.0
		9.1	162	-6.3	-9.5
SGR(VS)-RGR	Very Slow	-3.1	36.1	-6.6	-12.5
		0.7	60.0	-6.9	-12.4
		2.9	80.3	-7.5	-12.1
		4.5	98.5	-7.5	-11.7
		7.6	132.9	-6.5	-10.1
		8.9	158	-6.3	-9.6
SDR	Slow dissociation	13.7	40.1	-	3.5
		17.3	66.2	-	3.5
		19.2	89.8	-	3.5
		20.2	109.1	-	3.5
		21.8	150.2	-	3.5
		22.7	183.9	-	3.5

Table 4-21. Experimental natural gas hydrate CGI region data for 1.0 mass% Luvicap Bio aqueous (relative to water) with 20 mass% MEG (relative to water + Luvicap Bio).

CGR boundary	Growth rate	T / °C (±0.5)	P / bar (±0.2)	ΔTs-I / °C (±0.5)	ΔTs-II / °C (±0.5)
CIR-SGR(VS)	No growth	-6.5	33.6	-6.4	-12.4
		-2.4	58.7	-7.2	-12.4
		-0.2	83.5	-7.8	-12.4
		0.9	103	-8.2	-12.5
		3.0	132	-7.8	-11.5
		4.3	157.9	-7.6	-11.0
SGR(VS)-RGR	Very Slow	-7.1	33.6	-7.0	-13.0
		-2.8	59.1	-7.7	-12.9
		-0.6	83.9	-8.3	-12.9
		0.5	102.5	-8.6	-12.9
		2.4	131.4	-8.4	-12.1
		3.8	157.7	-8.1	-11.5
SDR	Slow dissociation	10.1	36.9	-	3.5
		14.3	65.8	-	3.5
		16.3	92.9	-	3.5
		17.4	115.9	-	3.5
		18.6	149	-	3.5
		19.4	180.9	-	3.5

Table 4-22. Experimental natural gas hydrate CGI region data for 1.0 mass% Luvicap Bio aqueous (relative to water) with 30 mass% MEG (relative to water + Luvicap Bio).

CGR boundary	Growth rate	T / °C (±0.5)	P / bar (±0.2)	ΔTs-I / °C (±0.5)	ΔTs-II / °C (±0.5)
CIR-SGR(VS)	No growth	-10.1	34	-6.4	-12.8
		-5.5	58.7	-6.4	-11.8
		-2.9	81.5	-6.4	-11.2
		-1.3	104.1	-6.4	-10.8
		0.4	128.8	-6.1	-10.0
		2.5	162.3	-5.5	-8.9
SGR(VS)-RGR	Very Slow	-11.0	34	-7.3	-13.7
		-6.4	58.7	-7.3	-12.7
		-3.8	81.1	-7.2	-12.0
		-1.7	103.8	-6.8	-11.2
		0.0	128.4	-6.5	-10.4
		1.8	160.9	-6.1	-9.6
SDR	Slow dissociation	6.6	37.7	-	3.5
		10.4	64.9	-	3.5
		12.3	90.7	-	3.5
		13.5	116.5	-	3.5
		14.5	145.5	-	3.5
		15.4	183.3	-	3.5

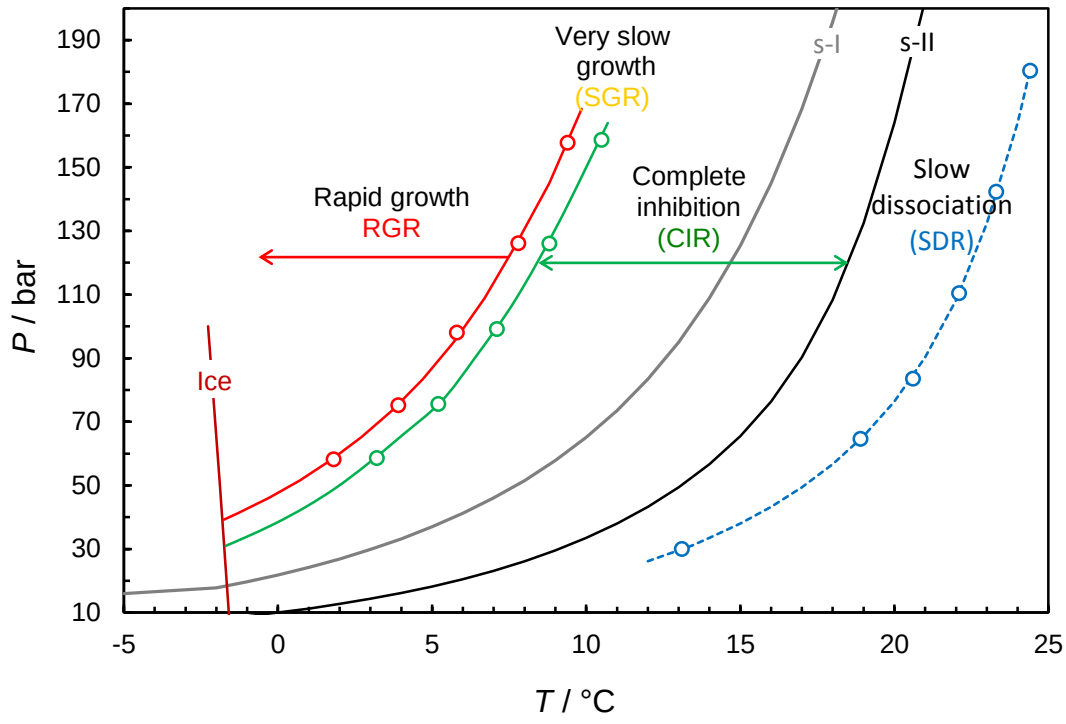

Figure 4-42. Experimental natural gas hydrate CGI region data for 1.0 mass% Luvicap Bio aqueous with 5.0 mass% MEG (relative to water + Luvicap) showing CGI regions determined from changes in relative hydrate growth rates.

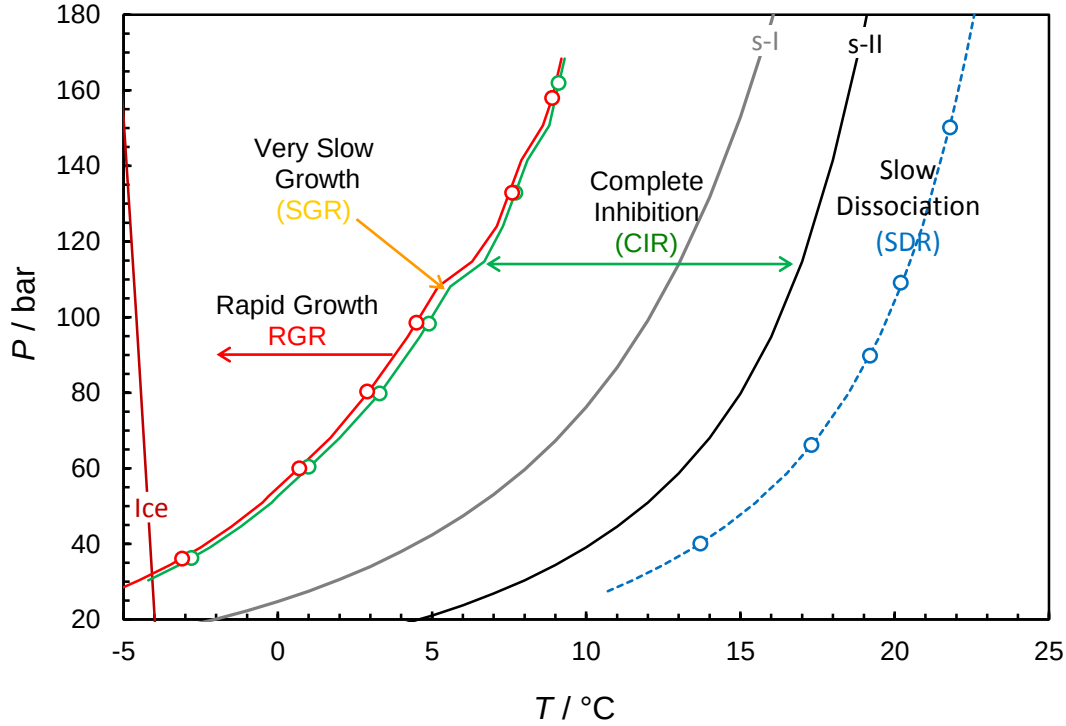

Figure 4-43. Experimental natural gas hydrate CGI region data for 1.0 mass% Luvicap Bio aqueous with 10 mass% MEG (relative to water + Luvicap) showing CGI regions determined from changes in relative hydrate growth rates.

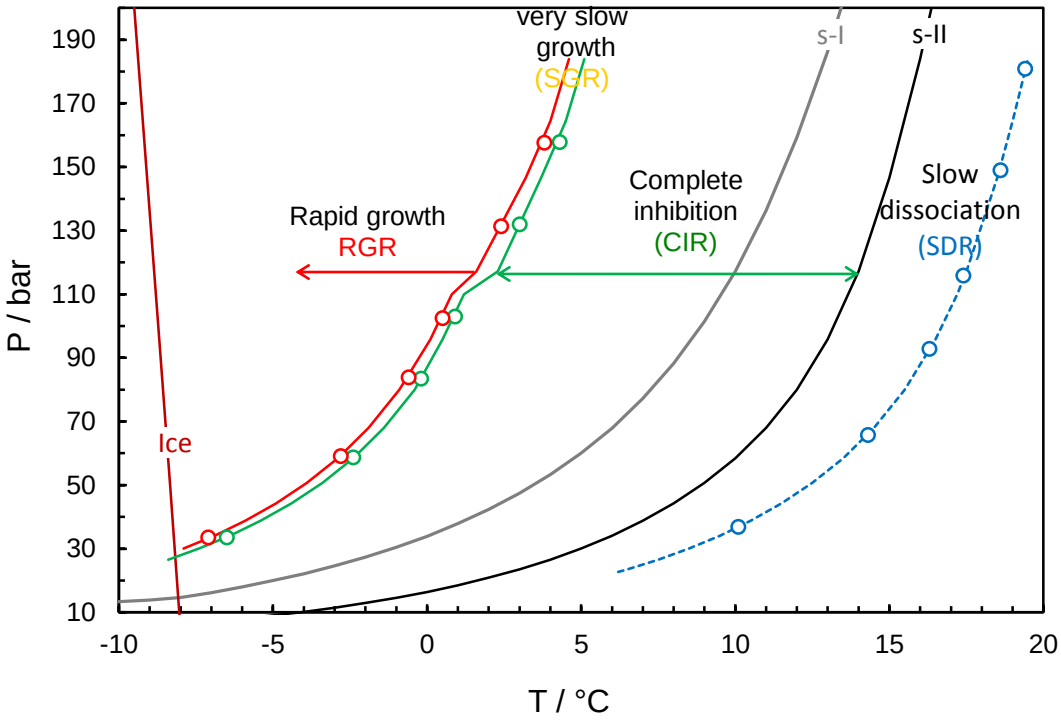

Figure 4-44. Experimental natural gas hydrate CGI region data for 1.0 mass% Luvicap Bio aqueous with 20 mass% MEG (relative to water + Luvicap) showing CGI regions determined from changes in relative hydrate growth rates.

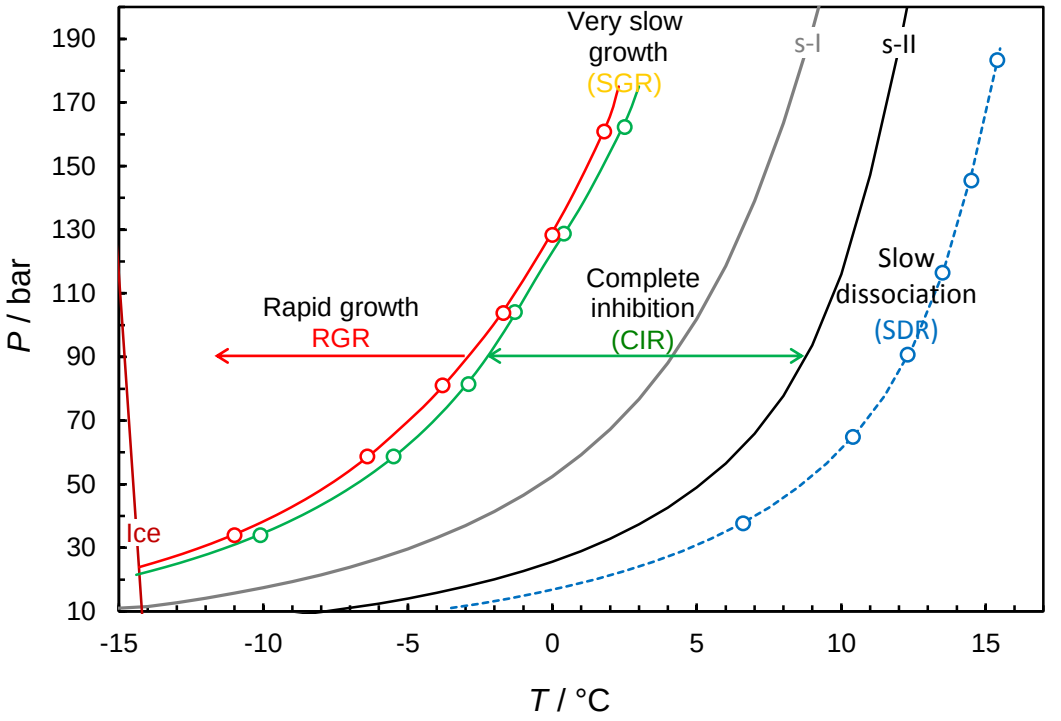

Figure 4-45. Experimental natural gas hydrate CGI region data for 1.0 mass% Luvicap Bio aqueous with 30 mass% MEG (relative to water + Luvicap) showing CGI regions determined from changes in relative hydrate growth rates.

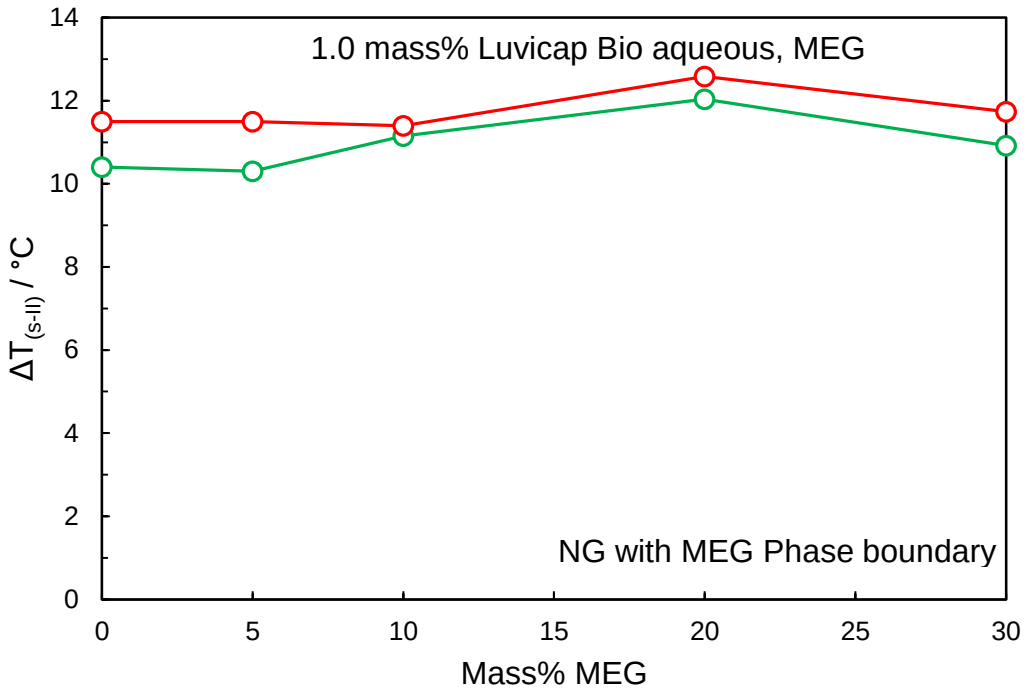

Figure 4-46. Average (25 to 150 bar) Luvicap Bio induced CGI regions for 1.0 mass% Luvicap Bio aqueous as a function of MEG mass% (relative to water + Luvicap Bio) relative to the MEG-inhibited s-II boundary for the natural gas-MEG-water system.

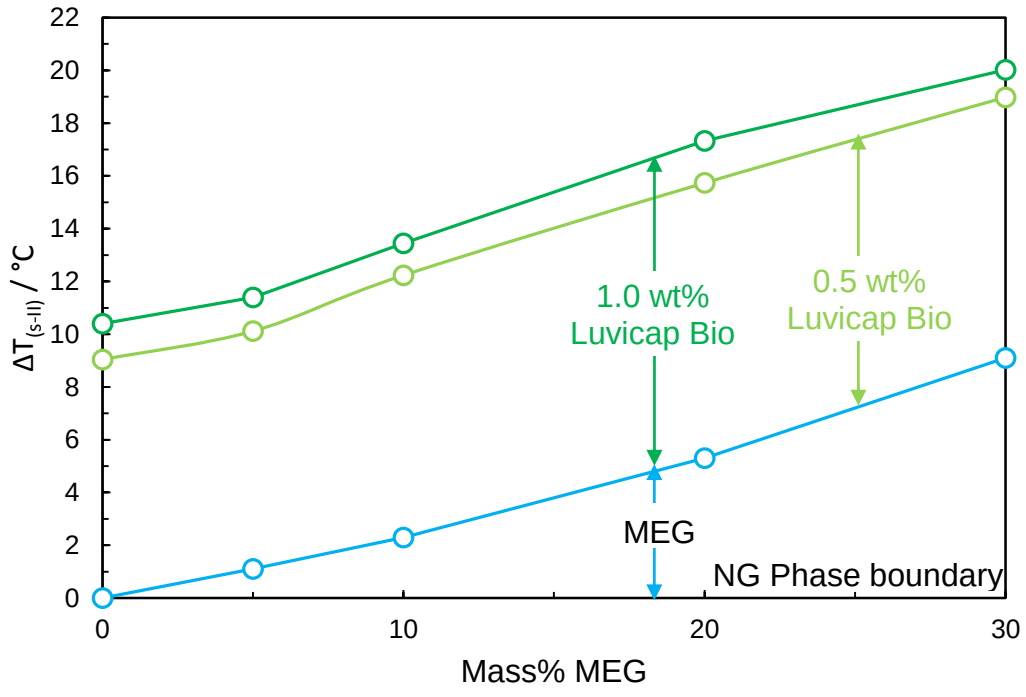

Figure 4-47. Average (25 to 150 bar) Luvicap Bio induced CIR region for 1.0 and 0.5 mass% Luvicap Bio aqueous as a function of MEG mass% (relative to water + Luvicap Bio) + MEG thermodynamic inhibition for the natural gas-water system.

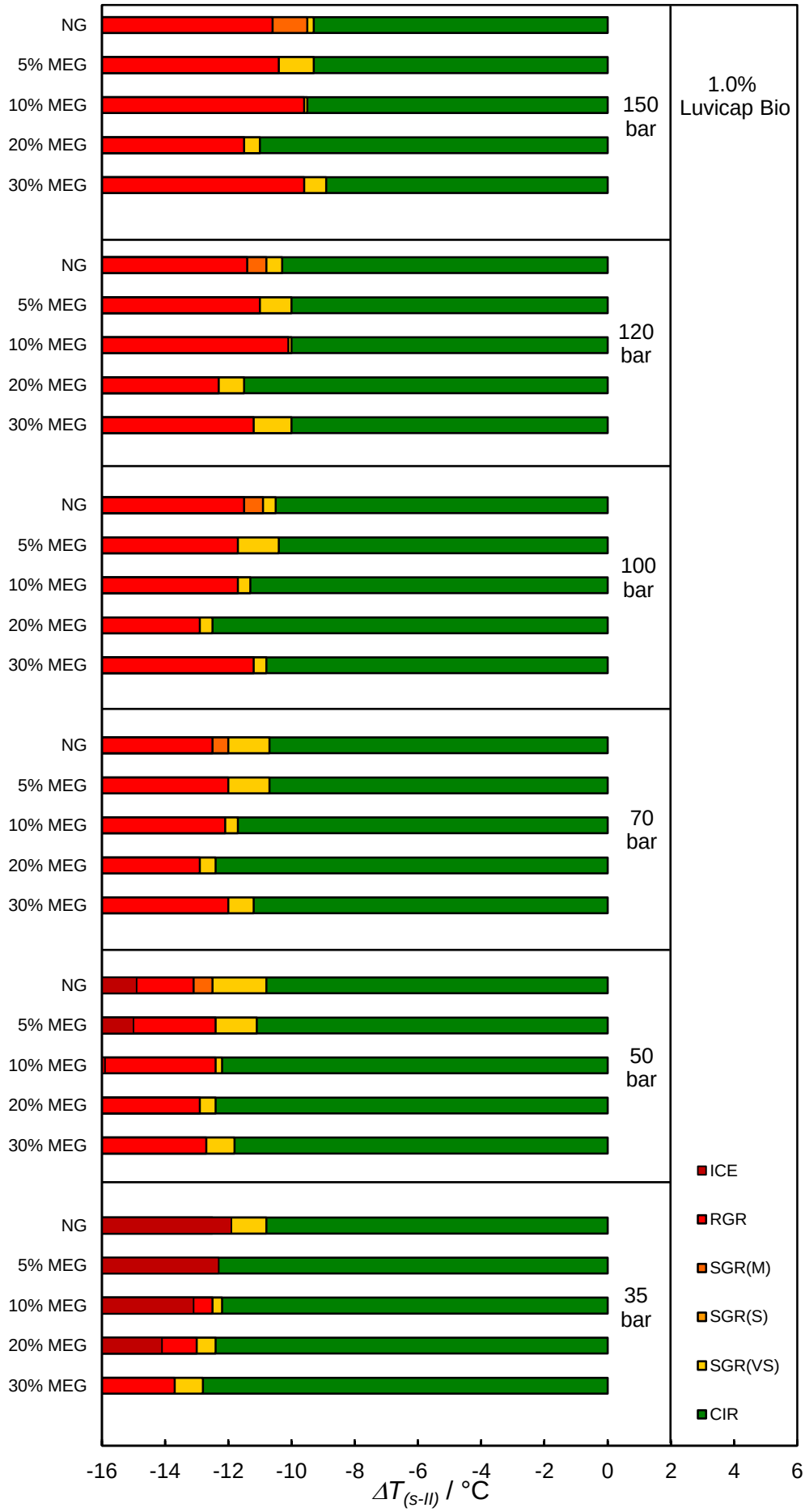

Figure 4-48. Comparison of subcooling extents of CGI regions from the s-II phase boundary for 1.0 mass% Luvicap Bio aqueous with natural gas and different methanol mass%.

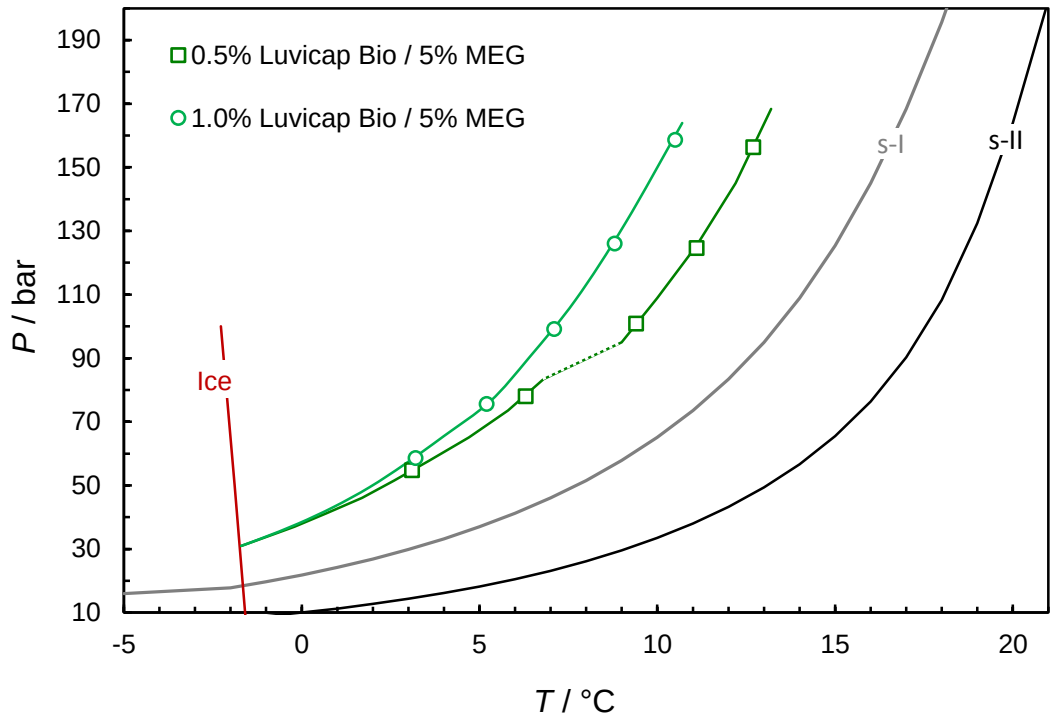

Figure 4-49. Comparison of measured CIR boundaries for 0.5 and 1.0 mass% Luvicap Bio, both with 5 mass% MEG and natural gas.

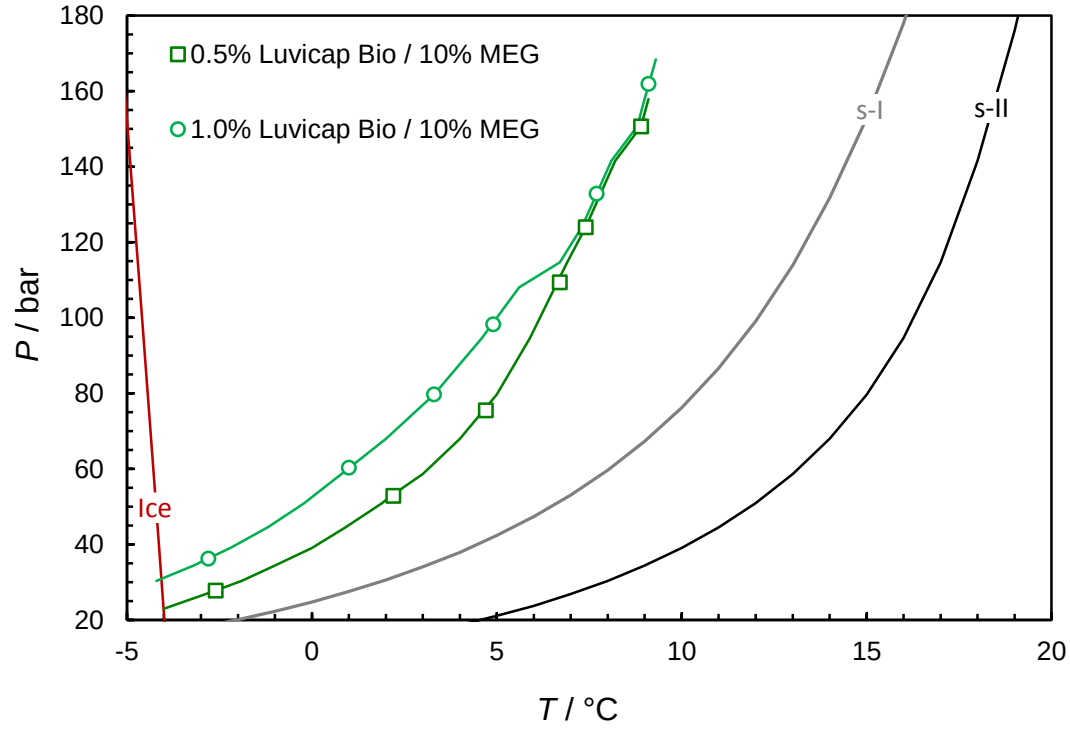

Figure 4-50. Comparison of measured CIR boundaries for 0.5 mass% Luvicap Bio and 1.0 mass% Luvicap Bio with 10 mass% MEG and natural gas.

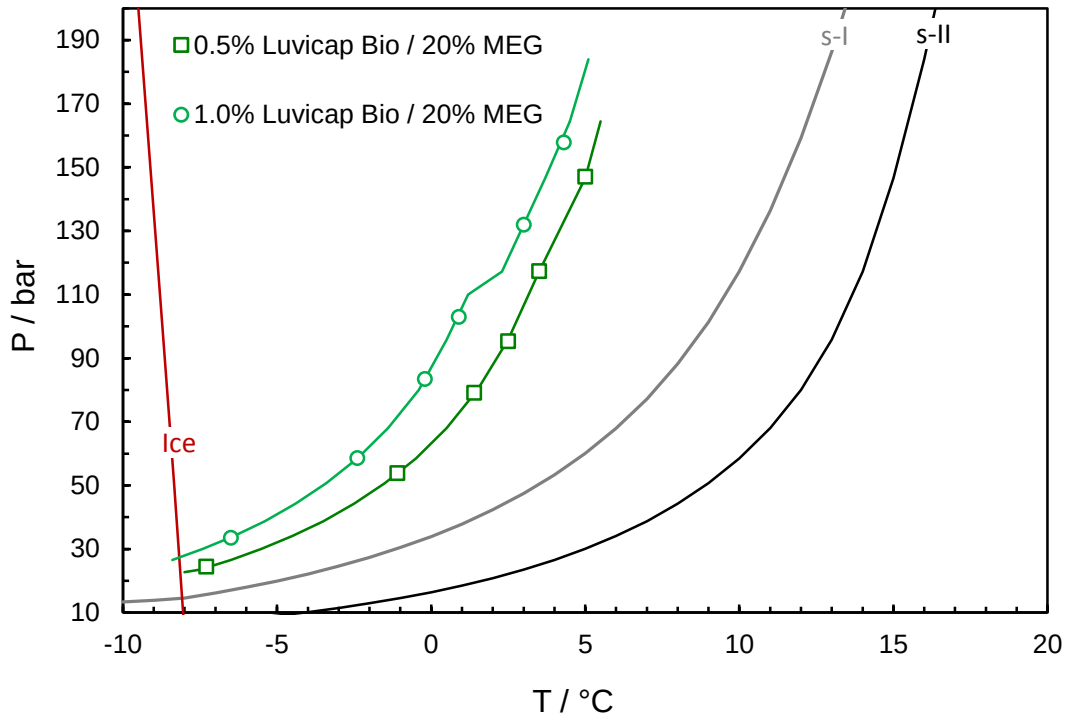

Figure 4-51. Comparison of measured CIR boundaries for 0.5 mass% Luvicap Bio and 1.0 mass% Luvicap Bio with 20 mass% MEG and natural gas.

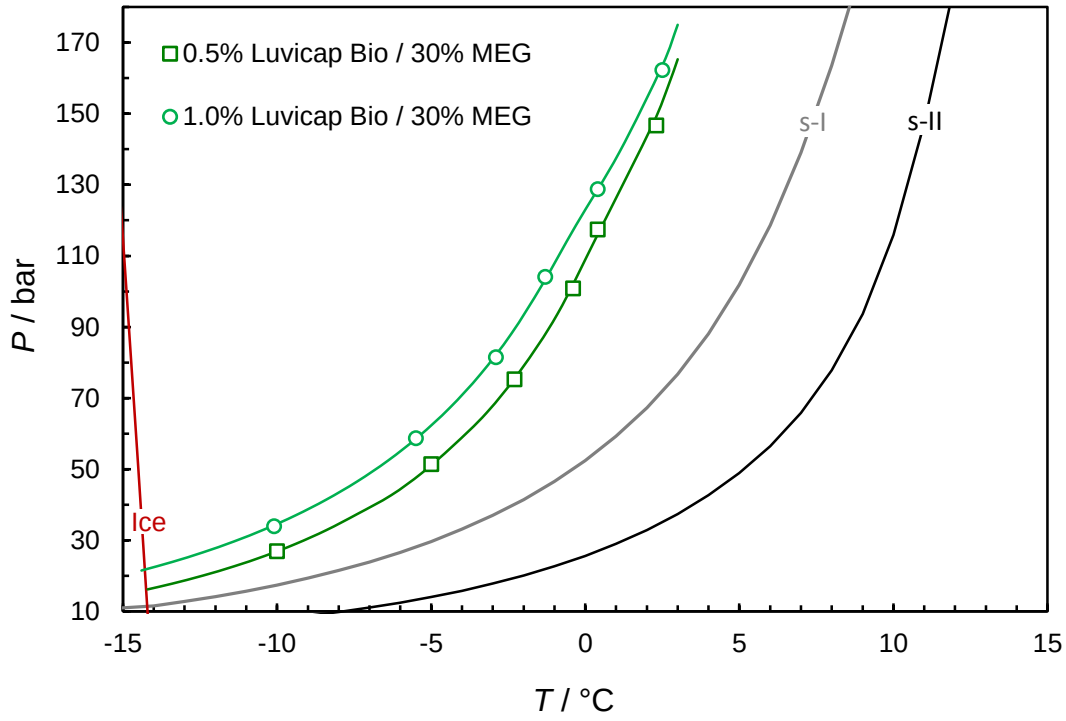

Figure 4-52. Comparison of measured CIR boundaries for 0.5 mass% Luvicap Bio and 1.0 mass% Luvicap Bio with 30 mass% MEG and natural gas.

4.4 Summary

From the results of CGI region studies on 0.5 mass% Luvicap Bio aqueous with 5-50 mass% methanol (relative to Luvicap Bio and water) and natural gas, the following is concluded:

- In contrast to results for PVCap (and other non-bio KHIs), methanol acts much more as a top-up inhibitor for Luvicap Bio, particularly up to 30 mass% MeOH

- The most important CIR is largely retained for the concentrations and pressures tested

- Only at higher methanol concentrations does the CIR begin to reduce, notably for 50 mass%, but with significant reduction largely confined to lower pressures (below 100 bar) here

- Results, therefore, show significant potential for using Luvicap Bio to reduce methanol requirements for hydrate inhibition; just 0.5% Bio can replace ~23 mass% MeOH while at higher subcooling requirements, e.g. 0.5% Bio + 26% methanol offers the inhibition equivalent of 40 mass% methanol; a 35% MeOH reduction

- Finally, while not explored in depth, contrasting results for Luvicap Bio (general top-up effect) and PVCap (increasingly negative) for methanol points increasingly towards MeOH (and ethanol) partial enclathration as the factor behind the contrasting top-up effects observed for different KHI polymers

From the results of CGI studies on 1.0 mass% Luvicap Bio aqueous with 5, 10, 20, and 30 mass% methanol in a natural gas system, the following is concluded:

- At 1.0 mass% Luvicap Bio, as was the case for 0.5 mass%, methanol was found to generally act as a good top-up inhibitor for the MeOH concentrations tested, which is unusual for methanol and KHIs

- However, for both polymer doses, there was a modest but increasingly negative effect of MeOH at higher concentrations and pressures, making top-up not fully additive

- While the higher 1.0% polymer concentration did offer better inhibition in terms of a larger CIR extent, this was overall fairly marginal, and the net CGI gains of using 1.0% Bio compared to 0.5% are quite limited per unit dose

- Data suggest that the benefits of using a higher polymer concentration are most evident at the lowest methanol concentrations (e.g. ~2°C extra CIR for 1.0% Bio + 5% MeOH compared to 0.5% Bio with 5 % MeOH)

From the results of CGI region studies on 0.5 mass% Luvicap Bio aqueous with 5 to 30 mass% ethanol in a natural gas system, the following is concluded:

- Unlike PVCap, ethanol does act reasonably well as a top-up inhibitor for Luvicap Bio, although there is a degree of negative effect, making it not a full top-up

- This negative effect increases with pressure and steadily with ethanol concentration

- Overall, ethanol offers some promise for combination with Luvicap Bio as alternative to the more toxic methanol

Finally, from the results of CGI region studies on 0.5 mass% Luvicap Bio aqueous with 5 to 30 mass% MEG in a natural gas system, the following is concluded:

- The important CIR is largely preserved, giving a general full top-up effect up to 30 mass% MEG, at least at lower pressures

- At lower MEG concentrations, however, e.g. 5 mass%, the CIR is measurably reduced at higher pressures, in contrast to the behaviour seen for MEG + PVCap where there is essentially a full top-up effect

- The apparent ‘generic’ top up effect of MEG, which contrasts that for methanol and ethanol (strongly negative for PVCap, but much less so for Luvicap Bio) is speculated as being related to the fact the latter two can enter hydrate cavities, while MEG cannot, although the exact mechanisms remain unknown

From the results of CGI studies on 1.0 mass% Luvicap Bio aqueous with 5, 10, 20, and 30 mass% MEG in a natural gas system, the following is concluded:

- At 1.0 mass% Luvicap Bio, as was the case for 0.5 mass%, MEG not only acts as a full top-up inhibitor, but also it has a positive, synergistic effect, modestly extending CGI regions, including the CIR

- The synergistic effect of MEG on Luvicap Bio performance is most evident at the 1% polymer dose

- For both Luvicap doses (0.5 and 1.0 mass%) tested, the best synergism (largest CIR) is observed at 20 mass% MEG

Generally, from the results of CGI region studies on a combination of Luvicap Bio and THIs (MEG, methanol, and ethanol), it is concluded that Luvicap Bio could be used to reduce the required THIs dosage for hydrate inhibition. It is very important to industry and real application with respect to the environment that the green Bio KHI replacing could be used to reduce MEG and MeOH which are toxic.

4.5 Reference

[1] E. D. Sloan, S. Subramanian, P. N. Matthews, J. P. Lederhos, and A. A. Khokhar, "Quantifying hydrate formation and kinetic inhibition," *Ind. Eng. Chem. Res.*, vol. 37, no. 8, pp. 3124–3132, 1998.

[2] M. Pakulski and D. Hurd, "Uncovering a dual nature of polyether amines hydrate inhibitors," in *Proceedings of the Fifth International Conference on Gas Hydrates*, 2005.

[3] M. R. Anklam, J. D. York, L. Helmerich, and A. Firoozabadi, "Effects of antiagglomerants on the interactions between hydrate particles," *AIChE J.*, vol. 54, no. 2, pp. 565–574, 2008.

[4] J. D. York and A. Firoozabadi, "Alcohol cosurfactants in hydrate antiagglomeration," *J. Phys. Chem. B*, vol. 112, no. 34, pp. 10455–10465, 2008.

[5] B. Tohidi and R. Anderson, "Evaluation of low dosage hydrate inhibitors" Edinburgh:Heriot-Watt University, Institute of Petroleum Engineering- Joint Industry Project Report-2006-2009.

[6] B. Tohidi, R. Anderson, H. Mozaffar, and R. Azarinezhad, "Evaluation of low dosage hydrate inhibitors" Edinburgh:Heriot-Watt University, Institute of Petroleum Engineering- Joint Industry Project Report-2009-2012.

[7] B. Tohidi, R. Anderson, H. Mozaffar, and F. Tohidi, "Evaluation of low dosage hydrate inhibitors" Edinburgh:Heriot-Watt University, Institute of Petroleum Engineering- Joint Industry Project Report-2012-2015.

[8] A. K. Soper and J. L. Finney, "Hydration of methanol in aqueous solution," *Phys. Rev. Lett.*, vol. 71, no. 26, p. 4346, 1993.

[9] S. Dixit, W. C. K. Poon, and J. Crain, "Hydration of methanol in aqueous solutions: a Raman spectroscopic study," *J. Phys. Condens. Matter*, vol. 12, no. 21, p. L323, 2000.

[10] R. Anderson, A. Chapoy, H. Haghighi, and B. Tohidi, "Binary Ethanol- Methane Clathrate Hydrate Formation in the System CH_4-C_2H_5OH-H_2O: Phase Equilibria and Compositional Analyses," *J. Phys. Chem. C*, vol. 113, no. 28, pp. 12602–12607, 2009.

[11] D. Blake, L. Allamandola, S. Sandford, D. Hudgins, and F. Freund, "Clathrate hydrate formation in amorphous cometary ice analogs in vacuo," *Science (80)*, vol. 254, no. 5031, pp. 548–551, 1991.

Chapter 5 – Remediation of Hydrate Using MEG and MeOH

5.1 Introduction

If KHIs are used for hydrate prevention, it may still need THIs for e.g. cold restart after shut-in. Although KHIs are able to dissociate hydrates (see Chapter 6), it may need THI for plug removal, i.e., as even with KHI it might have to resort to THI for hydrate removal. In addition, it is speculated that the density of THI play an important role in hydrate removal. Therefore, this chapter investigates hydrate plug removal using THIs in vertical pipes with a focus on the effect of density of THI on hydrate plug removal.

Although there are options/strategies to inhibit hydrate formation (see Section 1.4), hydrate blockage can occur in some cases. Hydrate blockage is still a major flow assurance challenge and can form as a result of different scenarios such as restart following an unplanned shut-in, failure of inhibitor delivery pumps, or increased water cut. There have been a lot of investigations in association with hydrate blockage and its removal strategies in the literature along with case studies [5.1][5.2][5.3][5.4].

In Section 1.3, different remediation options and hydrate blockage removal strategies have been discussed including depressurization, chemical injection, thermal method, and mechanical method. In many cases, more than one methods was used to dissociate and remove hydrate. As discussed in Section 1.5.1, in some cases, depressurization is not possible in the vertical pipes e.g. riser, i.e., depressurization is not possible due to hydrostatic pressure of liquid. Therefore, other methods e.g. chemical injection (thermodynamic inhibitors e.g. MEG and methanol) may be used to remove hydrate blockage in vertical pipes. The mechanism and process of hydrate dissociation using thermodynamic inhibitors have been discussed in Section 1.5.1.

In the light of above, it raises the potential demand to investigate the ability of THIs (e.g. MEG and MeOH) in hydrate dissociation after hydrate blockage in vertical pipes e.g. risers. This chapter covers the results of three experiments including the use of MEG, MeOH, and combination of MEG/MeOH in removing gas hydrate blockage in vertical pipes. In all tests, during chemical injections and hydrate dissociation, the pressure was kept relatively constant using batch removal of gas from the top of the cell. The other results of this chapter include pressure response due to hydrate dissociation, the possibility of reformation of gas hydrates, and possibility of ice formation as a result of gas hydrate dissociation (due to endothermic nature of hydrate dissociation).

5.2 Experimental

5.2.1 Materials

The purity of MEG and Methanol used was 99.8 weight% and supplied by Fisher Scientific (catalogue numbers E177-20 and A452-1, respectively). Deionized water was used in all experiments. The composition of natural gas mixture used in the tests is given in Table 5-1.

5.2.2 Equipment

Evaluation and effectiveness of MEG and methanol in hydrate blockage dissociation and removal were examined using an in-house designed/ built long cylindrical and windowed experimental rig with full temperature gradient control along the 1.5 meters cylindrical body of the cell (75 mm internal diameter).

The set-up consists of 12 soda-lime glass windows (6 pairs), enabling visual monitoring of the system. Images and videos can be recorded through the windows while the light is shining through the opposite side of windows. The total volume of the cell is approximately 6.8 litres with the ability to reduce the volume by a moving piston inside the cell. It is possible to change the orientation of set-up: horizontal, vertical, or any other position. The cell has a pressure rating of 300 bara and it is made of titanium; which allows working with some corrosive materials such as salts.

The temperature along the rig is controlled using 6 separate jackets each connected to a programmable constant temperature bath. The temperature inside the cell is monitored by 12 platinum resistance thermometers (PRT) with a measurement accuracy of 0.1 °C. These thermometers are placed through the cell and each section consists of two thermometers which are placed in opposite directions and against each other.

Table 5-1. Composition of natural gases used in experiments.

Component	Mole%
Methane	87.93
Ethane	6.00
Propane	2.04
i-Butane	0.20
n-Butane	0.30
CO2	2.03
Nitrogen	1.50

Cell pressure is measured by two Druck strain gauges (±0.07 bar), calibrated using a Budenberg dead weight tester. The pressure transducers are placed at each end of the rig. All thermometers and pressure transducers are connected to a data acquisition unit and a computer with the ability to continuously record the temperature of each section and the cell pressure.

A stirrer with blades and a magnetic motor is mounted at the bottom of the cell for mixing the cell contents to reduce the time required for reaching thermodynamic and thermal equilibrium. Figure 5-1.a and Figure 5-1.b show a detailed schematic illustration of the cell and its picture, respectively.

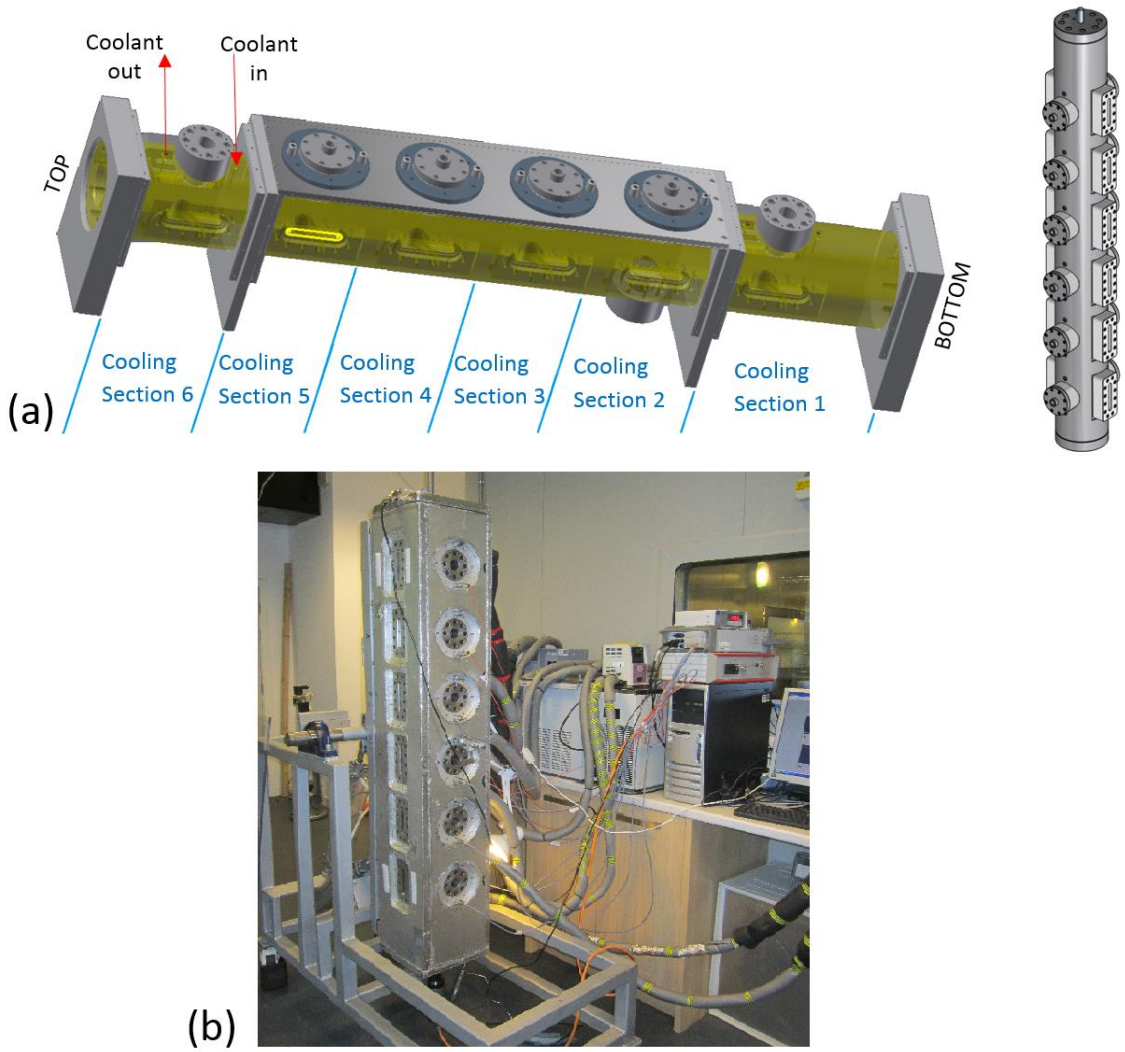

Figure 5-1. a) Illustration of the window positions and the coolant system of the long windowed rig. b) Picture of the long winnowed rig.

5.2.3 Procedure

As mentioned, the orientation of the cell can be changed from completely horizontal to vertical to simulate various configurations, from horizontal pipelines to vertical wells/risers. To simulate hydrate formation, hydrate blockage, and hydrate dissociation by THI in vertical pipes, the experimental setup was positioned in vertical orientation.

The system can be loaded with different water cuts and gas can be injected from both ends into the cell. To compare the results of experiments, the volume ratio of water/gas was approximately 0.44 in all tests in this chapter.

However, in these series of experiments, the shut-in condition for hydrate formation/blockage was simulated. In order to simulate shut-in condition, the gas injection can be stopped and the temperature can be adjusted to seabed temperature or any other desired temperature. The system can be held at a specific P and T conditions for any time required to form enough hydrates and induce a blockage (which may take several days).

The system was loaded with deionized water, and then vacuumed and pressurized with natural gas. The details of gas injection of each experiment are discussed in result and discussion section of this chapter. In order to initiate hydrates, the temperature was set to 1-4 °C and the mixer was switched on. The logic behind setting the temperature at 1-4 °C is discussed later in each section. In order to block the system, it was allowed to form hydrates as much as possible.

After hydrate blockage, MEG or methanol can be injected from both ends of the experimental setup to induce hydrate dissociation and finally remove the hydrate blockage. Hydrate dissociation and potential reformation can be investigated both qualitatively and quantitatively, i.e., visual observation and changes in the system pressure and temperature. The system pressure was kept constant and the gas released from hydrate dissociation was removed from the top of the cell and measured by a gasometer at ambient conditions.

5.3 Results and discussion

5.3.1 Hydrate blockage removal using MEG in vertical pipes

To investigate the effect of MEG on hydrate blockage removal in vertical pipes, the long windowed rig was located in the vertical position and loaded with 2064 g of deionized water. The system was vacuumed and then pressurized with 460 g≈25 moles of natural gas (it was measured using a balance) at 96.5 bara and 20 °C. The volume ratio of liquid/gas was approximately 0.44. In order to form hydrates, the system temperature was set to 1 °C and the mixer was turned on. The logic behind setting the temperature at 1 °C was to avoid ice formation during cooling/hydrate formation (as conversion ice to hydrate is expected to be a very slow process). Also at the same time providing a better opportunity for investigating the possibility of ice formation during endothermic hydrate dissociation due to inhibitor injection (from non-homogenous aqueous phase).

In the initial cooling step, some 10 mass% of water was converted into hydrate (WCH %) over 3 days, which resulted in the mixer stoppage. At this point, the mixer was switched off and was not used in the rest of the experiment. Although the mixer stopped due to the presence of hydrates in the system, the system was not completely blocked as both pressure transducers at top and bottom of the cell showed the same pressure, indicating pressure communication through the system. In order to simulate constant pressure conditions and block the system completely, natural gas was injected multiple times from the bottom of the cell. The aim of this procedure was to encourage the system to form hydrates by mixing the system (by the bubbling gas, i.e., the injection of gas from the bottom of the cell, generated gas bubbles inside the aqueous phase) and increasing water/gas interface during gas injection. The system was allowed to form more hydrates for several days (listed in Table 5-2) after each gas injection. Details of each gas injection are reported in Table 5-2. Finally, after 51 days, 89 mass% water was converted to hydrates and the system became completely blocked. The pressures at top and bottom of the cell were 79 bara and 90 bara at 1 °C respectively, indicating complete hydrate blockage without any pressure communication in the system. The pressure data at top and bottom of the cell shows that it took a long time (51 days in this case) to get complete blockage and there was pressure communication through the hydrate body even at high 80 WCH%.

The next step is to remove hydrate blockage using MEG and investigate its effectiveness in removing hydrate blockage. It was decided to use stepwise MEG injection at relative constant pressure (±5 bar). MEG was tested first due to its high density, assuming to be more effective than methanol in removing hydrate blockage in vertical pipes.

Gas hydrate phase boundaries of the system with different amount of MEG are shown in Figure 5-2. Software calculation shows that 45 mass% MEG in the aqueous phase is enough to dissociate all hydrates in the system. Different batches of MEG were injected from the top of the cell as listed in Table 5-3. The main reason for the injection of batches of MEG was to examine if it is possible to remove the hydrate plug with a lower amount of MEG than thermodynamic requirements, i.e., it is not necessary to dissociate all hydrates to remove the blockage.

Table 5-2. Details of gas injection including the amount of gas injected, calculated percent water converted to hydrate after the end of each gas injection period -MEG injection test.

No.	Amount of gas injected in each step		Total water mole fraction	WCH%	No. of days
	g	mole			
1	460	25	0.82	10	3
2	100	5.4	0.79	26	7
3	80	4.4	0.77	37	8
4	74	4	0.75	82	37
5	92	5	0.72	89	51

Table 5-3. Details of MEG injection into the long windowed rig.

No. of injection	Type	Mass / g	Volume / cc	Total Mass %
1	MEG	230	206	10
2	MEG	230	206	19
3	MEG	230	206	25
4	MEG	220	197	30
5	MEG	228	204	35
6	MEG	400	358	42
7	MEG	450	403	49
8	Methanol	222	282	5

The temperature and pressure of the injected MEG were the lab temperature (around 20 °C) and the cell pressure, respectively. As the pressure increased due to inhibitor injection and gas hydrate dissociation, gas was removed from the top of the cell to keep the pressure constant (depressurization was very slow to minimize temperature reduction due to Joule–Thomson effect). The volume of the gas removed from the system at different steps in hydrate blockage removal process was measured using a gasometer at ambient condition and it is shown in Figure 5-3.

Figure 5-3 also shows the pressure at the top of the cell indicating the pressure response to MEG during gas hydrate dissociation. After each MEG injection, time was given to the system until the pressure became constant and it is possible to say that the system roughly reaches to a new equilibrium point. In fact, the system was not homogenous because of the absence of any active mixing in the system. Beside this, both pressures at the top and bottom of the long windowed rig were monitored simultaneously to see at what point pressure communication will be established.

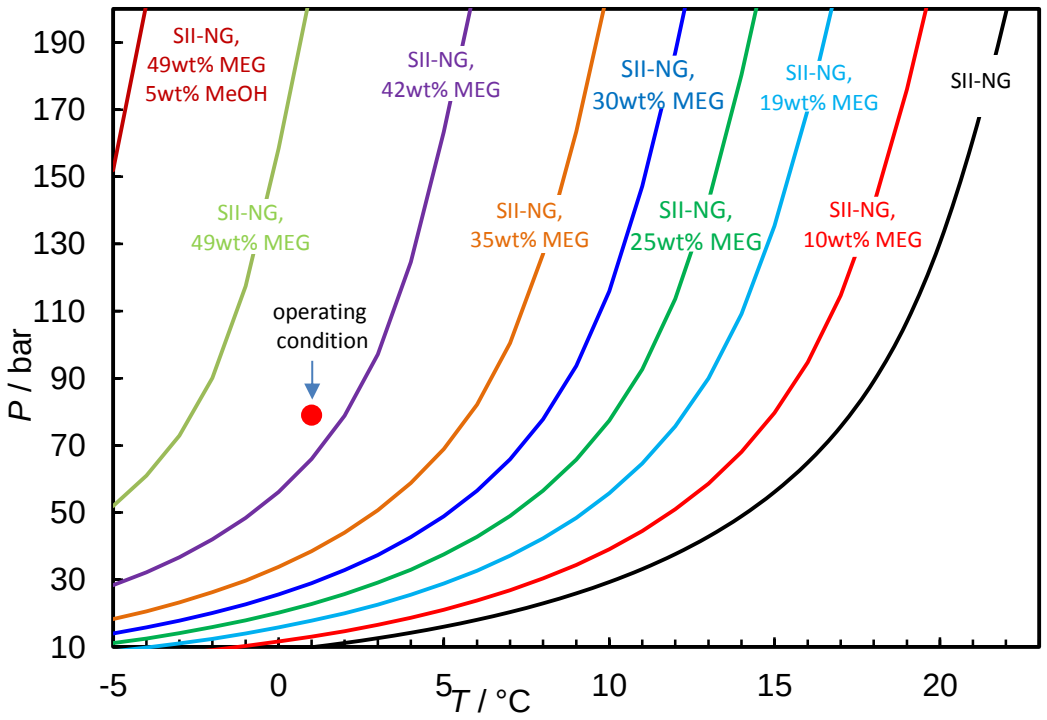

Figure 5-2. Hydrate phase boundary for natural gas system with different amount of MEG (and also 49% MEG + 5% MeOH) and operating condition.

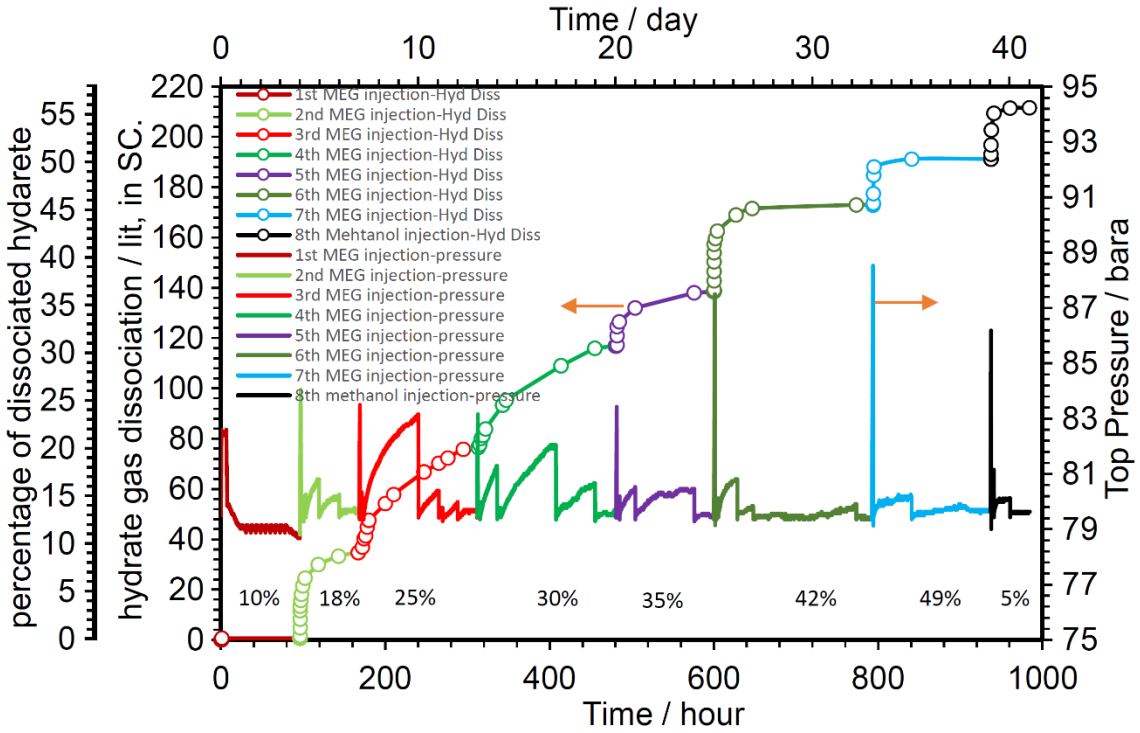

Figure 5-3. Volume of gas from hydrate dissociation at standard conditions, percentage of dissociated hydrate, and pressure response due to MEG injection and hydrate dissociation versus time. The pressure build-up due to MEG injection was calculated based on the volume of MEG injected considering the volume of gas released due to hydrate dissociation. Use the curve with the points for both hydrate gas dissociation and percentage of dissociation hydrate.

Once MEG was added to the system, a layer of MEG was formed on the top of the hydrates body during MEG injection because the system was completely blocked. As the density of MEG is higher than hydrate and water, MEG gradually penetrated into to the body of hydrates. Consequently, some hydrates dissociated and the pressure in the top section of the cell increased.

However, the system temperature is expected to decrease due to endothermic nature of hydrate dissociation and it is possible to form ice and block the system. This hypothesis was investigated by monitoring the cell temperature along its cell during MEG injection and hydrate dissociation. Some low temperatures, as low as -3 °C, were recorded in the hydrate zone during the hydrate dissociation process, indicating the possibility of ice formation during hydrate dissociation in the system. This low temperature was observed in window 3, i.e., fresh MEG came into contact with hydrates in window 3. The system temperature in each section of the setup during the MEG injection is shown in Figure 5-4.

Temperature reduction from 1 °C to -3 °C shows how the endothermic nature of hydrate dissociation could reduce the system temperature. The sharp increase in temperature of the system after each THI injection is due to the fact that the injected MEG was at ambient

lab temperature, i.e., this temperature rise only occurred at contact surfaces of MEG and hydrate in the system. Although depressurization process was very slow, a small temperature reduction was observed only at the top of the cell (window 6) during depressurization, indicating observed sub-zero temperature was not due to pressure reduction. For example, as shown in Figure 5-3, a depressurization was conducted at ~620 hours, and Figure 5-4 shows 0.4 °C reduction in the temperature which was only observed at the top of the cell (window 6).

The hydrate dissociation rate after each MEG injection varies due to non-homogenous nature of the system e.g. the hydrate dissociation rate in the early time of injection in the second and third MEG injections were 2.4 and 0.3 $^{\%\text{ hydrate dissociation}}/_{hour}$ respectively. However, the data shown in Figure 5-3 demonstrates that hydrate dissociation gradually stopped and hence pressure stabilized after each MEG injection, indicating a gradual reduction of MEG effect in every single batch of MEG injection. In other words, in the first few hours of each MEG injection, because there was a high concentration of MEG in the system, some hydrates dissociated fast and the rate of hydrate dissociation gradually decreased and finally stopped. This behaviour happened in every single batch of MEG injection. It can possibly describe how the injection rate is important to remove the hydrate blockage in the system and explain advantages and disadvantages of continuous/stepwise MEG injection.

The main reasons for this behaviour –reduction of MEG effect on hydrate dissociation in every single batch of MEG injection- can be listed as (assuming batch gas removal is efficient in maintaining the system pressure):

1. Dilution of MEG. Hydrate dissociation results in fresh water which could dilute the injected MEG, hence reducing its effectiveness

2. Non-homogeneous MEG distribution/concentration. In the absence of any active mixing, the MEG-water seems to remain non-homogeneous in the limited test time, i.e., high MEG concentration may not come into contact with hydrates

3. Localised low temperature. Hydrate dissociation is endothermic which results in a reduction in local temperature, hence moving the system back to the hydrate stability zone.

4. Localised compositional variations. Again in the absence of active mixing, there is a good possibility of non-homogeneous hydrocarbon composition in the gas phase.

Hydrate blockage was removed after injection of 49 mass% MEG into the system. The system remained blocked before this MEG injection, i.e., more than 45% of hydrates was dissociated before 7th batch of MEG injection. The data show that during this MEG injection, hydrate blockage was removed quickly as both pressure transducers showed the same pressure. It suggests that the amount of THI required for removing gas hydrate blockage in the system can be more than the amount calculated due to lack of active mixing in the system.

Figure 5-5 shows that hydrate blockage shifted upward after MEG injection. There were no hydrates in window 3 and 4 before MEG injection, but after MEG injection these two windows became blocked. It is potentially due to the reformation of hydrates in upper section precisely because of produced fresh water from gas hydrate dissociation. In other words, hydrate dissociation produced fresh water which moves upward due to lower density and hence hydrates reformed again in the interface between the gas and aqueous phase. Consequently, if there is enough time between each MEG injection, hydrates can form and block the system again in the upper section. Another potential reason for this behaviour could be shifting the preformed hydrates upward. Nonetheless, no matter what the reason is, hydrate blockage can shift upward in vertical pipes after MEG injection and it needs to be considered.

Some hydrates did not dissociate after the 7th MEG injection potentially due to non-homogeneous MEG distribution and lack of mixing in the system as shown in Figure 5-5 (see window 4). In order to dissociate the remaining hydrates, it was decided to inject methanol to see if it is possible to remove the remaining hydrates. After methanol injection, a layer of methanol was formed on the top of initial aqueous phase. As it was expected, methanol couldn't penetrate into the aqueous phase due to lower density.

Consequently, only some of those hydrates that came into contact with methanol at the top of the aqueous phase dissociated. Therefore, methanol was not able to dissociate most of the hydrate which remained in the initial aqueous phase. The system pressure did not increase any more after a few hours of methanol injection. This could be explained by the lack of methanol mixing with aqueous phase as Li, Gjertsen, and Austvik (2000) pointed out the problems associated with using methanol for hydrate dissociation in a system without good mixing [5.5].

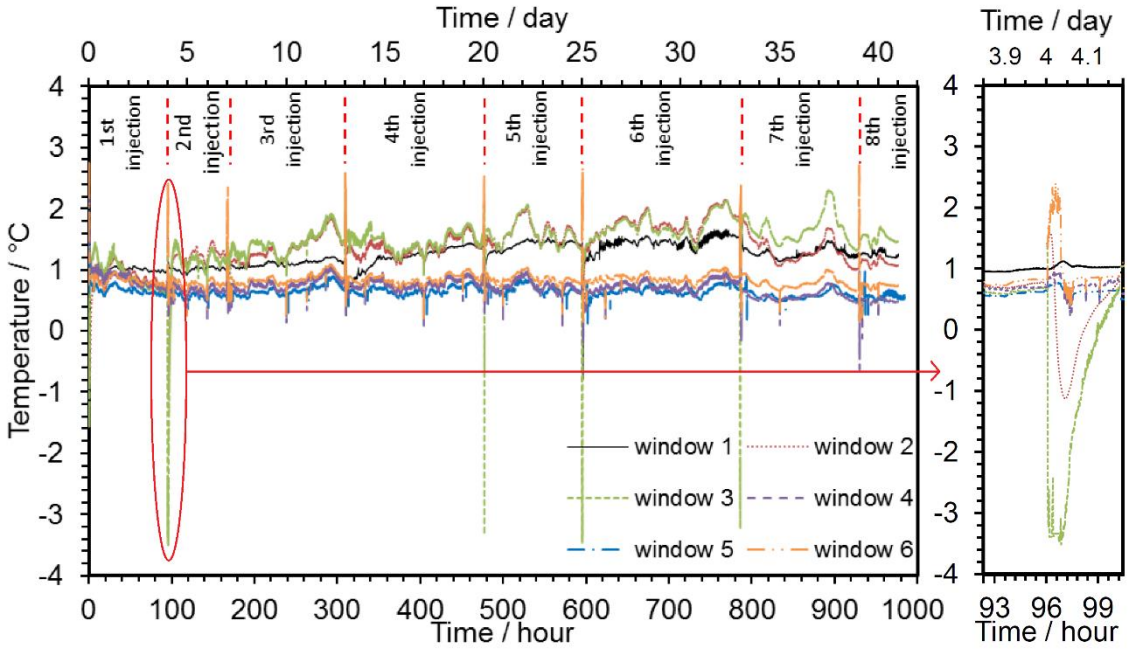

Figure 5-4. Temperature profile for the different sections of the rig during MEG injection.

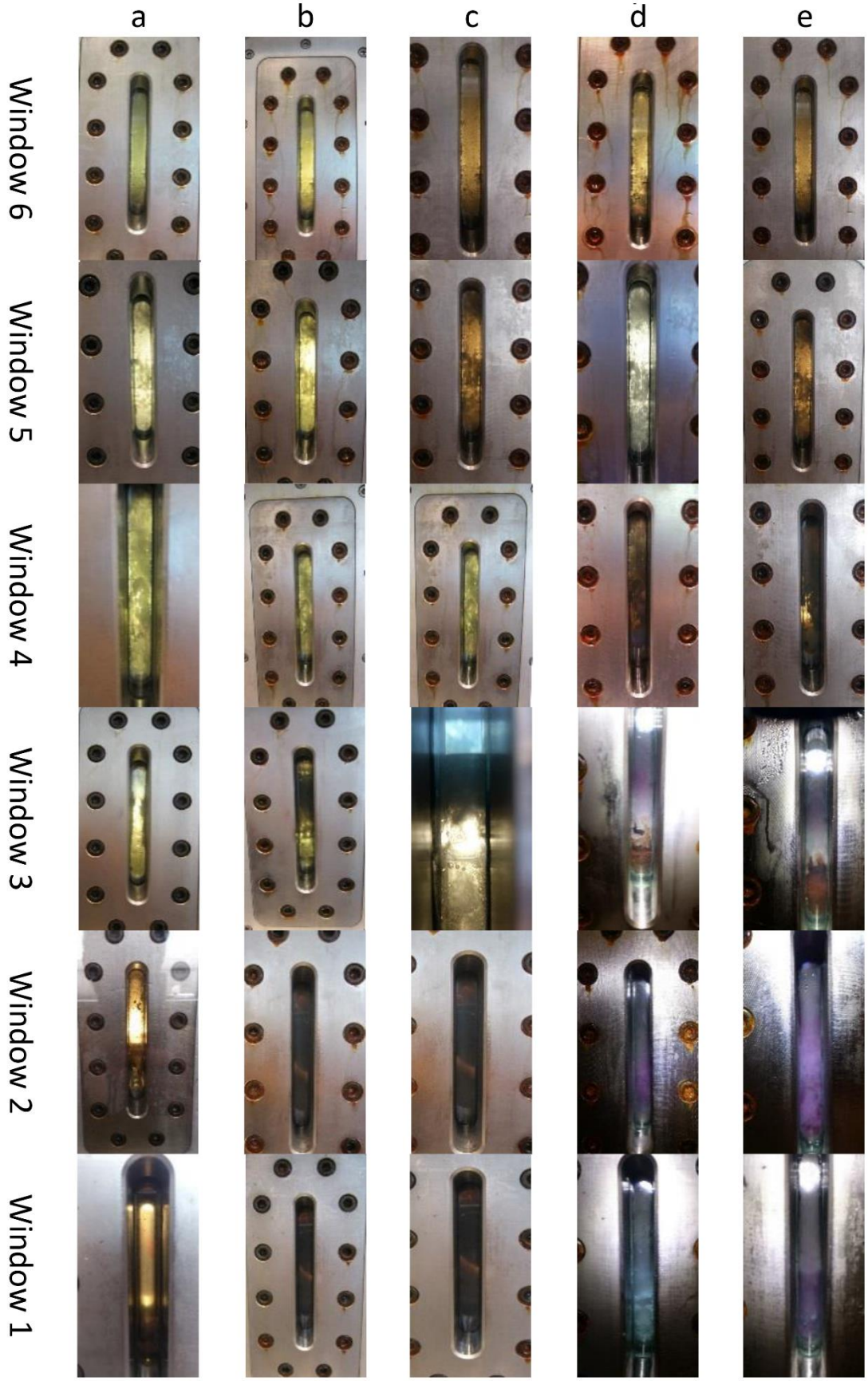

Figure 5-5. Hydrate formation and dissociation, hence hydrate blockage removal during MEG injection at 1 °C and ~80 bara. (a) first gas injection-no hydrate present, (b) last gas injection-blocked with hydrates, (c) 10 mass% MEG, (d) 19 mass% MEG, (e) 25 mass% MEG, (f) 30 mass% MEG, (g) 35 mass% MEG, (h) 42 mass% MEG, (i) 49 mass% MEG, (j) 5 mass% methanol, in addition to the amount of injected MEG .

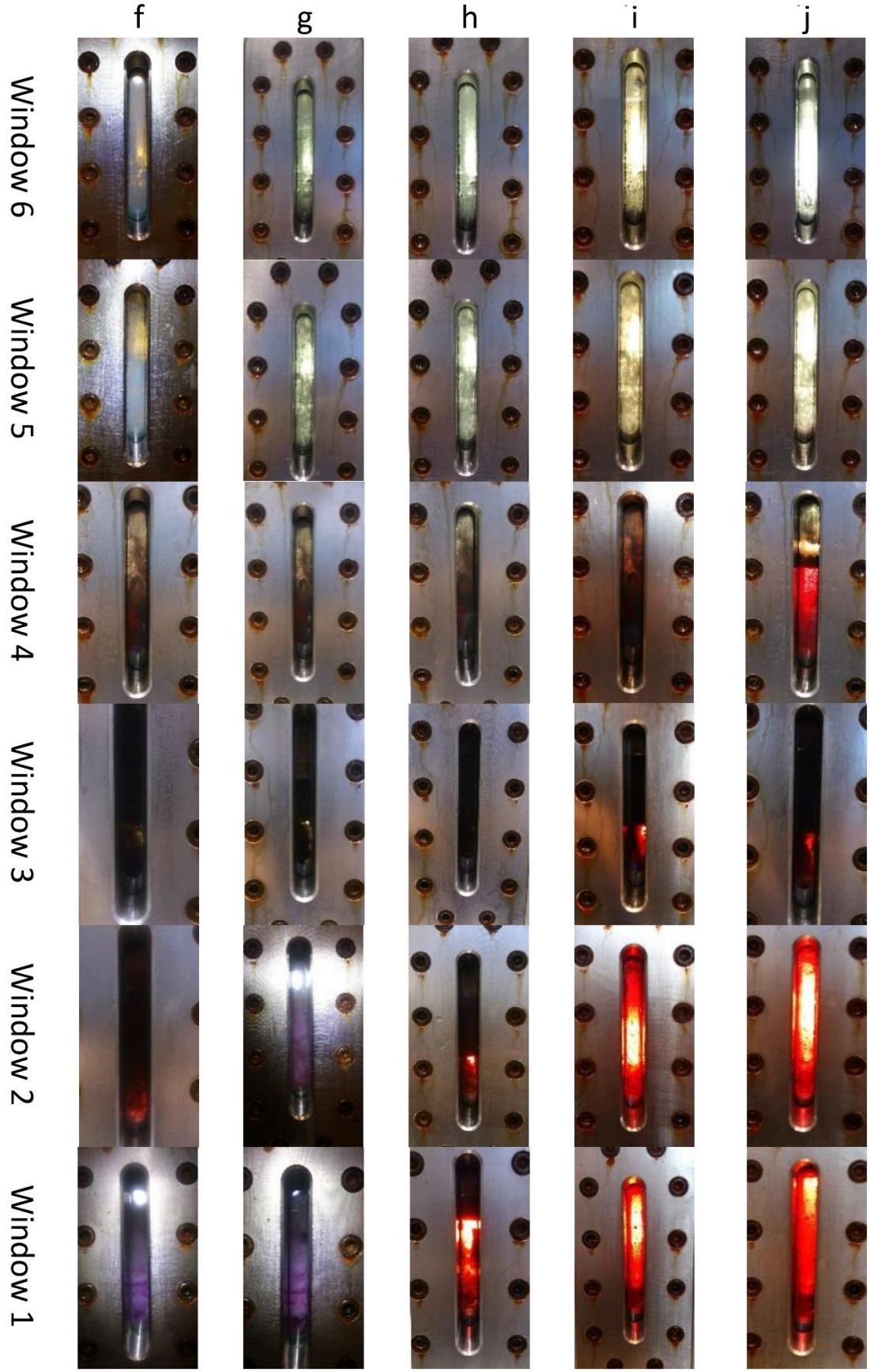

Figure 5.5. Continued.

5.3.2 Hydrate blockage removal using methanol in vertical pipes

This section presents the results of experiments which have done to investigate hydrate blockage removal using methanol in vertical pipes. In order to compare the results of this section with hydrate blockage removal using MEG in vertical pipes, the same procedure which is mentioned in the previous section was followed.

2066 g of deionized water was used in the long window rig which was positioned in vertical orientation. The vacuumed cell was pressurized with a single injection of 675 g of natural gas with a composition listed in Table 5-1. The volume ratio of liquid/gas in the cell was 0.44. In this case, the system temperature was set to 4.5 °C which is more realistic and close to seabed temperature.

Calculation using the data pressure which was recorded during hydrate formation shows that 73 mass% of water was converted to hydrates over 30 days. The stirrer was also used, but it stopped after formation of roughly 12% hydrates. This suggests that it is possible to form huge quantities of hydrates in the absence of any active mixing, i.e., the stirrer stopped and there was nothing to encourage the system to form hydrates by mixing the system or increasing water/gas interface, e.g. bubbling gas (there was not multiple gas injection and gas was injected from the top of the cell in one step). The pressure transducers showed different values of pressures at top and bottom of the cell, indicating complete hydrate blockage in the system. Figure 5-10 shows that the first two windows were completely blocked with hydrates and most of water was converted to hydrates.

To remove hydrate blockage, 18, 26, and 30 mass% methanol were injected at constant pressure as listed in

Table 5-5. Similar to the previous test, in order to keep the pressure constant, gas was removed from the top of the system and measured by gasometer. Figure 5-6 shows that 30 mass% methanol can dissociate all hydrates if there is a good mixing in the system.

Table 5-4. Details of gas injection including amount of gas injected, calculated percent water converted to hydrate 30 days after the beginning of the experiment of the methanol injection test.

Amount of gas		Total water mole fraction	WCH%	No. of days
g	mole			
675	36.7	0.76	73	30

Table 5-5. Details of methanol injection into the long windowed rig

No. of injection	Type	Mass / g	Volume / cc	Total Mass %
1	methanol	516	651	18
2	methanol	203	256	26
3	methanol	200	252	30

Figure 5-10 clearly shows that once methanol injected into the system, methanol located in window 3 (on the top of the hydrates body). Due to the direct contact of methanol and hydrates at the interface of methanol/hydrates body, some of those hydrates started to dissociate. Figure 5-7 indicates that hydrate dissociation started immediately after methanol injection. As shown in Figure 5-7, the rate of hydrate dissociation in the first few hours of the first methanol injection was very high, but it gradually decreased. The main reason is that there was no mixing in the system. Another reason could be due to the fresh water which came from hydrate dissociation and diluted the methanol and reduced its effectiveness.

Figure 5-10 shows that methanol could not penetrate into the hydrates body, i.e., dyed methanol was injected into the system and colour of hydrates in the first two windows did not change to red. Consequently, only those hydrates which have contacted to methanol at the top of the hydrates body dissociated. Recorded temperatures along the cell also confirm it. The temperature in the first two windows did not change, but data acquisition system recorded reduction of temperature in the hydrate-methanol contact zone during hydrate dissociation and recorded some temperature as low as -2 °C. This low temperature -similar to MEG injection test- confirms the possibility of ice formation during hydrate dissociation. The system temperature in each section of the rig during the methanol injection is shown in Figure 5-8.

As mentioned, the effect of methanol gradually diminished after the first injection and then hydrate dissociation stopped, so it was decided to inject more methanol, 26 and 30 mass% methanol. Figure 5-7 shows that the last two methanol injections could not dissociate the remaining hydrates. Although the total methanol concentration in the system after the last methanol injection was 30 mass% (software calculation shows that this system with 30 mass% methanol at this operating condition is out of hydrate stability zone, Figure 5-6), the system was still blocked. The main reason for this behaviour could

be due to the lower density of methanol compared to water and hydrate. Basically, the produced fresh water (as a result of hydrate dissociation) prevents methanol to penetrate into the hydrate plug due to its lower density.

Dilution of methanol, non-homogeneous methanol distribution/concentration in the absence of any active mixing in the system, localized low temperature, and localized compositional variations could be the other reasons for the aforementioned behaviour of methanol in removing and dissociating of gas hydrates.

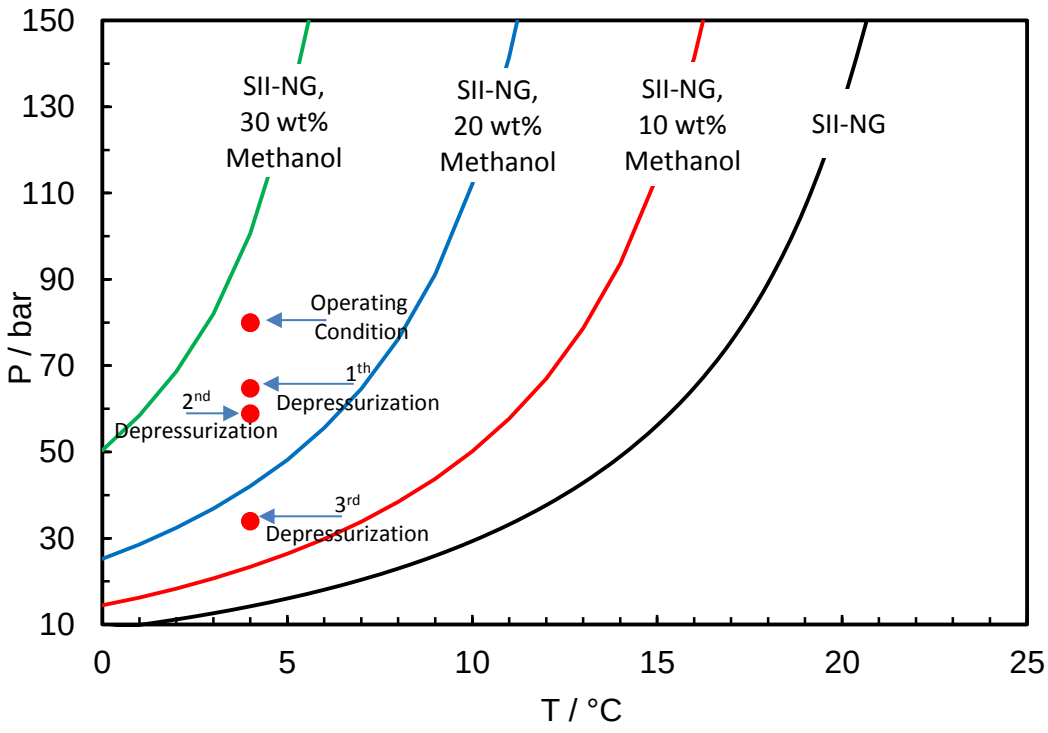

Figure 5-6. Hydrate phase boundary for natural gas system with different amount of methanol and operating condition.

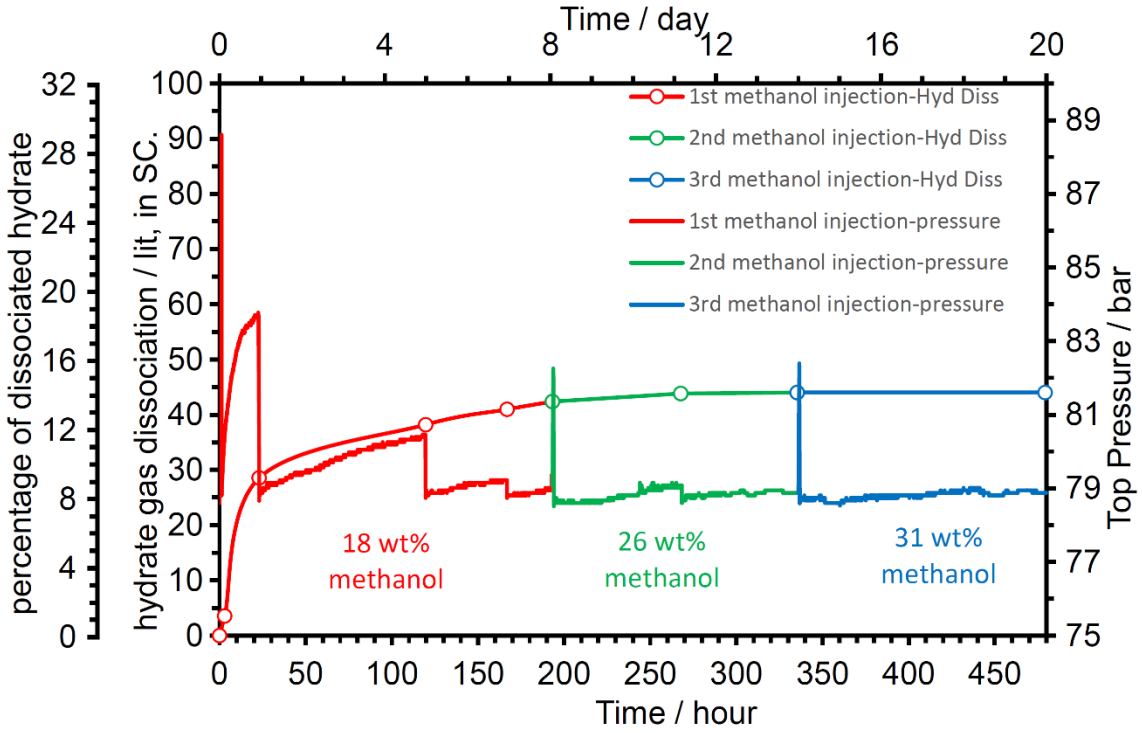

Figure 5-7. Volume of gas from hydrate dissociation at standard conditions, percentage of dissociated hydrate, and pressure response due to methanol injection versus time. The pressure build-up due to methanol injection was calculated based on the volume of methanol injected considering the volume of gas released due to hydrate dissociation. Use the curve with the points for both hydrate gas dissociation and percentage of dissociation hydrate.

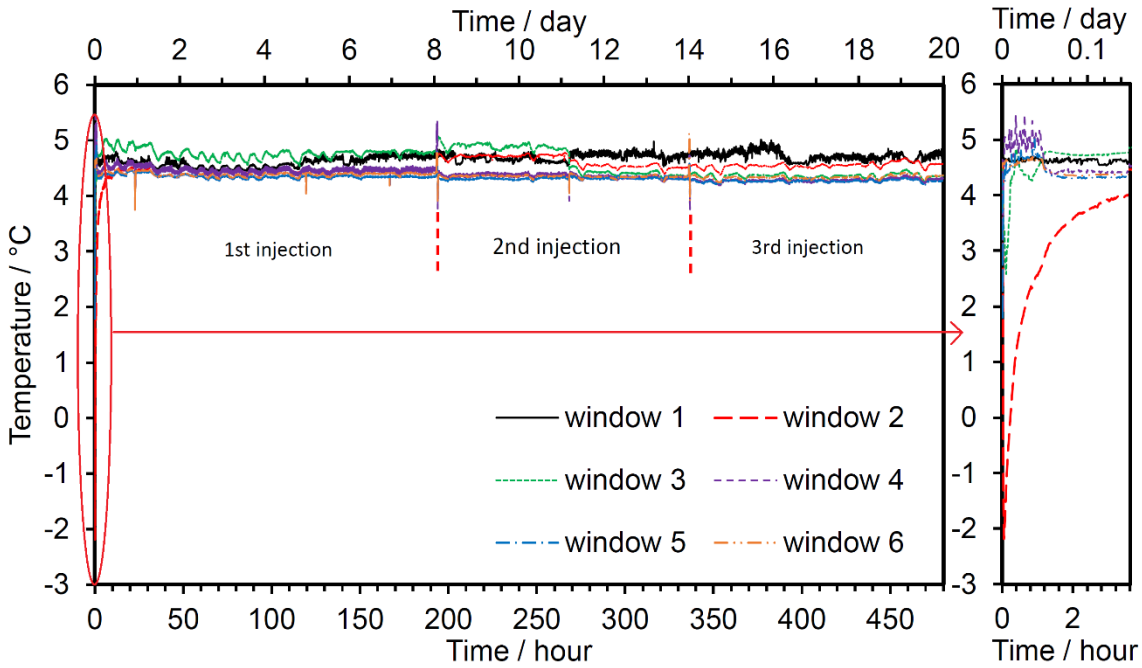

Figure 5-8. Temperature profile for the different sections of the rig during methanol injection.

As hydrate blockage was not removed from the system by methanol injection, it was decided to depressurize the system to investigate the possibility of hydrate dissociation and hydrate blockage removal using depressurization. Therefore, the gas was removed from the system in 3 steps to decrease the top pressure from 79 to 65, 59, and 34 bara respectively as shown in Figure 5-6.

Figure 5-9 shows the pressures at above and below the hydrates body during the depressurizing. The main aim of this work was to promote hydrate dissociation by keeping the system farther away from the hydrate phase boundary. Another aim was to mix the system by releasing of dissolved gas which could happen during depressurization of the system, i.e., this could homogenize the system and distribute the methanol in the system.

Figure 5-9 shows that hydrate did not dissociate in the first two steps of depressurization. It means that keeping the system farther away from the hydrate phase boundary using depressurizing could not dissociate the remaining hydrates for this system. It also indicates that mixing due to gas bubbling from the depressurization was not efficient to homogenize the system if there is large quantities of hydrates. Accordingly, as there was a small amount of liquid and large quantities of hydrates in the system, the bubbling dissolved gas using depressurization could not mix the system and hence hydrate blockage was not removed in the first two steps of depressurization.

Finally, the last depressurization was done and the pressure above the hydrates body decreased to 34 bara. As there was no pressure communication through the hydrates body, the pressure difference between the ends of hydrates body increased to 47 bara (the bottom pressure was 81 bara). Due to this high pressure difference, hydrate blockage moved up and the system became turbulent and mixed intensely.

Data shows that at this time the bottom pressure decreased immediately and after a few hours both top and bottom pressure transducers showed the same pressure. Although hydrate blockage was removed from the system, some hydrates remained in the system as Figure 5-9 shows increasing of the system pressure after hydrate blockage removal. Because of the efficient mixing due to hydrate plug movement, methanol was distributed in the system and contacted with the remaining hydrates. The pressure, therefore,

increased fast due to hydrate dissociation. As it is clear from Figure 5-10, all hydrates dissociated in the last step of depressurization and dyed methanol was distributed through the first three windows indicating the homogeneous system.

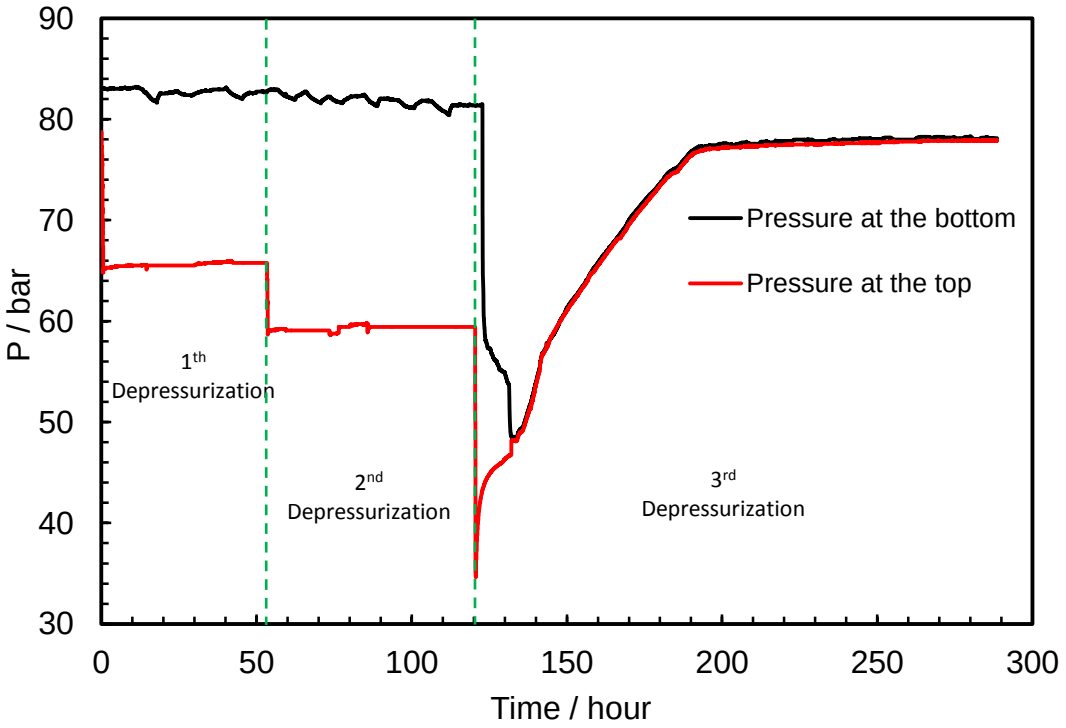

Figure 5-9. Top and bottom pressures of the long windowed rig during depressurization-methanol injection test.

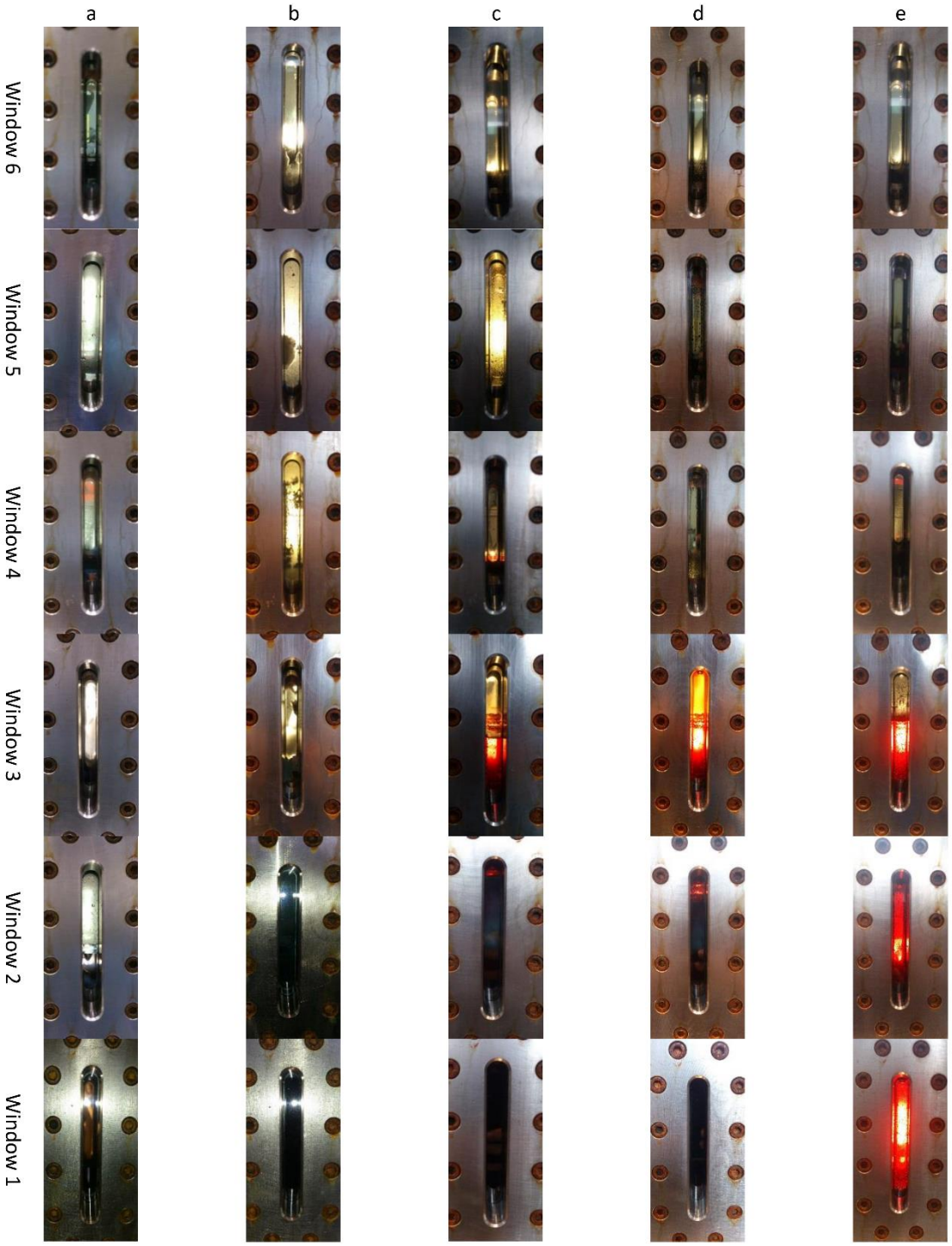

Figure 5-10. Hydrate formation and dissociation, hence hydrate blockage removal during gas methanol injection at 4.5 °C and ~81 bara. (a) no hydrate present, (b) blocked windows with hydrates before methanol, (c) 18 mass% methanol, (d) 26 mass% methanol, (e) after depressurizing to 34 bara.

5.3.3 Hydrate blockage removal using a mixture of methanol/MEG in vertical Pipes

Previous results (removing hydrate blockage using MEG and methanol in the vertical pipes) confirm that density of THI plays an important role in removing hydrate blockage in the vertical pipes. Therefore, the relative density of methanol and MEG needs to be considered in vertical pipes. In order to do more investigation of THI density role in hydrate blockage removal in vertical pipes, a mixture of methanol and MEG was used. The aim of this work was to adjust its density to 1 g/cc (equal to water density). This mixture could penetrate into the hydrate plug, i.e., the density of hydrates is lower than 1 g/cc. However, the possibility of hydrate reformation due to produced fresh water from hydrate dissociation could be minimized by adjusting the chemical density to 1 g/cc.

The same procedure for hydrate formation and blockage removal -similar to the previous tests- was carried out. The details of natural gas injection and the amount of hydrates formed in this test are listed in Table 5-6. The system temperature was set to 4.5 °C. 65 mass% of the water was converted to hydrates over 30 days, and the system became completely blocked as indicated by a lack of pressure communication through the hydrate bulk. This amount of hydrates indicates that the system can be blocked completely with different amount of hydrates, i.e., in this test, the system became blocked after formation of 65% of hydrates which is lower than the amount of hydrates required to block the system in the previous tests (roughly 85 %). In reality, the amount of hydrates required to block the system completely, e.g. no pressure communication, is much more than the amount of hydrates required to prevent fluid movement in pipes. Roughly 12 mass% hydrates resulted in stirrer stoppage, potentially preventing fluid movement in pipes. There are many factors that could affect the pipeline blockage due to hydrate formation e.g. amount of hydrates, subcooling temperature, hydrate growth rate, gas composition, and pipe diameter.

Table 5-6. Details of gas injection including amount of gas injected, calculated percent water converted to hydrate after 30 days from the beginning of the experiment-methanol/MEG injection test.

Amount of gas		Total water mole fraction	WCH %	No. of days
g	mole			
598	32.5	0.78	65	30

Software calculation (HydraFLASH®) shows that injection of 36 mass% of chemical which consists of methanol and MEG so that its total density is 1 g/cc, can dissociate and remove all hydrates if there is a good mixing in the system. Figure 5-11 shows the gas hydrate phase boundary of natural gas with different amounts of THIs (methanol/MEG). It was again decided to use stepwise chemical injection. The details of chemical injections are given in Table 5-7. Similar to the previous tests, the system pressure was kept constant during hydrate dissociation by removing the gas from the top of the cell.

The measured gas volume produced from hydrate dissociation and pressure response due to chemical injection and hydrate dissociation are plotted in Figure 5-12. The system temperature for each chemical injection is shown in Figure 5-13. As it was expected, the hydrate dissociation rate in the early times of each chemical injection was very high and it gradually decreased. It is notable that the hydrate dissociation rate in this case (methanol/MEG) is much higher than MEG injection case. The main reason for this behaviour could be the presence of methanol and MEG simultaneously. In terms of mass%, methanol shifts the hydrate phase boundary to lower temperature and higher pressures compared to MEG. The primary reason for the difference by mass is that MEG has a much higher molecular mass, so less moles per gram. They should be much more comparable if mole% is used, i.e., in fact, a quick model freezing point check suggests MEG is more inhibiting per mole. That could be down to it having two OH groups per CH_2 group, so more polar / more attractive to water in terms of hydrogen bonding. Certainly, the industry does injection based on volumes, and by volume, methanol is better than MEG (even though methanol density is lower) as there are still more moles per volume. Therefore, as these experiments were conducted based on mass%, the mixture of methanol/MEG could be more efficient. The temperature reduction of the system during hydrate dissociation in the case of MEG and methanol injection which were 4 °C (from 1 °C to -3 °C) and 6.5 °C (from 4.5 °C to -2°C) respectively, confirms this, i.e., temperature reduction for the methanol case was higher than MEG case. The temperature reduction for the methanol/MEG injection was 8.5 °C (from 4.5 °C to -4 °C). It is notable that, ice formation is possible in all cases during hydrate dissociation.

Table 5-7. Details of methanol/MEG injection into the long windowed rig.

No.	ρ_{THI} g/cc	Type	Mass / g	Total / g	Volume / cc	Mass %	Total Mass% (relative to aqueous phase)
1	1	MeOH	56.4	200	200	2.5	8.8
		MEG	143.6			6.3	
2	1	MeOH	56.4	200	200	4.6	16.3
		MEG	143.6			11.7	
3	1	MeOH	56.4	200	200	6.9	23.1
		MEG	143.6			16.2	
4	1	MeOH	56.4	200	200	7.9	27.9
		MEG	143.6			20.0	
5	1	MeOH	56.4	200	200	9.2	32.6
		MEG	143.6			23.4	
6	1	MeOH	56.4	200	200	10.4	36.8
		MEG	143.6			26.4	
7	0.9	MeOH	41.4	100	111	11.3	38.6
		MEG	58.6			27.3	

Although methanol is better than MEG for hydrate dissociation (if the same mass% of chemical is used), it does not have an ability to penetrate and remove hydrate blockage in vertical pipes due to its density. Therefore, using a mixture of MEG/methanol can increase the efficiency of hydrate blockage removal using chemical injection in the vertical pipes. Beside this, the mixture of methanol and MEG with a density of 1 g/cc can decrease the possibility of hydrate reformation, i.e., the density of methanol/MEG mixture and produced fresh water are the same, so the possibility of hydrate reformation in the upper section can be reduced. In addition, the hydrostatic pressure of injected chemical in the vertical pipes can be reduced by injection of MEG/methanol rather than MEG alone, i.e., MEG/methanol is stronger than MEG for shifting the hydrate phase boundary to lower temperature and higher pressure (if a same mass% chemical is used), hence less MEG/methanol mixture is required to remove hydrate blockage from the system.

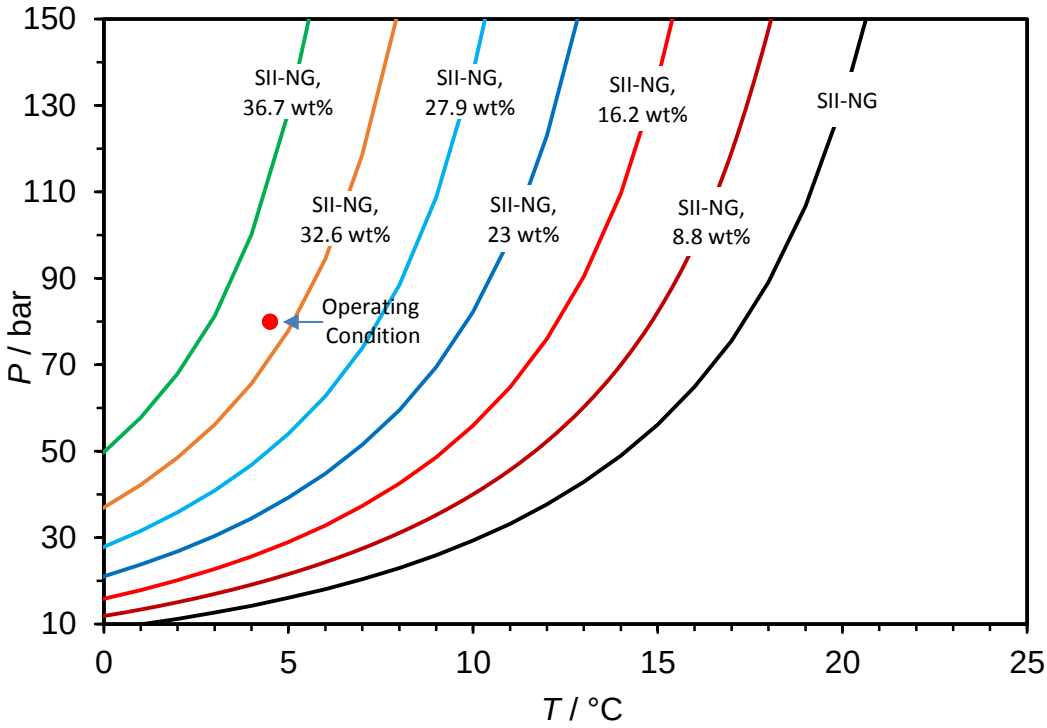

Figure 5-11. Hydrate phase boundary for natural gas system with different amount of THI, i.e., injected chemical consists of methanol and MEG so that its total density is 1, and operating condition.

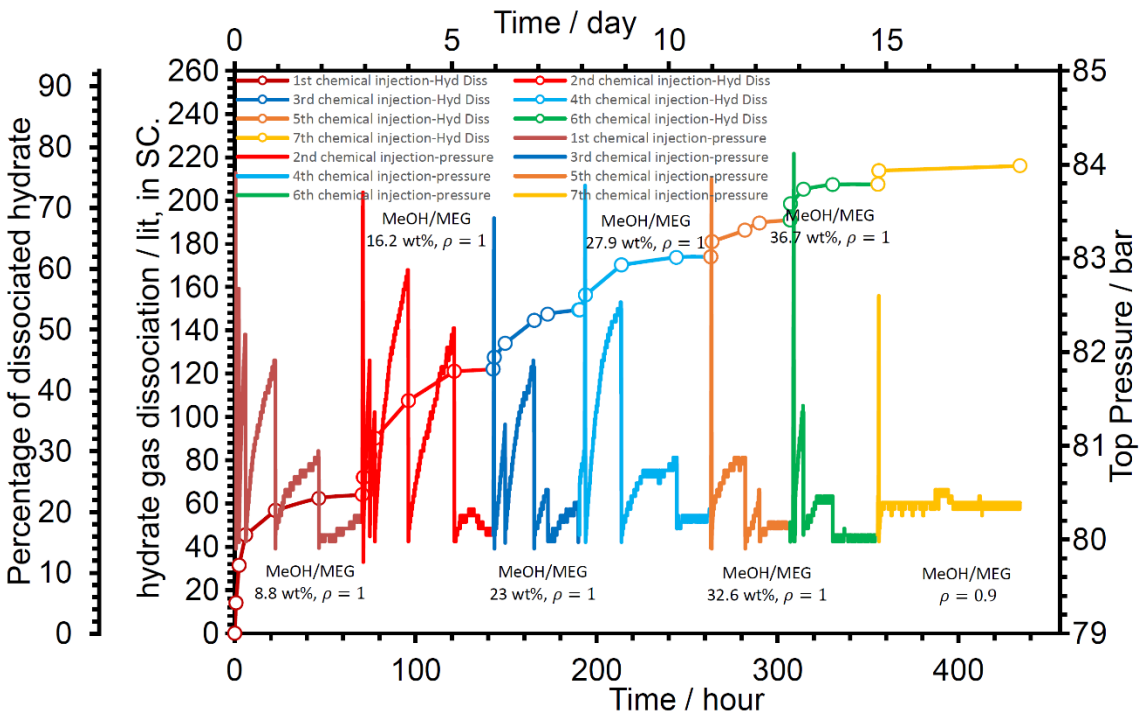

Figure 5-12. Volume of gas from hydrate dissociation at standard conditions, percentage of dissociated hydrate, and pressure response due to methanol/MEG injection versus time. The pressure build-up due to injection was calculated based on the volume of chemical injected considering the volume of gas released due to hydrate dissociation. Use the curve with the points for both hydrate gas dissociation and percentage of dissociation hydrate.

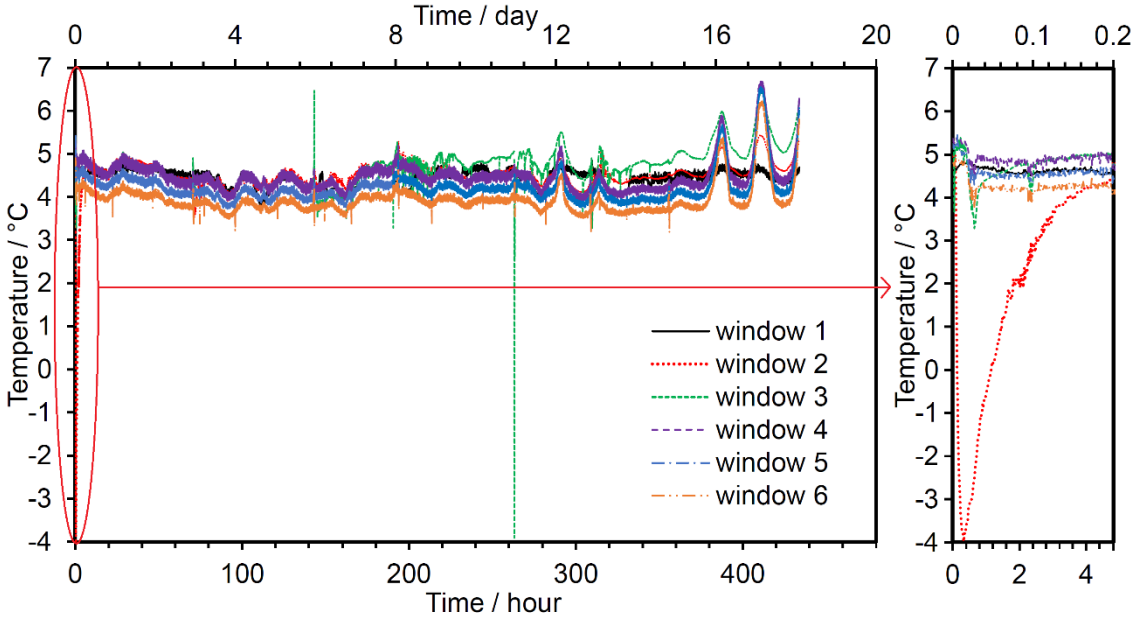

Figure 5-13. Temperature profile for the different sections of the rig during MEG/methanol injection.

Finally, after injection of 6th chemical injection (36 mass% mixture of methanol/MEG with a density of 1 g/cc) both pressure transducers at top and bottom of the cell showed the same pressure, indicating hydrate blockage was removed. Figure 5-14 shows that in this stage the hydrate blockage was removed in windows 1 and 2.

Although the most of the hydrates dissociated and hydrate blockage removed, there were still some hydrates at the top of the aqueous phase, window 3 in Figure 5-14. These hydrates could be from hydrate reformation or pre-formed hydrates. Pre-formed hydrates could detach from hydrates body during hydrate dissociation and then move up, at the top of the aqueous phase, due to being less dense. As the previous results show that methanol, MEG, and methanol/MEG with a density of 1 g/cc are not able to dissociate these hydrates, it was, therefore, decided to inject a mixture of methanol/MEG with a density of 0.9 g/cc, its details are listed in

Table 5-7. The density of methane hydrate is roughly approximated 0.91-0.94 g/cc at 273.15 K and 25.1 atmospheres [5.6]. This mixture of Methanol/MEG was injected with different colour, violet (the previous mixture of methanol/MEG was red). Figure 5-14 shows that this mixture could dissociate all hydrates in window 3 which did not dissociate by injection of methanol/MEG mixture with a density of 1 g/cc. It indicates that density is the most important factor in selection of chemical (MEG, methanol, and methanol/MEG mixture) to remove hydrates in vertical pipes.

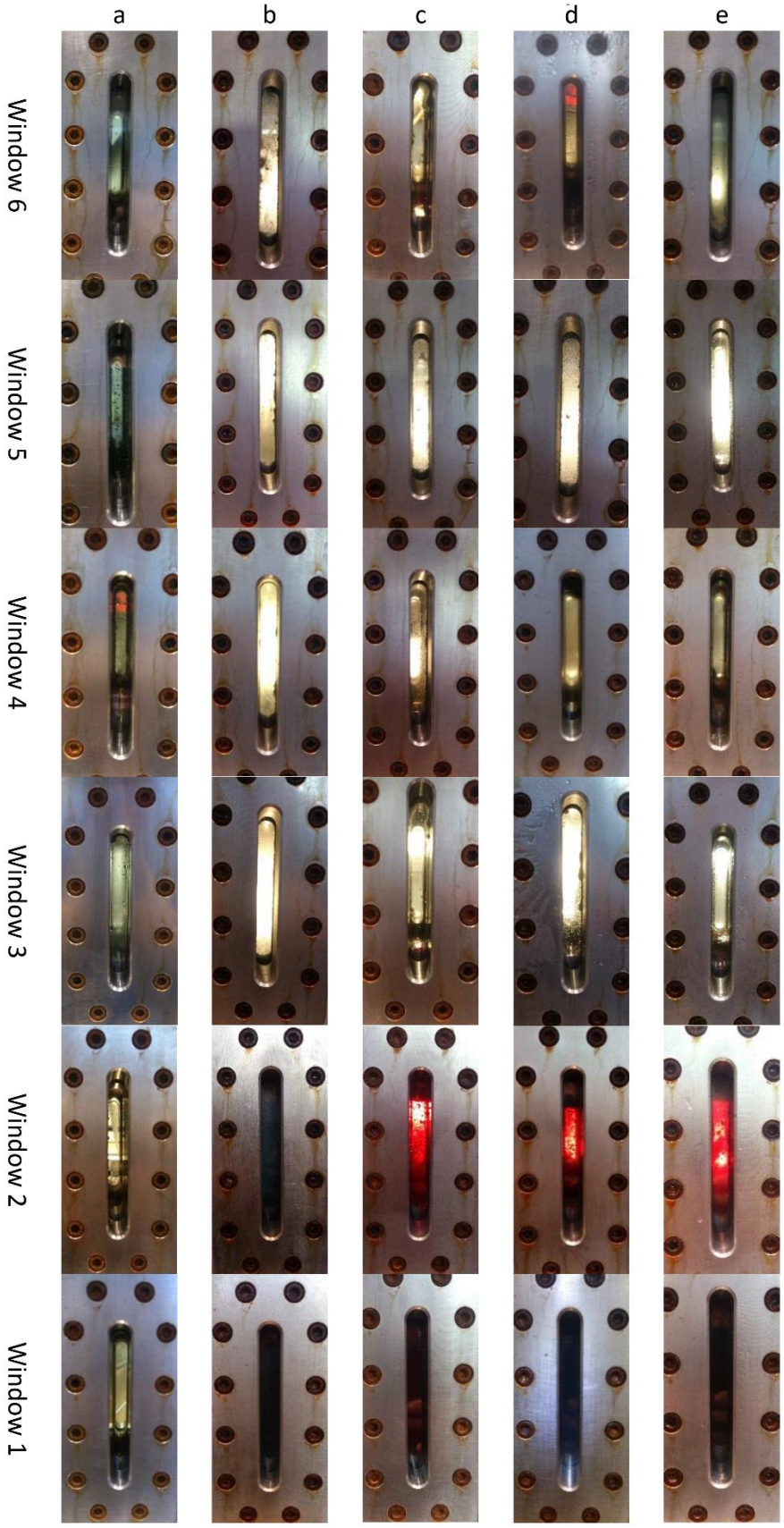

Figure 5-14. Hydrate formation and dissociation, hence hydrate blockage removal during MEG/methanol injection at 4.5 °C and ~80 bara. (a) no hydrate present, (b) blocked windows with hydrates before methanol/MEG injection, (c) 8.8 mass% chemical*, (d) 16.2 mass% chemical*, (e) 23 mass% chemical*, (f) 27.9 mass% chemical*, (g) 32.6 mass% chemical*, (h) 36.7 mass% chemical*, (i) 3 mass% chemical†.

*** Injected chemical consists of methanol and MEG so that its total density is 1.**

† Injected chemical consists of methanol and MEG so that its total density is 0.9.

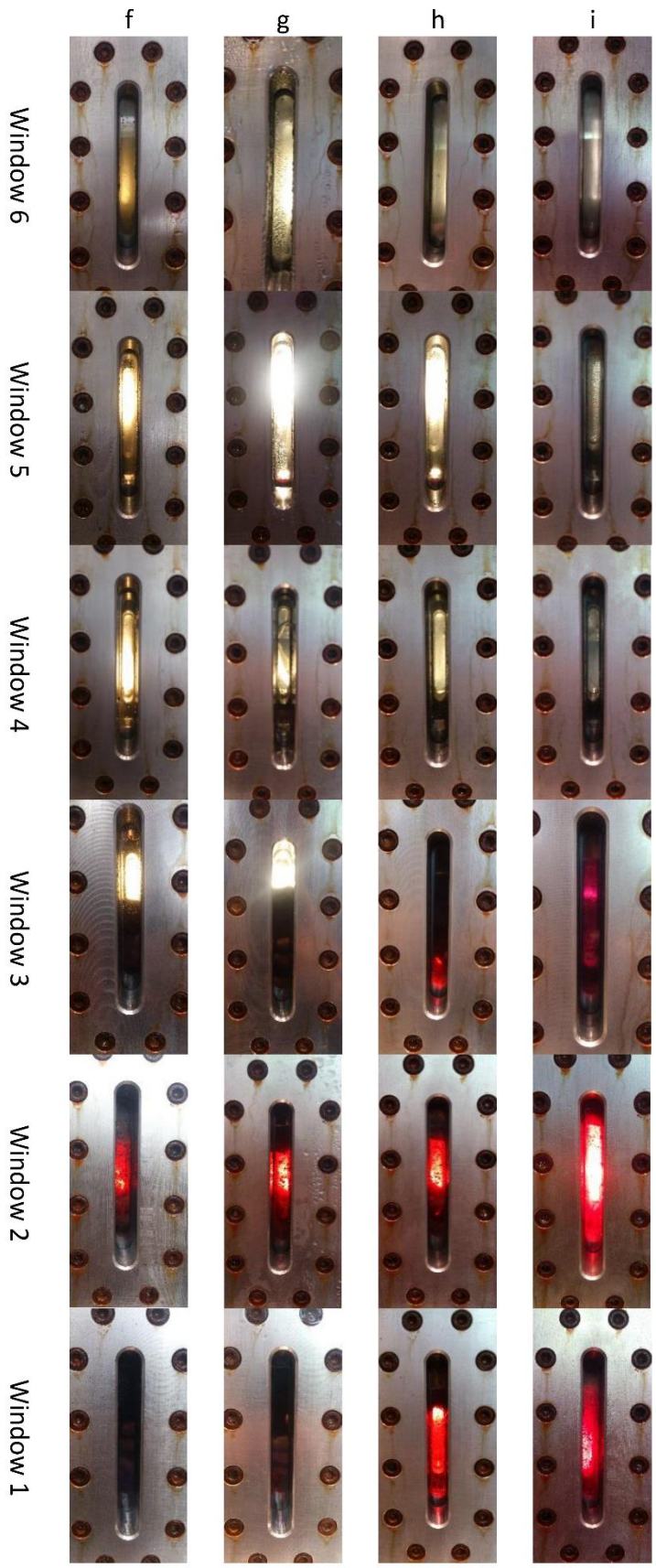

Figure 5-14. Continued.

5.4 Summary

This chapter presents details of a novel 1.5 meters, windowed cylindrical (75 mm internal diameter) experimental setup that can be used for studying of the hydrate blockage formation and removal. In addition, the setup is equipped with separate temperature controlled jackets along its length for establishing a temperature gradient.

In this chapter, the results of hydrate blockage formation from a North Sea natural gas with deionized water, and its subsequent removal using batch inhibitor injection (initially MEG followed by methanol, methanol, and methanol/MEG mixture) were presented. The following conclusions could be drawn:

- Injected MEG dissociated some hydrates at the top and penetrate into the body of hydrates

- Methanol injection can only dissociate those hydrates which contact with methanol at the top of the hydrates body, and can't penetrate into the body of hydrates

- The mixture of methanol/MEG with a density of 1 g/cc is a better option for dissociating and removing hydrates in the vertical pipelines, i.e., hydrate dissociation rate of this case is higher than the case of methanol or MEG injection alone

- The amount of chemical required for injection in terms of mass% could be reduced by injection of methanol/MEG mixture. This also results in a reduction of hydrostatic pressure during chemical injection

- Water generated as a result of hydrate dissociation moved upward and re-formed hydrates/blockage

- Hydrate reformation as a result of water generated due to hydrate dissociation could change the location of the blockage. In addition, those hydrates which are detached from the hydrate plug can move up and block the system

- A mixture of methanol/MEG with a density of 0.9 g/cc can dissociate those hydrates which are at the top of the aqueous phase

- The THI-water system seems to remain non-homogeneous, indicating that the mixing due to gas release/bubbling and diffusion is not very efficient in the limited test time

- The endothermic nature of hydrate dissociation resulted in sub-zero temperatures, hence ice formation/blockage

- Due to non-homogeneous nature of the system, the amount of THI required is more than what is calculated by thermodynamic modelling

- Density of injected inhibitor plays an important role in effectiveness of hydrate blockage removal

5.5 Reference

[1] S. Cochran, "Hydrate control and remediation best practices in deepwater oil developments," in Offshore Technology Conference, OTC 15255. Houston, TX, 2003.

[2] Sloan, E. D.; Koh, C. A.; Sum, A.; Ballard, A. L.; Creek, J. L.; Eaton, M.; Lachance, J.; McMullen, N.; Palermo, T.; Shoup, G.; Talley, L., 2010. Natural Gas Hydrates in Flow Assurance; Gulf Professional Publishing (Elsevier): Oxford, U.K., ISBN: 978-1-85617-945-4

[3] J. Lee, B. Hampton, R. R. Alapati, E. a Sanford, and S. O'Brien, "OTC 20171 Innovative Technique for Flowline Plug Remediation," *Otc*, no. May, pp. 4–7, 2009.

[4] M. Piemontese, M. Rotondi, A. Genesio, A. Perciante, and F. Iolli, "Successful experience of hydrate plug removal from deepwater gas injection flowline" 12th Offshore Mediterr. Conf., pp. 1–9, 2015.

[5] X. Li, L. H. Gjertsen, and T. Austvik, "Thermodynamic inhibitors for hydrate plug melting," *Ann. N. Y. Acad. Sci.*, vol. 912, no. 1, pp. 822–831, 2000.

[6] E. D. Sloan Jr and C. Koh, *Clathrate hydrates of natural gases*. CRC press, 2007.

Chapter 6– Bio KHI-Induced Dissociation of Gas Hydrate

6.1 Introduction

Generally, Kinetic Hydrate Inhibitors (KHIs) which are water-soluble polymers, are known as an option for prevention/delay of hydrate nucleation or reduce hydrate growth rate by influencing hydrate surface properties at low concentrations. The industry opinion is that KHIs cannot be used for remediation, i.e., if THI is replaced with KHI, it still might need THI to remove plugs. As there is very little literature data on the effect of KHIs on hydrate dissociation inside the hydrate region (see Section 1.5.2), the question may then arise: could KHIs help to remove plugs by causing dissociation? The main objective of this chapter is to investigate very abnormal hydrate dissociation using Luvicap Bio inside the hydrate regions. In addition, PVCap was used as a well-known reference / benchmark to compare the performance of Bio KHIs.

There has been a lot of experimental and theoretical work to find the mechanism of KHIs. Despite this, none of them explains completely all of the KHIs behaviours e.g. induction time, crystal growth inhibition (CGI) regions (see Section 1.4.4.2), hydrate nucleation, sudden hydrate growth, hydrate morphology, or structure change. As discussed in Section 1.5.2, although some limited evidence shows PVCap could induce hydrate dissociation inside the hydrate stability zone [6.1], the ability to influence hydrate dissociation has not been focused and investigated in detail.

Anderson et al. (2005) showed two KHIs mechanisms using molecular dynamic by accepting local structure mechanism of hydrate nucleation [6.2]. They proposed that KHIs increase the energy barrier to nucleation by disruption of the organization of the water and guest molecules and once hydrate nuclei are created, the inhibitor molecules bind to the hydrate crystals and retard further hydrate growth. In addition, Yang and Tohidi (2011) showed experimentally two different KHIs mechanisms (nucleation inhibition and growth inhibition) [6.3]. Most of the studies which have been done suggest the influence of KHIs on hydrate crystal surface as a main mechanism of KHIs which can only inhibit hydrate formation, not dissociation [6.2-6.5].

In addition, hydrate formation can form as a result of different scenarios e.g. failure of inhibitor delivery, increased water content / unpredicted free water appearance, unplanned shut-in, and poor KHI distribution. With respect to the field, the scenario of hydrate formation in the absence of KHIs (free-KHIs system) is realistic. Therefore, the question may then arise: could KHIs inhibit or even dissociate pre-formed hydrates (the

KHIs mechanisms only suggest hydrate nucleation/growth prevention). If KHIs cause dissociation, it raises the question of whether they can be used to remove plugs.

The molecules of KHI inhibitors can bind to the hydrate crystals and retard further hydrate growth and some results showed the ability of KHIs in hydrate dissociation [6.1]. As a result, if KHIs are able to dissociate hydrates, the question may then arise as whether disruption/induced-dissociation of pre-formed hydrate crystals is another mechanism of KHIs in addition to aforementioned KHIs mechanisms e.g. disruption of the organization of the water and guest molecules during hydrate nucleation.

Therefore, this chapter focuses on the abnormal hydrate dissociation in the presence of KHIs. Hence, experiments have been done to answer this question, i.e., whether KHIs (Luvicap-EG and Luvicap Bio in this study) can dissociate hydrates inside the hydrate stability zone and what is the reason behind this behaviour. In addition, the ability of KHIs in prevention of hydrates in pre-formed hydrate systems (hydrates formed in the absence of KHIs) was investigated.

Furthermore, this chapter investigates if there is a difference between the hydrate crystal growth patterns (CGI regions) of the systems with hydrate formation in the presence and absence of KHIs. Experimental work was carried out to see whether KHIs can successfully inhibit those hydrates which formed in the free-KHIs systems.

6.2 Experimental Methods and Materials

Tests were undertaken on simple methane + PVCap (BASF Luvicap-EG), methane + Luvicap Bio, and natural gas + Luvicap Bio. Experiments were carried out using stirred autoclaves (see Section 2.2). The purity of methane gas used was 99.99%. The composition of natural gas used is given in Table 2-1. Distilled water was used in all tests. Standard commercial Luvicap-EG, supplied by BASF, was used; vacuum oven dried PVCap (from Luvicap-EG) has been used for PVCap studies, however, Luvicap-EG provides a liquid form that can be injected with the small fraction of MEG solvent having a negligible effect on CGI patterns.

Cells were filled 50% by volume with distilled water. The thermodynamic hydrate phase boundary was predicted using HydraFLASH®, a thermodynamic model by Hydrafact Ltd and Heriot-Watt University. The estimated percentage of water converted to hydrate (WCH %) was calculated based on the calculation presented in Appendix B.

To investigate the ability of KHIs in inhibition of hydrate growth in pre-formed hydrate system, the CGI method (See Section 1.4.4.2) was used. Standard CGI method determines different regions as a function of subcoolings. These regions and their description are listed in Table 1-2. Complete inhibition region (infinite induction time)/green zone, partial inhibition region /amber zone, and rapid failure region/red zone are three main regions which are highly repeatable. In this technique usually, KHI is mixed with the aqueous phase before loading, and then the standard CGI procedure is applied, i.e., the system is cooled rapidly to form hydrates and then is heated to dissociate most of hydrates but leaving a small fraction of hydrates and re-cooled the system again. Therefore, the following procedure was used to simulate the pre-formed hydrate system.

As discussed in the next section, to simulate the pre-formed hydrate systems, Luvicap-EG was injected (to a concentration of ~0.5% polymer aqueous) after hydrate formation. The Luvicap-EG injection was done using a piston vessel. The appropriate volume of Luvicap-EG was placed in one side of the piston vessel with a high pressure water behind the piston (this pressure was applied using hand pump). The Luvicap-EG side of the piston vessel was connected to the cell inlet/outlet valve. It is worth to mention that, as the necessary volume of Luvicap-EG to achieve a concentration of ~0.5% polymer aqueous is low, this injection did not increase the cell pressure significantly. As discussed later, two separate tests have been carried out for Luvicap-EG to investigate repeatability. In addition, the capability of Luvicap-EG in hydrate dissociation was investigated.

Furthermore, shut-in/restart (SIR) tests (see Section 3.3.2) have been carried out for the methane-Luvicap Bio system to investigate whether Bio KHIs e.g. Luvicap Bio is able to dissociate hydrates.

6.3 Result and discussion

As PVCap is the only polymer which has been reported for hydrate dissociation using KHI inside the hydrate phase boundary [6.1], abnormal hydrate dissociation was investigated first using PVCap for the reference / benchmark. Therefore, two tests (test-A and test-B) have been carried out for the methane + Luvicap-EG system at similar conditions (~100 bar at 20 °C) with the same procedure for injection of Luvicap-EG as discussed in the previous section. These tests have been carried out to confirm the ability of KHIs (e.g. PVCap) for hydrate dissociation inside the hydrate stability zone, including whether it occurs if KHI is injected after hydrate formation (in the pre-formed hydrate system). Therefore, this was to confirm the process with a KHI that should cause abnormal hydrate dissociation and to give the benchmark case.

To show the ability of Luvicap Bio for hydrate dissociation, the test has been carried out for Luvicap Bio + natural gas system. In addition, to confirm this abnormal hydrate dissociation, SIR tests have been carried out for Luvicap Bio in methane system.

The following sections describe the results of these experiments indicating the ability of KHIs in hydrate dissociation and inhibition of pre-formed hydrates growth.

6.3.1 Luvicap-EG + Methane System

6.3.1.1 Test-A: Inhibition / Dissociation of Pre-formed Hydrates

Figure 6-1 shows pressure-temperature cycles for the methane + Luvicap-EG (PVCap) system inside the thermodynamically stable hydrate region. In this figure, the various CGI regions for the 0.5 mass% PVCap + methane system are also shown, i.e., the boundary lines of 5.2, 7.2, and 9.7 °C subcooling temperatures refer to CIR, SGR, and RGR respectively [6.1].

Firstly, the ability of KHIs in inhibition of pre-formed hydrates systems is discussed. To simulate the pre-formed hydrate system, hydrate should form in the absence of KHIs. Therefore, as shown in Figure 6-1, the system which is free-KHI was cooled down to ~4.5 °C (No. 1). The system was mixed during cooling and was allowed ~24 hrs to form hydrates as much as possible. As can be seen in Figure 6-1, this cooling pathway did not cross the s-II phase boundary of methane which is predicted by HydraFLASH (the

potential formation of s-II methane are discussed in Chapter 3). This strongly suggests that only s-I methane was formed during this cooling.

In the next step (No. 2), the system was fast heated to 11.5 °C to dissociate most of the hydrates but retaining ~6% of water converted to hydrates. At this condition, the system was left for ~24 hrs to reach the equilibrium condition (s-I methane phase boundary).

Following this, the system was cooled down to 9.5 °C (~2 °C subcooling temperature) inside the hydrate stability zone without mixing (the stirrer motor was shut off). This cooling without mixing prevents any hydrate formation inside the hydrate region. Then, the Luvicap-EG was injected into the system based on the procedure described in the previous section. At this point, the stirrer motor was started. As can be seen in Figure 6-1, not only hydrates did not form but also this 6% hydrates completely dissociated even though the dissociation process was very slow (over a 475 hrs period). This confirms that the CIR extent could be applied to the system even though KHI is injected into the system after hydrate formation (pre-formed hydrates in KHI-free system).

Following this complete hydrate dissociation (No. 4), the system was cooled at the rate of 1.0 °C/hr to discover the CGI regions. As shown in Figure 6-1, the hydrates formed beyond the ~9.7 °C subcooling temperature which is the RGR extent for 0.5% PVCap in the methane systems without any hydrate history. This probably suggests that the PVCap not only could dissociate all hydrates inside the thermodynamic hydrate stability zone but also caused removing the hydrate nuclei (hydrate memory/history).

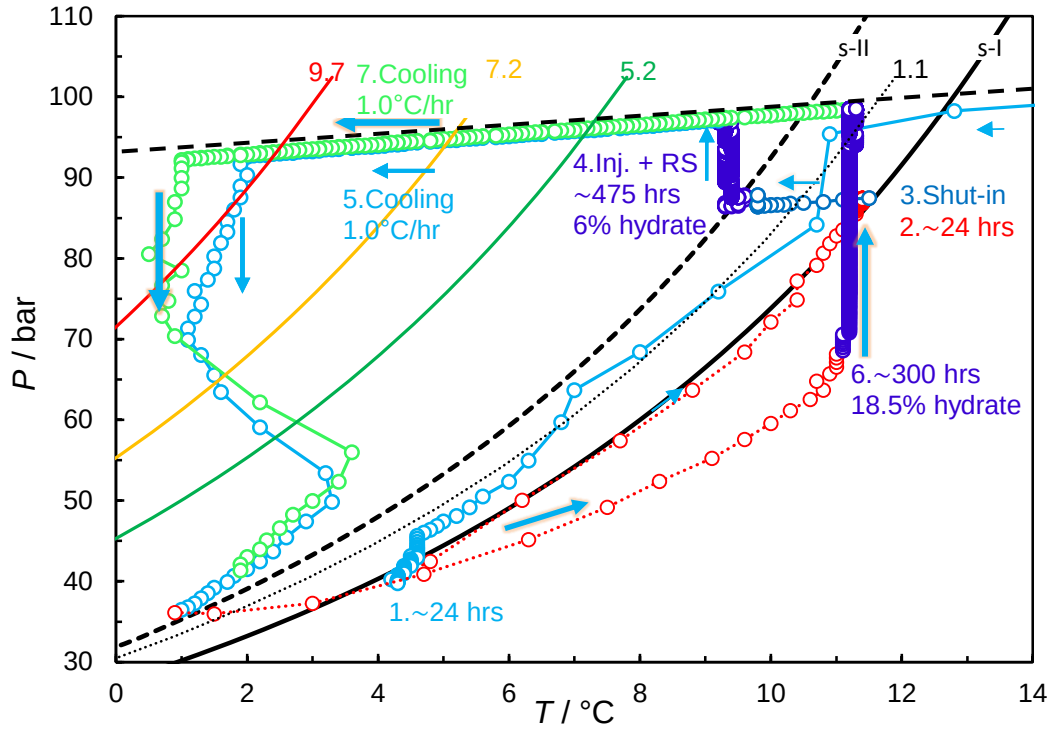

Figure 6-1. Plot of complete PT cycle for post-hydrate formation Luvicap-EG (PVCap) injection Test-A system. See text for description. Inj. = KHI injection condition. RS = Restart. The green line (5.2 °C subcooling) is the standard extent of the CIR for the concentration of KHI injected for methane-water [6.1].

Although hydrate dissociation inside the hydrate region using KHIs was observed before [6.1], the reason for this kind of hydrate dissociation in presence of PVCap in the CIR region (e.g. in step 4) was not fully explained. One of the potential reason could be the recrystallization of hydrate to achieve more stable crystals with a lower surface to volume ratio. For example, if hydrates are formed at a very low temperature (high subcooling) hence high growth rate, it results in creating hydrate crystals with high surface to volume ratio (e.g. dendrites, needles). These hydrates crystals may not be thermodynamically stable and need to recrystallize to the lower surface to volume ratio hydrates. However, the process of recrystallization needs dissociation and re-growth respectively. Therefore, KHIs allow dissociation but prevent formation. Consequently, net dissociation would result. This potential mechanism is shown in Figure 6-2. Nonetheless, this hypothesis can be argued as in this case, the system was left 48 hrs to equilibrate on the hydrate phase boundary before KHI-injection. One of the potential explanation for this argument could be that recrystallization process may be very slow in the absence of KHI and once KHIs are injected into the system, this process could be accelerated. The other potential reason could be disruption of pre-formed hydrates crystals in CIR by KHIs, i.e., KHI polymers bind to hydrate crystals and disrupt them. If it is true, disruption of hydrates crystals could be another mechanism of KHIs.

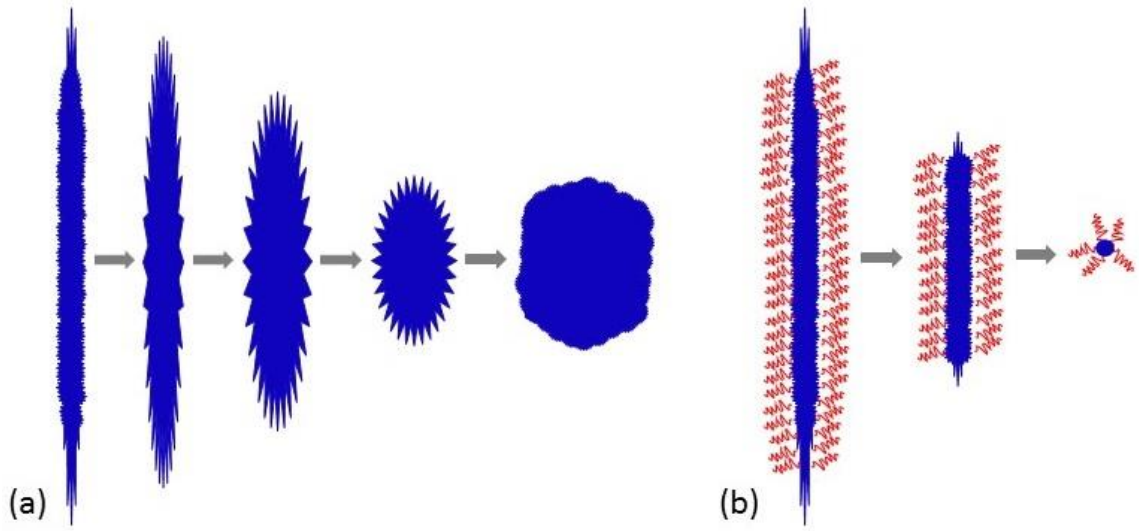

Figure 6-2. Recrystallization of hydrates in a system a) without KHIs, results in to form more stable crystals with a lower surface to volume ratio b) with KHIs, results in hydrate dissociation. Zigzag lines are KHI polymers

Hydrate structure change at different subcooling could be another reason for this behaviour, i.e., different hydrate structures could be formed which are thermodynamically stable at different subcooling temperature as discussed in Chapter 3. Therefore, if one structure e.g. s-II methane is not stable and has to change to another stable structure e.g. s-I, it needs the process of recrystallization (dissociate and then regrowth). As a result, KHIs allow dissociation but prevent formation which leads to net dissociation. In theory, s-II of methane hydrates can be stable at lower temperatures/ higher pressures which other researchers observed [6.6 - 6.9].

Figure 6-3 shows structural transition as one of the potential mechanism of hydrate dissociation. As shown in Figure 6-3, transition from metastable s-II to s-I needs dissociation of hydrate crystals and then reformation, and although dissociation occurs in both cases (a: without KHIs, b: with KHIs), reformation is prevented in the case with KHIs Polymers.

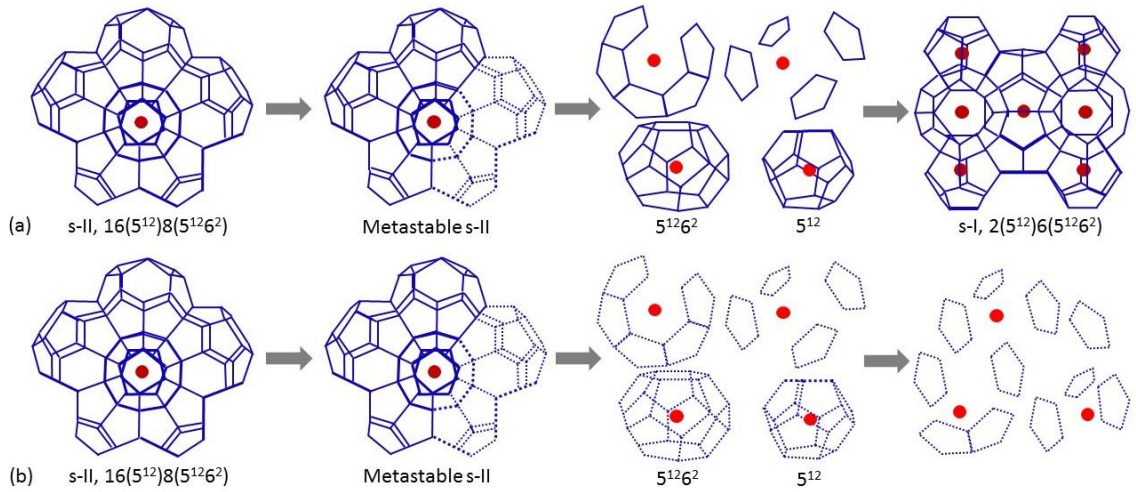

Figure 6-3. Structural transition mechanism of hydrate crystals (e.g. s-II to s-I), a) Without KHIs polymers: metastable s-II melt and $5^{12}6^2$ and 5^{12} cavities formed which result in formation of s-I. b) In the presence of KHI polymers: metastable s-II melt and s-I could not be formed due to KHI polymers. Red circles and zigzag lines are methane and KHI polymers respectively.

6.3.1.2 Test-A: Extent of IDR

Nevertheless, hydrate dissociation in the presence of KHIs could be due to any reasons, and it is important to find the regions where hydrate crystals could be dissociated by Luvicap-EG. Therefore, different cooling/heating steps were carried out for the test-A. Figure 6-4 to Figure 6-7 show all cooling, heating, and constant temperature curves for the test-A system to find the Inhibition-Dissociation Region (IDR). The results strongly suggest that subcooling temperature and amount of hydrates are two factors in determining IDR. For example, although hydrate dissociation stopped at 6.1 °C and 53 bara in step 16 of Figure 6-5, hydrates dissociated at the same temperature but different amount of hydrates in step 18 in Figure 6-6. It indicates the effect of hydrates amount on IDR. However, steps 24 and 25 in Figure 6-7 indicate the effect of subcooling on IDR, i.e., hydrates formed in step 24 but hydrates dissociated in step 25 with the same amount of hydrates but lower subcooling.

Figure 6-8 shows the IDR for the test-A system which is concluded from the different paths carried out for the test-A system. IDR suggests that if the system is anywhere inside this regions, hydrates could be possibly dissociated using KHIs e.g. step 4 in Figure 6-1. On the other hand, if the system is out of IDR, hydrates form with different growth rates, depending on subcooling temperature and pressure.

Although hydrates could dissociate inside IDR, it is notable that, it does not guarantee that hydrate formation path cannot cross the green zone and go through IDR, e.g. hydrate

formation path of step 26 as shown in Figure 6-8. Actually, hydrate formation rate of step 26 was very high (points were recorded every 5 minutes), so hydrates formation continued even inside IDR. It may give a clue that if hydrate formation rate is high, KHI polymers do not have enough time to bind to the hydrate crystals to inhibit further hydrate formation. On the other hand, hydrates formation of step 27 in Figure 6-8 stopped near the boundary of IDR, i.e., hydrate formation rate of step 27 was very low, so KHI polymers could bind to the hydrate crystals, hence hydrate formation stopped after 24 hours. Therefore, hydrate formation rate could affect the ability of KHIs in terms of inhibition, i.e., this would imply that the IDR is not fixed if it is affected by rate which is in turn affected by e.g. mixing. In addition, this IDR only applies to a fixed composition system.

In addition to IDR region, there is another region with a phase boundary of 1.1 °C subcooling temperature from s-I methane phase boundary that hydrate crystals can dissociate very slow inside this region, as shown in Figure 6-8.

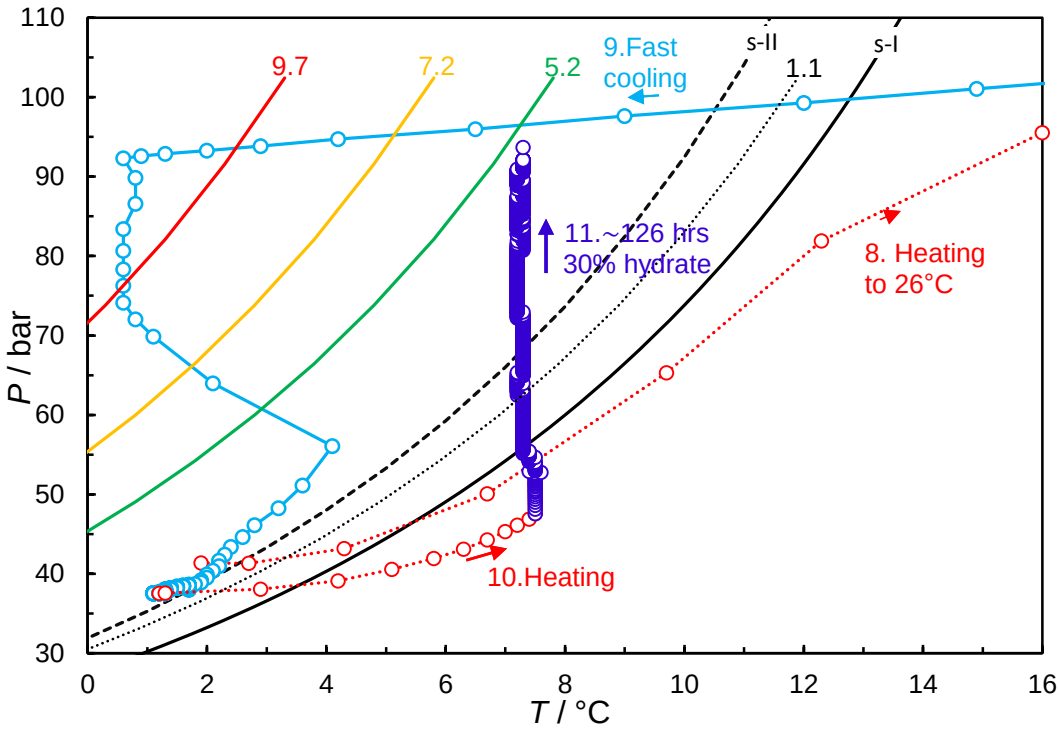

Figure 6-4. Continuation plot of PT cycle for post-hydrate formation Luvicap-EG injection Test-A.

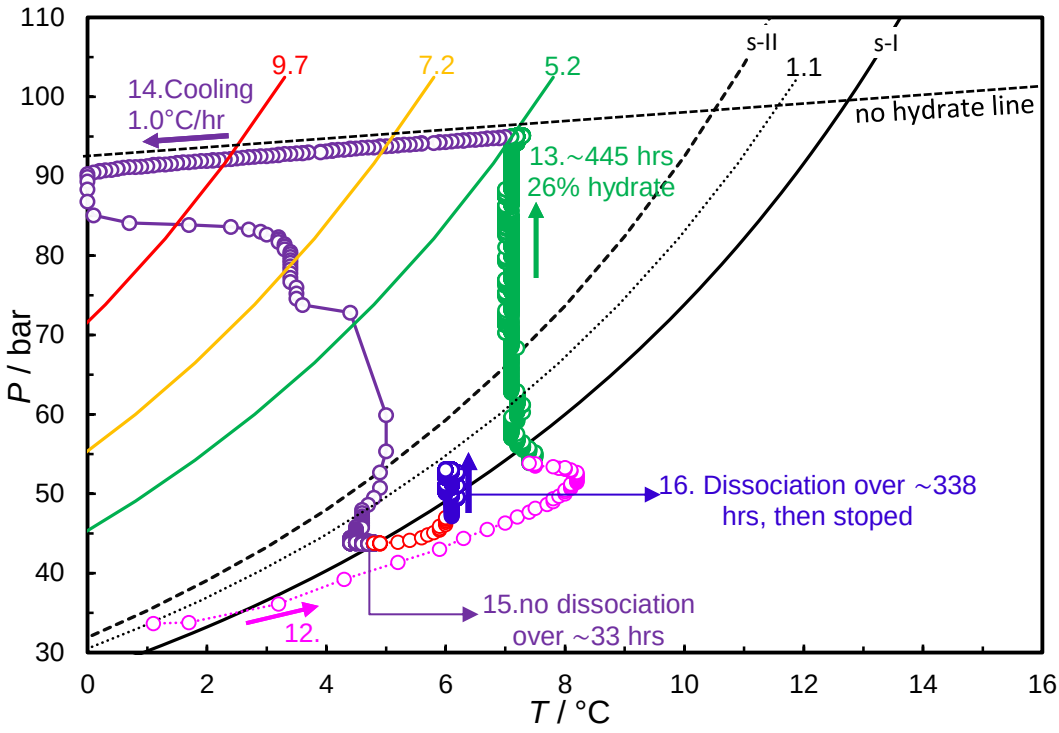

Figure 6-5. Continuation plot of PT cycle for post-hydrate formation Luvicap-EG injection Test-A.

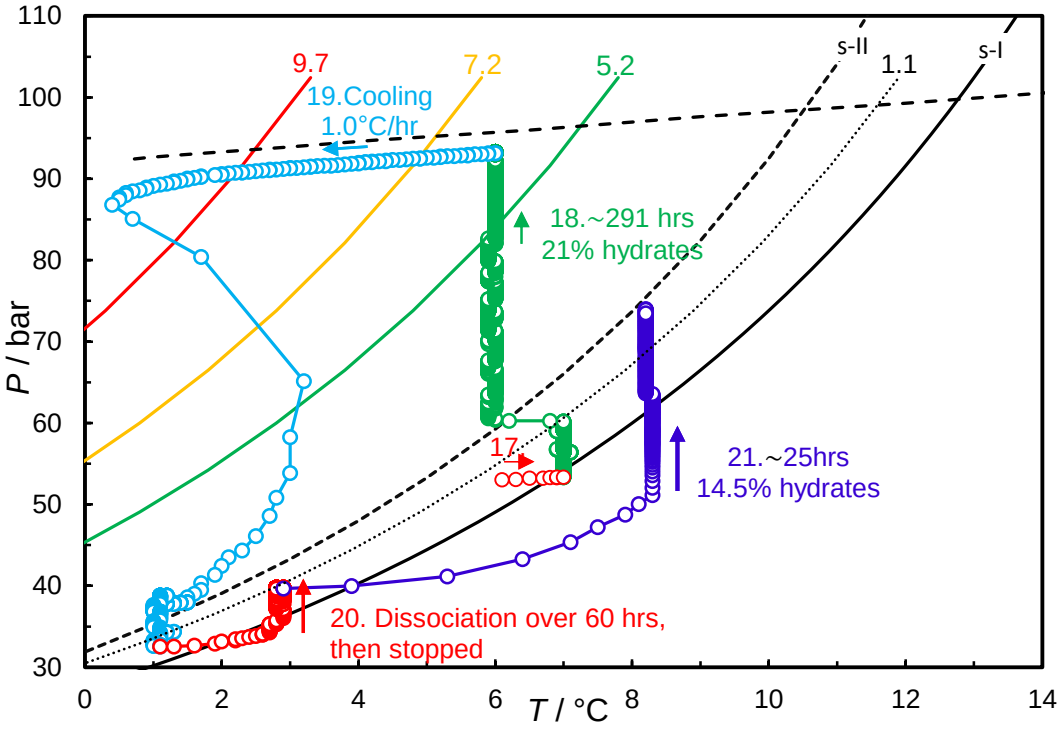

Figure 6-6. Continuation plot of PT cycle for post-hydrate formation Luvicap-EG injection Test-A.

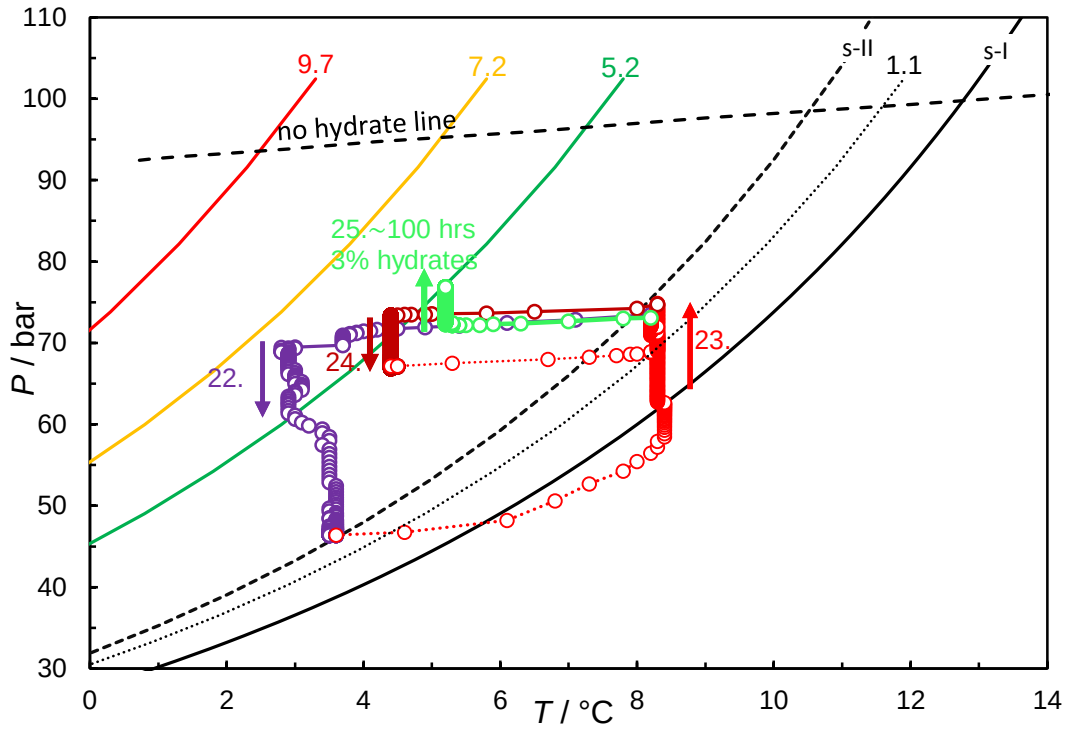

Figure 6-7. Continuation plot of PT cycle for post-hydrate formation Luvicap-EG injection Test-A.

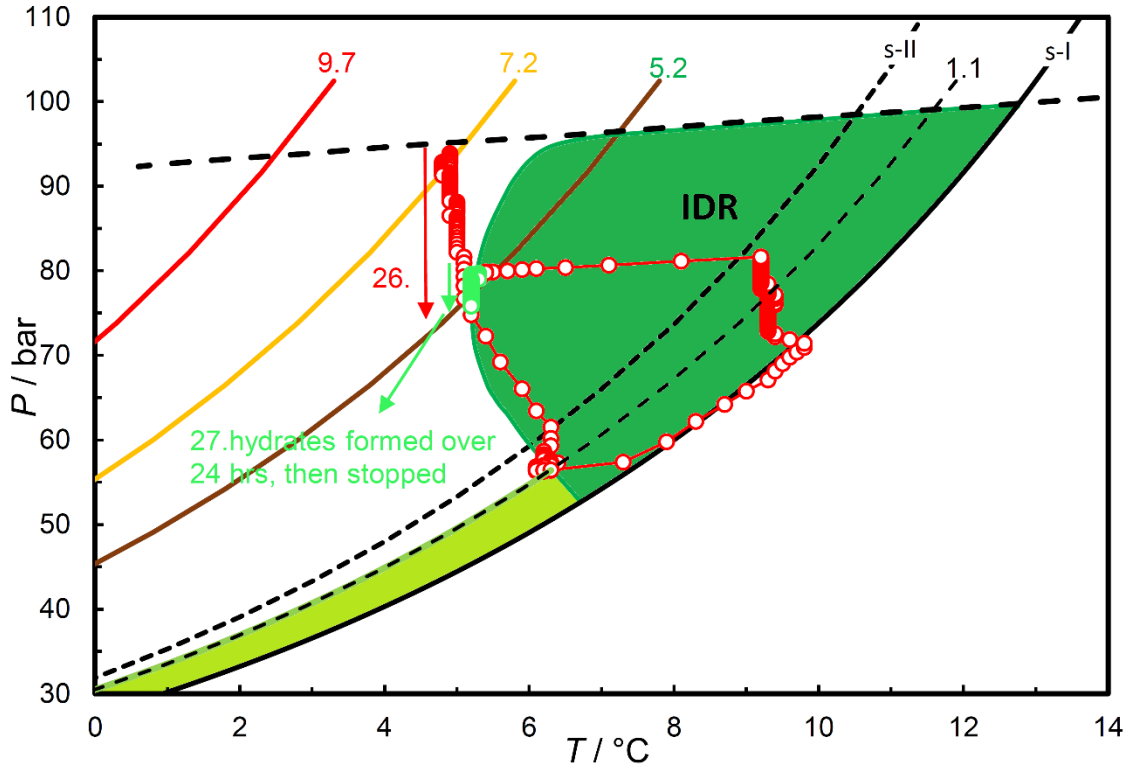

Figure 6-8. Inhibition-Dissociation Region (IDR) for post-hydrate formation Luvicap-EG (PVCap) injection Test-A system.

6.3.1.3 Test-B

Further investigation on this topic has been done in Test-B. The system for Test-B is as same as Test-A (same pressure / temperature condition and water cut) but in a different cell. The main purpose of Test-B is to confirm the repeatability of Test-A. Figure 6-9 shows pressure-temperature plot for the methane system inside the thermodynamically hydrate stability region with identified various CGI regions for the 0.5 mass% PVCap + methane system.

Similar to Test-A, the methane system without KHIs was cooled down to ~ 2.5 °C to form hydrate as much as possible. In the Test-B, as shown in Figure 6-9, the first cooling curve (light blue curve) crossed the hydrate phase boundary of s-II methane as predicted by HydraFLASH, suggesting the possibility of nucleation s-II methane hydrate. The system was left for ~65 hrs and then fast heated to 11.7 °C to dissociate most of the hydrates, but retaining ~6% of water converted to hydrates, similar to Test-A. The system was left at this condition for ~46 hrs (No. 2). The reason for leaving the Test-B system for a longer time at these two conditions (No. 1 and No. 2) compared to Test-A is to allow the system to generate hydrate recrystallization, as discussed in the previous section.

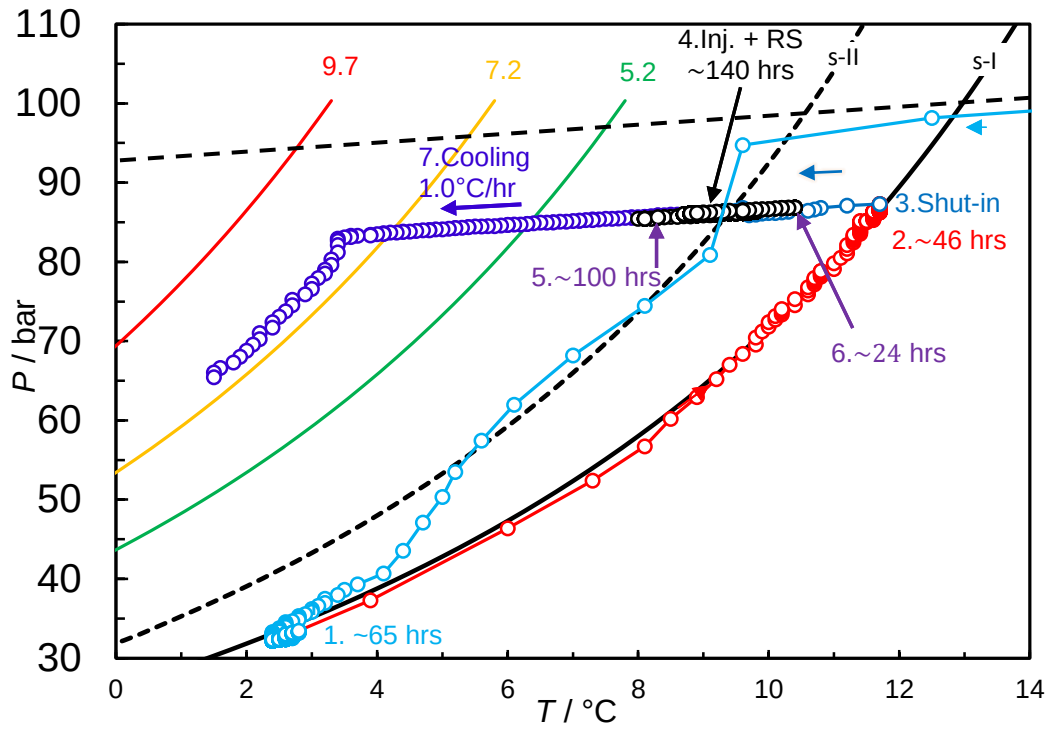

Figure 6-9. Plot of complete PT cycle for the post-hydrate formation Luvicap-EG (PVCap) injection Test-B. See text for description. Inj. = KHI injection condition. RS = Restart. Green line (5.2 °C subcooling) is the standard extent of the CIR for the concentration of KHI injected for methane-water [6.1].

Similar to Test-A, the motor stirrer was shut off (No. 3) and the system was cooled down to 9.5 °C (~2 °C subcooling temperature) inside the hydrate stability zone and then the Luvicap-EG was injected with the similar procedure as discussed. At this point, the stirrer motor was started.

As can be seen in Figure 6-9, the injected Luvicap-EG prevented the hydrate formation confirming CIR conditions. In contrast to Test-A, although the system was left for ~ 140 hrs (No. 4), no hydrate dissociation was observed. As shown in Figure 6-9, the temperature was changed to 8 °C (No. 5) and then 10.5 °C (No. 6) and left for ~ 100 hrs and ~ 24 hrs respectively, to explore the possibility of hydrates formation / dissociation. Despite this, neither hydrate formation nor hydrate dissociation was observed and the fraction of hydrate remained constant.

Similar to Test-A, the Test-B system was cooled at the standard cooling rate of 1.0 °C/hr to investigate the CGI regions (No. 7). The CIR, SGR (M) and RGR extents found for Test-B were exactly as expected for 0.5 % PVCap in methane system indicating the preserving CGI regions for KHIs systems even though KHIs are injected after hydrate formation (pre-formed hydrates system).

Although the reasons for different behaviours seen between Test-A and Test-B in terms of hydrates dissociation inside the hydrate stability zone in the presence of KHIs are not very clear, there are two potential reasons for these different behaviours as discussed in the following.

The first potential reason could be due to recrystallization. As discussed, if the recrystallization is needed to reduce the surface to volume ratio of hydrate crystals, the net dissociation of hydrates would be expected, i.e., recrystallization needs dissociation and then re-growth, meanwhile KHIs allow the dissociation but prevent the formation. As mentioned, Test-B was left for a longer time (over twice) compared to Test-A in steps No.1 and No.2. Therefore, if this abnormal hydrate dissociation is due to recrystallization, it suggests that the recrystallization process in Test-B was completed before Luvicap-EG injection (dissociation was not observed) but was not completed for Test-A (dissociation was observed).

The second potential reason is that more than one hydrate structure could be nucleated and formed in the system (in this case s-I and s-II methane) and these hydrate structures are stable at different conditions. If one structure is metastable at the conditions of KHI injection, this metastable structure should change to a stable structure. This structure change needs dissociation and re-growth. Meanwhile, the KHIs allow dissociation but prevent formation. As a result, the net dissociation of hydrates would be expected. However, if all hydrate structures are stable under the conditions of KHIs injection, the dissociation of hydrates would not be expected even though KHIs prevent growth. If the second reason was the case, it means that when Luvicap-EG was injected all hydrate structures in test-B were stable or could not convert to another structure (but it was not the case for Test-A).

Although the first cooling step in Test-B crossed the s-II methane phase boundary (but did not cross in Test-A), both Test-A and Test-B equilibrated on the s-I phase boundary at the end of the first cooling step. This suggests any s-II methane hydrates initially formed should convert to s-I, i.e., evidence in the literature suggests the conversion of initial formed s-II methane to s-I when the condition is reached to s-I methane phase boundary [6.10] [6.11]. Therefore, it could be concluded that all hydrates in step No. 3 in both Test-A and test-B were s-I methane hydrates, so when Luvicap-EG was injected, all methane hydrates were s-I in both cases. As hydrate dissociation was observed in Test-A, s-II methane should have nucleated when Luvicap-EG was injected in Test-A. In contrast to Test-A, s-II methane should not have nucleated in Test-B. As a result, if s-II methane at Luvicap-EG injection condition is a stable phase, the net dissociation would be expected in Test-A (transition from s-I to s-II is required in Test-A, meanwhile PVCap allows dissociation of s-I but prevents formation of s-II). In contrast in Test-B, because the s-II was not nucleated, the s-I methane hydrate was the only stable phase, and so PVCap could prevent formation not dissociation.

This theory requires that s-II methane hydrate should be a stable phase (not a metastable). However, this work in this section and some evidence as discussed in Chapter 3 show that s-II methane hydrate should be a stable phase at some pressure-temperature conditions.

6.3.2 Hydrate Dissociation Using Luvicap Bio

6.3.2.1 In Natural Gas System

To assess anomalous dissociation of hydrate in the presence of Luvicap Bio, work progressed onto the 0.25 mass% Luvicap Bio in the natural gas system. Figure 6-10 shows experimental cooling / heating curve data for the 0.25 mass% Luvicap Bio aqueous in the natural gas system. To determine the CGI regions (see Section 1.4.4.2), the system was initially cooled down rapidly to form a large fraction of hydrates at high subcooling. Temperature was then increased to outside the hydrate region, allowing some dissociation at a constant temperature. System was subsequently cooled slowly again (1 °C/hour) into the hydrate stability zone, then stepped cooled (1 °C / 24 hours). As shown in Figure 6-10, the CIR extent for this system is 8.5 °C subcooling temperature form s-II phase boundary.

The abnormal hydrate dissociation using Luvicap Bio was investigated at two subcoolings; 3.5 °C and 7 °C. As shown in Figure 6-10, the green data points definitely confirm the ability of Luvicap Bio to induce hydrate dissociation in the CIR. In addition, the results show that hydrate dissociation rate using Luvicap Bio in the CIR decreases as subcooling temperature increases, i.e., while 30 psi (~ 2.1 bar) increased over 121 hours at 3.5 °C subcooling, it took 196 hours to increase 20 psi (~ 1.4 bar) at 7 °C subcooling.

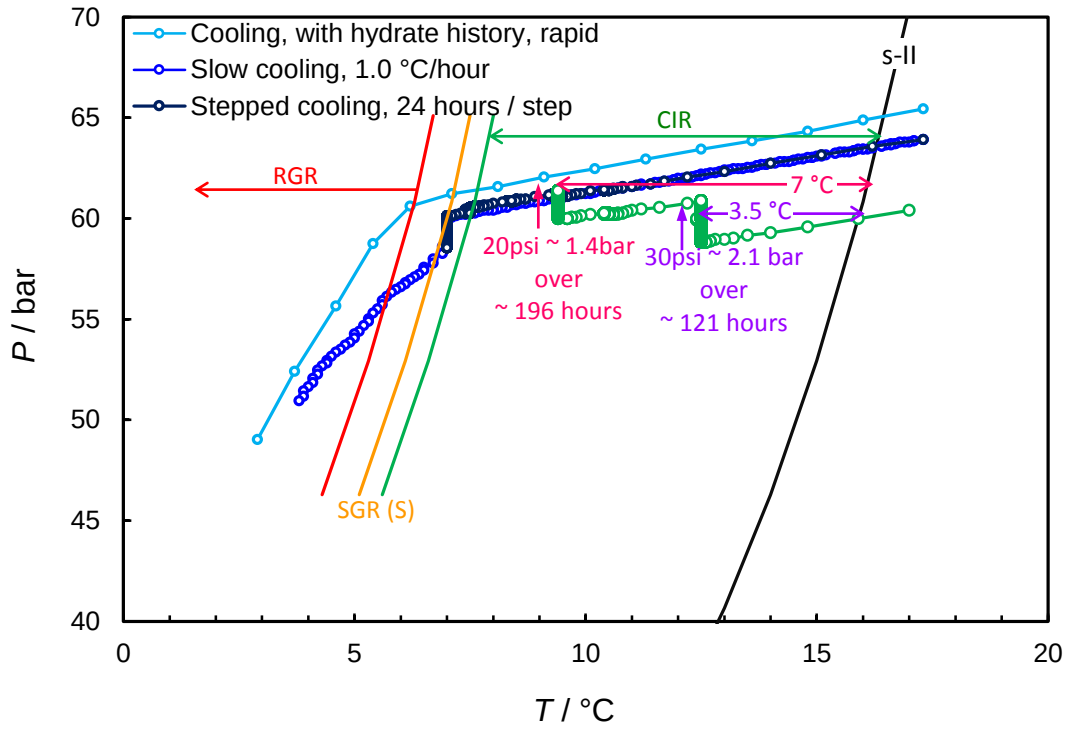

Figure 6-10. PT plot of cooling/heating curve data for the 0.25 mass% Luvicap Bio with natural gas system. The green line (8.5 °C subcooling) is the standard extent of CGI CIR.

6.3.2.2 In Methane system

Another test with the different procedure (SIR run) was carried out in Luvicap Bio + methane system to clarify the behavior of KHIs in terms of hydrate dissociation inside the hydrate stability zone. A number of different tests were carried out to assess the performance of Luvicap Bio, including SIR type test (see Section 3.3.2). When doing SIR type tests for Luvicap Bio in the methane system, a very abnormal and new phenomenon was noticed which was 'Self Induced Dissociation'. This 'Self Induced Dissociation' phenomenon for Luvicap Bio in the methane system is described here.

In this test, 0.5 mass% Luvicap Bio in the aqueous phase was loaded to the methane system at ~100 bara and 20 °C. The system was cooled to a high subcooling temperature to form hydrates and heated up at or close to the phase boundary to dissociate most of the hydrates, but allowing to have a small %hydrate in the system (less than 1%) or have a hydrate memory (seeded system). Then, in contrast to previous tests, Shut-in / Restart (SIR) hydrate growth rate was carried out. Based on the SIR procedure, the stirrer motor was shut off and the seeded system was cooled at a set subcooling temperature; the lack of mixing preventing any measurable hydrate growth during cooling. The mixing was immediately restarted allowing hydrates to form. The SIR run, as shown in Figure 6-11, was carried out for Luvicap Bio + methane system at different temperatures, e.g. 7.5, 5, and 3 °C.

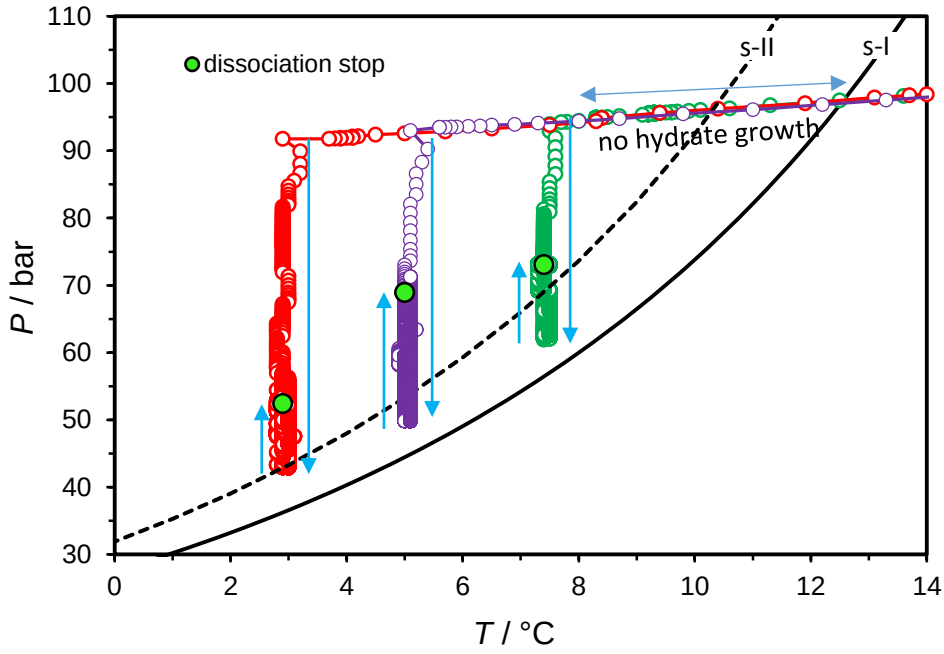

Figure 6-11. PT data for multiple growth rate measurement runs at different subcoolings for the 70:30 water to gas volume ratio, 0.5 mass% Luvicap Bio + methane system. Points are every 5 minutes.

As it was expected, no hydrates formed in the complete inhibition region (CIR) as shown in Figure 6-11, i.e., the CIR extent is 3 °C subcooling temperature for 0.5 mass% Luvicap Bio + methane system. At those subcooling temperatures higher than the CIR extent, hydrate can form at different growth rates. As shown in Figure 6-11, at these three SIR runs, hydrate started to form after restarting the mixing and the system tried to reach the s-I methane phase boundary, i.e., there was no limitation for hydrate formation as there was enough water and no blockage was occurred in the system during the test. Despite this, after a long period of time, hydrate started to dissociate in all three SIR runs. For example, for SIR run at 7.5 °C, hydrate started to dissociate after ~100 hrs. This hydrate dissociation in the presence of Bio KHI inside the hydrate region after a long period of time is abnormal.

In addition, results showed that this kind of hydrate dissociation took a long time indicating a very slow process of hydrate dissociation using Luvicap Bio. Figure 6-12 and Figure 6-13 show the plot of pressure and temperature as a function of time for SIR runs initiated at 7.5 and 3 °C respectively. As shown in Figure 6-12, hydrate formation stopped after 75 hours and stabilized for 25 hours, i.e., at this condition 9% water was converted to hydrates. It seems that during this 25 hours, Luvicap Bio managed to come close to hydrate/water interface or even to connect the hydrate cavities. After this period, hydrates suddenly started to dissociate which is very abnormal, i.e., this is very abnormal because while nothing has changed, hydrate grew and then dissociated itself. During 350 hours, 4% hydrate dissociated which would constitute 45% hydrate reduction in the system. Finally, the system pressure was approximately constant with little a bit oscillation in pressure, showing a very little hydrate dissociation and reformation in the system.

This hydrate dissociation and reformation in the presence of KHIs is more obvious at 3 °C. As shown in Figure 6-13, increasing/decreasing of pressure at a constant temperature indicates hydrate formation/dissociation suggesting KHIs polymers sometimes could overcome to the hydrate cavities and dissociate them and sometimes fail to inhibit hydrate formation. Although this behaviour of KHIs is unclear and needs more investigation, some potential reasons and explanation can describe this abnormal hydrate dissociation and reformation. In the following, it is described the potential reasons for this behaviour.

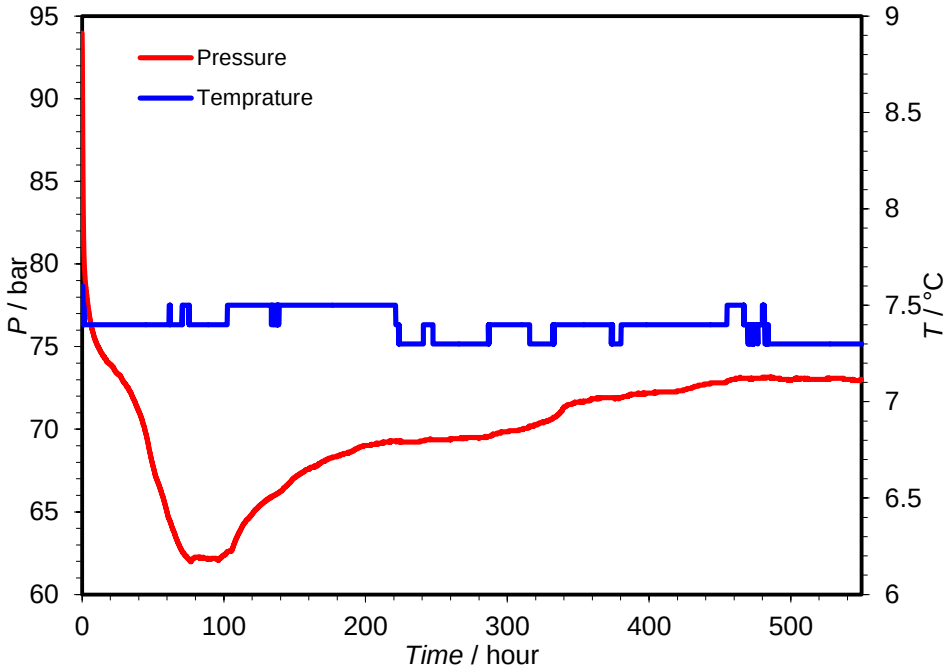

Figure 6-12. Plot of pressure and temperature versus time for 0.5 mass Luvicap Bio + methane run initiated at 7.5 °C subcooling.

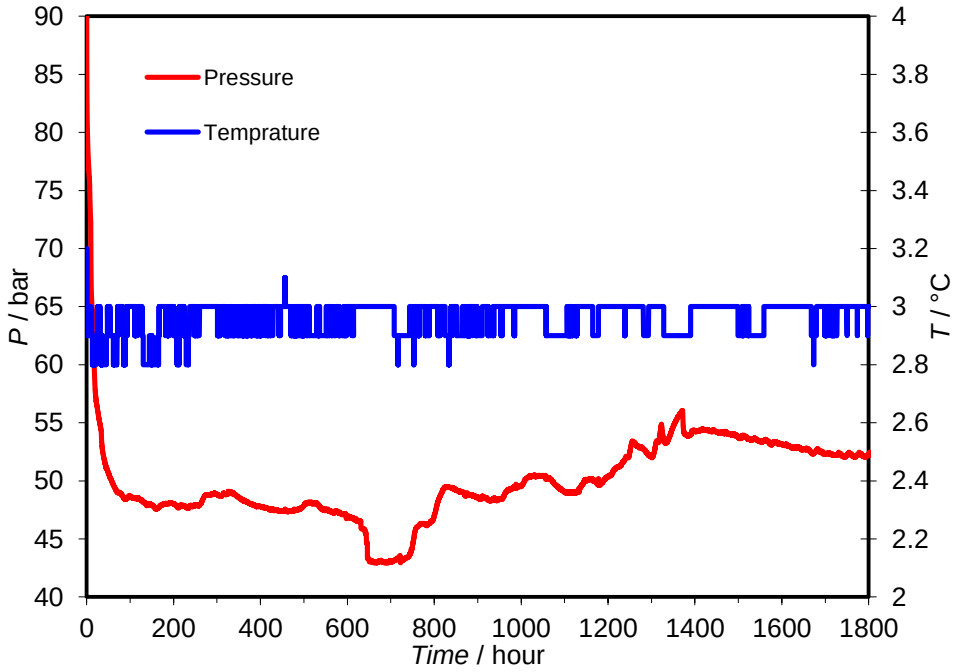

Figure 6-13. Plot of pressure and temperature versus time for 0.5 mass Luvicap Bio + methane run initiated at 3.0 °C subcooling.

As discussed, the formation of s-II methane can be a potential reason for hydrate dissociation using KHIs. In this experiment, if s-II methane hydrate was formed as a stable phase and became unstable at lower pressure (as pressure decreased due to hydrate formation), s-II methane hydrate should have dissociated and converted to s-I. KHI polymers allow dissociation of s-II methane but prevent formation of s-I methane and this would result in hydrate dissociation and pressure increase in the system. Therefore, different hydrate structures formation and their stability/instability at different pressure/temperature condition in the system with KHIs can result in hydrate dissociation inside hydrate stability region.

The coexisting of s-I and s-II methane hydrates at conditions of 30 to 90 bar and 1.5 to 12 °C is reported by Schicks and Ripmeester (2004) [6.10]. However, they emphasized that the s-II methane hydrates were metastable and finally converted to s-I (the condition for this transition is not mentioned in this work). Nevertheless, there was a potential for formation of s-II methane hydrate at the initial pressure drop of SIR run which could be even more stable than s-I. At the same time, the system could have s-I methane hydrates which formed initially and continued to grow. As pressure reduced due to hydrate formation, the system exited the s-II methane hydrate stable region. Therefore, although s-II hydrate formation stopped, s-I continued to grow and the system entered into the s-I stable region. Consequently, s-I became more stable than s-II and s-II tended to transition to s-I (needs dissociation and then re-growth). In addition, because the subcooling temperature reduced due to pressure drop, KHI could inhibit further hydrate formation. As a result, KHIs prevented s-I formation but allowed dissociation of s-II methane, resulted in net dissociation. This dissociation should have continued to reach to either phase boundary of the stable region of s-II or end of the CIR or IDR region as discussed before.

Kvamme et al. showed using molecular dynamic simulations that kinetic hydrate inhibitors like PVCap could dissociate hydrates [6.12]. They indicated the hydrate dissociation and reformation in the presence of KHIs. They showed that the PVCap monomer could make a hydrogen bond with the hydrate at the water-hydrate interface and dissociate the hydrate in two steps; slow dissociation of half cages and then rapid dissolution of the other side of hydrate crystal. Therefore, the finding of molecular dynamic simulation and the results of this experimental work strongly suggest the ability of KHIs monomer in hydrate dissociation and destruction of hydrate cavities.

Another point is that, as more hydrate cavities are dissociated by KHIs, more gas is released which results in increasing methane content in the aqueous phase and eventually forming a methane bubble. This methane bubble is attractive for surfactant such as PVP [6.12]. This can result in withdrawal of KHIs polymer and reduce the free KHI monomer dosage. Consequently, this reduction of available KHI monomers can cause the system to fail in terms of hydrate formation inhibition. Therefore, as shown in Figure 6-13, reformation of hydrate at some conditions could be due to limited access to free KHI monomers.

6.4 Summary

The results of this work, investigating the ability of KHIs (Luvicap-EG) to inhibit hydrates pre-formed in uninhibited systems and ability of KHIs (Luvicap-EG and Luvicap Bio) to dissociate hydrates, show that:

- PVCap (Luvicap-EG) can apparently inhibit hydrates pre-formed in KHI-free systems, the CIR is preserved even though PVCap is injected into the system with pre-formed hydrates

- The injection of PVCap (Luvicap-EG) caused either complete growth inhibition or hydrate dissociation in CIR region

- Luvicap Bio caused hydrate dissociation or hydrate 'Self Induced Dissociation' in methane system during SIR runs

- One of the reasons for the behavior seen for Luvicap-EG and Luvicap Bio in terms of hydrate dissociation can be speculated as formation of s-I and s-II hydrates, with one of these being metastable under some conditions. If the hydrate phase in the system is unstable in some conditions and have to transit to the more stable hydrate structure, it needs melting and then re-growth. Meanwhile, KHIs allow dissociation but prevent formation, results in net dissociation

- The other potential reason for hydrate dissociation in the presence of KHI polymers is recrystallization to achieve more stable crystals with a lower surface to volume ratio

- As discussed KHIs monomers can bind to hydrate crystals by hydrogen bonding and destruct the hydrates cavities. Nevertheless, the stability and meta-stability of hydrates structures (e.g. s-I and s-II of methane hydrates) can affect the ability of KHIs in destruction of hydrates cavities and hydrate dissociation

- In addition, there is a region called Inhibition-Dissociation Region (IDR) which induced by KHIs. In this region, KHIs could prevent hydrate formation or even dissociate hydrates

- The subcooling temperature/pressure (may suggest which hydrate structure is stable) and amount of hydrates (may suggest the availability of free-KHI) are the factors which affect in locating the Inhibition-Dissociation Region (IDR)

- Hydrate formation rate is another factor which affects the KHIs performance, i.e., if hydrate growth rate is high, then a KHI with less ability would be expected as it doesn't have enough time to bind to hydrate crystals to inhibit further growth, and vice versa, a KHI with strong ability would be expected if hydrate growth rate is low

For application in the field and in oil and gas production pipeline, the findings are very significant with respect to the traditional use of KHIs for hydrate prevention. The results of this chapter imply that if hydrates are formed before KHIs injection (pre-formed hydrates), KHIs can be used in the pipeline. In addition, it offers novel possibilities for plug removal using KHIs. Similarly, biodegradable polymer injection might present a means to induce the dissociation of naturally occurring gas hydrate in sediments for the purposes of methane gas production.

6.5 Reference

[1] R. Anderson, H. Mozaffar, and B. Tohidi, "Development of a crystal growth inhibition based method for the evaluation of kinetic hydrate inhibitors," in *Proceedings of the 7th International Conference on Gas Hydrates*, 2011, pp. 17–21.

[2] Anderson, B.J., Tester, J.W., Borghi, G.P. and Trout, B.L., 2005. Properties of inhibitors of methane hydrate formation via molecular dynamics simulations. Journal of the American Chemical Society, 127(50), pp.17852-17862.

[3] Yang, J. and Tohidi, B., 2011. Characterization of inhibition mechanisms of kinetic hydrate inhibitors using ultrasonic test technique. Chemical engineering science, 66(3), pp.278-283.

[4] Hutter, J.L., King, H.E. and Lin, M.Y., 2000. Polymeric hydrate− inhibitor adsorption measured by neutron scattering. Macromolecules, 33(7), pp.2670-2679.

[5] Storr, M.T., Taylor, P.C., Monfort, J.P. and Rodger, P.M., 2004. Kinetic inhibitor of hydrate crystallization. Journal of the American Chemical Society, 126(5), pp.1569-1576.

[6] I.-M. Chou, A. Sharma, R. C. Burruss, J. Shu, H. Mao, R. J. Hemley, A. F. Goncharov, L. A. Stern, and S. H. Kirby, "Transformations in methane hydrates," *Proc. Natl. Acad. Sci.*, vol. 97, no. 25, pp. 13484–13487, 2000.

[7] H. Shimizu, T. Kumazaki, T. Kume, and S. Sasaki, "In situ observations of high-pressure phase transformations in a synthetic methane hydrate," *J. Phys. Chem. B*, vol. 106, no. 1, pp. 30–33, 2002.

[8] H. Hirai, T. Kondo, M. Hasegawa, T. Yagi, Y. Yamamoto, T. Komai, K. Nagashima, M. Sakashita, H. Fujihisa, and K. Aoki, "Methane hydrate behavior under high pressure," *J. Phys. Chem. B*, vol. 104, no. 7, pp. 1429–1433, 2000.

[9] J. S. Loveday, R. J. Nelmes, M. Guthrie, S. A. Belmonte, D. R. Allan, D. D. Klug, J. S. Tse, and Y. P. Handa, "Stable methane hydrate above 2 GPa and the source of Titan's atmospheric methane," *Nature*, vol. 410, no. 6829, pp. 661–663, 2001.

[10] Schicks, J.M. and Ripmeester, J.A., 2004. The coexistence of two different methane hydrate phases under moderate pressure and temperature conditions: Kinetic versus thermodynamic products. Angewandte Chemie International Edition, 43(25), pp.3310-3313.

[11] Staykova, D.K., Kuhs, W.F., Salamatin, A.N. and Hansen, T., 2003. Formation of porous gas hydrates from ice powders: Diffraction experiments and multistage model. The Journal of Physical Chemistry B, 107(37), pp.10299-10311.

[12] B. Kvamme, T. Kuznetsova, and K. Aasoldsen, "Molecular dynamics simulations for selection of kinetic hydrate inhibitors," *J. Mol. Graph. Model.*, vol. 23, no. 6, pp. 524–536, 2005.

Chapter 7– Conclusion and Recommendations

7.1 Conclusions

The main objective of this thesis is to study inhibition and dissociation of gas hydrate using biodegradable kinetic hydrate inhibitors and their potential combination with thermodynamic hydrate inhibitors. In addition to this main objective, some works have been carried out including investigation of hydrate growth rate/structure pattern and its effect on inhibition/dissociation of gas hydrates.

In Chapter 2, the performance of three green KHIs which have been reported / are produced (Luvicap Bio, ECO-530, and pectin) was evaluated experimentally using CGI method. As a result, Luvicap Bio shows strong Bio KHI properties, so Luvicap Bio was selected for further investigation for KHI in this thesis. In addition, the well-known PVCap was also investigated as a reference / benchmark.

In Chapter 3, the effect of hydrate fraction tolerance on Luvicap Bio and PVCap in the methane systems was investigated. In was concluded that as the hydrate fraction increases, inhibition performance reduces for both Luvicap Bio and PVCap, as typified by a reduction in the crucial CIR (complete inhibition region). In addition, it was observed a weak inhibition region (SGR) before the 'Semi' CIR at higher subcooling for Luvicap Bio + methane system; it is a very unusual phenomenon for KHIs. It can probably only be explained by structural changes. It was concluded that Luvicap Bio is a better inhibitor for s-I hydrate than for s-II. In contrast to Luvicap Bio, PVCap is a better s-II hydrate inhibitor. Furthermore, the CGI test on combined 0.25% Luvicap Bio + 0.25% PVCap with both methane and natural gas shows significant improvement of hydrate inhibition region compared to these polymers alone, suggesting the synergism effect of Luvicap Bio and PVCap; Luvicap Bio is better for s-I and PVCap is better for s-II. Further work associated with structure effects inhibition studies have been carried out to investigate hydrate growth rate regions/patterns and hydrate structure in the simple gas and multicomponent gas systems. The results for simple methane and ethane systems show clear and distinct changes in hydrate growth rates which probably correspond to the new hydrate phase/structure, e.g. formation of s-II hydrate in the simple methane or ethane systems. Moreover, exothermic heat release rates in the methane system support the theory of formation both s-I and s-II methane hydrate. In contrast to the methane and ethane system, the clear change in hydrate growth rate or exothermic heat release rate was not observed in simple propane system which can form only s-II due to its large molecular diameter. In addition, equilibrium step heating/cooling measurements in the

multi-component gas systems ($C_1 + C_3$ and $C_1 + C_2 + C_3$) suggest the formation of multiple hydrate structures e.g. C_3 s-II, C_2 s-II, C_2 s-I, and C_1 s-I. These various hydrate structures with a sequential formation can be formed in order of decreasing stability (C_3 s-II → C_2 s-II → C_2 s-I → C_1 s-I).

In Chapter 4, to see if Luvicap Bio could be used to reduce or eliminate THIs (particularly methanol), the performance of combined Luvicap Bio / THIs was evaluated using the CGI method in terms of hydrate inhibition in the natural gas systems. Methanol, ethanol, and MEG which are most commonly THIs used for hydrate inhibition were used to evaluate whether these THIs are top-up inhibitors for Luvicap Bio. Results for 0.5 mass% Luvicap Bio with methanol show that methanol acts as a top-up inhibitor for Luvicap Bio which is in contrast to the PVCap and what is generally seen for KHIs, which is unusual and important. Only at higher methanol concentrations, notably for 50 mass%, a significant reduction in CIR extent was observed. At a higher Luvicap Bio concentration, 1.0 mass%, results show better inhibition in the system with methanol compared to the 0.5 mass% Luvicap Bio, although this was overall fairly marginal. Generally, for both polymer doses, there is an increasingly negative effect of methanol at higher concentrations and pressures, making top-up not fully additive. Results for ethanol + Luvicap Bio (0.5 mass%) in the natural gas system show that there is a degree of negative effect of ethanol on Luvicap Bio, but it does act reasonably well as a top-up inhibitor for Luvicap Bio. Further investigation on 0.5 and 1.0 mass% Luvicap Bio with 5 to 30 mass% MEG in the natural gas systems show that MEG not only does act as a full top-up inhibitor for Luvicap Bio but also has a positive, synergistic effect, modestly extending CGI regions, including the CIR, which is the same as for other KHIs in general. As an important conclusion, these results strongly suggest that Bio KHIs can be used to reduce or eliminate THI use in production operations, offering cost savings, logistical benefits, and environmental benefits.

The industry opinion is that even if KHIs are used for prevention, they cannot be used for remediation for e.g. cold restart. To address this industry opinion, in Chapter 5, works were carried out to investigate hydrate blockage removal using MEG or methanol in the vertical pipes. The results show that density was the key factor in hydrate blockage removal, so further works have been carried out to assess the effect of THI density on hydrate blockage removal in the vertical pipes and whether methanol/MEG mixture has advantages over methanol or MEG alone. The results indicate the advantages of

methanol/MEG mixture with a density of 1 g/cc over methanol and MEG alone, i.e., hydrate dissociation rate of this case is higher than the case of methanol or MEG injection alone. In addition, results showed that chemical injection into the blocked vertical pipes could change the location of the hydrate blockage. This relocation of hydrate blockage could be due to the hydrate reformation as a result of water generated from hydrate dissociation. Another reason for this relocation of hydrate blockage could be due to those hydrates which were detached from the hydrate plug so that could move up and block the system. In addition, the endothermic nature of hydrate dissociation resulted in sub-zero temperatures. Finally, results point out that density of inhibitor plays an important role in the effectiveness of hydrate blockage removal and the amount of THI required for hydrate blockage removal is more than what is calculated by thermodynamic modeling due to non-homogeneous nature of the system.

In Chapter 6, the novel possibility of using KHIs, including Bio KHIs, to dissociate hydrates inside the hydrate thermodynamically stability region was investigated; something which would never have been considered possible before. It was found that both PVCap (Luvicap EG, PVCap in mono-ethylene glycol) and Luvicap Bio not only can prevent hydrate nucleation/growth inside the hydrate stability zone in the methane system but also induce abnormal hydrate dissociation inside hydrate stability region in both methane and natural gas systems. Two recrystallization processes are suggested as being the potential reason of the hydrate dissociation inside hydrate stability region: (1) reformation/recrystallization to achieve more stable crystals with a lower surface to volume ratio, i.e., to reduce surface to volume ratios of needle-like / dendritic crystals formed initially and (2) the transition of metastable hydrate structures (e.g. s-II) to another stable hydrate structures (e.g. s-I). In both cases, KHIs allow dissociation but prevent formation, results in net dissociation. Results for Luvicap EG + methane indicate that there is a region called Inhibition-Dissociation Region (IDR) which induced by KHIs. In this region, KHIs could prevent hydrate formation or even dissociate hydrates. As discussed, while KHIs are usually used for inhibition of hydrate nucleation and hydrate growth, there are a number of situations where hydrates can form from produced waters which are KHI-free. The results for Luvicap EG showed that it can apparently inhibit hydrates pre-formed in KHI-free systems, the CIR is preserved even though Luvicap EG is injected into the system with pre-formed hydrates.

From the results of this thesis, it can be concluded that there is a quite good Bio KHI, Luvicap Bio, and it can be used to reduce or remove the need for THIs. In addition, while THIs are still the normal and most promising option for remediation, KHIs, Bio induced, could present a new and novel option for hydrate plug remediation or even for gas production from naturally occurring hydrates in oceanic/permafrost sediments here.

7.2 Recommendations and Future Works

With respect to hydrate prevention, although Luvicap Bio does seem to offer top-up green inhibitor for THIs (methanol, MEG, and ethanol), some other topics could be investigated including effect of salt with/without THIs on Luvicap Bio performance, effect of condensate / liquid hydrocarbons on Luvicap Bio performance, and effect of acid gases e.g. H_2S and CO_2 on Luvicap Bio performance. In addition, the performance of Luvicap Bio in a richer natural gas (a richer s-II forming gas) can be investigated, i.e., in this work, Luvicap Bio is understood as a better inhibitor for s-I hydrates, so its performance could be restricted to the lean natural gas.

As discussed, as the hydrate fraction increases, the CIR subcooling extent decreases for both Luvicap Bio and PVCap, so it is proposed to determine polymer-hydrate stoichiometry for these KHIs. In addition, although it is understood that Luvicap Bio is a better inhibitor for s-I than for s-II and PVCap is a better s-II hydrate inhibitor, it is recommended to do further detailed tests for clarifying the effectiveness of PVCap and Luvicap Bio in s-I vs s-II hydrates systems. In addition, the results and evidence suggest the multiple hydrate structures formation in the multi-component natural gas systems or even in the simple methane and ethane system. So, in order to confirm the formation of various hydrate structures, it is recommended to analyze the gas composition of the system in different steps of hydrate formation in SIR runs using a capillary sampler.

In addition, with respect to plug remediation, works carried out for hydrate dissociation using THIs in the vertical pipes show that the density of THIs plays an important role in the effectiveness of hydrate blockage removal. With respect to future work, it is proposed to investigate and find an optimum density for THIs injection into the vertical pipe in order to hydrate blockage removal. Moreover, it is proposed to use and investigate the effectiveness of combined THIs and KHIs in removing/remediation of hydrate blockage.

With respect to Bio KHI-induced dissociation of gas hydrate, the results show that KHIs can offer a novel possible method for plug removal, so it is proposed to do research and investigate about the effectiveness of KHIs (or combined KHIs + THIs) in hydrate plug removal. Likewise, biodegradable polymer injection (e.g. Luvicap Bio) might present a means to induce the dissociation of naturally occurring gas hydrate in sediments for the purposes of methane gas production. So, it is highly recommended to do experiments to induce hydrate dissociation using KHIs in sediments.

Appendix A: PT plot for measurement of CGI regions of Luvicap Bio + THI + NG systems

Chapter 4, as discussed, reports the effect of methanol, ethanol, and MEG on Luvicap Bio (biodegradable polymer) in the natural gas system. To investigate this, the crystal growth inhibition method (CGI) (see Section 1.4.4.2) was used and then the experimental CGI region data points for various systems (as listed in table 1) are reported. These CGI region data point which reported in Chapter 5 are determined based on cooling curves with different cooling rate e.g. 1 °C / 1 hour or 1 °C / 24 hours.

In this section, pressure / temperature plots showing measured experimental points delineating the various crystal growth inhibition regions for all systems are reported. The summary of these systems with the range of pressure tested for each system are listed in Table A-1. In the following all plots are reported.

However, PT plot showing measured experimental points delineating the various crystal growth inhibition regions for 0.5 and 1.0 mass% Luvicap alone with natural gas are reported in Section A.6.

Table A-1. Summary of all systems used to study the performance of Luvicap Bio in the presence of thermodynamic hydrate inhibitors in the natural gas system using the CGI method. For example, the green highlighted cell indicates the system which consists of 30 mass% methanol + 0.5 mass% Luvicap Bio + natural gas and the CGI regions were measured for this system up to 280 bara. The composition of natural gas system is given in Table 4-1.

THI \ **KHI** Concentration mass%		0.5 mass% Luvicap Bio	1.0 mass% Luvicap Bio
MeOH	5	< 135 bara	< 150 bara
	10	< 135 bara	< 150 bara
	20	< 125 bara	< 150 bara
	30	< 280 bara	< 290 bara
	50	< 320 bara	-
EtOH	5	< 160 bara	-
	10	< 170 bara	
	20	< 310 bara	
	30	< 160 bara	
MEG	5	< 150 bara	< 150 bara
	10	< 150 bara	< 150 bara
	20	< 150 bara	< 150 bara
	30	< 150 bara	< 150 bara

A.1 0.5 Mass% Luvicap Bio with Methanol in a Natural Gas System

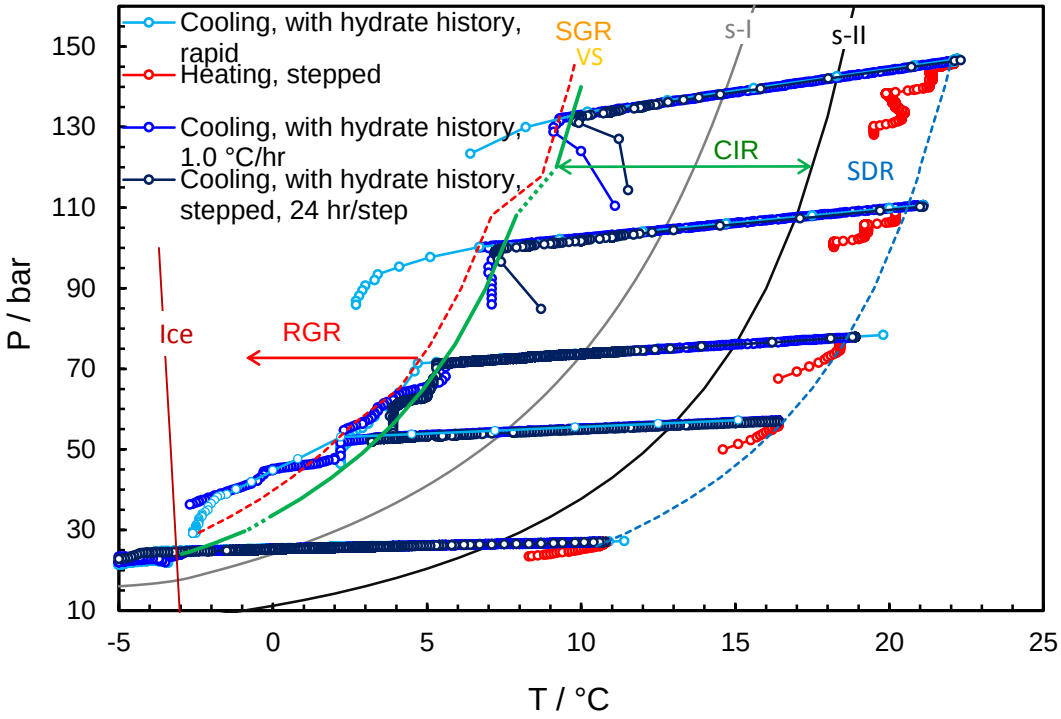

Figure A-1. PT plot showing measured experimental points delineating the various crystal growth inhibition regions for 0.5 mass% Luvicap Bio / 5 mass% methanol aqueous with natural gas.

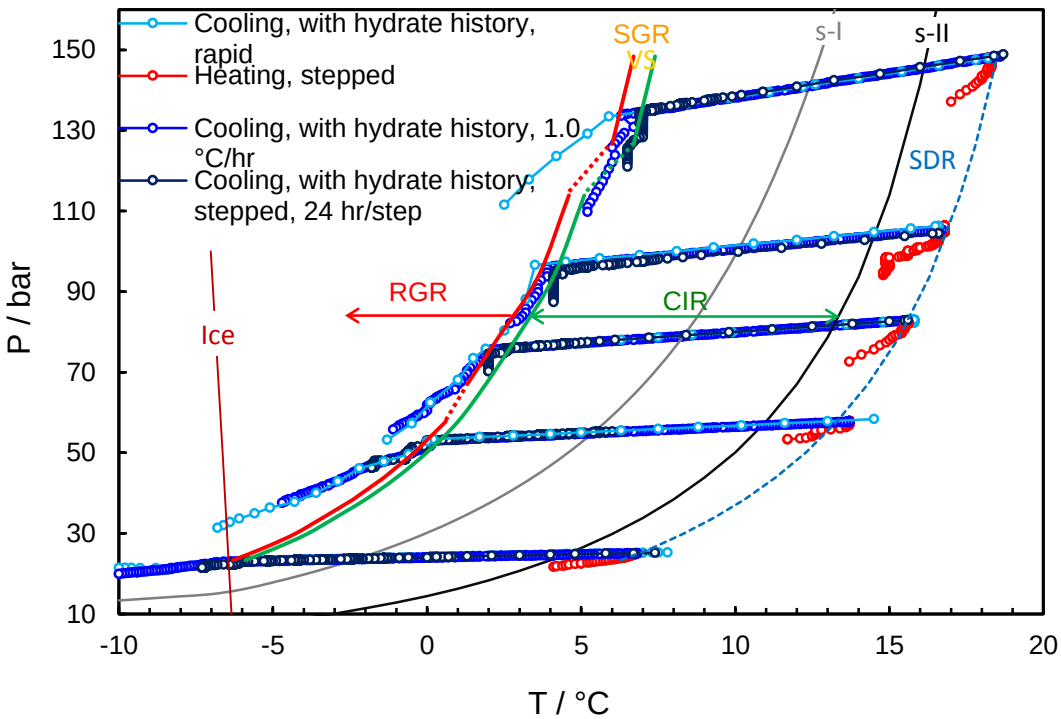

Figure A-2. PT plot showing measured experimental points delineating the various crystal growth inhibition regions for 0.5 mass% Luvicap Bio / 10 mass% methanol aqueous with natural gas.

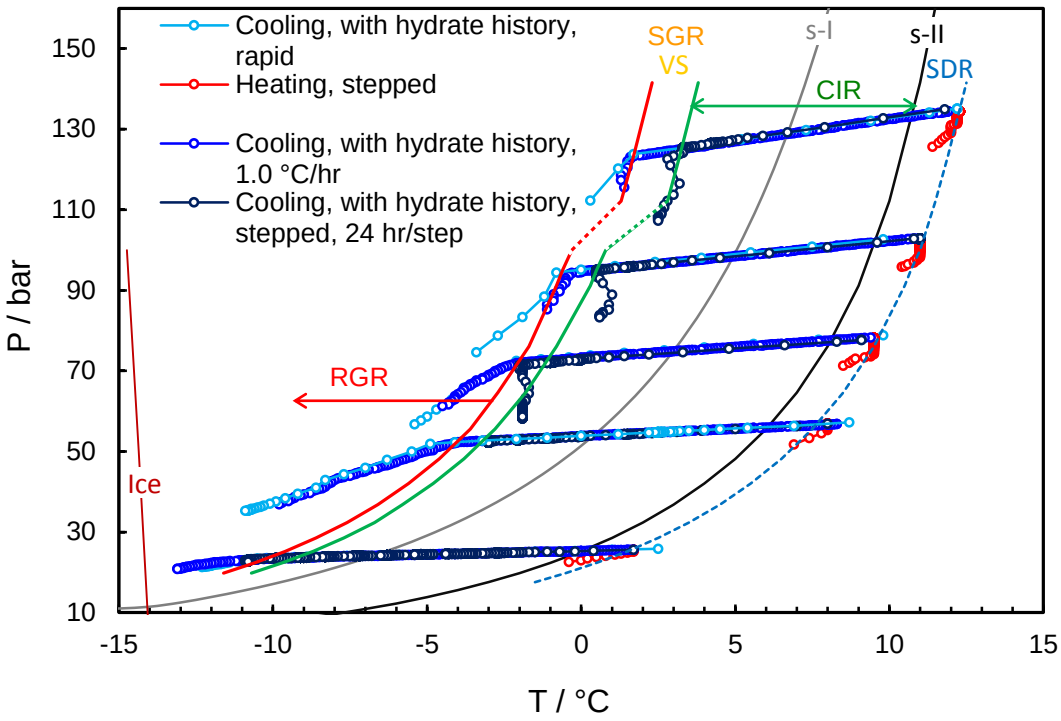

Figure A-3. PT plot showing measured experimental points delineating the various crystal growth inhibition regions for 0.5 mass% Luvicap Bio / 20 mass% methanol aqueous with natural gas.

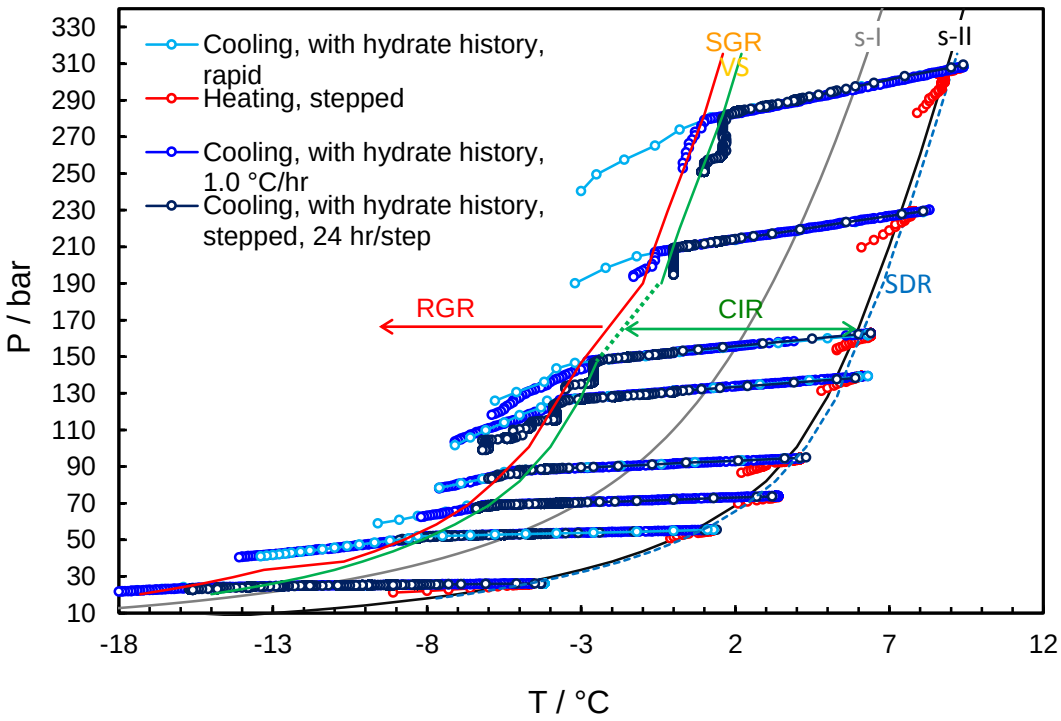

Figure A-4. PT plot showing measured experimental points delineating the various crystal growth inhibition regions for 0.5 mass% Luvicap Bio / 30 mass% methanol aqueous with natural gas.

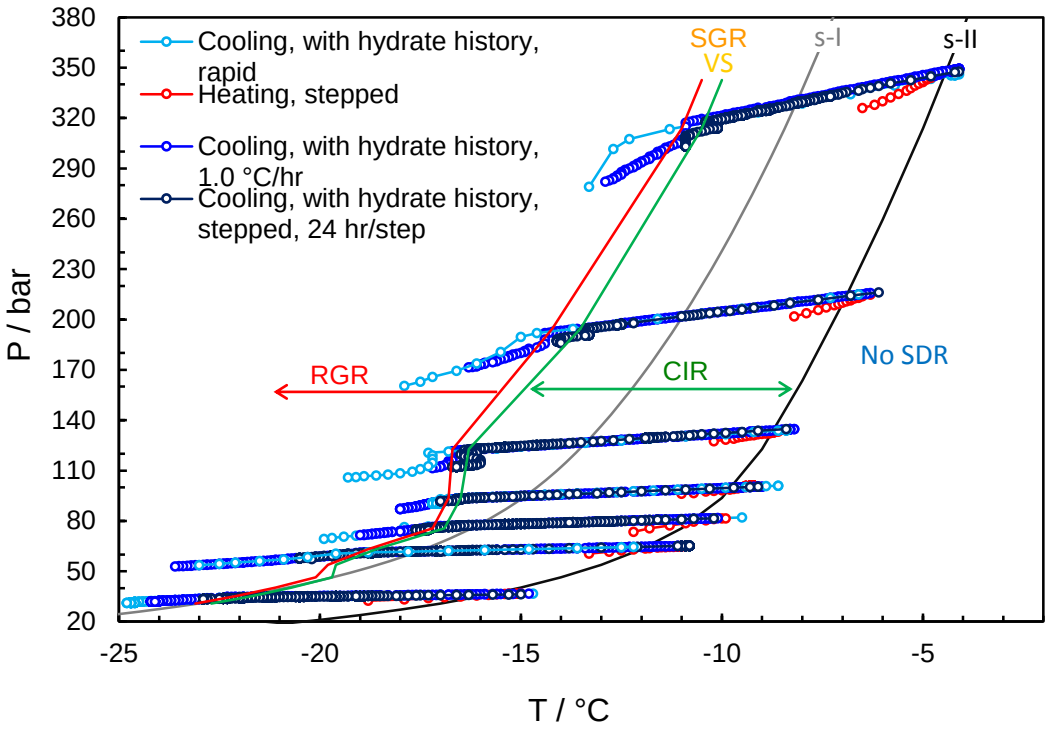

Figure A-5. PT plot showing measured experimental points delineating the various crystal growth inhibition regions for 0.5 mass% Luvicap Bio / 50 mass% methanol aqueous with natural gas.

A.2 1.0 Mass% Luvicap Bio with Methanol in a Natural Gas System

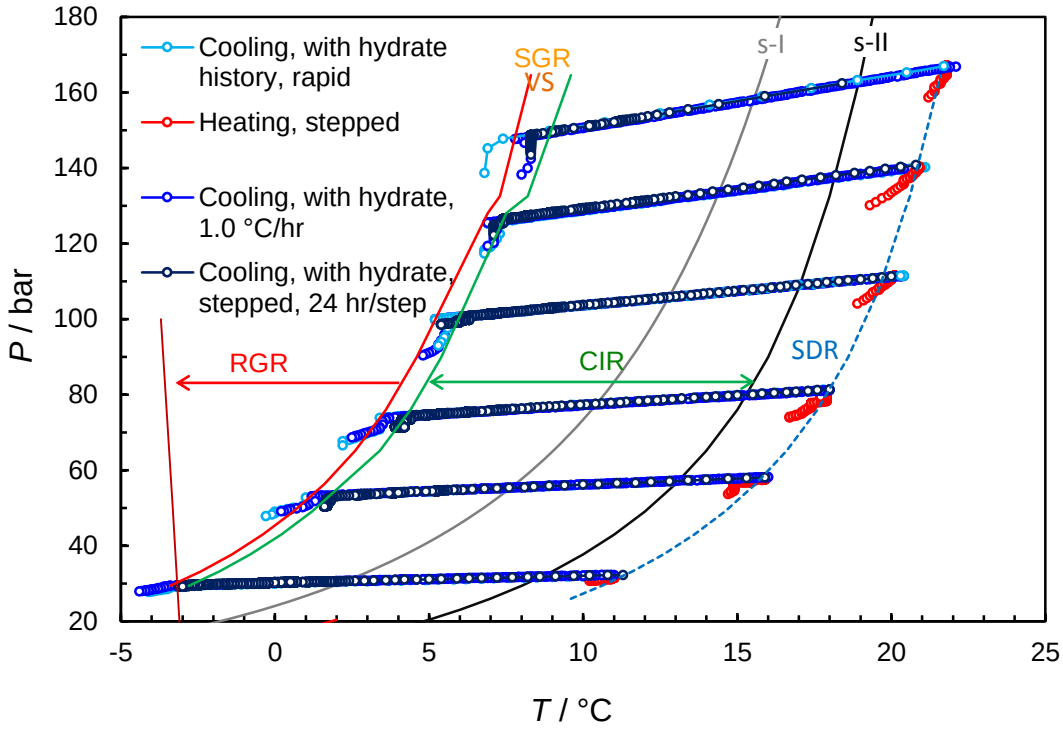

Figure A-6. PT plot showing measured experimental points delineating the various crystal growth inhibition regions for 1 mass% Luvicap Bio / 5 mass% methanol aqueous with natural gas.

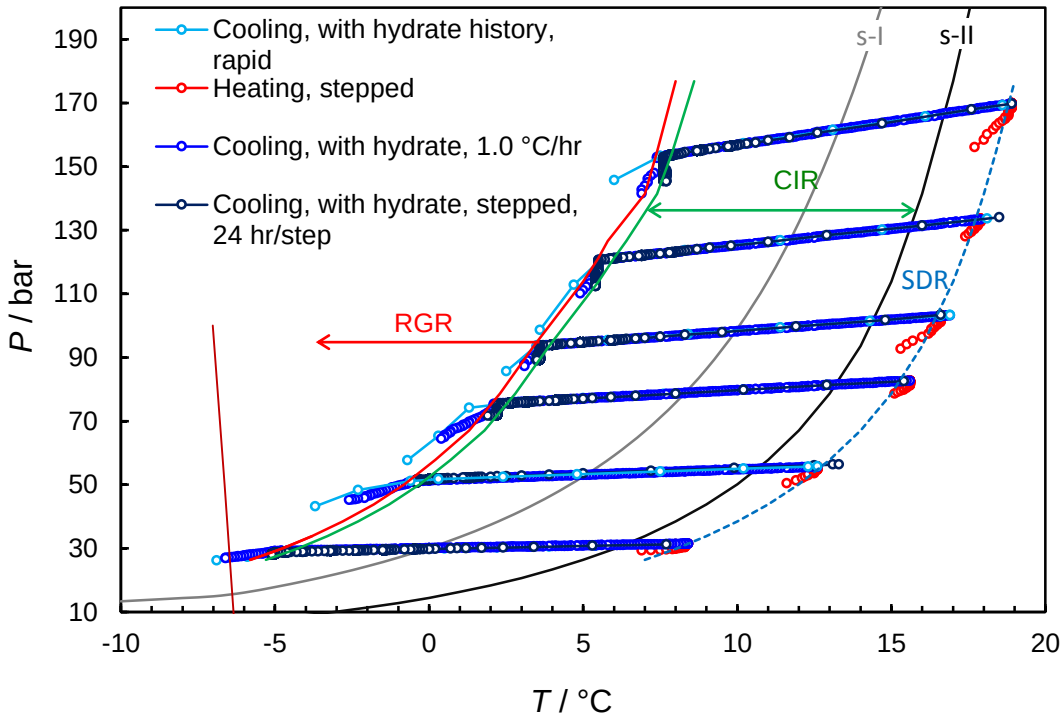

Figure A-7. PT plot showing measured experimental points delineating the various crystal growth inhibition regions for 1 mass% Luvicap Bio / 10 mass% methanol aqueous with natural gas.

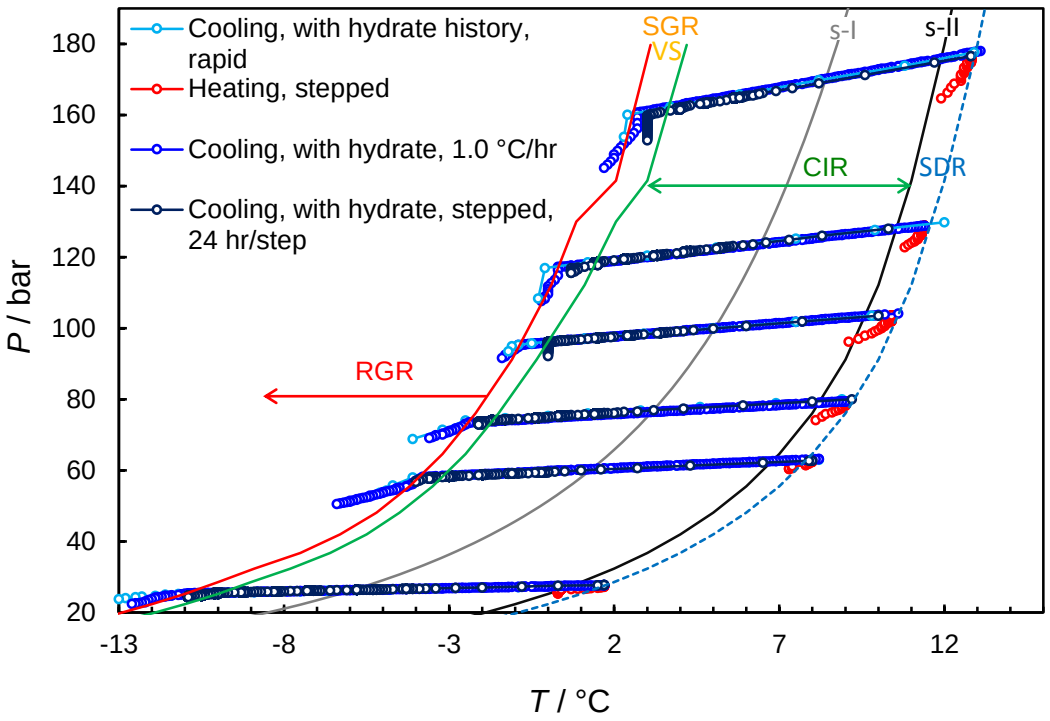

Figure A-8. PT plot showing measured experimental points delineating the various crystal growth inhibition regions for 1 mass% Luvicap Bio / 20 mass% methanol aqueous with natural gas.

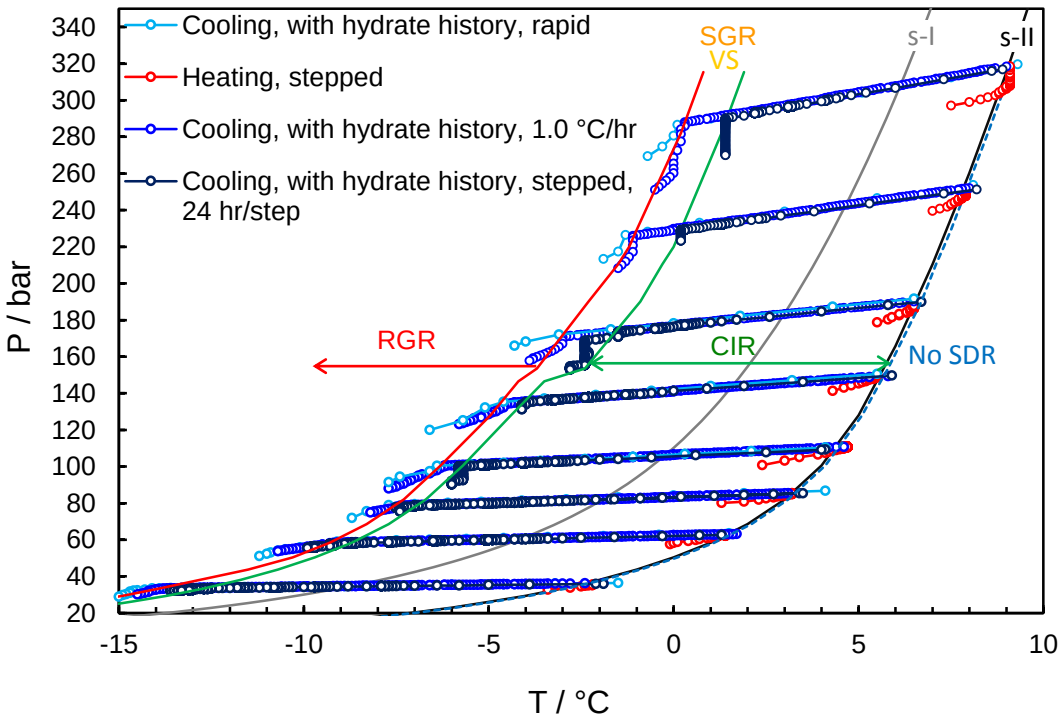

Figure A-9. PT plot showing measured experimental points delineating the various crystal growth inhibition regions for 1 mass% Luvicap Bio / 30 mass% methanol aqueous with natural gas.

A.3 0.5 Mass% Luvicap Bio with Ethanol in a Natural Gas system

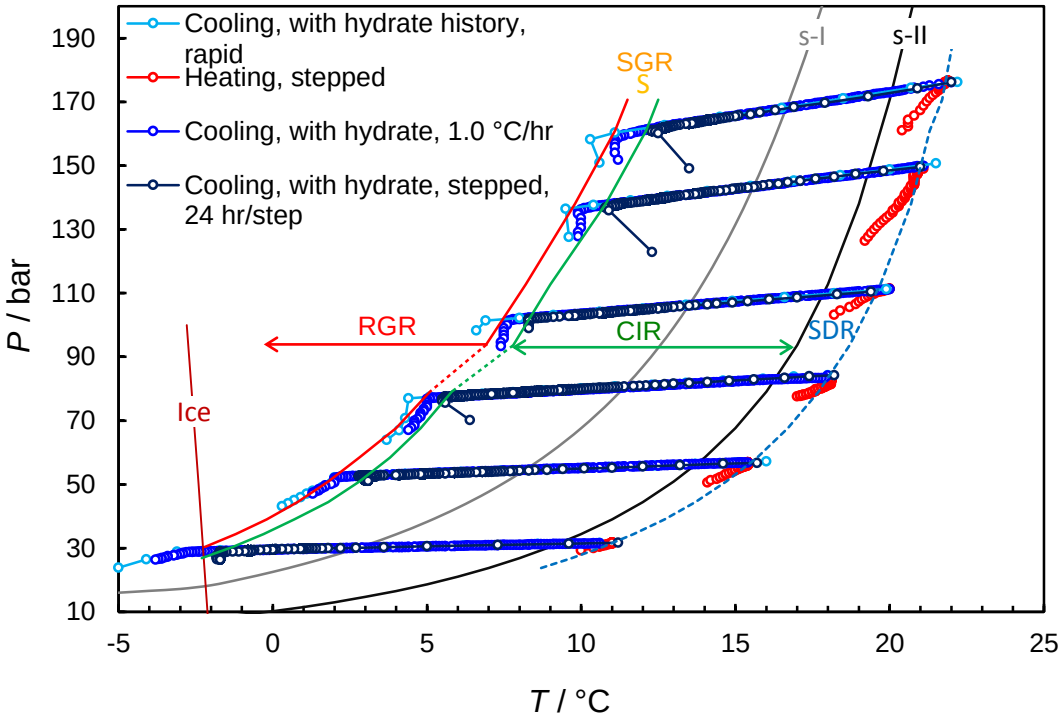

Figure A-10. PT plot showing measured experimental points delineating the various crystal growth inhibition regions for 0.5 mass% Luvicap Bio / 5 mass% ethanol aqueous with natural gas.

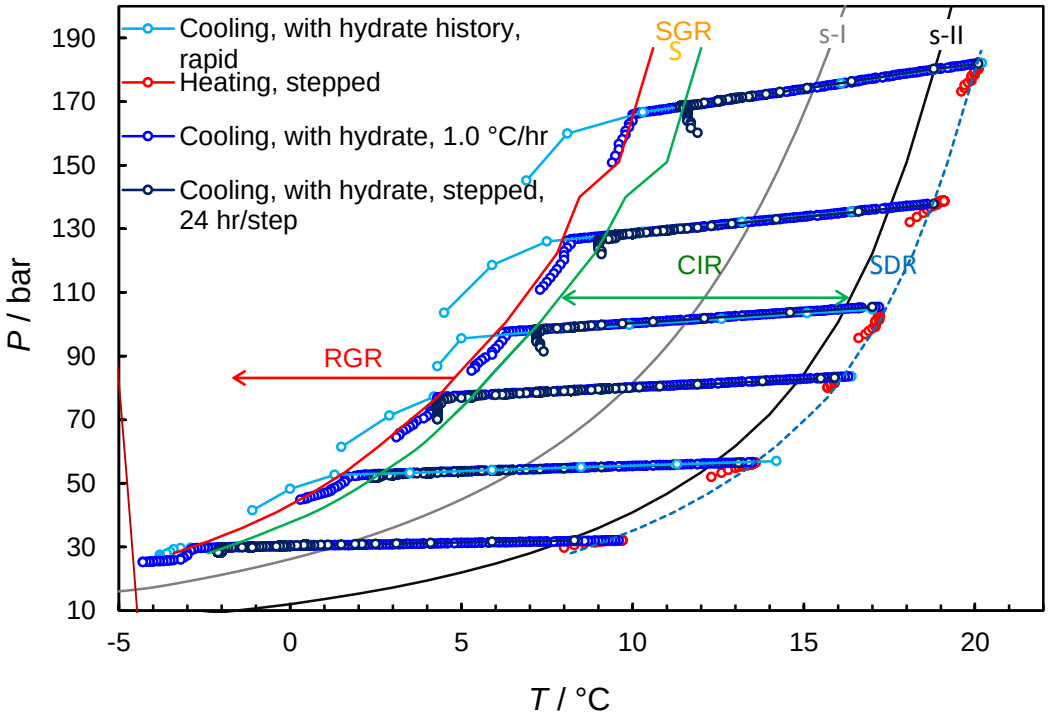

Figure A-11. PT plot showing measured experimental points delineating the various crystal growth inhibition regions for 0.5 mass% Luvicap Bio / 10 mass% ethanol aqueous with natural gas.

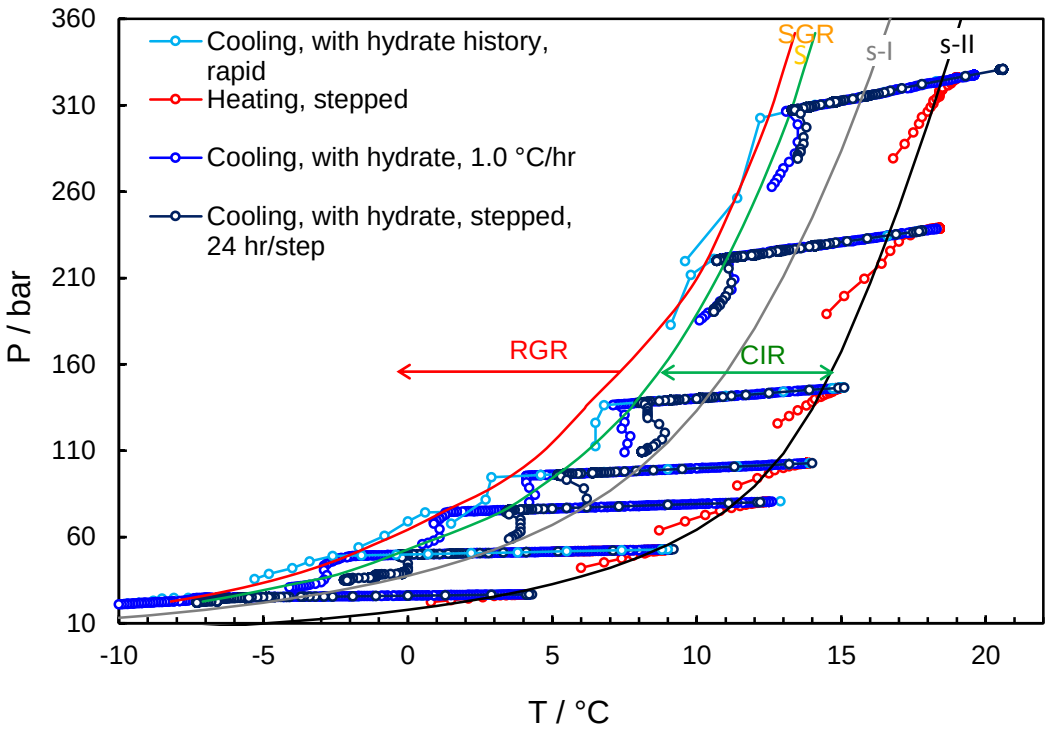

Figure A-12. PT plot showing measured experimental points delineating the various crystal growth inhibition regions for 0.5 mass% Luvicap Bio / 20 mass% ethanol aqueous with natural gas.

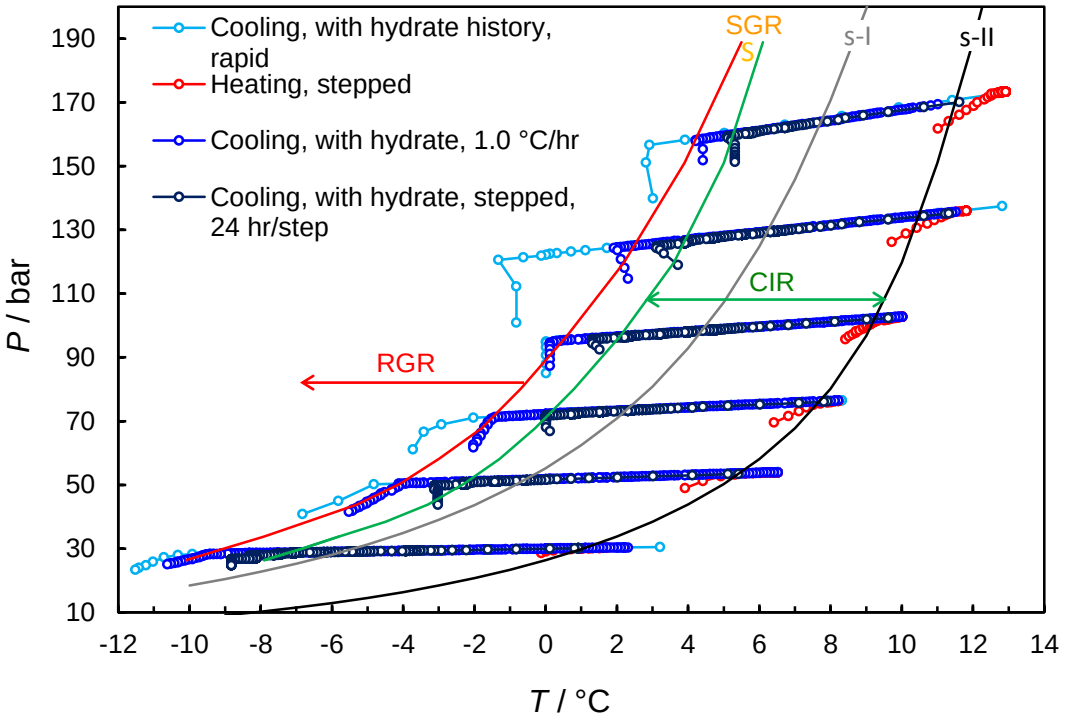

Figure A-13. PT plot showing measured experimental points delineating the various crystal growth inhibition regions for 0.5 mass% Luvicap Bio / 30 mass% ethanol aqueous with natural gas.

A.4 0.5 Mass% Luvicap Bio with MEG in a Natural Gas system

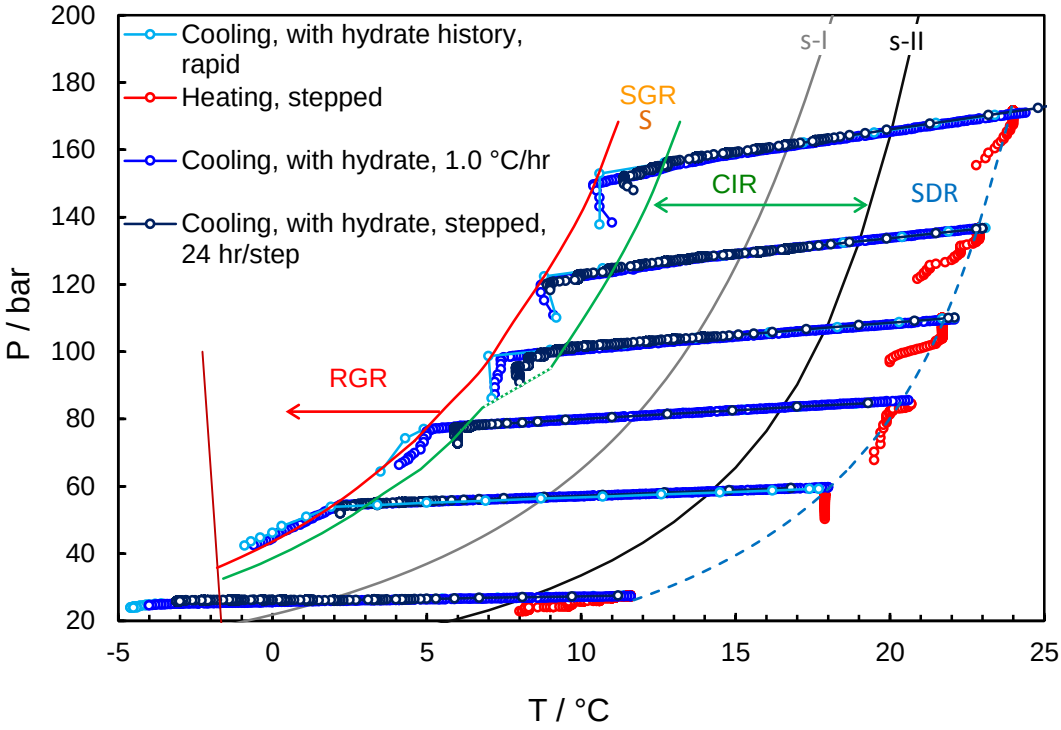

Figure A-14. PT plot showing measured experimental points delineating the various crystal growth inhibition regions for 0.5 mass% Luvicap Bio / 5 mass% MEG aqueous with natural gas.

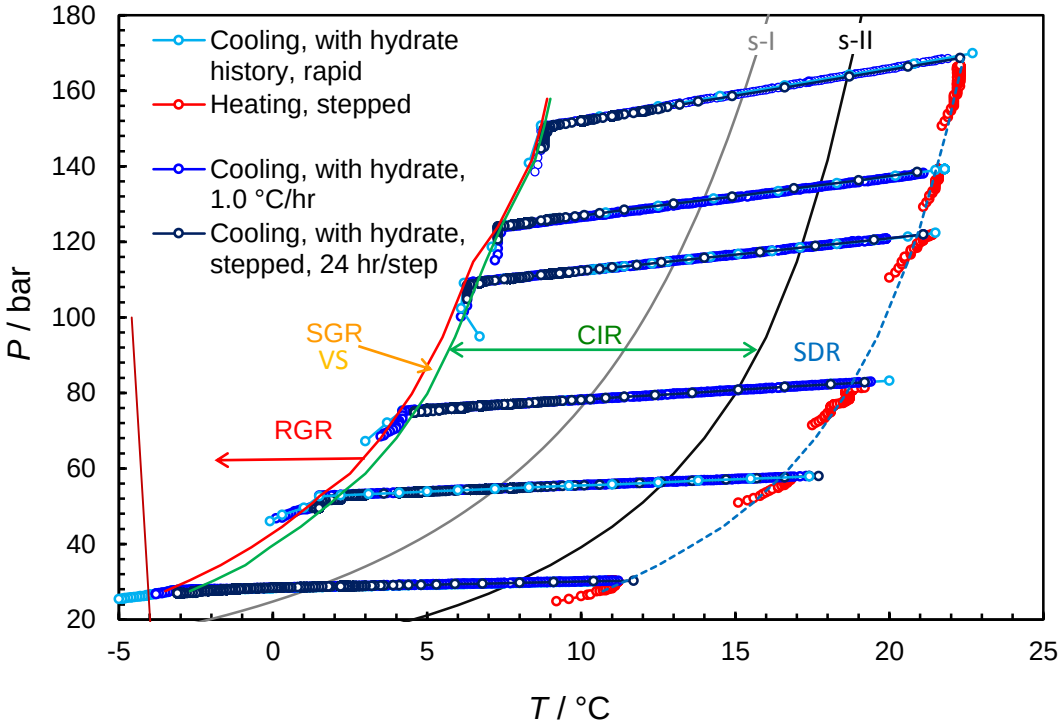

Figure A-15. PT plot showing measured experimental points delineating the various crystal growth inhibition regions for 0.5 mass% Luvicap Bio / 10 mass% MEG aqueous with natural gas.

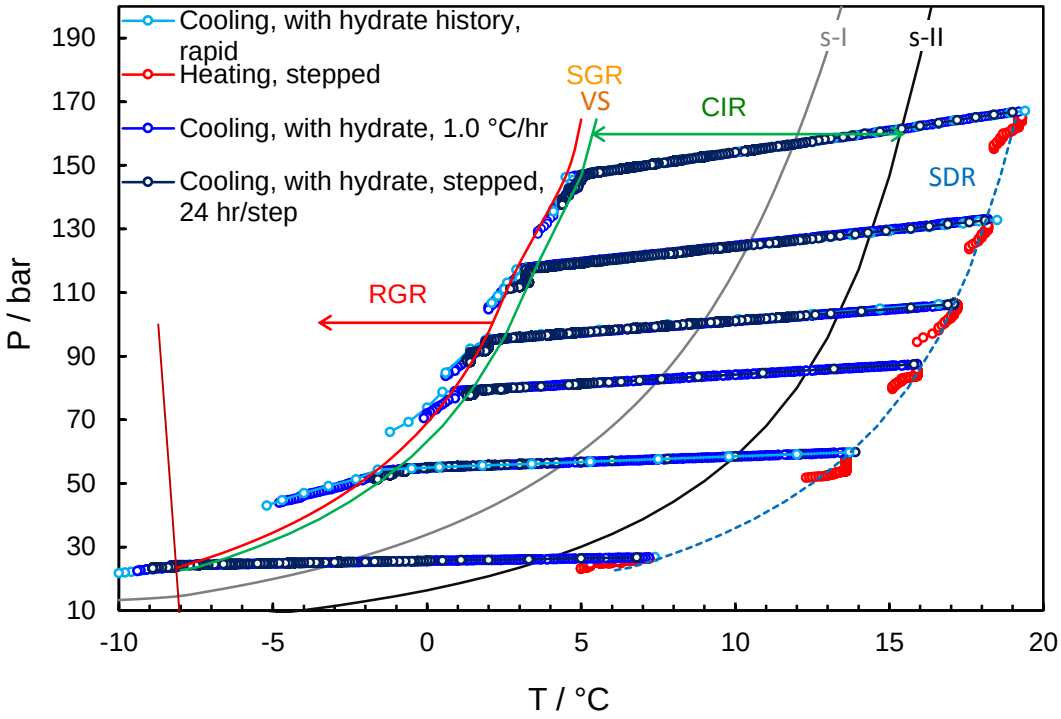

Figure A-16. PT plot showing measured experimental points delineating the various crystal growth inhibition regions for 0.5 mass% Luvicap Bio / 20 mass% MEG aqueous with natural gas.

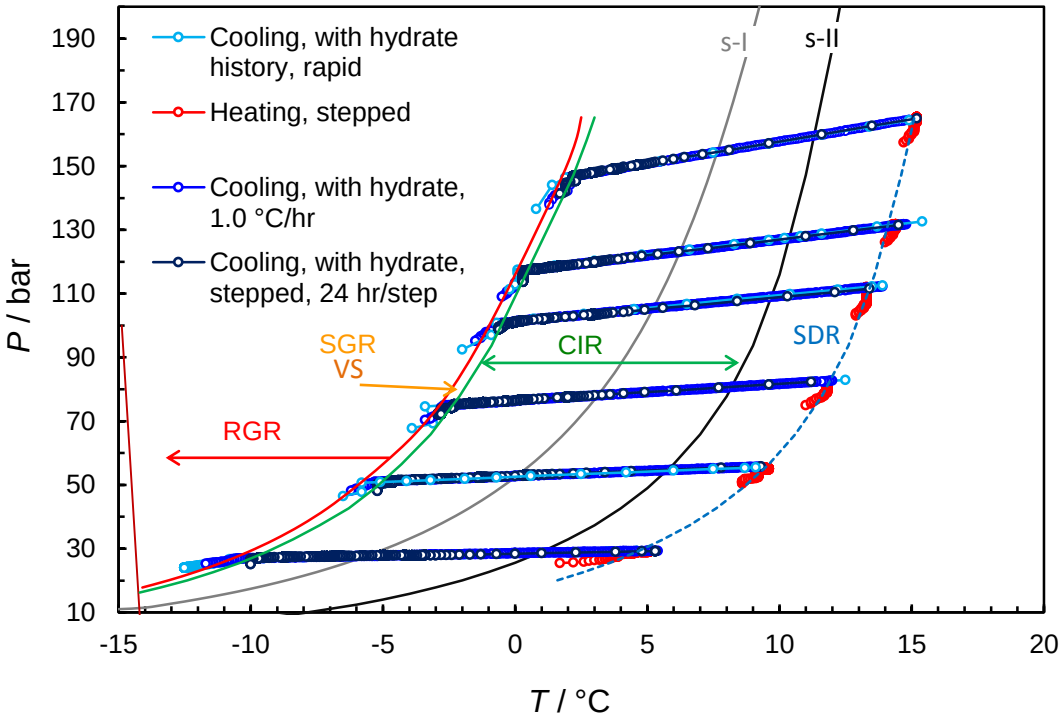

Figure A-17. PT plot showing measured experimental points delineating the various crystal growth inhibition regions for 0.5 mass% Luvicap Bio / 30 mass% MEG aqueous with natural gas.

A.5 1.0 Mass% Luvicap Bio with MEG in a Natural Gas system

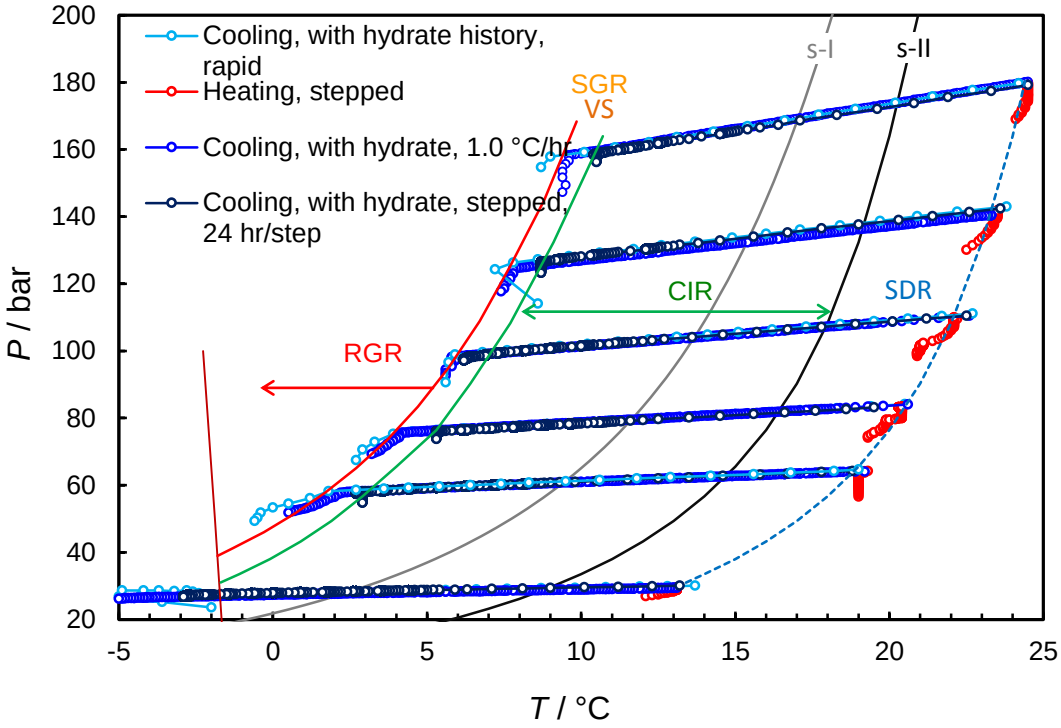

Figure A-18. PT plot showing measured experimental points delineating the various crystal growth inhibition regions for 1.0 mass% Luvicap Bio / 5 mass% MEG aqueous with natural gas.

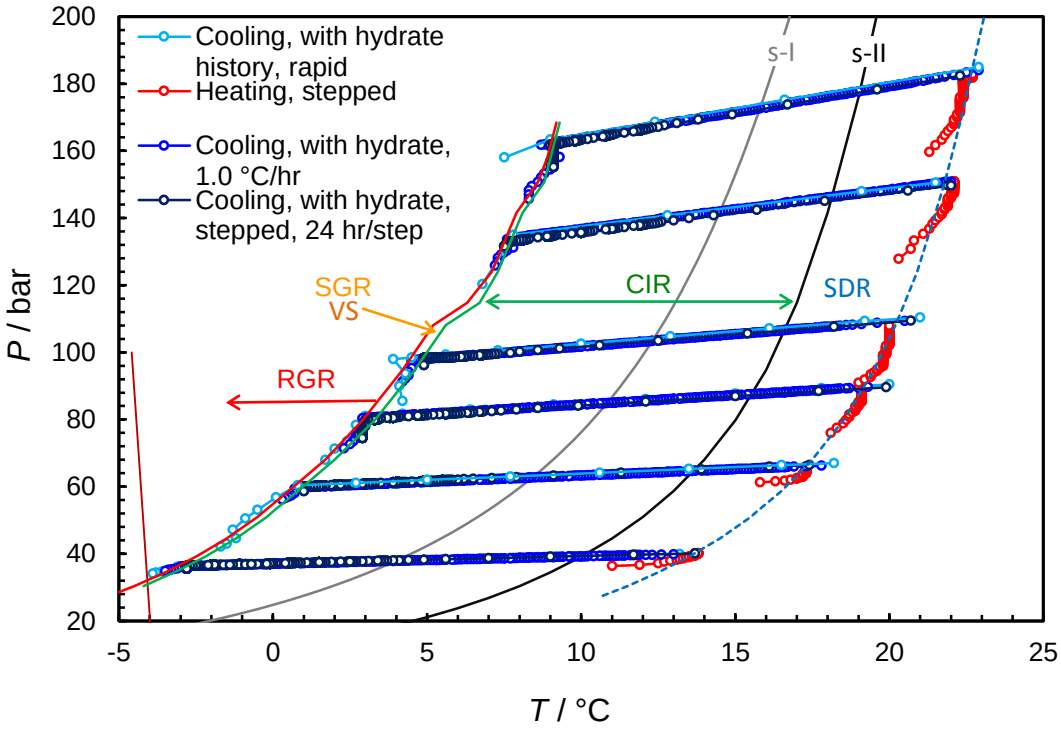

Figure A-19. PT plot showing measured experimental points delineating the various crystal growth inhibition regions for 1.0 mass% Luvicap Bio / 10 mass% MEG aqueous with natural gas.

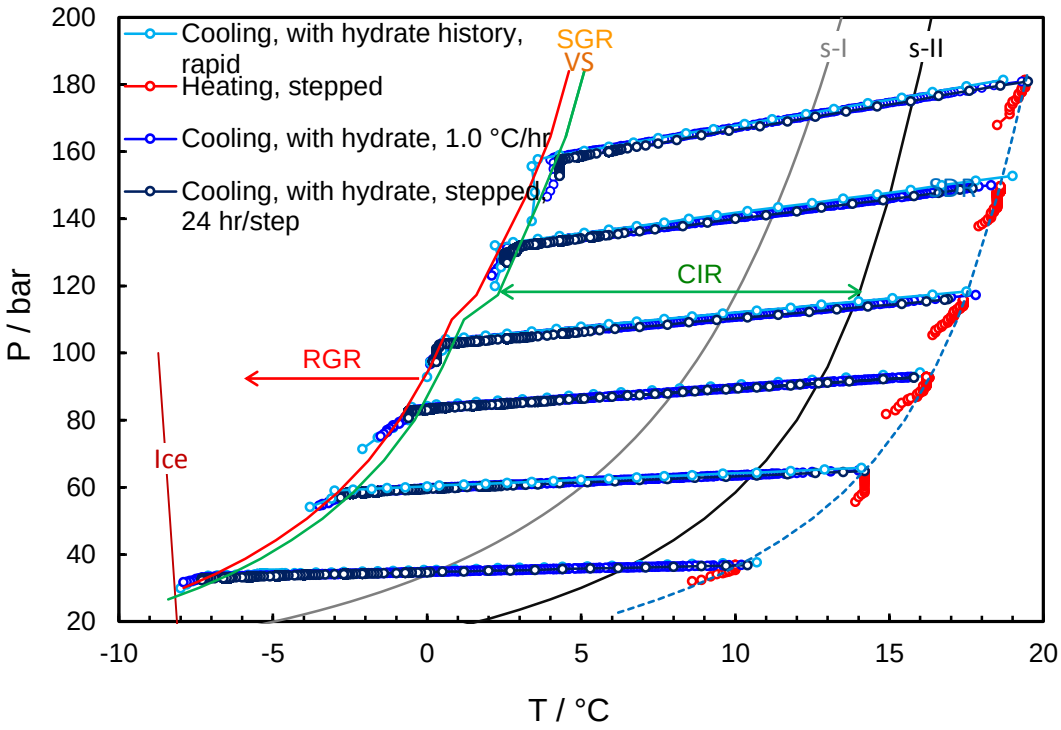

Figure A-20. PT plot showing measured experimental points delineating the various crystal growth inhibition regions for 1.0 mass% Luvicap Bio / 20 mass% MEG aqueous with natural gas.

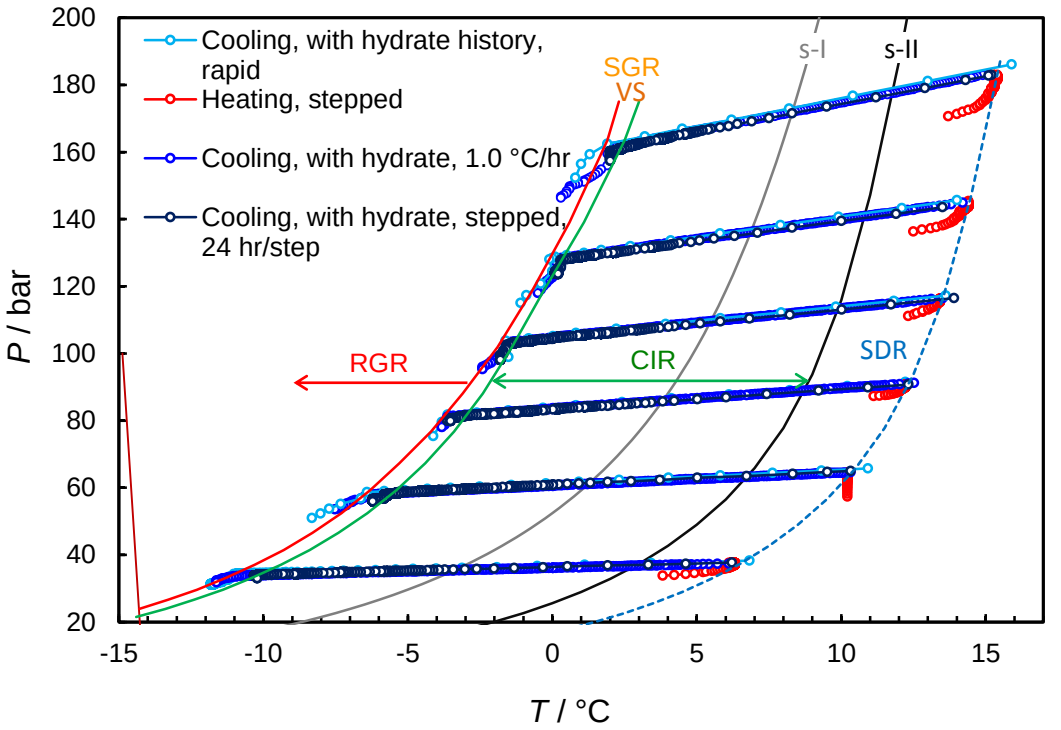

Figure A-21. PT plot showing measured experimental points delineating the various crystal growth inhibition regions for 1.0 mass% Luvicap Bio / 30 mass% MEG aqueous with natural gas.

A.6 0.5 and 1.0 Mass% Luvicap Bio alone in a Natural Gas system

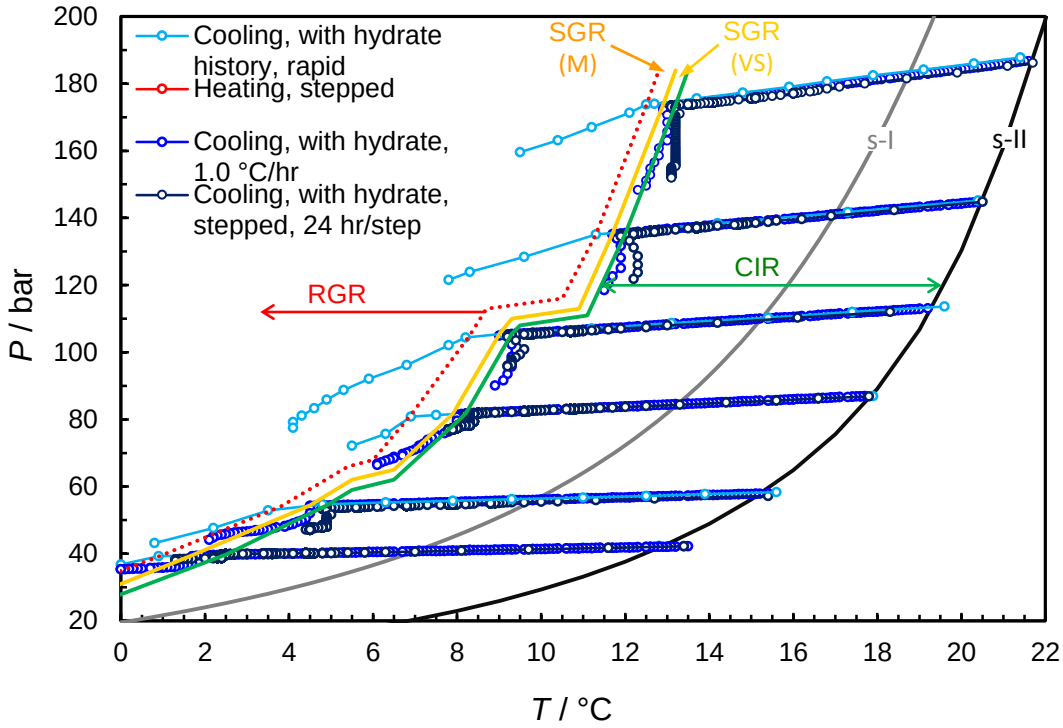

Figure A-22. PT plot showing measured experimental points delineating the various crystal growth inhibition regions for 0.5 mass% Luvicap Bio with natural gas.

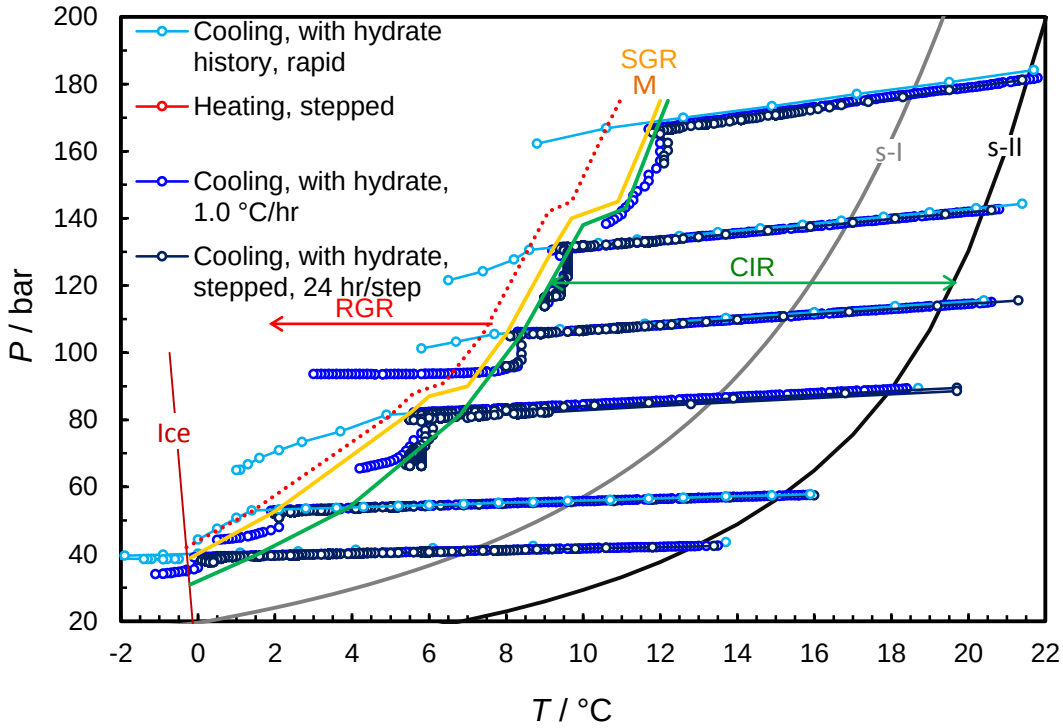

Figure A-23. PT plot showing measured experimental points delineating the various crystal growth inhibition regions for 1.0 mass% Luvicap Bio with natural gas.

Appendix B: Hydrate Calculation

The estimated percentage of water converted to hydrate (WCH %, defined as Equation 1) could be calculated based on pressure drop in the system (ΔP) and the hydration number (H_n), i.e., hydration number is defined as number of water molecules per gas molecule at a given P&T conditions, e.g. the hydration number is around 6 for methane hydrate s-I. The number of gas moles consumed due to hydrate formation, Δn_{gas}, is calculated using Equation 2 which is derived based on the gas law at constant temperature and volume.

$$\text{WCH } \% = \frac{\Delta n_{water}}{n_{water}} \tag{1}$$

$$\Delta n_{gas} = \frac{\Delta P}{P} n_{gas} \tag{2}$$

Here, n_{gas} is the number of gas moles in the gas phase before hydrate formation and P is the pressure of the system without hydrates at the desired temperature. If f_w is defined as water mole fraction, Equation 2 could be rewritten as Equation 4. As a result, the number of water moles used in hydrates (Δn_{water}) is calculated using Equation 5.

$$f_w = \frac{n_{water}}{n_{gas}+n_{water}} = \frac{n_{water}}{n_{tot}} \tag{3}$$

$$\Delta n_{gas} = \frac{\Delta P}{P}(1 - f_w) n_{tot} \tag{4}$$

$$\Delta n_{water} = H_n \frac{\Delta P}{P}(1 - f_w) n_{tot} \tag{5}$$

Therefore, substitution of Equations (5) and (3) in Equation (1) results in Equation (5) which could be applied in calculation of WCH %.

$$\text{WCH } \% = H_n \frac{\Delta P}{P} \frac{1-f_w}{f_w} \tag{6}$$

In this work, the hydration number is assumed constant and equal to 6 for simplicity.